Bangor University

DOCTOR OF PHILOSOPHY

DSP-based Real-Time Enabling Technologies for Future Cloud Access Networks

Al-Rawachy, Ehab

Award date:
2019

Awarding institution:
Bangor University

[Link to publication](#)

DSP-based Real-Time Enabling Technologies for Future Cloud Access Networks

Ehab Isam Dawood Al-Rawachy

PRIFYSGOL

BANGOR

UNIVERSITY

A thesis submitted for the degree of

Doctor of Philosophy

School of Computer Science and Electronic Engineering

Bangor University

October 2019

Abstract

Optical network technologies employed in access networks, metro networks and mobile fronthaul and backhaul must support the unyielding exponential growth in user bandwidth requirements whilst also providing adaptive connectivity solutions to meet the rapid evolution in the diversity of data traffic patterns and characteristics. Furthermore, it is essential that future optical networks support converged fixed and mobile data to leverage the associated cost advantages.. The three distinct 5G services to be supported are, enhanced mobile broadband (eMBB), massive machine type communication (mMTC) and ultra-reliable, low latency communications (uRLLC). As a consequence of the heterogeneous requirements, network slicing is a critical feature for 5G, this allows various services to be provisioned in independent logical channels on the same physical network infrastructure, with different quality of service (QoS) levels. To meet the abovementioned challenges in a cost effective way, the next generation of optical networks have to evolve to be extremely agile, offer highly elastic bandwidth provision and possess a highly reconfigurable network architecture supporting network sliceabilty and software defined networking (SDN), this will allow dynamic adaptation to the changing traffic patterns and enable use of network resources in a highly efficient manner, thus realising commercially viable solutions for network operators. To meet the aforementioned challenges cloud access networks (CANs) have been proposed as a cost effective solution for future optical networks which support converged access/metro networks and mobile fronthaul/backhaul networks. The CANs employ digital signal processing (DSP) to enable various dynamically reconfigurable network devices, network architectures and embedded algorithms for signal impairment mitigation. The fundamental concept of the CAN is built upon digital orthogonal filter-based channel multiplexing, implemented in DSP to achieve highly flexible physical layer connectivity at multi-sub-wavelength levels.

The main objective of this dissertation research is to comprehensively investigate fundamental technical concepts that enable the realisation of the CANs. Using both off-line processing-based experiments and fully real-time DSP-based experiments the technical feasibility of the following CAN technologies and techniques are investigated, i) a cross-channel interference cancellation (CCIC) technique to mitigate physical channel frequency response-induced interference between orthogonal channels, the technique is demonstrated

in 2 channel IMDD point-to-point (PTP) SMF-links and implemented with an offline receiver, ii) a real-time, intensity-modulation and direct-detection (IMDD) multipoint-to-point (MPTP)- digital filter multiple access (DFMA) passive optical networks (PONs) with four independent channels, incorporating a real-time ultra-low complexity CCIC technique embedded in a real-time optical line terminal (OLT) in a 26km SMF, IMDD DFMA PON consisting of two real-time ONUs and iii) a fully real-time soft reconfigurable optical add drop multiplexer (soft-ROADM) providing channel add/drop functions for channel switching within the CAN. The soft-ROADM is constructed with commercially-available low-cost electrical/optical components. In summary, this PhD thesis experimentally validates, performs detailed performance analyses and demonstrates the practical feasibility of various fundamental technologies required for the realisation of CANs, which are proposed as a cost effective solution for future optical networks.

Acknowledgements

Abbreviations

AAD	After-Add
ADC	Analogue to Digital Converter
ADM	Add Drop Multiplexer
ADR	After-Drop
AMOOFDM	Adaptively Modulated Optical OFDM
AON	Active Optical Network
ASE	Amplified Spontaneous Emission
ASIC	Application Specific Integrated Circuit
ATM	Asynchronous Transfer Mode
AWG	Arbitrary Waveform Generator
AWGN	Additive White Gaussian Noise
BAD	Before-Add
BB	BaseBand
BBU	BaseBand Unit
BDR	Before-Drop
BER	Bit Error Rate
BPON	Broadband Passive Optical Network
B&S	Broadcast And Select
BTB	Back to Back
CANs	Cloud Access Networks
CAP	Carrierless Amplitude and Phase
CAPEX	Capital Expenditure
CCI	Cross Channel Interference
CCIC	Cross Channel Interferences Cancellations
CD	Chromatic Dispersion
CDC	Colourless, Directionless and Contentionless
CDF	Cumulative Density Function
CDMA	Code Division Multiple Access
CES	Circuit Emulation Services
CFs	Center Frequencies
CFO	Carrier Frequency Offset

CO	Central Office
CP	Cyclic Prefix
CPRI	Common Public Radio Interface
CSI	Channel State Information
CU	Central Unit
C-RAN	Cloud Radio Access Network
E2E	End To End
DAC	Digital to Analogue Converter
DBA	Dynamic Bandwidth Allocation
DFMA	Digital Filter Multiple Access
DFB	Distributed Feedback Laser
DL	Delay Line
DML	Directly Modulated DFB Laser
DMT	Discrete Multitone Modulation
DOF	Digital Orthogonal Filter
DVB	Digital Video Broadcast
DSB	Double Sideband
DSO	Digital Storage Oscilloscope
DSP	Digital Signal Processing
EAM	Electro-Absorption Modulator
eCPRI	Enhanced Common Public Radio Interface
EDFA	Erbium-Doped Fibre Amplifier
EFM	Ethernet in The First Mile
eMBB	Enhanced Mobile Broadband
EML	Electro-absorption Modulated Laser
ETSI	European Telecommunication Standard Institute
EO	Electrical-to-Optical
EPON	Ethernet Passive Optical Network
FBG	Fibre Bragg Gratings
FDM	Frequency Division Multiplexing
FEC	Forward Error Correction
FIR	Finite Impulse Responses
FTTH(B/C/N)	Fiber-to-the-Home/Building/Curb/Neighbourhood
FFT	Fast Fourier Transform

FIR	Finite Impulse Response
FOP	Fixed Optical Power
FPGA	Field-Programmable Gate Array
FSAN	Full Service Access Network
GPON	Gigabit Passive Optical Network
HDTV	High-Definition Television
IC	Integrated Circuits
ICI	Inter-Channel-Interference
IIR	Infinite Impulse Responses
IFFT	Inverse Fast Fourier Transform
IMDD	Intensity Modulation and Direct Detection
IOT	Internet of Things
IPACT	Interleaved Polling with Adaptive Cycle Time
IP	Internet Protocol
IETF	Internet Engineering Task Force
MPLS	Multiprotocol Label Switching
IQ	In-Phase and Quadrature
ISI	Inter-Symbol-Interference
ITU	International Telecommunication Union
LAN	Local Area Network
LCOS	Liquid Crystal on Silicon
LMS	Least Mean Square
LO	Local Oscillator
LoS	Line of Sight
LR-PON	Long-Reach Passive Optical Network
MAC	Medium Access Control
MAI	Multiple Access Interference
MBH	Mobile Backhaul
MCSs	Multicast Switches
MEF	Metro Ethernet Forum
MEMS	Micro Electromechanical Systems
MF	Matching Filter
MFH	Mobile Fronthaul
MFL	Multi-Frequency Laser

MIMO	Multiple Input, Multiple Output
MMF	Multi-Mode Fiber
mMTC	Machine Type Communication
MSC	Mobile Switching Centre
MUD	Multi-User Detectors
MZM	Mach-Zehnder Modulator
NG-PONs	Next Generation Passive Optical Networks
NRZ	Non-Return-to-Zero
OADM	Optical Add/Drop Multiplexer
OBI	Optical Beat Interference
OBPFs	Optical Bandpass Filters
OC	Optical Coupler
ODN	Optical Distribution Network
OE	Optical-to-Electrical
OFDM	Orthogonal Frequency Division Multiplexing
OLT	Optical Line Terminal
ONU	Optical Network Unit
OOFDM	Optical Orthogonal Frequency Division Multiplexing
OOK	On/Off Keying
OSC	Optical Supervisory Channel
OSNR	Optical Signal-to-Noise Ratio
OTBPFs	Optical Tuneable Bandpass-Filters
PAM	Pulse Amplitude Modulation
PAPR	Peak-to-Average Power Ratio
PB	PassBand
PD	Photodetector
PDCP	Packet Data Convergence Protocol
PDH	Plesiochronous Digital Hierarchy
PIC	Parallel Interference Cancellation
PLC	Planar Lightwave Circuit
PMD	Polarization Mode Dispersion
PON	Passive Optical Network
PPM	Parts Per Million(PPM)
PRBS	Pseudo Random Bit Sequences

PS	Power Splitters
PTP	Point To Point
PTMP	Point To MultiPoint
P/S	Parallel-to-Serial
PSK	Phase Shift Keying
QAM	Quadrature Amplitude Modulation
OBSAI	Open Base Station Architecture Initiative
ORI	Open Radio Equipment Interface
OSNR	Optical Signal-To-Noise Ratio
QoS	Quality Of Services
RAN	Radio Access Unit
RAT	Radio Access Technology
RF	Radio Frequency
ROADM	Reconfigurable Optical Add/Drop Multiplexer
ROP	Received Optical Power
ROT	Reconfigurable Optical Transceivers
RPs	Reference Points
RRH	Remote Radio Head
RLC	Radio Link Control
RU	Radio Unit
R&S	Route and Select
S-BVT	Sliceable Bandwidth Variable Transceiver
SCO	Sampling Clock Offset
SDH	Synchronous Digital Hierarchy
SDN	Software Defined Networking
SF	Shaping Filter
SFO	Sampling Frequency Offset
SFP	Small Form-Factor Pluggable
S/H	Sample-and-Hold
SIC	Successive Interference Cancellation
SMF	Single-Mode Fiber
SNR	Signal-to-Noise Ratio
SONET	Synchronous Optical Network
S/P	Serial-to-Parallel

SSI	Subcarrier-Subcarrier-Intermixing
SSS	Spectrum Selective Switch
SIC	Successive Interference Cancellation
SIR	Signal to Interference Ratio
STO	Symbol Timing Offset/Sample Timing Offset
Sub- B	Sub-Band
Sub- λ	Sub-Wavelength
SUD	Single User Detector
TDM	Time Division Multiplexing
TET	Terminal Equipment Transceivers
TIA	Transimpedance Amplifier
TL	Teaunable Laser
TTF	Thin Film Filters
TSB	Targeted Sub-Band
TWDM	Time and Wavelength-Division Multiplexed
uRLLC	Ultra-Reliability Low Latency Communication
VNI	Visual Networking Index
VOA	Variable Optical Attenuator
VPN	Virtual Private Networks
VR	Virtual Reality
WAN	Wide Area Networks
WiMAX	Worldwide Interoperability for Microwave Access
WDM	Wavelength Division Multiplexing
WSS	Wavelength Selective Switches

Contents

1. Introduction

Contents

1. Introduction

1.1   Future Network Challenges and Cloud Access Networks

The advent of modern communication technologies has revolutionized the way people communicate [1]. In particular, the mobile communication revolution transformed the initial basic services from basic voice calls and text messaging, to advanced mobile applications such as video calling, web browsing, on-demand video, on-line gaming and navigation. Mobile technologies are continuing to evolve to support a new generation of services in diverse fields of our lives, including health, entertainment, industrial and home automation and vehicular communication, etc. A significant factor influencing the rapid growth of mobile applications is that people and organizations continually leverage the communications technologies for purposes very different of those initially conceived by the designers of the technology [2]. A clear example is the use of mobile communications to link autonomous devices such as sensors and machines in the emerging Internet of Things (IoT). Another factor influencing the growth in communications is that nowadays, the worldwide spread of social media networking means that users do not just consume content but have become avid content generators themselves. Statistics in July 2019 showed that for example, Facebook has more than 2.375 billion active users, whereas YouTube has more than 2 billion active users [3]. Moreover, recent statistics [4] show the number of smartphones in the US is predicted to increase approximately four fold from 2010 to 2023.

As a direct result of the aforementioned facts, the rapid increase in mobile network traffic has continued in recent years and this trend is predicted to continue in the foreseeable future. Fig 1.1 illustrates the overall mobile data traffic growth, predicted until 2022, there is an approximate seven-fold increase due to an annual growth rate of 46 percent from 2017 to 2022 [5]. Consequently, to support the growth in mobile traffic, ongoing improvements to the associated optical network's capabilities and performance are therefore undeniably critical.
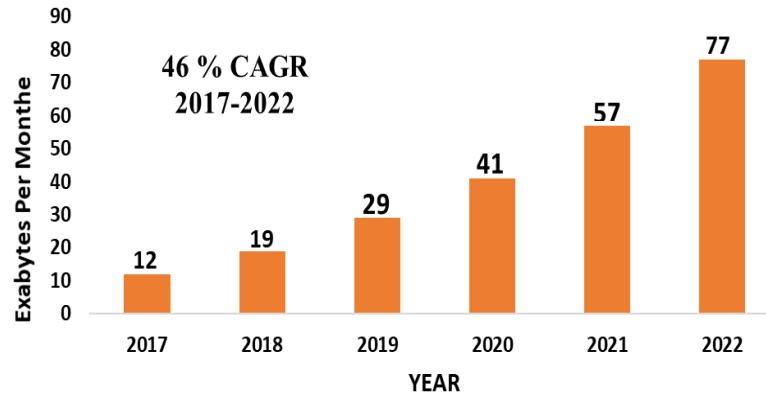
Fig. 1.1 Forecast of global volume of mobile data traffic per month.[5]

Apart from the capacity increase, the newly emerging applications are also posing unprecedented challenges in terms of latency, reliability and scalability on the future networks. Other factors are also exacerbating the challenges to the future networks, such as the vast heterogeneity of the applications, network functions and mobile devices [6]. To meet the aforementioned challenges the 5th generation (5G) mobile network will become widely adopted worldwide, to accommodate the trend of explosive mobile traffic and achieve the necessary improvements in the network performance. 5G is planned to provide all types of connectivity to any type of device with different quality of services (QoS) requirements. 5G thus aims to support a vast array of services with enormously heterogeneous requirements. Enhanced mobile broadband (eMBB) is one of the main characteristics of 5G [6, 7]. Technically speaking, in terms of signal bitrate, 5G aims to provide a 10-100 times increase in comparison to 4G. While in terms of traffic density, in 2020, the volume of mobile data per geographical area is predicted to increase 1000 times compared to that in 2010 [8, 9] .

In addition to the improved network transmission capacity, 5G should also offer ultra-reliable low-latency communications (URLLC) for real-time, safety-critical systems. From the network's physical-layer perspective, the URLLC requirement imposes strict conditions on its latency and reliability [10]. Generally speaking, network latency simply refers to the time taken for a packet of data to travel between two points in the network [11]. While the end-to-end (E2E) latency of a complete network connection, contains the over-the-air transmission delay, queuing delay, processing/computing delay and retransmissions (when needed). 1ms is the target E2E latency required for 5G mobile systems and it is interesting to note that, due to speed of light restrictions, ~150 km is the maximum transmission distance over which this can be achieved [6]. Whereas, reliability refers to the probability that a given amount of the data will be transferred in a given time period. Industrial automation is an

example application where high reliability levels are critical. For example, time-critical processes such as real-time, closed loop, robotic control can required reliability levels of 99.9999% [12]. Another clear example of a URLLC safety-critical application requiring ultra-reliability, is remote surgical operations involving real-time sensors with the use of haptic feedback thus enabling the concept of a remote operating theatre [13]. URLLC can also serve sport fans by realising a virtual reality (VR) headset with a 360-degree courtside view to give a fully immersive crowd experience from the comfort of the home[14].

Another key feature supported by 5G is massive machine-type communications (mMTCs), which is defined as an immense number of machine-type devices simultaneously connected through wireless internet technologies to allow automated data generation, processing, transfer and exchange amongst them with minimum human interaction. In general, mMTC has to support a wide range of applications, spanning from low-complexity devices, such as simple sensors, to highly complex and advanced devices such as used in the automotive industry, transportation, public safety and healthcare. Moreover, it is expected that [6] there would be tens of billions of connected devices, which would surpass the number of the connected human user devices by 2020 [15, 16] . In 2020, the device density which 5G aims to support is 1 million/km^2 [4,11].

A wide range of technologies are being utilised to achieve the practical implementation of 5G networks. Firstly, the use of the millimetre wave spectrum (30-300 GHz) is proposed to leverage the unused wide spectral bands available at these frequencies, thus permitting greatly increased signal bit rates. It should be noted however that the adopted RF carrier frequencies themselves do not directly impact the capacity requirements of the underlying radio access network (RAN). Secondly, massive multiple input multiple output (MIMO) antenna arrays with steerable beam forming capability are a key technology to be adopted in 5G to enhance the signal transmission capacity by improving spectral efficiency and also reducing radio interference across the cell. Thirdly, small-cell networks (SCNs) are also widely adopted where the cells use low power transmitters to provide coverage of ~10 meters to a few kilometres, compared to up to ~35km for conventional macro-cells. The SCNs thus fully exploit the frequency reuse principle of cellular networks to provide increased mobile device density through increased spectrum utilisation. The peak mobile devise density in an area must therefore be predicated in order to deploy a sufficiently high density of small cells.

The combination of increased user bandwidths, multiple antenna techniques and high density SCNs leads to a vast increase in the required capacity of the underlying 5G RAN, compared to the existing 4G RANs, particularly as the 5G RAN capacity is directly dependent on the user bit rates, number of antennas and number of cells.
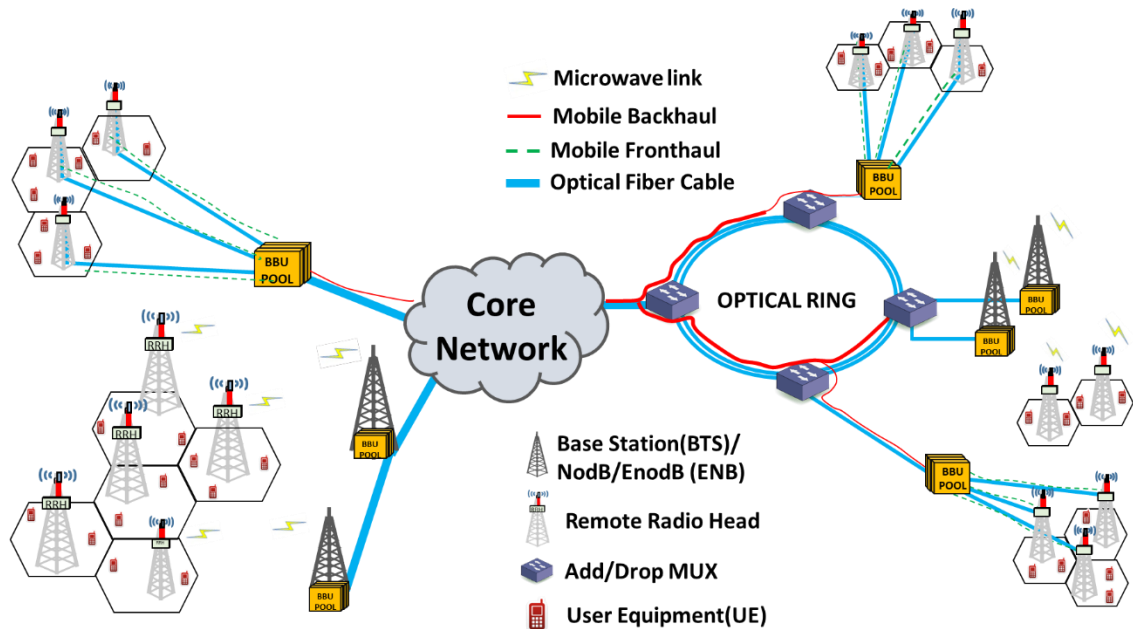
Fig. 1.2 The mobile backhaul and fronthaul network infrastructure for Centralised-RAN

5G networks will adopt the centralised radio access network (C-RAN) architecture as depicted in Fig 1.2, which is a centralised RAN architecture now being deployed in 4G to replace the traditional distributed RAN architecture. This is necessary in order to leverage the associated cost benefits and increased operational flexibility of the C-RAN. In the C-RAN, remote radio heads (RRH) connect via mobile fronthaul (MFH) links to a centralised pool of baseband units (BBUs) which in turn connect via mobile backhaul (MBH) links to the mobile switching centre in the core network. The RRH performs functions of, digital-to-analogue and analogue-to-digital conversions (DAC/ADC), frequency up and down conversions, power and low-noise amplification and antenna interfacing. Whereas the pool of BBUs at the centralised site, perform physical layer processing of the baseband radio signals such as digital processing to modulate/demodulate the baseband radio signals according to the employed radio access technology and the BBUs include all functions of the upper layers and traffic management.

As the mobile device density and distribution exhibits highly temporal variation across the cells within a C-RAN and as the instantaneous capacity requirements of individual mobile devices is also continually changing, the co-located pool of BBUs can dynamically allocate and share their resources amongst the RRHs based on the current network traffic requirements. Thus the BBU processing functions are utilised in a highly efficient manner. The traditional C-RAN employs point-to-point (PTP) links for the MFH between the RRHs and centralised BBUs, however the PTP architecture can be highly inefficient when supporting dynamically allocated network capacity.

For an optical network architecture where multiple end nodes connect to a single centralised node (or nodes) and where cost-effectiveness is paramount, as in the 5G C-RAN, passive optical networks (PONs) have become a highly popular technical solution. PONs that employ intensity-modulation and direct-detection (IMDD) transmission systems are particularly cost effective as they employ simple optical transceiver front-ends in comparison to other optical transmission techniques such as coherent systems. Thus IMDD-based PONs offer low power consumption and minimal maintenance as there are no active devices deployed in the outside plant. In 2018, Nx25Gb/s Wavelength division multiplexing (WDM) PON-based 5G fronthaul was successfully validated in a live demonstration on China Telecomm's network [17], where the data rate and end-to-end latency was shown to be equal to that of PTP-based fibre connections. The WDM-PON-based 5G C-RAN however still suffers from limited flexibility as capacity cannot be shared between wavelengths. Thus, to deal with the aforementioned dynamic traffic patterns associated with the 5G C-RAN, it is highly advantageous if the PON is equipped with sufficient flexibility, elasticity and dynamic reconfigurability. Furthermore, if the PON is to support multiple mobile generations (e.g. 3G, 4G, 5G) for backwards compatibility, or even multiple network operators, the PON must have not only strong adaptability to highly dynamic traffic with arbitrary signal bandwidth granularity, but also excellent transparency to various traffic characteristics including signal modulation format, signal bit rate, different signal detection schemes, flexible WDM-grids, diversified network topologies and various multiple access techniques. Furthermore, it is crucial that the PON supports network slicing, which is a technique that splits the physical infrastructure into multiple logical slices (sub-networks), each one specified for a different QoS requirement, thus each mobile generation and/or network operator can be allocated a dedicated network slice acting as an independent network. The network slicing feature is also highly applicable to 5G in order to support the

highly heterogeneous applications as previously stated. As dynamic provision of fast on-demand network connections and slices is required with fine granularity and high connection/slice count, it is essential that a single optical wavelength can be subdivided into multiple logical connections at the subwavelength and sub-band levels. WDM can, however, still be employed, as necessary, to increase the aggregate capacity in the PON. To achieve effective delivery of the aforementioned PON network features, the implementation of software-defined networking (SDN) down to the physical layer, is also critical [18, 19] , as SDN makes use of centralized network resource abstraction and network infrastructure virtualization to easily and dynamically reconfigure the networks.

Fixed optical fibre-based access networks are almost exclusively based on IMDD PONs due to the aforementioned advantages of low deployment and operational costs. The latest PON standards support multi-10Gb/s aggregate bit rates, however there is continuing demand for higher and higher end-user capacity in the fixed access networks and it is expected that in the near future operators need to offer 1-10 Gb/s peak connection speeds to individual subscribers [20]. Provision of such high connection speeds based on an essentially static network architecture with limited flexibility in capacity allocation amongst users is highly challenging due to the associated high costs and as the users are not ready to pay significantly more for the increased internet speeds. Operators are therefore facing the dilemma of the decoupling effect between increased bit rate and revenue growth. High costs are associated with increased bit rates as it is technically challenging to implement low cost, high speed networks because the physical impairments of both electrical/optical components and the fibre transmission have significant impact on signal quality at higher bit rates when traditional on-off keying modulation is used, thus advanced and therefore costly components and/or techniques are needed to mitigate the physical impairments. Alternatively, WDM is a mature technology capable of increasing PON capacity, but this is a costly solution due to the need for expensive tuneable lasers, arrayed wave guides (AWGs) and/or tuneable optical filters. The future PONs for fixed data access networks must therefore incorporate advanced modulation techniques for increased bit rates, but importantly, must possess the features of flexibility, elasticity and dynamic reconfigurability down to the physical layer to use the available PON capacity in a highly efficient manner and support features such as network sliceabilty and signal modulation transparency for highly versatile service delivery. The statistical characteristics of the user capacity requirements over time can be exploited, as the capacity requirements of each user are highly dynamic, therefore dynamic bandwidth

allocation (DBA) with arbitrary and fine granularity allows the PON to adapt to the prevailing traffic conditions and share the available PON capacity in a highly efficient manner. The fixed access PONs can also utilise SDN as an effective control system for dynamic PON reconfiguration. To achieve flexibility in the currently deployed time division multiple access (TDMA)-based PONs, many techniques have been proposed to achieve DBA based on the dynamic allocation of timeslots to ONUs based on traffic loading. Interleaved Polling with Adaptive Cycle Time (IPACT) [21] is an algorithm developed for use with Ethernet PONs (EPON), where the OLT distributes timeslots with dynamic window size according to the instantaneous number of packets buffered in the ONUs and reported by the ONU request messages. The DBA algorithms based on dynamic timeslot allocation operate at the medium access control (MAC) layer and so cannot achieve the same level of PON flexibility and reconfigurability possible by physical layer reconfigurability. It is important to highlight that the recent NG-PON2 ITU-T standard is essentially targeted at providing higher PON aggregate capacity (40Gb/s or more) and is still effectively a static architecture, thus NG-PON2 cannot solve the abovementioned challenges.

The flexible, adaptive and elastic PONs are therefore highly suitable for application in both MFH/MBH networks and fixed optical access networks, consequently it can be highly beneficial if the flexible PON simultaneously supports both mobile and optical access networks, thus forming a converged fixed-mobile network to replace the traditional independently developed and deployed networks. The seamless convergence of fixed optical access and mobile data networks in a single PON allows network resources to be shared between the fixed access and mobile data traffic thus increasing network flexibility and allowing for more efficient use of network resources, which reduces the overall cost of network ownership. The benefit of a converged network is clear if the end users' usage patterns are considered. In general, users typically connect to the internet either via fixed optical access or mobile connections at certain times of the day, thus network resources can be switched between fixed optical access and mobile data connections to match the usage patterns of the end users. SDN control can be fully exploited to effectively manage the allocation of PON resources between the fixed access and mobile data connections and furthermore, such SDN-based network operations will also allow network operators to change their business model from fixed bandwidth provision, to a more on-demand real-time bandwidth provision-based model with on-demand "pay as you grow" services.

A significantly increased level of flexibility in the PON-based converged optical network can be achieved if multiple PONs are interconnected via reconfigurable switching elements which can dynamically distribute the total network capacity between the PONs and the operator's central office, thus providing inter-PON bandwidth allocation for greatly enhanced network flexibility and efficiency. The switching elements could also provide flexible interconnections between the PONs for highly flexible network deployment. Being one of the most important network switching devices offering connectivity between an large number of individual optical networks, reconfigurable optical add/drop multiplexers (ROADMs) with advanced configurations and flexible functionalities are thus expected to play a vital role in ensuring the achievement of the aforementioned highly flexible converged networks [22, 23] , however ROADMs with low implementation and operational costs are critical for the cost sensitive converged network scenario.
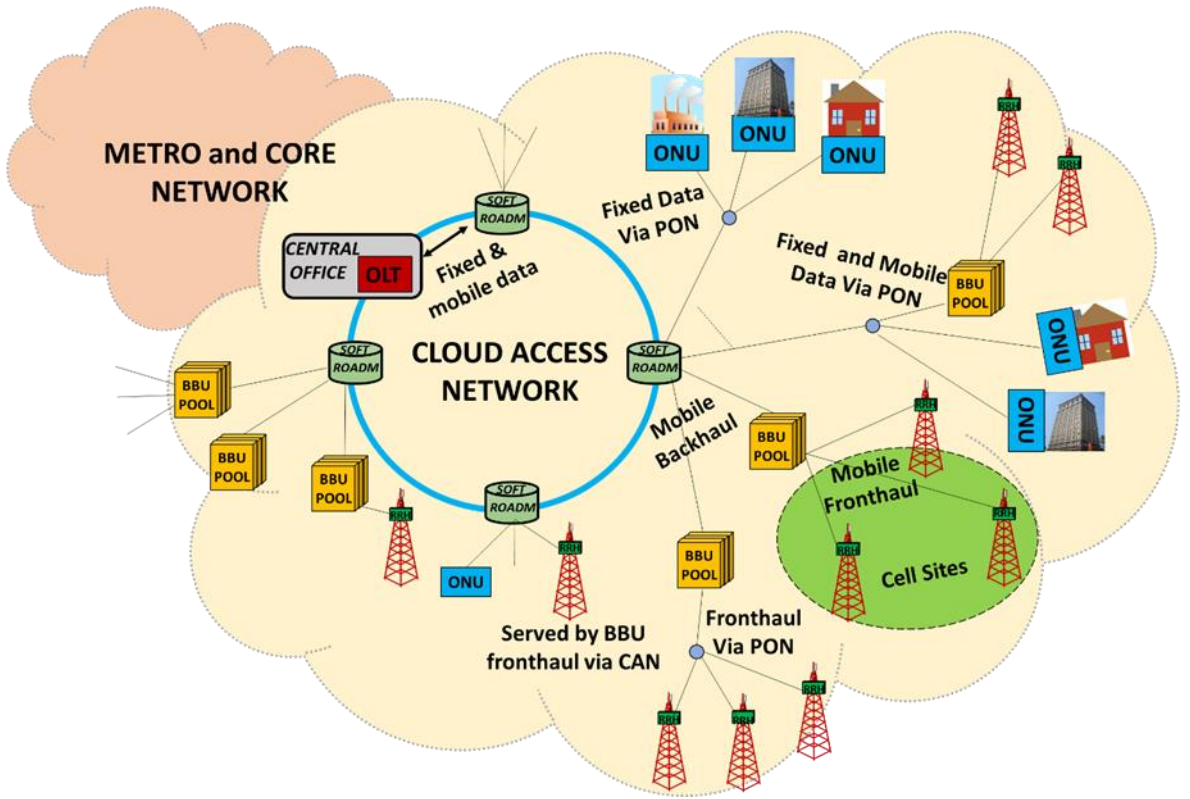
Fig. 1.3 Cloud Access Network (CAN) Architecture

Fig. 1.3 shows an example converged network consisting of a ring of ROADMs which connect to various network end points via flexible PONs and PTP links. This newly proposed network has been termed a cloud access network (CAN) [24] as it offers a highly configurable network architecture, enabling dynamic and flexible connectivity between the

connected network devices. The CAN thus flexibly connects multiple end-points to an optical line terminal (OLT) in the operator's central office (CO), where the connectivity to the core network is provisioned. The dynamically reconfigurable data connections within the CAN thus support connectivity to optical network units (ONUs) for fixed access data links, BBUs for backhaul links and RRHs for fronthaul links. The CAN also supports direct connectivity between end-points within the CAN, thus completely bypassing the OLT. For example, fronthaul links can be established between BBUs and RRHs at different locations in the CAN and dedicated fixed data links can be established between two end users connected to the CAN, such as a private network between two different offices of a business.

Considering the commercially available ROADMs widely deployed today, they typically employ expensive wavelength selective switches (WSSs), with the required number of WSSs depending on the degree of the ROADM. Furthermore, complex architectures are necessary to avoid any restrictions on wavelength/direction assignments and to prevent wavelength-contention conflicts [25]. The latest generation of ROADMs [25, 26] are also developed to possess advanced features including colourlessness, directionlessness, contentionlessness and gridlessness [27, 28]. All of the ROADM technologies however employ hard-wired switching elements [29] operating at the wavelength level only, as they are target long-haul optical metro and core networks. These ROADM's are therefore not suited to application in CANs as they do not support channel switching at subwavelength or sub-band levels and have prohibitively high deployment and operational costs. The ROADMs for application in CANs must therefore achieve switching at subwavelength and sub-band levels, with low end-to-end latency in a cost-effective manner. Conventional subwavelength switching involves O-E-O conversions and complex electrical domain processing, resulting in high latency, high-power and large footprint devices, making them unsuitable for application in CANs. Therefore, O-E-O free, SDN-controllable, highly versatile "soft-ROADMs" are essential for the realisation of CANs [27, 28].

The CAN-enabled converged fixed-mobile networks suffer from the high cost sensitivity associated with aggregation networks, therefore, it is necessary to use low complexity and low-cost network elements. One attractive approach is to use digital signal processing (DSP) to implement advanced modulation formats and advanced networking features, whilst using low-cost, low complexity IMDD-based optical transceiver front-ends. As DSP-based transceivers require DACs and ADCs it is beneficial if low resolution converters are used to

minimise cost. The IMDD optical transmission together with the non-ideal characteristics of the low-cost hardware will induce signal impairments which can considerably degrade transmission performance and also introduce significant cross channel interference in multi-channel application scenarios. Thus, modulation formats are required that are tolerant to, or can adapt to, the transmission impairments and furthermore, an effective interference cancellation scheme is required to maintain the relaxed component requirements and avoid the need for a less efficient network architecture with low cross channel interference, e.g. by avoiding spectrum sharing orthogonal channels and introducing large frequency guard bands.

To realise the aforementioned CANs, optical transceiver-embedded DSP has been utilised to implement a digital orthogonal filter-based multiplexing technique, to achieve multiplexed, independent optical channels at the wavelength, sub-wavelength and orthogonal sub-band levels [30, 31] , thus enabling CAN networks with the following salient features:

- o Seamless convergence of fixed optical access networks, Metro-networks and 4G/5G fronthaul and backhaul networks.
- o Provision of a sliceable and dynamically reconfigurable network which can efficiently support virtualised networks at multiple sub-wavelength connectivity levels with elastic bandwidth provision.
- o Full support of SDN for efficient control and management of the network configuration, with control extended to the physical layer.
- o Support of DSP-based advanced modulation formats to achieve spectrally efficient high-speed interconnections.
- o Channel transparency to underlying signal characteristics, such as bandwidth and modulation format.
- o Excellent backwards compatibility with existing optical transmission technologies as the baseband region in the optical domain can be allocated to existing TDM-based optical signals.
- o Dynamically reconfigurable and highly flexible network elements.
- o Exploitation of existing passive optical network (PON) infrastructures by the use of advanced multiple access techniques.

- o By completely eliminating O/E and E/O conversions within the network switching elements, the network's latency and power consumption efficiency are drastically improved.

- o Enhanced physical layer data security as the full details of the channel multiplexing parameters are required to perform data recovery.

- o An inherent "pay as you grow" network operation model, as the growing demand for aggregate capacity can be met by adding additional channels to the network as required.

To meet the challenges associated with the practical implementation of CANs this dissertation research experimentally demonstrates and thus technically verifies various critical CAN technologies. The verified CAN technologies are i) a newly proposed cross-channel interference cancellation (CCIC) technique to mitigate physical channel frequency response induced interference between orthogonal channels sharing the same spectral region, an offline CCIC technique is validated in a digital orthogonal filter (DOF) multiplexed two channel, PTP, IMDD, SMF-based link of various lengths and is shown to achieve significant improvements in various transmission parameters including as bit error rate (BER), capacity and power budget, demonstrating its great potential for improving the performance of CANs, ii) for the first time a fully real-time DSP-based digital filter multiple access (DFMA) PON is demonstrated which employs transceiver embeddedDOF-based multiplexing to dynamically share the PON capacity, 4 channels are successfully multiplexed in a two ONU DFMA PON, the OLT also incorporates a fully real-time low complexity CCIC function which is shown to drastically improve the transmission performance and robustness of all DFMA PON channels, iii) a soft-ROADM is demonstrated for the first time in a fully real-time 4 channel DFMA system, the soft-ROADM successfully adds various combinations of channels and drops any of the 4 channels from an aggregated signal with low power penalties and high robustness to variations in operating conditions and parameters. Overall, the research work technically validates various fundamental CAN techniques, demonstrating that CANs can be practically realised.

Major Achievements of the Dissertation Research

To tackle the aforementioned future network challenges the CAN has thus been proposed as a cost-effective solution, this dissertation research work has therefore been undertaken to

technically verify key CAN technologies to confirm the technical feasibility of the CAN concept. Experimental and/or numerical investigations of DSP-based fundamental CAN technologies are undertaken in terms of networks architectures, devices and functional elements, required to enable the SDN-controlled, reconfigurable, flexible and dynamically adaptive CANs. The major achievements of the research work are summarized as follows:

Experimental demonstration of a DSP-based cross-channel interference cancellation technique for application in digital filter multiple access PONs [32]

Practical optical transmission links employing IMDD and electrical/optical components with non-ideal characteristics, as used in cost sensitive CANs, will consequently suffer from a non-flat physical channel frequency response which typically has increasing attenuation with frequency. This effect can lead to severe cross channel interface (CCI) in the DOF multiplexed channels of the DFMA PON and CAN, the interference being the most severe between orthogonal spectrum sharing channels and so can drastically reduce the performance of the orthogonal channels. To address this problem and achieve channels with high transmission performance, for the first time, a cross-channel interference cancellation (CCIC) technique has been proposed, experimentally demonstrated and verified in a two-channel point-to-point (PTP) optical link, employing DOF-based channel multiplexing. The proposed DSP-based CCIC technique has a number of salient features, including, no dependency on the underlying signal modulation formats, fast convergence as only one iteration is sufficient, system performance is not dependent on initial system conditions and it requires low DSP complexity compared to other techniques such as successive interference cancellation (SIC).

The OLT-embedded CCIC function was experimentally demonstrated using a real-time transmitter (ONU) and offline processing-based receiver (OLT), in a PTP IMDD-based SMF-link of various lengths. OFDM modulated signals were employed in each channel. The offline receiver consisted of a real-time oscilloscope running MatLab-based code for the CCIC algorithm and OFDM signal detection. The CCIC technique achieved considerable improvement in network operation performance by mitigating the CCI effect under various system conditions. The CCIC technique was shown to improve the DOF-based optical transmission performance as follows; i) significant reduction in individual OFDM subcarrier BERs, ii) a substantial increase in transmission capacity which is independent to the fibre length and iii) considerable increase in the optical power budget in comparison with the case

of CCIC disable. This work thus shows that a low-cost DSP technique can be employedto overcome the non-ideal physical channel frequency responses-induced impairments associated with practical low-cost optical links and achieve high performance optical links application in CANs and DFMA PONs..

Experimental Demonstration of a Real-Time Digital Filter Multiple Access PON with Low Complexity DSP-Based Interference Cancellation [33]

As IMDD DFMA PONs are essential elements for realising reconfigurable CANs, the operation of the proposed DFMA PON and the associated DOF-based multiplexing technique must be practically verified, thus it is essential to experimentally demonstrate a fully operational multi-ONU and multi-channel DFMA PON exclusively employing real-time DSP Therefore, for the first time, a DFMA PON is experimentally demonstrated incorporating two real-time ONUs and a real-time OLT, with four independent channels. To combat physical channel frequency response-induced CCI, the offline verified, low complexity DSP-based CCIC function is incorporated in the real-time OLT receiver. The fully real-time DFMA-PON implementation, is dynamically reconfigurable in terms of channel spectral locations and signal modulation parameters.

The performance of the real-time DSP-based-low complexity CCIC function embedded in the OLT receiver is fully explored and optimised experimentally, it is shown to considerably improve the 26km SMF, IMDD-based, DFMA PON performance and robustness in terms of significant reductions in individual subcarrier BERs and total channel BERs, resulting in a significant increase in the capacity of each channel when CCIC is enabled. It is also clearly shown that the CCIC function reduces sensitivity to ONU synchronisation as the inter-ONU sample timing offset (STO) range is considerably increased. The real-time implementation also fully validates the abovementioned offline CCIC performance. The optimization of the CCIC function's filter, in terms of tap count and the DFMA PONs performance is explored to identify the optimum trade-off. In addition to full optimisation of the digital filter-based CCIC function's complexity a comprehensive analysis is undertaken of the DSP complexity of the associated shaping and matching DFMA filters and the CCIC filters for varying DFMA PON channel counts. It was shown that as the number of channels employed in the DFMA PON increases, the complexity of the shaping and matching filters does not change. Whereas, the complexity for the CCIC filter decreases to a fixed value of only 10 scalar multipliers per parallel signal sample.

Real-time experimental demonstration of DSP-enabled soft-ROADMs with multi-level flexible add/drop functions for cloud access networks [34][35] .

As low-cost channel switching elements are essential for realising reconfigurable CANs [36], soft-ROADMs have been proposed and their performance has been comprehensively investigated using numerical simulations [37, 38], 38]and its drop operation has also been experimentally demonstrated using an off-line DSP receiver [39], however to comprehensively and technically verify the practical operation and robustness of the soft-ROADMs, experimental demonstrations with multiple channels generated exclusively with real-time DSP are essential. Therefore, in this dissertation research, for the first time, a fully real-time soft-ROADM has been demonstrated in a 4 channel DOF-multiplexed system, employing commercially-available low-cost electrical/optical components. Drop elements are based on drop RF signal-driven intensity modulators and add elements are based on passive optical couplers (OC). The soft-ROADM implementation is free from both optical filters and O-E-O conversions and is inherently transparent to major network design characteristics. A fully real-time soft-ROADM was used to dynamically add/drop individual channels from a four channel, IMDD-based optical network, enabled by digital orthogonal filters embedded in real-time DSP-based transceivers.

The demonstration achieved highly flexible dynamic channel switching operations at sub-wavelength and sub-band levels in the physical layer. Extensive experimental work was also undertaken, to explore the performance robustness of the soft-ROADM add/drop operation characteristics against operating condition variations associated with practical networks. The soft-ROADM successfully demonstrated excellent performance and robustness as it was shown that relatively low power penalties are introduced for both add and drop operations and it was demonstrated that the soft-ROADM add operation achieves a high tolerance to differential optical input power for various add operation combinations. Furthermore, the soft-ROADM drop operation showed excellent robustness to variations in the drop RF signal characteristics. This work is a significant milestone, as it verifies the technical feasibility of employing the soft-ROADM to create a programmable networking environment capable of addressing elastic 5G slicing and the supporting the SDN paradigm.

1.3 Thesis Structure

This thesis consists of eight chapters. This chapter presents an introduction to the challenges facing optical networks required to support future fixed access networks and future mobile networks such as 5G, the chapter discusses the main requirements for next generation optical networks required to effectively support the various new emerging services and to meet the rapidly growing end-user demands. Also presented is an overview of the motivation for adopting CANs and the associated network architectures, elements and DSP functions, including DFMA PONs, soft-ROADMs and the CCIC technique. Also, the significance of the research work with regard to supporting 5G requirements is discussed.

Chapter 2 presents PON and MBH/MFH technologies in two subsections, in the first part of the chapter, an overview of the basic operating principle of the PON is introduced. Then an introduction is presented, to the current and the proposed multiplexing and multiple access technologies used in passive optical network (PON) systems, with the pros and the cons for each discussed. Details of the current PON and the next generation PON (NGPON) standards are also presented. The second part of chapter 2 discusses fixed optical networks for mobile systems. A brief introduction to the evolution of the radio access network and its main elements and architecture are presented. The main advantages and disadvantages of employing the emerging C-RAN architecture based on point-to-point and various PON architectures are also discussed. The evolution of MBH and MFH technologies are discussed, with focus on the adopted interface protocols and physical transport standards adopted in current networks. In addition, and most importantly, next generation MFH/MBH and emerging midhaul technologies under consideration for supporting 5G are presented. The great challenges for these next generation technologies to meet the ambitious 5G requirements are outlined. Finally, the application of the CAN for next generation MFH/MBH/midhaul is discussed and the associated salient advantages are clearly highlighted.

In chapter 3, the CAN concept is presented in detail. In the first part of the chapter, an introduction to the need for the CANs to support the flexible, converged fixed-mobile networks is presented. The main network elements of a CAN are briefly discussed along with how these network elements are used to build a CAN. The challenges and the requirements of future PONs are also explained. For the next generation PONs, the

importance of the reconfigurable optical transceivers to achieve a flexible network architecture to support 5G requirements is discussed in detail. The DOF multiplexing principle, which is fundamental to CAN operation, is also explained. Subsequently, the operating principle of the DOF-based DFMA PON is explained. In the third section of chapter 3, an overview of the evolution of network switching technologies is presented, including a brief introduction to the legacy OEO-based add drop multiplexers (ADM) and their limitations are considered. A detailed explanation of optical ADMs (OADMs) and their associated main architectures is also included, followed by a detailed discussion of reconfigurable OADMs (ROADMs) as they are key network elements providing full optical wavelength switching in combination with WDM technology. The two common types of ROADM architectures are explained in detail, as well as how more advanced ROADM features can be achieved. Finally, the motivation for the need of the soft-ROADM in CAN applications is discussed. The top-level architecture of the soft-ROADM is explained in detail, along with a detailed theory of operation of the associated add/drop elements.

In chapter 4, firstly an overview of the multiple access interference (MAI) problem in a shared transmission medium is presented, with an explanation of its effects in a communication system employing orthogonal channels. Then, complementary to the detailed explanation in chapter 3 of the orthogonal channel multiplexing principle, the associated cross-channel interference mechanism, due to a non-ideal physical channel frequency responses, is explained in depth. In addition, detailed explanations of some currently adopted techniques in the post interference cancellation category, are presented. Finally, the mathematical theory and a detailed explanation of the adopted CCIC technique for application in DFMA-based PONs and CANs is presented.

In chapter 5, the proposed CCIC technique is experimentally demonstrated using a field programmable gate array (FPGA)-based real-time transmitter (see Appendix A) and a digital storage oscilloscope (DSO), running MatLab, as an offline receiver. The employed experimental system is a two-channel PTP, IMDD, SMF-link of various lengths. Experimental investigations are undertaken to verify the basic operation of the technique and also evaluate the resulting improvements in subcarrier and channel BERs, capacity and power budget. The measured channel frequency response of the PTP, IMDD, optical link shows a significant roll-off of 10.5dB, this high roll-off value having a direct impact on channel orthogonality and the resulting CCI severely limits system performance. The offline

CCIC technique achieves significant improvements in the DOF-based transmission link performance. The measured BERs of each individual OFDM subcarrier, over a 26 km SSMF link at a received optical power (ROP) of -14dBm, show that the total average BER of the last 10 subcarriers in the I (Q) channel are as low as 1.0×10^{-4}(6×10^{-5})() with CCIC enabled, compared to achieving only 3 (0) operational subcarriers in the I (Q) channel with CCIC disabled. The experiment shows that only one CCIC iteration is enough to effectively minimize the roll-off effect and that it can reduce the BER of individual subcarriers by more than 1000 times. The second investigation in the CCIC PTP offline demonstration examines the impact of the adopted technique on the maximum signal transmission capacity for various fibre lengths of 10, 26 and 36 km for the cases of CCIC enabled and disabled at an ROP of -16.6dBm. The experimental demonstration shows that I (Q) channels can only support 0.2 (0) Gb/s respectively for a fibre length of 10km SMF in case of the CCIC disabled. Whilst, with CCIC enabled, it is shown that the net signal transmission capacity is drastically increased to 1 (0.9) Gb/s for I (Q) channels respectively. In addition, the total signal capacity increase due to CCIC, over a 36km SMF, is from 0.1Gb/s to 1.9Gb/s, to achieve a 19 times improvement. The last part of chapter 5 investigates the CCIC-induced power budget improvements. The adopted measurements show that the CCIC can give ~3.5 dB power budget improvement for both I and Q channels under the condition of using a fixed aggregated signal transmission capacity of 1.2Gb/s at 36km SMF.

Chapter 6 presents the first experimental demonstration of a real-time 4-channel, DFMA-PON incorporating the demonstration of a real-time DSP-based, OLT-embedded CCIC function. The number of taps in the CCIC filter are designed to be dynamically adjusted to explore the trade-off between CCIC filter complexity and system performance, thus the optimum CCIC filter tap count is determined. The obtained results verified the effectiveness of the CCIC technique in a fully real-time system, as it achieves significant improvements in transmission performance and robustness of the IMDD DFMA PON as follows: The first part of the result verifies the operation of the real-time CCIC function in a PTP link, where the number of the operational subcarriers is 11 and 14 out of 15 for the baseband (BB) and passband (PB) sub-wavelength bands, respectively. With CCIC enabled, total BER performance can reach below the FEC limit at a specific ROP, whereas with CCIC disabled, the system cannot achieve the required BER below the FEC limit at any ROP. It is determined that the optimum tap count for the CCIC filter is 42 taps, as it provides a good trade-off between the CCIC filter complexity and the channel performances. This tap count

thus being adopted for all subsequent measurements. The second part of the results validates the CCIC technique for the case of a two ONU DFMA PON. For the PON case, the real-time CCIC technique also gives significant improvements in the BER of individual subcarriers, by approximately as much as 100-300 times. The results also show that the total channel capacity is significant increased, by a factor of the order of ≥12 times. In addition, for the DFMA PON, real-time exploration of total channel BER versus ROP was undertaken for the PB channels each with 13 subcarriers enabled. With CCIC enabled, the total BER performance could reach acceptable levels, below the adopted FEC limit, whilst with CCIC off, neither of the PB channels can achieve total BERs below the FEC limit at any ROP level.

Furthermore, the measurement of the inter-ONU STO tolerance is explored to evaluate the impact of timing synchronization between ONUs occupying the same signal spectral region. The adopted ROP is -9 dBm and only the 6 highest frequency subcarriers are employed. The results show the BB in-phase channel exhibits an increase of approximately 5 times in the inter-STO timing range from 0.04ns for CCIC off to 0.2ns for CCIC on. Whereas the BB quadrature channel exhibits an increase of approximately 15 times in the inter-STO timing range from ~0.01ns for CCIC off to 0.15ns for CCIC on. In addition, the transparency of the CCIC function to the interfering channel's modulation format is also examined, it is shown that the CCIC operation has no dependency on the modulation format, as there is negligible change in the observed subcarrier BERs when applying either 16QAM or 32QAM modulation formats on the interfering orthogonal channel's subcarriers. The final part of the chapter mathematically examines the DSP complexity of the required CCIC, shaping and matching filters in terms of the required digital multipliers. It is shown, crucially, that the complexity of the shaping and matching does not scale with the implemented channel count. Furthermore, for the implemented CCIC filter, the results show a 73% reduction in optimised filter complexity in comparison to the non-optimised full-length CCIC filter. The complexity of the CCIC filter for varying channel counts is also investigated, it is shown that, if the number of employed channels is ≥ 4, the CCIC filter only needs to process ~10 interference-inducing samples per wanted signal sample, resulting in only ~10 multipliers per parallel filter in the CCIC filter, thus achieving an ultra-low complexity implementation.

Chapter 7 presents the experimental demonstration of a soft-ROADM using real-time DSP-based transceivers for signal generation and detection. A 4-channel, DFMA system based on

two independent ONUs, a passive OC -based add element and an intensity modulator-based drop element are employed to implement a cost effective soft-ROADM which is free from both optical filters and O-E-O conversions. Real-time experimental investigations are undertaken to evaluate the add/drop operations' characteristics and exploration their performance robustness to real-time operating condition variations. The obtained results verify the technical feasibility of the soft-ROADM for CAN application, as follows: The first part of the results assesses the soft-ROADM add operation by measuring BER curves for various channel add combinations. The results showed the soft-ROADM add operation induces a considerably low power penalty at a FEC limit of 1.0×10^{-3} of $\leq$ 1dB for sub-wavelength add and $\leq$ 1.4dB for sub-band add operations. While there is less than 2dB power penalty for the drop operation case at a FEC limit of 1.0×10^{-3}.

The second part of the experimental investigation evaluates the soft-ROADM add operation performance robustness to differential optical input power variation. The results verify the soft-ROADM add operations can tolerate a large differential optical power range of 6dB and 1.5dB for sub-wavelength add and sub-band add respectively, where the ROP is -10dBm at a FEC limit of 1.0×10^{-3}. The last part of the experimental investigation evaluates the soft-ROADM drop operation tolerance to variations in the drop RF signal characteristics. The results measure the BER variation whilst varying the drop RF signal amplitude and phase for both PB sub-band channels. The results showed that the drop operation can tolerate an amplitude (phase) variation of 1.4Vpp (16°) of the drop RF signal as it varied about the optimum value of ~3Vpp (0°) at a FEC limit 1.0×10^{-3}.

A conclusion of the whole thesis and areas of future research work are presented in chapter 8 and finally an appendix provides details of the employed DSP design environment and the FPGA-based DSP logic designs.

References

[1]   X. Foukas, "Towards a Programmable and Virtualized Mobile Radio Access Network Architecture," PhD thesis,University Edinburgh, 2018.

[2]   M. Castells, J. L. Qiu, Mireia Fernandez-Ardevol, and A. Sey, "The Mobile Communication Society A cross - cultural analysis of available evidence on the social uses of wireless communication technology," Int. Work. Wirel. Commun. Policies Prospect., 2004.

[3]   Statista, "Most popular social networks worldwide as of July 2019, ranked by number of active users (in millions)," 2019. [Online]. Available: https://www.statista.com/statistics/272014/global-social-networks-ranked-by-number-of-users.

[4]   Statista, "Number of smartphone users in the United States from 2010 to 2023 (in millions)," 2019. [Online]. Available: https://www.statista.com/statistics/201182/forecast-of-smartphone-users-in-the-us.

[5]   Cisco, "Cisco visual networking index global mobile data traffic Forecast Update, 2017–2022," Available at https://www.cisco.com, 2019. .

[6]   M. Bennis, M. Debbah, and H. V. Poor, "Ultrareliable and Low-Latency Wireless Communication: Tail, Risk, and Scale," Proc. IEEE, vol. 106, no. 10, pp. 1834–1853, 2018.

[7]   P. Popovski, K. F. Trillingsgaard, O. Simeone, and G. Durisi, "5G wireless network slicing for eMBB, URLLC, and mMTC: A communication-theoretic view," IEEE Access, vol. 6, pp. 55765–55779, 2018.

[8]   T. Nakamura, A. Benjebbour, Y. Kishiyama, S. Suyama, and T. Imai, "5G Radio access: Requirements, concept and experimental trials," IEICE Trans. Commun., vol. E98B, no. 8, pp. 1397–1406, 2015.

[9]   A. Gupta and R. K. Jha, "A Survey of 5G Network: Architecture and Emerging Technologies," IEEE Access, vol. 3, pp. 1206–1232, 2015.

[10]   A. E. Kalør, R. Guillaume, J. J. Nielsen, A. Mueller, and P. Popovski, "Network Slicing for Ultra-Reliable Low Latency Communication in Industry 4.0 Scenarios,"

pp. 1–11, 2017.

[11] Z. Tayq, "Fronthaul integration and monitoring in 5G networks," PhD thesis Univ. Limoges, 2018.

[12] G. Brown, "Ultra-Reliable Low-Latency 5G for Industrial Automation," 2017. [Online]. Available: https://www.qualcomm.com/media/documents/files/read-the-white-paper-by-heavy-reading.pdf.

[13] B. J. Challacombe, L. R. Kavoussi, and P. Dasgupta, "Trans-oceanic telerobotic surgery," BJU Int., vol. 92, no. 7, pp. 678–680, 2003.

[14] E. Bastug, M. Bennis, M. Medard, and M. Debbah, "Toward Interconnected Virtual Reality: Opportunities, Challenges, and Enablers," IEEE Commun. Mag., vol. 55, no. 6, pp. 110–117, 2017.

[15] International Telecommunications Union, "FG IMT-2020: Report on Standards Gap Analysis," no. TD 208 (PLEN/13), pp. 1–172, 2016.

[16] A. A. Gebremariam, "Resource Abstraction and Virtualization Solutions for Wireless Networks," phd thesis, no. March, 2017.

[17] "WDM-PON: a Key Innovation to Enable 5G+FTTH Converged Gigaband Access," 2019. [Online]. Available: https://www.mobileworldlive.com/zte-updates-2019-20/wdm-pon-a-key-innovation-to-enable-5gftth-converged-gigaband-access/.

[18] P. Chanclou, L. A. Neto, K. Grzybowski, Z. Tayq, F. Saliou, and N. Genay, "Mobile fronthaul architecture and technologies: A RAN equipment assessment [invited]," J. Opt. Commun. Netw., vol. 10, no. 1, pp. A1–A7, 2018.

[19] I. Chih-Lin, H. Li, J. Korhonen, J. Huang, and L. Han, "RAN Revolution with NGFI (xhaul) for 5G," J. Light. Technol., vol. 36, no. 2, pp. 541–550, 2018.

[20] J. I. Kani, J. Terada, K. I. Suzuki, and A. Otaka, "Solutions for Future Mobile Fronthaul and Access-Network Convergence," J. Light. Technol., vol. 35, no. 3, pp. 527–534, 2017.

[21] P. G. Kramer G, Mukherjee B, "Interleaved polling with adaptive cycle time (IPACT): a dynamic bandwidth distribution scheme in an optical access network," Photonic Netw. Commun., pp. 89–107, 2002.

[22] M. Ruffini, "Multidimensional Convergence in Future 5G Networks," J. Light. Technol., vol. 35, no. 3, pp. 535–549, 2017.

[23] D. Nesset, "PON roadmap [invited]," J. Opt. Commun. Netw., vol. 9, no. 1, pp. A71–A76, 2017.

[24] R. Giddings, X. Duan, E. Al-Rawachy, and M. Mao, "A Review of DSP-based enabling technologies for Cloud Access Networks," Futur. Internet, vol. 10, no. 11, 2018.

[25] S. Perrin, "Next-Generation ROADM Architectures & Benefits." [Online]. Available: www.fujitsu.com/us/Images/Fujitsu-NGROADM.%0Apdf.

[26] W. Way, "Optimum Architecture for M × N Multicast Switch-Based Colorless, Directionless, Contentionless, and Flexible-Grid ROADM," in OFC/NFOEC, 2012, pp. 5–7.

[27] A. Peters, E. Hugues-Salas, M. Gunkel, and G. Zervas, "Key performance indicators for elastic optical transponders and ROADMs: The role of flexibility," Opt. Switch. Netw., vol. 25, no. November 2016, pp. 1–12, 2017.

[28] S. Thiagarajan and S. Ass, "Nodal contention in colorless, directionless ROADMs using traffic growth models," Natl. Fiber Opt. Eng. Conf. NFOEC 2012, paper no. Nw3F.2, 2012.

[29] A. Muhammad, G. Zervas, G. Saridis, E. H. Salas, D. Simeonidou, and R. Forchheimer, "Flexible and synthetic SDM networks with multi-core-fibers implemented by programmable ROADMs," Eur. Conf. Opt. Commun. ECOC, no. 1, pp. 1–3, 2014.

[30] M. Bolea, R. P. Giddings, and J. M. Tang, "Digital orthogonal filter-enabled optical OFDM channel multiplexing for software-reconfigurable elastic PONs," J. Light. Technol., vol. 32, no. 6, pp. 1200–1206, 2014.

[31] M. Bolea, R. P. Giddings, M. Bouich, C. Aupetit-Berthelemot, and J. M. Tang, "Digital Filter Multiple Access PONs With DSP-Enabled Software Reconfigurability," J. Opt. Commun. Netw., vol. 7, no. 4, p. 215, 2015.

[32] E. AL-Rawachy, R. P. Giddings, and J. M. Tang, "Experimental Demonstration of Cross-Channel Interference Cancellation for Digital Filter Multiple Access PONs," Opt. Express, vol. 25, no. 4, p. Th3C.5, 2016.

[33] E. Al-Rawachy, R. P. Giddings, and J. Tang, "Experimental Demonstration of a Real-Time Digital Filter Multiple Access PON with Low Complexity DSP-Based

Interference Cancellation," J. Light. Technol., vol. PP, no. c, pp. 1–1, 2019.

[34] E. Al-Rawachy, R. P. Giddings, and J. M. Tang, "Real-time experimental demonstration of DSP-enabled soft-ROADMs with multi-level flexible add/drop functions for cloud access networks," Opt. Express, vol. 27, no. 1, p. 16, 2019.

[35] E. Al-Rawachy, R. P. Giddings, and J. M. Tang, "Experimental Demonstration of Real-Time Add/Drop Operations in DSP-enabled Flexible ROADMs for Converging Fixed and Mobile Networks," 2018 Opt. Fiber Commun. Conf. Expo., paper W2A-33, 2018.

[36] Jin, W., Duan, X., Bolea, M., Giddings, R.P., Jing, N., Zhang, C.F., Qiu, K. and Tang, J.M., 2015, March. New ROADMs with DSP-enabled dynamic and flexible operations for elastic optical networks. In Optical Fiber Communication Conference (pp. Th2A-50). Optical Society of America.

[37] Jin, W., Duan, X., Dong, Y., Cao, B., Giddings, R.P., Zhang, C., Qiu, K. and Tang, J.M., 2015. DSP-enabled flexible ROADMs without optical filters and OEO conversions. Journal of Lightwave Technology, 33(19), pp.4124-4131.

[38] Jin, W., Zhang, C., Duan, X., Kadhum, M.R., Dong, Y.X., Giddings, R.P., Jiang, N., Qiu, K. and Tang, J.M., 2016. Improved performance robustness of DSP-enabled flexible ROADMs free from optical filters and OEO conversions. Journal of Optical Communications and Networking, 8(8), pp.521-529.

[39] X. Duan, M. L. Deng, W. Jin, R. P. Giddings, S. Mansoor, and J. M. Tang, "Experimental Demonstration of DSP-enabled Drop Operations of Flexible ROADMs Excluding Optical Filters and O-E-O Conversions," 2016 Opt. Fiber Commun. Conf. Exhib., no. Im, p. M3E.4, 2016.

2. Current Optical Network Technologies for Fixed Access and Mobile Fronthaul/Backhaul Networks

Contents

2.1 Introduction

This chapter provides an introduction to the essential aspects of the current multiplexing technologies used in PON systems and the details of current and future PON standards are presented, in addition an overview is given, of fixed optical networks employed in the evolution of the mobile radio access network.

It is worth noting that although optical fibre based access networks are the most popular type of deployed access network today, other technologies are used for fixed access where fibre deployment is challenging or prohibitively expensive, such as WiMAX which is based on wireless RF links. Also other new access technologies are being researched such as optical wireless communications (OWC) which uses free space optical (FSO) links.

2.2 PON Technologies for Fixed Data Networks

2.2.1 PON Concept and Categories

Using optical fiber instead of twisted pair copper cable as a transmission media in the access network is considered an essential solution to meet the requirements of long distance reach and high data rate [1]. Fiber access networks are generally referred to as Fiber-to-the-Home/Building/Curb/Neighbourhood (FTTH/B/C/N), etc., depending on the fiber termination point, a universal term for these networks is FTTx. FTTH strictly refers to the case where the fiber goes all the way to the end users' premises. FTTH can be classified as PTP or PTMP. A PTP network architecture provides individual fiber links from the central office (CO) to the end users and is therefore the most expensive architecture due to the high cost of optical fiber installation. Alternately, to serve a large number of subscribers using a single fiber link, the PON with multiple access functionality leverages PTMP networks to reduce the total fiber deployed in the field [2]. In the PON, no active power components are employed in the path between the source and destination. Typical PONs, as shown in Fig. 2.1, consist of several main parts: an (OLT at the service provider's CO, a number of ONUs near or at the end users' premises and a passive optical splitter/combiner located at a remote node (RN) near to ONUs. The optical distribution network (ODN) refers to the passive network portion between the OLT and the ONUs. The ODN consists of a feeder fiber between the OLT and RN and distribution fibers between the RN and ONUs.
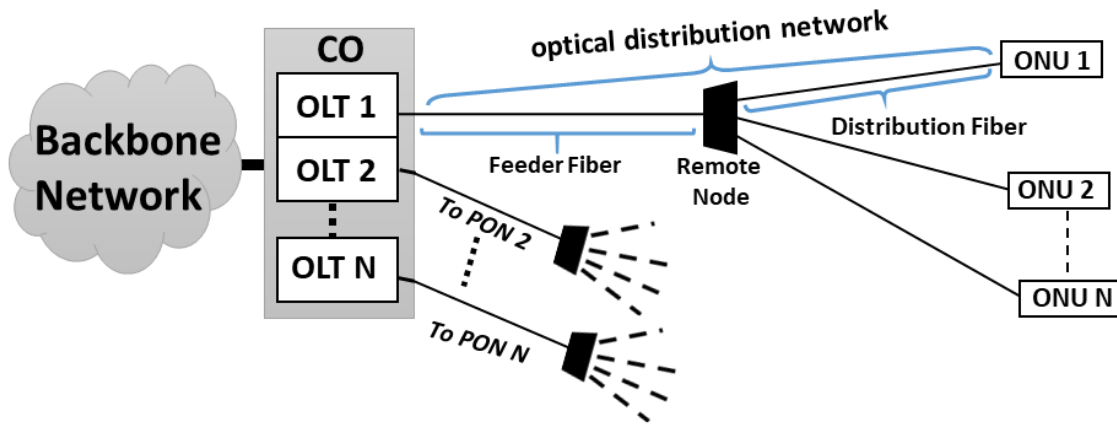
Fig. 2.1 Typical PON architecture

The PON architecture generally supports in the region of 16 to 32 ONUs with a covered transmission distance of typically 10 to 60 kilometres [2]. The CO contains multiple OLTs, which connect to the backbone network as shown in Fig. 2.1, each OLT connects with its own ONUs through the ODN using its own dedicated PON. For bidirectional communication, two-separate fibers, or one fiber with two different wavelengths, is used to support both the upstream direction (from ONUs to OLT) and the downstream direction (from OLT to ONUs). An active optical network (AON) employs an active network node at the RN, however, the PON out performs the AON as follow:

1. The employment of widespread passive optical devices instead of active optoelectronic and electronic devices located at the RN, results in lower capital expenditure costs and significantly reduced maintenance costs.
2. The power splitter/combiner can be easily located anywhere along the fibre link as to provide great flexibility in the network topology.
3. There is no power source required at the RN, which is beneficial for both operator energy saving and global energy saving.

A key draw back of the PON, in comparison to the AON, is a reduced transmission reach due to the inherent power loss of the passive splitter at the RN, however despite this, PON deployment is highly prevalent due to the aforementioned advantages. Traditional PON multiplexing techniques include: time division multiplexing-PON (TDM-PON), wavelength division multiplexing-PON (WDM-PON). In addition, optical OFDMA-PON (OOFDMA-PON) and Code-Division Multiple Access-PON (CDMA-PON) havealso been widely researched as a future PON candidate technology.

2.2.1.1 **TDM-PON**

TDM PONs use different time slots to multiplex/demultiplex individual ONU channels to/from the aggregated PON signal, as shown in Fig. 2.2. Thus, in TDM, multiple users access and share the available bandwidth in the time domain. To share a common optical fiber the upstream (downstream) traffic is carried on a dedicated wavelength of 1310 nm (1490 nm), for example. For downstream traffic, the OLT continuously broadcasts timeslots to all ONUs, and each ONU selects the timeslots allocated to it and discards the timeslots allocated to other ONUs. For the upstream direction, as there is a common fibre and a shared optical receiver, the synchronisation of transmissions from the ONUs is critical to avoid contention between ONUs, Therefore, a TDMA scheme such as Ethernet PON (EPON) or Gigabit PON (GPON) is adopted. The OLT performs the scheduling of the connected ONUs to ensure they transmit their own data in the allocated timeslots only. Furthermore, an ONU's transmission time should be adjusted to take into account of the varying ONU transmission delays in the upstream direction [3], the OLT thus adopts a ranging process to synchronise the timings between the ONUs and the OLT, this is typically based on the timed ONU responses to OLT-range requests. The OLT then instructs the ONUs to adjust their timing to allow them to send their data at exactly the right moment to avoid collision between timeslots at the OLT. The TDMA schemes commonly adopt equal timeslot assignment amongst users for fixed bandwidth allocation, although adaptive algorithms have been adopted, such as Interleaved Polling with Adaptive Cycle Time (IPACT) [4],for more efficient timeslot assignment and thus allowing dynamic bandwidth allocation. The modulation format that has been adopted in all standardised TDM access network architectures is Non-Return-to-Zero (NRZ).

The first TDM PONs standardised 1:16 or 1:32 as the typical maximum splitting ratio. A higher splitting ratio would let a higher number of ONUs share the OLT bandwidth, however, as the splitting ratio increases, the optical transceiver requirements also increase, such as the need for high transmitter optical power and/or higher receiver sensitivity as the higher loss associated with a higher splitting ratio directly affects the system power budget. Various TDM PON standards are discussed in detail in section 2.2.2.1.
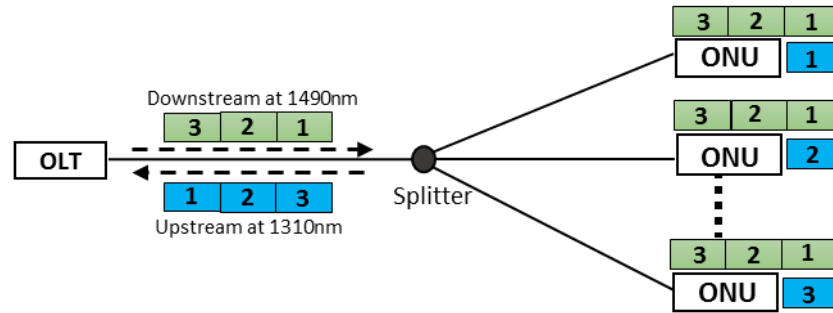
Fig. 2.2 A typical structure of a TDM-PON

2.2.1.2 **WDM-PON**

WDM is a multiplexing technique which can also be used to share a common optical fibre between multiple ONUs in a PON. In a WDM-PON, a pair of dedicated wavelengths are assigned to carry transmitted data to/from a particular ONU, one wavelength provides the upstream transmission and the other wavelength the downstream transmission. Thus in each direction an ONU as can utilise the full bandwidth provisioned by the dedicated wavelength[5].
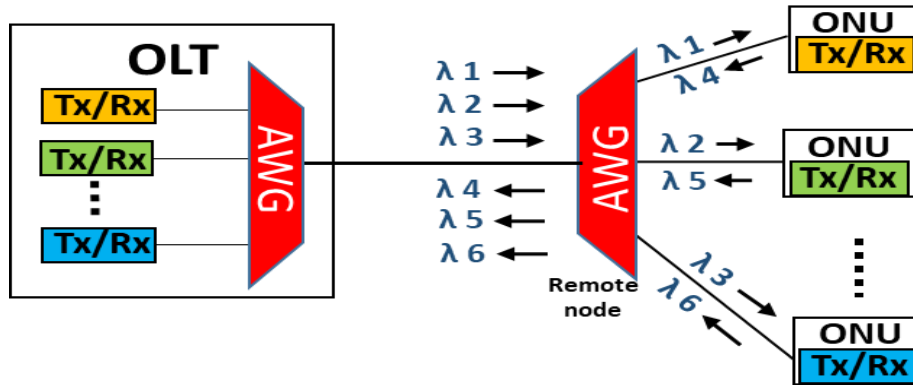
Fig. 2.3 A Typical WDM-PON architecture

Instead of using an optical power splitter, as in a TDM-PON, an AWG operates as the passive WDM routing component to multiplex/demultiplex different ONU transmissions at the remote node, as shown in Fig. 2.3. In the upstream direction, an individual wavelength is dedicated to each ONU to carry its own signal, and the AWG at the remote node, is used to combine different ONUs' signals on to the common feeder fiber link. Another AWG located in the OLT is used to demultiplex the received WDM signals and multiple photodetectors are used to detect the different wavelength signals. In the downstream direction, a mixed

wavelength laser array or a Multi-Frequency Laser (MFL) is used to generate the downstream optical signals, which are individually modulated before being multiplexed via the AWG in the OLT to form the downstream WDM signal. The generated downstream WDM signal is separated into individual wavelengths by the AWG in the RN, and the individual wavelengths are routed via the distribution fibres to the various ONUs. WDM-PONs have the key advantages of providing, i) high bandwidth per ONU as the capacity of a single wavelength is not shared by multiple users, ii) increased reach due to lower losses of the AWG compared to a passive splitter, iii) transparency to underlying signal modulation formats and iv) can be easily overlaid onto a legacy PON infrastructure. However, in comparison to the TDM PON, it requires dedicated optical hardware for each user at the OLT and tuneable laser sources are required to achieve colourless transceivers, these factors result in high deployment costs, which has restricted the widespread deployment of WDM-PONs [6].

2.2.1.3   **TWDM-PONs**

To alleviate the disadvantages of WDM PONs, a new technique has been proposed which combines the both TDM and WDM technology and uses them in a single network called a hybrid TDM/WDM-PON (TWDM-PON)[7], this PON architecture has been adopted for the ITU-T NG-PON2 standard, as described in section 2.2.2.3. The architecture of a typical TWDM-PON is shown in Fig. 2.4.

TWDM-PONs help to increase ONU count, transmission distance, system scalability and capacity[8]. TWDM consists of multiple wavelengths assigned in the up/down stream directions for communications between an OLT and a number of ONUs to serve multiple users in a single PON by using the TDM technique, thus multiple TDM PONs are combined together using WDM to form TWDM. The TWDM-PON possesses a number of advantages from both WDM and TDM such as the ability to increase total PON capacity and to keep costs down by still sharing wavelengths between users. In addition, with the increased number of customers and transmission distance enabled by the TWDM PON, the number of COs can also be reduced leading to considerable power and maintenance cost savings.
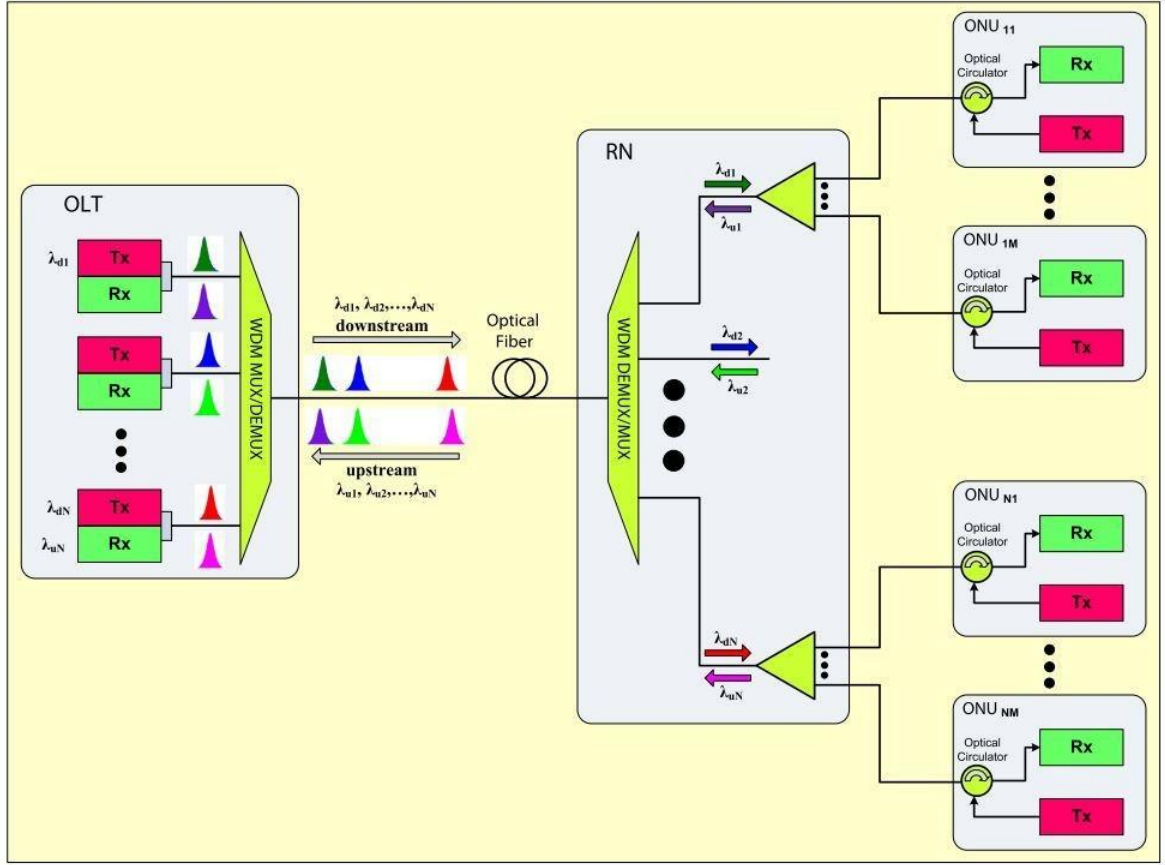
Fig. 2.4 A Typical TWDM-PON architecture [41]

2.2.1.4 **OOFDM-PONs**

OFDM is a multi-carrier modulation, where each orthogonal subcarrier is modulated independently. OFDM is employed in a variety of communication standards such as 802.11b wireless Ethernet (Wi-Fi), digital video broadcast (DVB) and Worldwide Interoperability for Microwave Access (WiMAX)[9]. The OFDM working principle relies on quadrature amplitude modulation (QAM) modulation, where both the amplitude and phase of a sinusoidal subcarrier are modulated in comparison to traditional amplitude only or phase only modulation techniques, thus considerably increasing data rate and spectral efficiency. QAM is represented by a constellation diagram with different symbols represented by different points, typically arranged in a square grid with equal horizontal and vertical spacing. A group of data bits are mapped into a single information symbol hence encoding multiple bits simultaneously. Thus a QAM symbol can encode different numbers of bits to create varying forms of constellation diagram. For example; each symbol in 16-QAM (32-QAM) contain 4 (5) bits, in general 2^N QAM will encode N bits at a time. Fig. 2.5 (a, b and

c) shows examples of constellations for 16-QAM, 32-QAM and 64-QAM respectively. Using higher QAM levels means more bits will be encoded in one QAM symbol, thus for a fixed peak signal power, the constellation points get closer together so there is consequently less resilience to noise and distortion. QAM modulation of a single carrier can be implemented by amplitude and phase control of a single local oscillator, however OFDM requires precise synchronisation of subcarrier frequencies so can only be implemented by a DSP-based IFFT/FFT and DAC/ADC.

Fig. 2.5 Example constellation diagrams. a) 16-QAM, b) 32-QAM, c) 64-QAM

The optical OFDM (OOFDM) PON combines OFDM modulation together with TDM in a PON architecture as shown in Fig. 2.6.

Fig. 2.6 A typical structure of an OOFDM-PON system [42]

In an OOFDM PON [10] the overall bandwidth is divided into orthogonal subcarriers and one or more subcarriers are allocated to each ONU, this bandwidth can be further shared among different applications/users via different time slots. In the OOFDM PON, the traffic is carried in the OFDM frames, where one frame contains all subcarriers and multiple timeslots, it should be noted that OOFDM PONs have not been standardised, so there is not

a standardised framing structure. However, a suitably designed framing structure can be used to allocate varying capacity to different ONUs in terms of both subcarrier and timeslot allocation. In the OOFDM transceivers, use can be made of low-cost optical devices for IM, such as directly modulated lasers (DMLs), to generate the optical OFDM signals [11] for transmission over the fibre, andDD via PIN detectors can be used for signal recovery, thus low-cost IM-DD links can be exploited. It is important to mention that OFDM is of great interest, due to its high spectral efficiency which can increase the capacity of a single wavelength in a highly cost effective way. Currently, the performance of OOFDM PONs is mainly limited by the bandwidth of the available DACs/ADCs [8-10]and the required system power budgets. However, it should be noted that DAC/ADC technologies are developing rapidly and sample rates are now starting to exceed 100GS/s [12,13].

For downstream traffic, according to the frequency/time domain scheduling process at the OLT, the data for all ONUs will be encapsulated into the subcarriers and timeslots to create the complete OFDM frame. The OFDM frames are broadcast to all ONUs via the passive optical splitter at the remote node. When the frames reach the ONUs, each ONU recovers the OFDM frame and picks out its own data from its allocated subcarriers and timeslots[14]. For the upstream traffic, within its allocated timeslots, each ONU maps data to one or more subcarriers and the remaining subcarriers are set to zero. After the OC, one single OFDM frame will be generated that contains a combination of optical OFDM subcarriers and timeslots from multiple ONUs. In the OLT receiver a single photo-detector is then used to detect the optical OFDM signal. To maintain subcarrier orthogonality and symbol alignment at the OLT, stringent synchronization of the OFDM signals generated at the ONUs is needed, which is fully controlled by the OLT in order to minimise interference between ONUs in the upstream direction[15]. Furthermore, as in the TDMA PON, upstream timeslots must also be synchronised to avoid data collisions at the OLT. It should also be noted that a slightly different wavelength is required for each ONU to avoid the optical beat interference (OBI) noise effect [10,11], in practice wavelength control can be achieved by laser thermal detuning [17, 18] or alternative OBI mitigation methods [19,20] may be incorporated into the OFDM transceivers. It is of course feasible to also combine OFDM modulation with a WDM architecture which will produce a hybrid OOFDM-WDM PON. Therefore, OOFDM-WDM allows for further increases in both signal transmission capacity and flexibility. For example if one wavelength can support 25Gb/s using OFDM, 4 wavelengths would provide a 100Gb/s PON[11].

2.2.2 **Current PON standards**

In 1995, several of the global telecommunication operators and equipment vendors agreed to form the full service access network (FSAN) group. One of the main goals of this group is to promote common PON standards to reduce the cost of the fiber-optic access systems[21]. The International Telecommunication Union (ITU) is a European standardisation body that has worked with FSAN to introduce PON standards[22, 23].

In 1998, the FSAN/ITU-T approved the Asynchronous Transfer Mode (ATM) PON (APON) as the ITU-T G983 standard. Then in approximately 2001, a higher speed version of APON was standardized, which was known as Broadband PON (BPON). Both APON and BPON employ ATM cells for data framing and TDMA (TDM) for access in the upstream (downstream) direction. 155Mb/s is the signal line rates in the upstream direction for both APON and BPON with this same data rate in the APON downstream direction, while BPON downstream direction achieves approximately 4 times higher speed to reach to 622Mb/s. Both APON and BPON supports a maximum physical transmission distance of up 20km [10-12]. APON and BPONs are essentially now obsolete as they are not commonly used nowadays and have been superseded by more advanced PON technologies, the following discussion will therefore focus on the commercially deployed PON standards in use today. The ITU-T standards, developed in collaboration with FSAN, include the GPON and X-GPON standards. The IEEE has also developed the Ethernet-based PON standards of EPON and 10G-EPON[24].

2.2.2.1 **ITU-T GPON and IEEE EPON**

The ITU-T G.984 series is an evolution of the ITU-T G.983 BPON standard, and is called Gigabit PON (GPON) due to supporting bit rates of ~1-2 Gb/s. GPON was selected in 2003 by many telecommunication operators to deliver the triple-play (video, voice, and data) services [25]. In GPON, the transmission speed increases 4 times compared with BPON to reach to 2.488 Gb/s downstream and 1.244 Gb/s or 2.488 Gb/s upstream [16]. GPON supports a maximum physical transmission distance of up to 60km and split ratios up to 1:128. GPON also defines different sets of wavelengths used in the transmission depending on whether single fiber or dual fiber is used in the ODN. An example wavelength plan is 1260-1360nm for upstream and 1480-1500nm for downstream in a single fiber, and the use

of 1260-1360nm for both up and down stream used in dual fiber, with 1550nm reserved for video broadcasting for both cases.

Approximately at the same time as GPON emerged, a new PON specification was adopted by the Ethernet in the first mile (EFM) group and established as a standard by IEEE. This new 802.3ah standard was ratified in June 2004 and called Ethernet PON (EPON)[24]. Ethernet is used for data networking due to high bandwidth, low cost, and ease of use and installation, which made it a logical choice for adaptation into a PON standard. The EPON architecture implements the transmission of data via the transport of Ethernet frames. The EPON's transmission speed is 1.25 Gbps for both upstream and downstream with a transmission distance of up to 20 km and supports split ratios of up to 128. It uses the same wavelength plan as GPON and can support a video broadcast in a similar manner. Data transmission via Ethernet frames is gradually becoming more and more popular in telecommunication networks and is penetrating further into the core network, mainly due to the ease with which higher layer protocols can be encapsulated, thus EPONs are ideally placed to enable the creation of end-to-end cohesive networks. EPON has become particularly widely spread in East Asian countries, especially Japan and Korea[26].

2.2.2.2   **ITU-T XG-PON and IEEE 10G-EPON (NG-PON1):**

To meet the ever increasing demand of future high bandwidth applications and services such as video on demand, voice over IP (VoIP), video conferencing, online gaming and peer to peer networking it was essential to develop new PON standards with increased performance. Therefore 10G PON standards, supporting 10Gb/s transmission rates, were developed which include ITU-T XG-PON and IEEE 10G-EPON[27]. These 10G PONs are commonly referred to as the first next generation PONs (NG-PON1). There are no significant changes in both 10G-EPON and 10G-PON architectures compared with EPON and GPON respectively, both new standards also support TDM/TDMA PON systems as in the GPON and EPON architectures but operate at higher data-rates[28]. 10G-PON (ITU-T G.987) series is an evolution of the ITU-T G.984 GPON standard, and is also called XG-PON. The XG-PON standard was approved in 2010 and is an extension of current GPON. The customer can be seamlessly upgraded from the current GPON to the new XG-PON on the same ODN without affecting or disrupting the existing services for customers served by GPON[28]. ITU-T defines asymmetrical bit rates of 10Gb/s for downstream and 2.5Gb/s for upstream

under the name of XG-PON, and symmetrical bit rates of 10Gb/s for both downstream and upstream under the name of XGS-PON. For XG-PON, the set of wavelengths are 1260-1280nm allocated for upstream and of 1575-1580nm specified for downstream with a physical transmission distance of at least 20 km and a splitting ratio of at least 1:64 (scalable to 1:256).

In the IEEE standards, as mentioned previously, the EPON's bit rate with IEEE 802.3ah standard reached up to approximately 1Gbps for both upstream and downstream directions. Therefore, to increase the transmission capacity of EPONs, the IEEE 802.3av standard, known as 10G-EPON, was ratified in 2009. The 10G-EPON supports two configurations, in the asymmetric configuration, the PON would operate at 10 Gbps in the downstream direction and 1 Gbps in the upstream direction. Whereas for symmetric configuration, the transmission speed will reach up to 10 Gbps in both upstream and downstream directions. 10G-EPON adopts the same wavelength plan as used in 10G-PON. In the downstream direction, the 1480-1500 nm band is specified for 1 Gbps transmission and the 1575-1580 nm band for 10 Gbps transmission. However, in the upstream direction side, 1 Gbps band extends from 1260-1360 nm and 10 Gbps span from 1260 to 1280 nm band[29]. The supported splitting ratios for10G-EPON are 1:16 to 1:32, with up to 20km maximum reach.

2.2.2.3   **NG-PON2**

Fig. 2.7 shows the evolution roadmap of PON technologies, showing it is essential to further upgrade the PON networks in order to meet the rapidly growing bandwidth requirements for ultra-high data speed transmission[30]. The FSAN groups and ITU- T defined the next-generation PON stage 2 (NG-PON2) in 2011. In FSAN, from the network operators' prospective, NG PON2 is required to be compatible with the previously deployed systems i.e., G-PON and XG-PON without disrupting services for customers on the legacy PON systems[31]. Time and wavelength-division multiplexed (TWDM) PON (4 wavelengths with 10Gbps each) was the selected technology to implement the 40 Gb/s architecture required by NG-PON2[32], this selection was essentially due to the maturity of the technology. However, from an economic prospective, TWDM is not very cost effective, for example, the provision of four tuneable lasers in the OLT and one in each ONU and the corresponding tuneable optical filters to achieve 4x 10GPON (40 Gb/s), is currently an expensive solution. Therefore, utilizing OOFDM technology when it is sufficiently mature, could be a considerably more cost effective solution to achieve 40Gb/s or more on a single

wavelength due to the utilization of low-cost mass produced electronics for implementing the required DSP and avoiding the need for multiple tuneable lasers and optical filters, thus OOFDM-PONs are a potential candidate for future third generation PON (NG-PON3)[33].

In addition, the IEEE P802.3ca standard or so called 100G-EPON (25Gb/s per wavelength) is currently under consideration by the IEEE P802.3ca 100G-EPON task force. The 100G-EPON is based on 25Gb/s per channel providing 25, 50 and 100G PON. In 100G-EPON, the taskforce also take into consideration the requirement to maintain coexistence with 10G EPON, thus avoiding disruption of services for customers on the legacy PON systems[34].
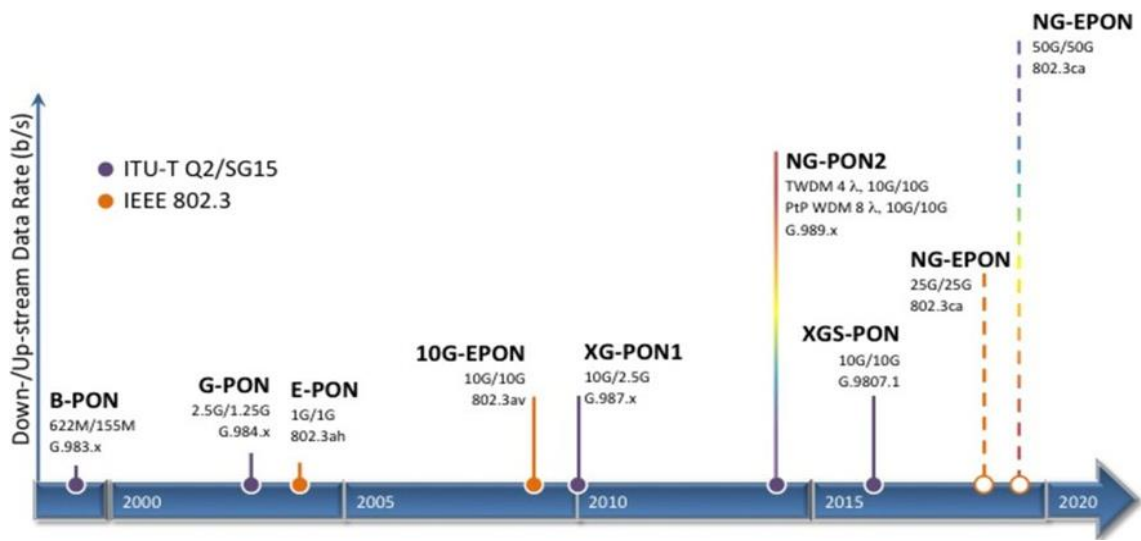
Fig. 2.7 NG-PON evolution roadmap from ITU-T [35]

2.3 Backhaul and Fronthaul for Mobile Networks

An overview of the evolution of the radio access network (RAN) architecture and the associated fronthaul/backhaul network links are presented in this section.

2.3.1 Evolution of the Radio Access Network Architecture

In the traditional radio access network architecture (RAN), the radio unit (RU) and theBBU are integrated into an all-in-one solution in the same physical unit, known as the base station (BS), which is located at the cell site. The physical transmission lines in the RAN between the BS and the mobile switching centre (MSC) in the core network are known as MBH. The

RAN also supports logical network connections between BSs in neighbouring cells to allow control data exchange, for the purpose of call handover for example [36]. The Radio Access Technology (RAT) is the standard that defines the radio interface between the BS and the mobile user equipment and specifies modulation formats, carrier frequencies, interfaces and protocols assigned to the RAN nodes and mobile devices (e.g. WCDMA/HSPA, LTE, WiMAX, etc.)[37]. Different transmission medium, like copper, optical fiber or microwave connections are utilized in the backhaul connection[38]. In the traditional RAN, coaxial cable was employed, as depicted in Fig. 2.8, to connect the RU with the antenna, however, the coaxial cable exhibits high losses at the high frequencies employed by the radio interface, which is undesirable as it leads to high power consumption and also limits the transmission to a short distance[38], thus the BS must be located close to the antenna site. This traditional RAN architecture was highly popular in 1G and 2 G mobile network deployments[39].
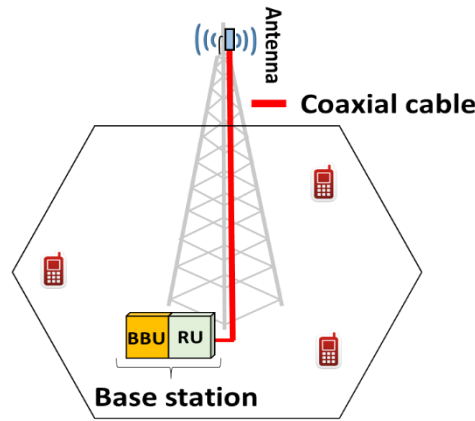
Fig. 2.8 Traditional base station

The next stage of the RAN evolution is shown in Fig. 2.9. To overcome the high losses induced by a coaxial cable feeding the antenna, the BBU and RU were separated as each element has clearly defined and independent functionality. The RU can be placed at the top of the tower in the cell site and is called the RRH. The RRH can thus use a short coaxial link to the antenna and can also leverage efficient cooling which also results in a saving on cooling requirements in the BBU housing. The RRH and BBU are linked by a digital link, carrying only digitised baseband radio signals [40],which consists of a standardised high speed digital mobile fronthaul interface (MFHI) employing a standard, such as the common public radio interface (CPRI)[41], which is designed to carry the digitally sampled, baseband radio signals, including both the in-phase and quadrature (IQ) data, as well as necessary

control and synchronisation information. To efficiently carry the digitally sampled IQ data, the BBU-RRH link is thus a bidirectional interface with a suitably high bit rate, which requires accurate synchronization and strict latency control. Other standardised interfaces for the BBU-RRH link are Open Base Station Architecture Initiative (OBSAI) [42]and Open Radio equipment Interface (ORI)[43].
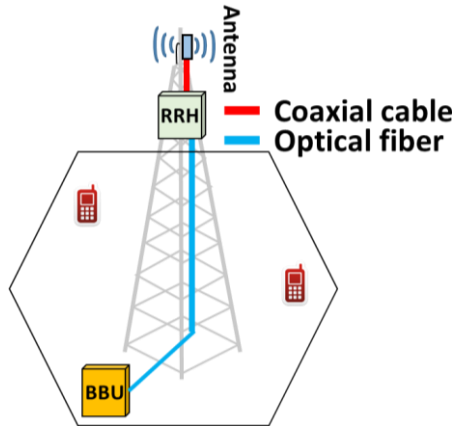
Fig. 2.9 Basestation with RRH architecture

Fig. 2.10 depicts the internal architectures of the BBU and RRH systems. The BBU provides the interface with the backhauling network and performs physical layer digital processing of the baseband radio signals such as digital signal processing to modulate/demodulate the baseband radio signals according to the employed RAT, and includes all functions of the upper layers and traffic management.

 While the RRH executes the remaining physical layer functions of DACs and I/Q frequency up-conversion for downstream signals, I/Q frequency down-conversion and ADCs for upstream signals, power amplification, duplexing and filtering (to share a common antenna for up-link and down-link) and interfacing with the antenna via coaxial cables[37]. It should also be noted that in advanced radio systems incorporating MIMO technologies, which utilise multiple antennas, the RRH becomes more complex as components must be duplicated as required to support each antenna.
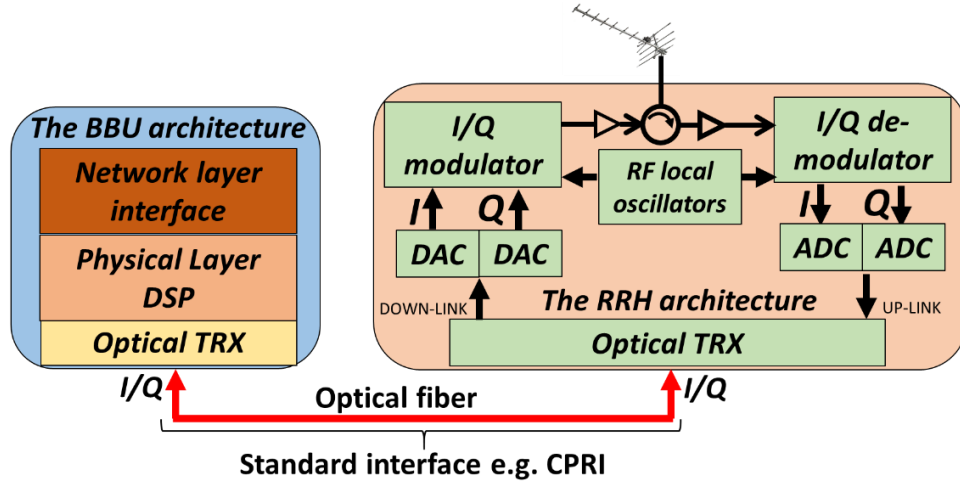
Fig. 2.10 The internal block diagram of the BBU and RRH.

The RAN architecture has evolved from the aforementioned distributed architectures, to a C-RAN as shown in Fig. 2.11. In the C-RAN architecture, the BBU is no longer located at the cell site but it is moved to a shared central location, containing multiple co-located BBUs which serves a large group of RRHs, hence the BBUs are known as centralized BBUs. The BBU resources can be pooled and so shared between the RRHs for improved operational efficiency and reductions in cost and power consumption. A further evolution of the RAN is the Cloud-RAN, also known as C-RAN. Cloud-RAN is closely related to centralised-RAN but employs a different architecture implementation, where the baseband processing is handled in software run on a generic servers located closer to the core network. Thus, the evolution of the C-RAN is undergoing a two stage implementation. In stage 1, the baseband resources are placed in a central location and pooled while baseband processing is done using specialized baseband DSP chips. Pooling the BBUs, groups them at a unified cite and re-implements their functions in fewer devices that are designed to share some of their hardware/software resources. In stage 2, the baseband resources are virtualized in software running on generic servers[39]. Virtualization techniques can have significant impact on mobile networks [44], as they enable the decoupling of network functions, like baseband processing, from network hardware in order to reduce the network cost and to enable flexible deployment of services. The evolution from the traditional distributed RAN to the C-RAN offers; i) Adaptability to non-uniform traffic and network scalability, ii) Energy and cost savings, iii) Increase in traffic throughput and iv) Ease in network upgrades and maintenance [[39]. In addition there are also benefits regarding the total cost of ownership in terms of both capital expenditure (CAPEX) and operating expenditure (OPEX). The C-RAN reduces the CAPEX as fewer BBUs are needed in comparison to the traditional architecture. This

also leads to a significant decrease in the OPEX, as power consumption is reduced in comparison to the traditional distributed RAN. The Cloud-RAN based on the aforementioned virtualised BBUs, has the additional advantages of increased cost savings due to generic hardware and drastically improved scalability as the virtual BBUs are now software based. The network connection between the RRH at the cell site and the centralized BBU at the remote site is known as MFH. The aforementioned CPRI, OBSAI and ORI interface standards are still used here to convey the digital baseband radio signal between the RRH and the centralized BBUs[45]. Using these standards, the MFH link can be extended up to several tens of kilometres, where the limitations originate from the processing and propagation delays and the strict timing requirements of the RAT's retransmission mechanisms[39].

Fig. 2.11 shows the traditional MFH with point-to-point connections for the optical access systems. Currently, this type of the connection is the most common deployed for macro cell connections, where the MFH connections can carry multiple CPRI/OBSAI/ORI signals, e.g. for the various sectors in a multi-sector antenna, for different generations of mobile technologies, as well as different components of MIMO signals[45]. The MFH latency here is related to light-propagation delay only[46].
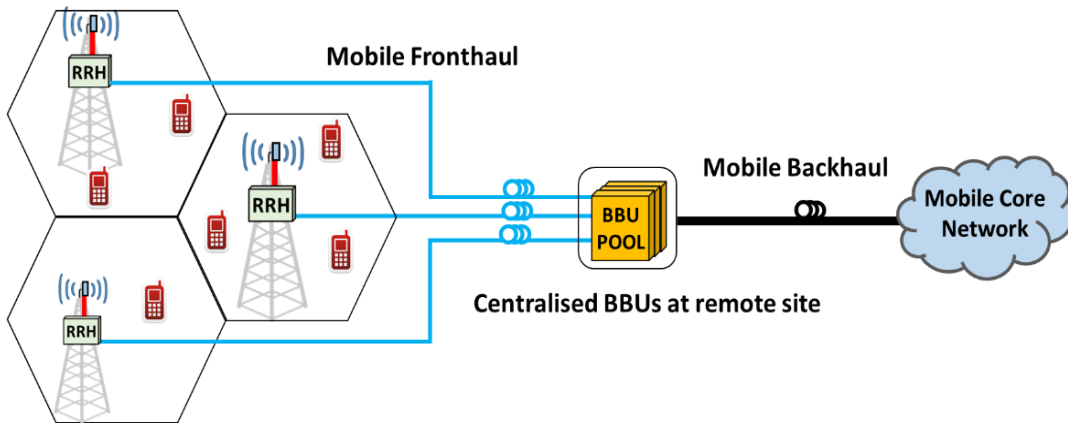
Fig. 2.11 Traditional C-RAN with RRHs and centralised BBUs using point-to-point architecture

For future 5G mobile networks, it is necessary to provide ubiquitous Gbit/s to 10 Gbit/s access speeds per user[47]. Therefore, it is essential for the future MFH to accommodate a large number of huge-capacity, small cells to effectively provide such high bandwidth signals and extend coverage for massive device connectivity [47]. Furthermore, the emerging need for fixed-mobile convergence requires a consolidated platform for optical

access network infrastructure to support both fixed and mobile data. From an economical point of view, the PON can be effectively employed to support the MFH connectivity to small cells in densely deployed areas, whilst supporting both fixed and mobile traffic simultaneously. TDM-PON, WDM-PON and TWDM-PON are example PON categories that can be employed to support the small cells. Fig. 2.12 depicts the TDM PON scheme for the next generation MFH. It provides a cost effective solution for constructing MHF due to the TDM PON features explained in section 2.2.1.1. However, from a technical point of view, the latency in the TDM PON-based MFH can be an issue when employing DBA for the upstream transmission, resulting in a latency of approximately 1ms, due to the need for information exchanges between ONU and OLT, which exceeds the future MFH requirements of several 100 µs [45-48] .
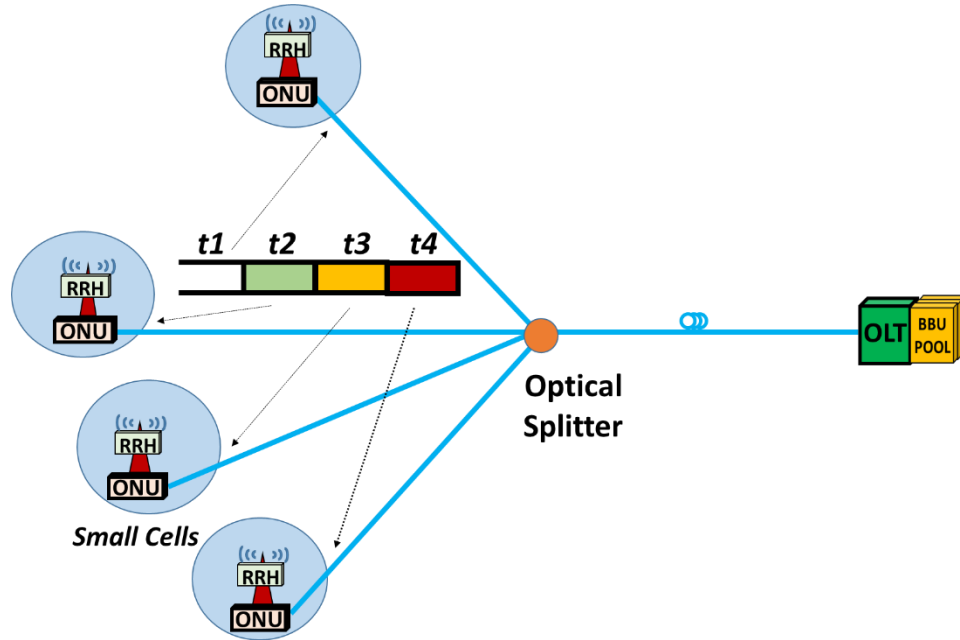
Fig. 2.12 C-RAN for future MFH using TDM-PON architecture

Fig. 2.13 depicts a WDM PON-based MFH. Two wavelength mux/demux components are needed at between the ONUs and the OLT to group/separate multiple wavelengths, as explained in section 2.2.1.2. A WDM PON generally requires dedicated transceivers for each single wavelength signal in both ONU and OLT. Therefore, it is more expensive than the TDM PON-based MFH. The WDM PON however introduces lower latency and larger bandwidth in comparison with the TDM PON[46].
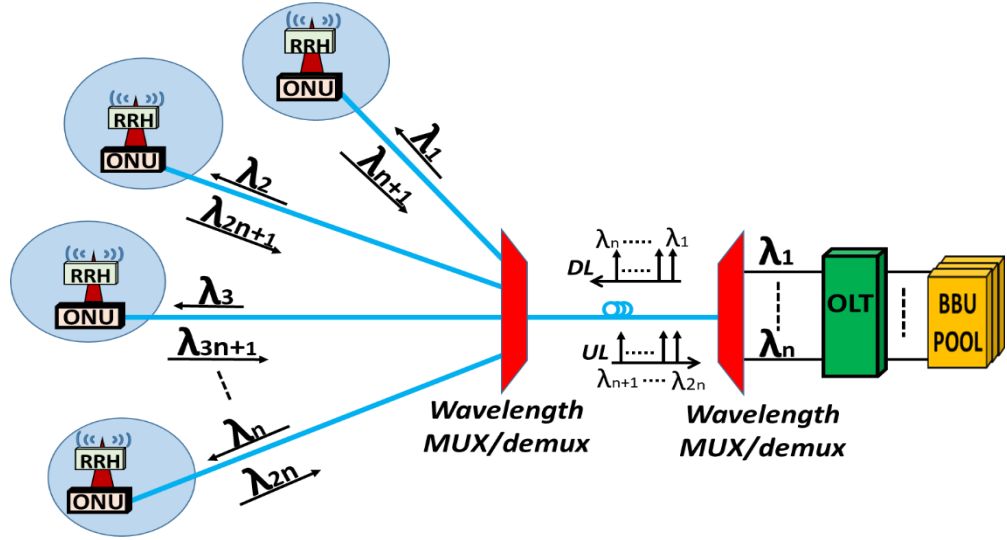
Fig. 2.13 C-RAN for future MFH using WDM-PON architecture

In addition, a WDM-RING can be employed to reduce the number of employed fibers and to further improves network flexibility and reliability. Fig. 2.14 shows the WDM-Ring-based MFH. The wavelength's can employ fixed (dynamic) routing via OADMs (ROADMs) located at the intermediate nodes. Employing ROADMs offers increased flexibility as MFH capacity can be dynamically allocated according to traffic demand, however the cost of existing ROADM technologies, developed for core network applications, makes the deployment of cost effectiveness WDM-Ring-based MFH highly challenging.
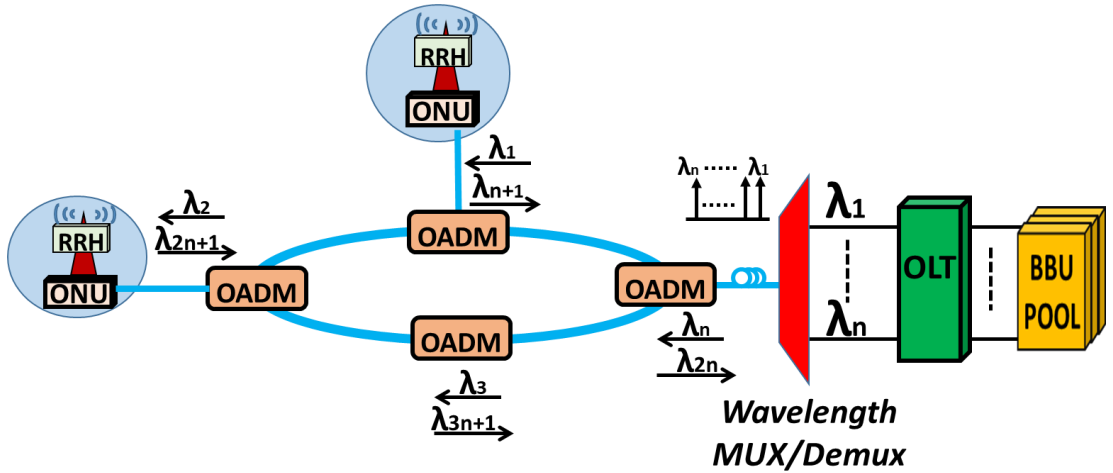
Fig. 2.14 C-RAN for future MFH using WDM RING-PON architecture

TDMPONs can also be used to support MFH, but this solution still faces the challenge of latency associated with DBA in TDM PONs and the low cost effectiveness of WDM PONs

2.3.2 **Backhaul Technologies**

As previously stated, backhaul is the link between the BS/BBU and the core network for all generations of mobile technologies in both uplink and downlink directions. The backhaul network supports various physical configurations depending on the requirement, as shown in Fig. 1.2, in chapter 1, where a simple approach adopts a point-to-point configuration to connect each BS/BBU directly to the core network [45], or alternatively , a ring network topology can be used with add/drop multiplexers to connect BS/BBUs to the core network in a more efficient and cost-effective manner. By using WDM and reconfigurable add drop multiplexers (ADMs) in a ring topology, backhaul capacity can be significantly increased and on demand configuration of paths between the BS/BBUs and the core network, allow for dynamic allocation and thus efficient use of the available backhaul capacity. This is very suitable for mobile networks because the dynamic traffic changes created by the massive movement of end users can be addressed by the ADM-based ring reconfiguration feature[45].

Optical fiber is now the predominant physical transmission medium used in backhaul networks, to a lesser extent, there are also legacy copper cables and microwave radio connections in use. The use of copper cables for MBH was initially widely adopted in the first mobile systems up to 2G, the circuit switch networks employed were initially deployed to carrying predominantly voice traffic and low data rate internet protocol (IP) traffic. Different connections can be deployed in MBH such as point-to-point systems, connecting BS/BBUs directly to the core network, or aggregation networks over plesiochronous digital hierarchy (PDH) or, more commonly, synchronous digital hierarchy (SDH) multiplexing-based systems. The required MBH capacities began to rise as successive mobile generations were providing increasing data connectivity speeds,[49]. However, the optical fiber links, used to carry the high data rate MBH traffic in the SDH standard, also evolved over time to support higher capacities, as indicated by the progressive development of the SDH interface standards fromSTM-1 (155.52 Mbit/s), STM-4 (622 Mbit/s), STM-16 (2.4 Gbit/s) to STM-64 (10Gb/s). SDH standards are typically deployed in Europe and the rest of the world, except in North America, where the prevailing and corresponding standard is Synchronous Optical Network (SONET). Some backhaul deployments employ a microwave radio as an alternative solution, especially in geographically challenging places where wired connections are difficult to deploy[45]. Microwave links require Line of Sight (LoS)

between the core network connection site and the BSs (BBUs) at the cell site (centralised BBU site). In rural environments long distance links can be achieved, however in urban environments shorter links must be used due to the LoS restriction. While the utilized frequency spectrum in wireless microwave links offers a trade-off between the capacity provision and distance coverage, the higher the microwave carrier frequency, the greater the capacity (due to higher bandwidths being available) and the shorter the coverage range and vice versa. The digital multiplexing technique employed over the microwave links can be based on PDH, SDH/SONET or Ethernet (e.g. Gigabit Ethernet)[49]. As the mobile generations evolved they began using packet switched radio services [50]. Therefore, in the early phases of 4G, the backhaul technology began to evolve into more advanced high speed packet-based networks with cost-effective and efficient backhaul transport. MBH to support 3G/4G mobile data services was provided by packet switched networks using popular technologies such as Carrier Ethernet and IP multiprotocol label switching (IP/MPLS). The backhaul transport thus consists of a packet-switched network, which can be implemented with various topologies including ring and mesh architectures. As mobile systems using the legacy TDM-based services still had to be supported, it was critical that the new packet-centric MBH technologies also support circuit emulation services (CES) to efficiently carry the TDM-based MBH traffic.

Carrier Ethernet is a widespread technology for packet-based backhaul transport. First envisioned by the Metro Ethernet Forum (MEF) in 2001, the objective was to naturally extend the Ethernet protocol from local area networks (LANs) to provide Wide Area Network (WAN) connectivity. The Carrier Ethernet network employs Ethernet as the core protocol and enables broadband applications across wide geographical areas [16], with additional key attributes of: flexible bandwidth scalability, increased reliability, QoS levels to meet a wide range of performance metrics and enhanced service management capabilities. Carrier Ethernet supports speeds of 1GbE, 10GbE, 40GbE and 100GbE [51].

The internet engineering task force (IETF) proposed MPLS in the late 1990s as a protocol-agnostic routing technique designed to speed up traffic flows across enterprise WANs and service provider networks. MPLS is an alternative to traditional IP routing, designed to reduce packet routing time and consume less hardware resource to identify a packet's next hop at each router, this is achieved by defining a label based on the packet's destination IP address and a predetermined network route, thus avoiding the need to consult a routing table

at each network node [52, 53]. As both the latest generation mobile broadband services and the MBH are now both based on packet switched technologies, this provides a cost effective and scalable solution and eliminates the TDM/packet mix that adds unnecessary complexity and can slow down the network. In addition, the more efficient packet switched MBH solutions are more able to support the use of the emerging advanced radio features for LTE Advanced (LTE-A), such as radio coordination, higher order MIMO and larger spectrum bandwidths as these all contribute to increased backhaul traffic[54].

2.3.3 Fronthaul Technologies

The main design requirements of the mobile fronthaul links are to minimise the degradation of the RF signal and to permit transmission over several tens of kilometres, whilst achieving low cost and low power consumption [54]. In the MFH link, certain control and framing information is added to the digitised I/Q baseband samples using a standardised protocol such as CPRI, OBSAI and ORI, as stated in section 2.3.1, which is transmitted using a suitable digital electrical or optical transport link between the RRH and the BBU.

The CPRI standard [41] defines a MFH protocol, which was released in 2003. It can be considered as a standardized interface for the front haul link, which defines a frame structure containing 'I' and 'Q' samples resulting from radio signal digitization, synchronization information and some control and management information. TDM is utilized to multiplex different IQ samples from different users in different time slots. CPRI fronthaul transceivers are typically based on standard modules such as small form-factor pluggable (SFP), where the physical layer is typically optical fiber based connectivity[55], employing IMDD for low cost, enabled with either a single bidirectional fiber or more commonly with dual fiber[56]. The CPRI standard dose not define a specific physical layer in the fronthaul link, however it has stringent requirements in term of BER and bitrates. A physical layer which achieves a BER of 10^{-12} is required to avoid the need for forward error correction (FEC). In terms of bit rate, the CPRI standard is based on a fixed and bidirectional high bit rate serial digital interface, 2.5 Gbit/s is the most popularly deployed type, but there are 10 supported bit rates ranging from 614.4 Mbit/s to 24.330 Gbit/s, which are selected according to the RAT, carrier bandwidth and MIMO implementation [54]. In CPRI, MIMO with different configurations are supported such as 2×2 MIMO or 4×4 MIMO. As an example of required data rates, for one LTE sector, assuming a digitisation sampling rate of 30.72 MS/s, a sample resolution

of 15 bits and control and coding overheads of 16/15 and 10/8 respectively, the resulting in data rates is 2.45 Gb/s (4.91 Gb/s) per sector for 2×2 (4×4) MIMO [55]. OBSAI [42] is an open standard forum that was launched in 2002, which supports a bit rate ranging from 768 Mb/s to 6.1 Gb/s. Different types of interfaces are defined in the OBSAI specification called reference points (RPs). RP3 performs a similar function to the CPRI interface, providing a MFH link between the BBU and the RRH [57]. It is important to note that RP3 has a stringent BER requirement of 10^{-15} [57]. The third MBH interface is the ORI standard [43] created by European Telecommunication Standard Institute (ETSI) in 2010[58]. The ORI interface is built on top of the interface already defined by the CPRI group. However, ORI adds many new options and removes unwanted options with the objective of making the interface fully interoperable, for flexible combination of BBUs and RRHs from different vendors. ORI Release 4, can supports bit rates up to 10.14 Gbit/s[59].

2.3.4 Next Generation Fronthaul/Backhaul and its Challenges

The next generation 5G networks aim to offer the end users an unprecedented user experience in terms of data rate, ultra-low latency and ubiquitous access. 5G will surpass 4G with better support for eMBB, uRLLC and mMTC services. However, the 5G network needs both new mobile radio technologies and a new 5G fixed network infrastructure, to accommodate such ambitious 5G requirements. On the road towards the 5G vision, it was realized that the MFH interface presented one of the biggest challenges facing the next generation 5G network. Currently CPRI is the most prevalent MFH interface which has been working well with mobile network generations up to 4G, but when it comes to future 5G technologies, CPRI is not viable due to the following drawbacks[60].

1) Even though the maximum data rate of CPRI is several 10s Gb/s, it can limit the centralisation scalability of the C-RAN. As an example, in the 4G network, if a RRH is equipped with 8 antennas, with a 20 MHz bandwidth, the CPRI MFH data rate is around 10 Gb/s and this is just for one cell. When multiple BBUs (and therefore many cells) are centralized as in the C-RAN case, a huge amount of transport bandwidth is required.

2) The transmission bit rate is constant regardless of the real network traffic behaviour. CPRI is designed with a constant transmission rate based on the TDM mechanism. Therefore, if there is no traffic on the MFH, the data rate on a CPRI link is still constant.

Therefore, it is clear that if bit rates adapt to the varying traffic load condition of the cell, the operation mode has highly increased efficiency.

3) Originally, the CPRI interface was designed for PTP architectures and so it lacks networking capability and so a huge number of optical fibers are required. While in a C-RAN system, there is the need for the central site/office to interconnect with multiple RRHs. The required switching capability in the MFH network would be relatively hard to realize with CPRI.

4) Implementing CPRI over a PON is challenging in terms of latency requirements, this is because existing commercial PONs, specifically TDM-PONs, are designed to support broadband services without strict latency requirements.

There are several solutions that have been proposed to solve the issues associated with C-RAN MFH, for example, an option of IQ compression to reduce the CPRI data rate based on optimized sampling speed and quantized bits has been demonstrated, resulting in 50% data compression[61]. WDM transmission technology is another option which has been applied in a cost effective manner compared to a point-to-point solution[62]. Unfortunately such proposed solutions are not sufficient to completely solve the MFH challenges in the 5G era. Consequently, both the interface and the transport technologies should be redesigned for smooth C-RAN evolution towards the next generation RAN (NG-RAN) to support 5G. Therefore, a Next Generation Fronthaul Interface (NGFI) was proposed in 2014 by China Mobile to overcome such aforementioned shortcomings of traditional MFH. NGFI 1914 is an IEEE working group created to develop a NGFI standard. The idea behind the NGFI relies on designing the MFH interface with two important features, firstly, the new MFH interface data rate should be traffic-dependent, whilst being independent of antenna count. The 5G mobile radio baseband protocol stack consists of different layers, including Packet Data Convergence Protocol (PDCP), Radio Link Control (RLC), Medium Access Control (MAC) and Physical layers. Such different layers have different requirements in terms of latency and bandwidth, this can be exploited by selecting the functional splits to control the network connectivity requirements. Whereas the traditional CPRI interface simply separates the baseband processing from the remote radio unit, the idea of NGFI is to employ an additional function split between two adjacent layers in the BBU and shifting the MFH functional split, allowing latency and bandwidth requirements to be controlled. Therefore, the NGFI solution now employs two functional splits, one is a split inside the baseband function while the other is a split located close to the RRH.

In the 5G era, by employing the additional function split in the BBU, the traditional BBU is divided into two main entities resulting in a new BS structure called the gNodeB (gNB). One gNB contains one central unit (CU) and multiple distributed units (DUs) located at different sites, as illustrated in Fig 2.15. In this sense, a gNB is a kind of mini-C-RAN. There are two types of transport networks in the proposed NG-RAN architecture. Fronthaul links the DU and RRH while midhaul provides the connection between CU and DUs. These combined 5G transport technologies are referred to as "NGFI-xhaul" since both midhaul and fronthaul originate from the idea of NGFI. As mentioned above, the crucial features [63] the NGFI should possess are: i) implementation is independent of the number of antennas, which provides better support for massive MIMO technologies and enables large-scale C-RAN deployment, ii) data rate should adapt to the NGFI traffic. In other words, the NGFI data rate should be dynamically varying with the real network traffic, this means that the NGFI data rate will not be constant, as in the 2G/3G/4G MFH standards, as if the MFH traffic changes (increases or decreases), the MFH data rate should be linearly changed (increases or decreases) too, this feature will make NGFI transmission more efficient in terms of both data transmission and power consumption, and iii) NGFI should be packet-based, which means that the MFH data would be packetized and transported via packet-switched networks. Therefore, it could be possible to adopt Ethernet technology due to its maturity and low cost which would further improve the flexibility of the transport network[60].
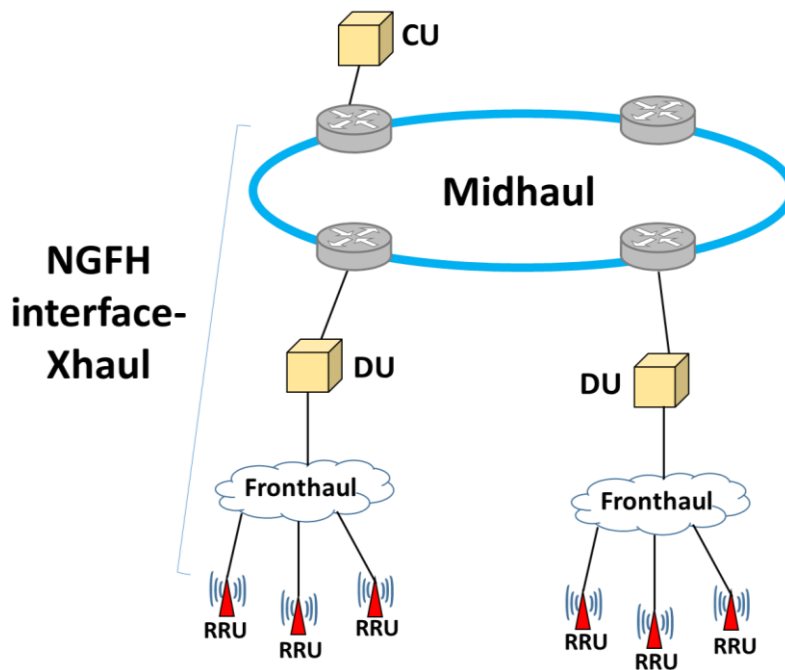

Fig. 2.15 5G C-RAN network

In addition, there is another project defined by the CPRI forum which is aimed at replacing the CPRI standard with the enhanced CPRI (eCPRI) [64]standard for 5G. eCPRI also relies on an additional functional split. It can be deployed over packet based transport network solutions, specifically Ethernet and IP[65], however it is not restrict to packet based transport networks[66]. The key features of eCPRI are as follows:

- Significant reduction of the required bandwidth in comparison with CPRI.
- More efficient utilization of the available bandwidth. In this way, the required bandwidth can scale flexibly according to the user plane traffic.
- Employs Ethernet and IP, therefore guaranteeing future evolutions.
- Compliance with the strict requirement of the radio technologies features in term of: bandwidth capacity, latency, timing/frequency accuracy and packet loss.
- Compatibility with Ethernet-based packet-switched networks to achieve cost reduction, hardware reuse and backwards compatibility [65].

Furthermore, the 5G MBH requirements are also greatly increased in order to meet the overall 5G performance targets, for example, the required 5G MBH capacity can be 1000 times higher compared to that in LTE/LTE-A networks, due to both the increased mobile data rates and the support for massive device connectivity to support services such mMTC and IoT technologies[67], this means MBH capacity requirements can be of the order of 100s Gb/s. Other crucial challenges to be met in the 5G MBH are, ultralow latency to meet the end-to-end 5G latency goal of 1 ms[68]. Ultra-high reliability is also critical as some 5G services, such as real-time monitoring and remote control, M2M applications etc. require a mission-critical network with high availability and tight security. In addidtion, future MBH must also be both energy and cost efficient. Consequently, it is a big challenge to develop commercially viable 5G backhaul to support the massive traffic capacity and maintain the required quality of service and low latency requirement for 5G[69].

To meet such aforementioned MBH/MFH 5G challenges, the DSP-enabled, CAN is proposed, which is introduced in chapter 1 and explained in detail in chapter 3. The CAN targets the seamless integration of traditional optical access networks, metropolitan area optical networks and 4G/5G MFH/MBH networks. The work presented in this dissertation research, focuses on investigating and demonstrating critical DSP-based or enabled technologies for the realisation of the proposed CANs. The requirements of future MBH/MFH for 5G which the CAN solves includes:

- A sliceable network, so different mobile technologies (3/4/5G), different network services or even different network operators can have a dedicated and isolated network slice. Network slicing is also a highly important feature needed to support the highly heterogeneous requirements of 5G services. The sliceability feature of the CAN being extensively demonstrated throughout the dissertation research.

- Ultra-low latency, provided by soft-ROADM enabled optical domain channel switching, as described in section 3.3.2.1, as delay-inducing OEO conversions are eliminated in the CAN's switching elements.

- Transport of both legacy TDM traffic and packet switched traffic in independent channels, as the CAN provides transparent channels.

- Convergence with fixed data traffic for cost-effectiveness.

- Dynamic reconfigurability to adapt the MFH/MBH connectivity to prevailing traffic needs.

- Transparency to different signal modulation formats.

- Low cost due to the exploitation of mass produced integrated circuits (ICs) for DSP implementation and E-O and O-E conversions strictly restricted to the network edges.

- High speed, high performance, spectrally efficient connections, enabled by a low-complexity, DSP-based interference cancellation technique, as detailed in section 4.4 and demonstrated in chapters 5 and 7.

- Massive device connectivity: The highly elastic channels with fine bandwidth granularity, combined with inherent transparency to multiple access techniques and modulation formats, allows for a high count of low bandwidth connections.

- Higher system capacity and flexibility: The CAN supports a large number of highly scalable aggregated elastic channels.

References

[1]   C. Lee and K. Choi, "Fiber to the Home," in LEOS 2007-IEEE Lasers and Electro-Optics Society Annual Meeting Conference Proceedings, 2007, vol. 2, pp. 937–938.

[2]   L. G. Kazovsky, W. Shaw, D. Gutierrez, N. Cheng, and S. Wong, "Next Generation Optical Access," J. Light. Technol., vol. 25, no. 11, pp. 3428–3442, 2007.

[3]   D. Van Veen and V. Houtsma, "High Speed TDM-PON Beyond 10G," Opt. Fiber Commun. Conf., pp. 3–5, 2016.

[4]   P. G. Kramer G, Mukherjee B, "Interleaved polling with adaptive cycle time (IPACT): a dynamic bandwidth distribution scheme in an optical access network," Photonic Netw. Commun., pp. 89–107, 2002.

[5]   J. I. Kani, "Enabling technologies for future scalable and flexible WDM-PON and WDM/TDM-PON systems," IEEE J. Sel. Top. Quantum Electron., vol. 16, no. 5, pp. 1290–1297, 2010.

[6]   K. Grobe and J. P. Elbers, "PON in adolescence: From TDMA to WDM-PON," IEEE Commun. Mag., vol. 46, no. 1, pp. 26–34, 2008.

[7]   Y. Cao, C. Gan, Y. Zhou, L. Shi, and L. Zhu, "A novel architecture of reconfigurable WDM/TDM-PON," WOCC Tech. Progr. - 19th Annu. Wirel. Opt. Commun. Conf. Converging Commun. Around Pacific, pp. 1–4, 2010.

[8]   R. Q. Shaddad, A. B. Mohammad, S. A. Al-Gailani, A. M. Al-Hetar, and M. A. Elmagzoub, "A survey on access technologies for broadband optical and wireless networks," J. Netw. Comput. Appl., vol. 41, no. 1, pp. 459–472, 2014.

[9]   National instruments white paper, "Quadrature Amplitude Modulation (QAM)," 2019. [Online]. Available: https://www.ni.com/en-gb/innovations/white-papers/06/quadrature-amplitude-modulation--qam-.html.

[10]   N. Cvijetic, D. Qian, J. Hu, and T. Wang, "Orthogonal frequency division multiple access PON (OFDMA-PON) for colorless upstream transmission beyond 10 Gb/s," IEEE J. Sel. Areas Commun., vol. 28, no. 6, pp. 781–790, 2010.

[11]   R. P. Giddings, E. Hugues-Salas, and J. M. Tang, "Experimental demonstration of record high 19.125Gb/s real-time end-to-end dual-band optical OFDM transmission over 25km SMF in a simple EML-based IMDD system," Opt. Express, vol. 20, no. 18, p. 20666, 2012.

[12]   A. Zandieh, P. Schvan, and S. P. Voinigescu, "A 2x-Oversampling, 128-GS/s 5-bit Flash ADC for 64-GBaud Applications," 2018 IEEE BiCMOS Compd. Semicond. Integr. Circuits Technol. Symp. BCICTS 2018, pp. 52–55, 2018.

[13]   C. Schmidt, C. Kottke, V. Jungnickel, and R. Freund, "High-speed digital-to-analog converter concepts," Next-Generation Opt. Commun. Components, Sub-Systems, Syst. VI, vol. 10130, no. January, p. 101300N, 2017.

[14]   Dayou Qian et al., "Experimental demonstration of a novel OFDM-a based 10 Gb/s PON architecture," 33rd Eur. Conf. Exhib. Opt. Commun. - ECOC, pp. 541–541, 2007.

[15]   R. Giddings, "Real-time digital signal processing for optical OFDM-based future optical access networks," J. Light. Technol., vol. 32, no. 4, pp. 553–570, 2014.

[16]   E. Al-Rawachy, R. P. Giddings, and J. M. Tang, "Real-time experimental demonstration of DSP-enabled soft-ROADMs with multi-level flexible add/drop functions for cloud access networks," Opt. Express, vol. 27, no. 1, p. 16, 2019.

[17]   X. Q. Jin and J. M. Tang, "Experimental investigations of wavelength spacing and colorlessness of RSOA-based ONUs in real-time optical OFDMA PONs," J. Light. Technol., vol. 30, no. 16, pp. 2603–2609, 2012.

[18]   A. Tsokanos et al., "Reductions of peak-to-average power ratio and optical beat interference in cost-effective OFDMA-PONs," Photonic Netw. Commun., vol. 26, no. 2–3, pp. 44–52, 2013.

[19]   S.-M. Jung, S.-M. Yang, K.-H. Mun, and S.-K. Han, "Optical beat interference noise reduction by using out-of-band RF clipping tone signal in remotely fed OFDMA-PON link," Opt. Express, vol. 22, no. 15, p. 18246, 2014.

[20]   Z. Li et al., "Simplified DSP-Based Signal-Signal Beat Interference Mitigation for Direct-Detection Subcarrier Modulation," p. W1A.3, 2016.

[21]   A. S. Tanenbaum, "Computer networks, 4-th edition," ed: Prentice Hall, 2003. .

[22]   "ITU-T, Recommendation G.983.1, Broadband optical access systems based on Passive Optical Networks (PON)," 1998. .

[23]   "All ITU-T, Recommendation G.983.3, A broadband optical access system with increased service capability by wavelength allocation," 2001. .

[24]   "IEEE 802.3ah Ethernet for the First Mile website, available from http://www.ieee802.org/3/ efm," 2005. .

[25]   "ITU-T G.983.2, ONT management and control interface specification for B-PON, 2005." .

[26]   "H. Shinohara, '"Broadband access in Japan: rapidly growing FTTH market,"' IEEE Commun. Mag., pp72–78, Sept. 2005." .

[27]   J. I. Kani et al., "Next-generation PON-part I: Technology roadmap and general requirements," IEEE Commun. Mag., vol. 47, no. 11, pp. 43–49, 2009.

[28]   M. Hajduczenia and H. J. A. Da Silva, "Next generation PON systems - Current status," in ICTON 2009: 11th International Conference on Transparent Optical Networks, 2009.

[29]   "Sameer Ashfaq Malik (2008). 10G EPON- Unleashing the Bandwidth Potential. ZTE White Papers." .

[30]   S. P. ⇑ Vivek Kachhatiya, "Downstream performance analysis and optimization of the next generation passive optical network stage 2 (NG-PON2)," Opt. Laser Technol., 2018.

[31]   D. Nesset, "NG-PON2 Technology and Standards," JOURNAL OF LIGHTWAVE TECHNOLOGY, VOL. 33, NO. 5, MARCH 1, 2015 NG-PON2 Technology and Standards, 2015. .

[32]   M. Gad, A. Zaki, and Y. M. Sabry, "Simulation of FDM-Based Next Generation Passive Optical Networks," 34th Natl. RADIO Sci. Conf. (NRSC 2017), March 13-16, 2017, Port Said, Egypt Arab Acad. Sci. Technol. Marit. Transp., no. Nrsc, pp. 400–406, 2017.

[33]   D. Nesset, "PON roadmap," IEEE/OSA J. Opt. Commun. Netw., vol. 9, no. 1, pp. A71–A76, 2017.

[34]   "Recent Progress on Standardization of Next-Generation 25, 50, and 100G EPONcuments," J. Light. Technol. VOL. 35, NO. 6, 2017.

[35]   J. S. Wey and J. Zhang, "Passive optical networks for 5G evolution," in Broadband Access Communication Technologies XII, Vol. 10559. International Society for Optics and Photonics, 2018..

[36]   T. Pfeiffer, "Next Generation Mobile Fronthaul and Midhaul Architectures [Invited]," J. Opt. Commun. Netw., vol. 7, no. 11, p. B38, 2015.

[37]   N. Carapellese, "BaseBand Unit Hotelling Architectures for Fixed-Mobile Converged Next-Generation Access and Aggregation Networks," 2015.

[38]   V. Diaz, "Networks Reshaped: 5G, Fronthaul and Fixed-Mobile Convergence - YouTube," 2016.

[39]   A. Checko, "Cloud radio access network architecture. Towards 5G mobile networks," PhD Thesis, Tech. Univ. Denmark, 2016.

[40]   G. Kardaras and C. Lanzani, "Advanced multimode radio for wireless & mobile broadband communication," 2009 Eur. Wirel. Technol. Conf., no. September, pp. 132–135, 2009.

[41]   Common Public Radio Interface, "CPRI Specification V7.0," Stand. Doc. Specif., vol. 0, p. 128, 2015.

[42]   C. Module and S. Version, "Open Base Station Architecture Initiative," Control, vol. 1, no. 1, pp. 1–29, 2006.

[43]   G. Specification, "ORI Interface Specification ;," vol. 1, no. Release 1, pp. 1–151, 2012.

[44]   Next Generation Mobile Networks Alliance 5G Initiative, "5G White Paper," A Deliv. by NGMN Alliance, p. 124, 2015.

[45]   J. I. Kani, S. Kuwano, and J. Terada, "Options for future mobile backhaul and fronthaul," Opt. Fiber Technol., vol. 26, pp. 42–49, 2015.

[46]   J. Zhang, Y. Xiao, H. Li, and Y. Ji, "Performance Analysis of Optical Mobile Fronthaul for Cloud Radio Access Networks," J. Phys. Conf. Ser., vol. 910, no. 1, 2017.

[47]   J. I. Kani, J. Terada, K. I. Suzuki, and A. Otaka, "Solutions for Future Mobile Fronthaul and Access-Network Convergence," J. Light. Technol., vol. 35, no. 3, pp. 527–534, 2017.

[48]   T. Tashiro et al., "A novel DBA scheme for TDM-PON based mobile fronthaul," Conf. Opt. Fiber Commun. Tech. Dig. Ser., no. c, pp. 1–3, 2014.

[49]   O. Tipmongkolsilp, S. Zaghloul, and A. Jukan, "The evolution of cellular backhaul technologies: Current issues and future trends," IEEE Commun. Surv. Tutorials, vol. 13, no. 1, pp. 97–113, 2011.

[50]   B. Lavallée, "Mobile Backhaul Ciena's Essential Series: Be in the know.," 2016.

[51]   J. Hawkins and Earl Follis, "Carrier Ethernet Ciena's Essential Series: Be in the know.," 2016.

[52]   J. S. Robert Sturt, "Multiprotocol Label Switching (MPLS)," 2018. [Online]. Available: https://searchnetworking.techtarget.com/definition/Multiprotocol-Label-Switching-MPLS.

[53]   Telco_Systems ABTM company, "Better backhaul with MPLS to the cell site," 2015. .

[54]   Z. Tayq, "Fronthaul integration and monitoring in 5G networks," PhD thesis Univ. Limoges, 2018.

[55]   A. Pizzinat, P. Chanclou, F. Saliou, and T. Diallo, "Things you should know about fronthaul," J. Light. Technol., vol. 33, no. 5, pp. 1077–1083, 2015.

[56]   J. W. Kwon et al., "AC-coupled burst-mode OLT SFP transceiver for gigabit ethernet PON systems," IEEE Photonics Technol. Lett., vol. 17, no. 7, pp. 1519–1521, 2005.

[57]   A. C. Christian Plante and Jason Wong, "Opening Base Station Architectures Part 1: An   Inside   Look   at   OBSAI,"   2004.   [Online].   Available: https://www.eetimes.com/document.asp?doc_id=1272038.

[58]   DHIMAN DEB CHOWDHURY, "Front Haul Wireless-Fiber Convergence: Does Ethernet At Front Haul Help The Case For Increase White Box Deployment In Telecom Network   Transformation?,"   2018.   [Online].   Available: http://www.dhimanchowdhury.com/2018/01/13/hello-world/.

[59]   R. Maiden, "ORI Overview," no. August, 2015.

[60]   I. Chih-Lin, H. Li, J. Korhonen, J. Huang, and L. Han, "RAN Revolution with NGFI (xhaul) for 5G," J. Light. Technol., vol. 36, no. 2, pp. 541–550, 2018.

[61]   B. Guo, W. Cao, A. Tao, and D. Samardzija, "CPRI compression transport for LTE and LTE-A signal in C-RAN," 2012 7th Int. ICST Conf. Commun. Netw. China, CHINACOM 2012 - Proc., pp. 843–849, 2012.

[62]   T. A. Diallo et al., "A Complete Fronthaul CWDM Single Fiber Solution including Improved Monitoring Scheme .," 2015 Eur. Conf. Networks Commun., pp. 325–329, 2015.

[63]   C. L. I, Y. Yuan, J. Huang, S. Ma, C. Cui, and R. Duan, "Rethink Fronthaul for Soft RAN," IEEE Commun. Mag., vol. 53, no. September, pp. 82–88, 2015.

[64]   "Common Public Radio Interface: eCPRI Interface specification V2." [Online]. Available: http://www.cpri.info/spec.html.

[65]   G. O. Perez, D. L. Lopez, and J. A. Hernandez, "5G New Radio Fronthaul Network Design for eCPRI-IEEE 802.1CM and Extreme Latency Percentiles," IEEE Access, vol. 7, pp. 82218–82230, 2019.

[66]   N. C. and N. Ericsson AB, Huawei Technologies Co. Ltd, "Common Public Radio Interface: eCPRI presentation," 2018. [Online]. Available: https://medium.com/5g-nr/cloud-ran-and-ecpri-fronthaul-in-5g-networks-a1f63d13df67.

[67]   C. J. Bernardos, A. De Domenico, J. Ortin, P. Rost, and D. Wübben, "Challenges of designing jointly the backhaul and radio access network in a cloud-based mobile network," in Future Network and Mobile Summit, 2013, pp. 1–10.

[68]   J. F. Monserrat, G. Mange, V. Braun, H. Tullberg, G. Zimmermann, and Ö. Bulakci, "METIS research advances towards the 5G mobile and wireless system definition," Eurasip J. Wirel. Commun. Netw., vol. 2015, no. 1, pp. 1–16, 2015.

[69]   M. M. Ahamed and S. Faruque, "5G Backhaul: Requirements, Challenges, and Emerging Technologies," in Broadband Communications Networks - Recent Advances and Lessons from Practice, no. October, 2018.

3. Cloud Access Networks for Future Converged Fixed and Mobile Networks

Contents

3 Cloud Access Networks for Future Converged Fixed and Mobile Networks

3.1 The Cloud Access Network Concept

As discussed in chapter 1, the CAN has been proposed [1-3] as a cost-effective "future-proof" network solution to not only meet the ever-increasing growth in data traffic capacity, but also to effectively support an increasing range of dynamic traffic types with widely varying characteristics. Chapter 1 introduced a basic overview of the CAN concept, in this section a more detailed description of the CAN and its associated technologies is presented.

To achieve sustainable business models for network operators, offering advanced services such as the rapid provision of on-demand, client-specific network interconnectivities is highly desirable, this requires CANs to be highly adaptive, resource-efficient and dynamically reconfigurable. To meet these requirements, CANs must be equipped with the vital networking functions of centralized software controller-based SDN, dynamic online network reconfigurability and fine granularity bandwidth provisioning performed at wavelength, sub-wavelength and/or sub-band levels. Furthermore, to achieve ultra-high flexibility and elasticity in network provisioning and adequate backward and forward compatibility, CANs are also envisaged to transparently accommodate a diverse range of important network design features such as signal modulation formats, signal detection schemes, flexible WDM grids, diversified network topologies and multiple access techniques[3]. Since PONs are being extensively deployed worldwide due to their cost effectiveness and inherent future-proof characteristics, CANs fully exploit the advantages of PON technologies by integrating together multiple PONs within a single CAN. The CAN requires advanced reconfigurable adaptive optical transceivers for signal generation and detection, together with low-cost ROADMs for optical domain switching, to enable the aforementioned CAN features. It is highly important to realize that software reconfigurable adaptive optical transceivers, ROADMs and flexible PONs enabled by high speed, digital integrated circuit (IC)-based DSP, play significant roles in enabling the SDN based CANs paradigm at the physical layer. The cost effective implementation together with high scalability and adaptability are essential for all the above mentioned elements. Therefore, DSP is considered as a key enabling technology for realising the future CANs by supporting various features such as advanced signal modulation, multiple access techniques, fast and

accurate synchronisation methods and adaptive linear/nonlinear compensations of network impairments[5,6].

3.2 Passive Optical Networks for Application in CANs

In this section, the key challenges and requirements of future PONs are first discussed in the context of the demanding needs of the future networks, as outlined in section 1.1. The concept of the DFMA PON is then described, which is designed to address the aforementioned challenges and requirements in a cost effective manner.

3.2.1 Challenges and Requirements of Future PONs

Basic On/Off Keying (OOK) is the traditional modulation format employed in existing optical fibre-based access networks. The main drawback of OOK is that it is not suitable for the high transmission speeds needed in future networks, this is because as the bit rate increases, distortion such as chromatic dispersion-induced inter-symbol interference (ISI) intensifies. However, OOK modulation has been used extensively for a long time due to various advantages such as provision of a cost-effective transceivers and robustness against noise and nonlinear impairments[6]. In addition, as current optical and electrical components exhibit strict bandwidth limitations, OOK is reaching the limit of its performance due to its fixed relationship between bit rate and bandwidth[7]. To support future PONs and CANs, advanced modulation formats [8] are therefore necessary to achieve higher bit rates through increased spectral efficiency and increased tolerance to channel dispersion. Examples of advanced modulation formats that have been extensively investigated for application in future PONs include OFDM [4][9], carrierless amplitude phase modulation (CAP)[10], quadrature amplitude modulation (QAM) [11]and multi-level pulse amplitude modulation (PAM)[12]. The increased complexity of these modulation formats, however, makes their generation and detection more challenging to achieve in a low cost, low power, small form factor transceiver, especially for the more complex modulation formats such as OFDM and CAP.

In addition to the challenges of implementing low-cost, advance modulation formats in future PONs, there are other challenges associated with the fixed characteristics of current networks. Traditional networks have been designed with an essentially static architecture to simultaneously provide individual end users with internet connections supporting

guaranteed peak bandwidths, although dynamic bandwidth allocation protocols are becoming widely employed to use the total network bandwidth more efficiently. If end users require a change to their peak connection speed this can require manual operator intervention and it can take significant time to implement as potentially physical hardware must be replaced, thus bandwidth provision is fundamentally static in nature [13]. The existing PONs effectively provide a fixed, peak bandwidth regardless of changing traffic demands, however as it is predicted that operators must offer peak internet connection speeds per user of 10Gb/s in the future [14], this operational model of essentially fixed bandwidth provision with limited flexibility, is unsustainable due to excessive costs. It is therefore essential that future PONs are highly adaptive and flexible in terms of dynamic end-user bandwidth allocation. Some of the additional key requirements to be taken into consideration for future PON technologies and there application in CANs are;

- Utilisation of existing commercially available optical and electrical components to provide the aforementioned higher bit rates, thus avoiding the need for higher bandwidth and consequently more expensive components.

- Transparency to the underlying network features, including, varying signal bandwidth, signal modulation formats, signal detection schemes, WDM grid and network topology. Such features providing a consolidating platform to greatly improve network flexibility, adaptability and elasticity.

- Excellent backwards compatibility with all existing PONs technologies.

- Considerably improved network operation reconfigurability and adaptability in both the electrical and optical domains, together with SDN network functionalities extended to the physical layer,

- Dynamic establishment of multiple virtual networks on the shared fiber infrastructure.

New network devices are thus required, which are capable of delivering the aforementioned required functionalities. Therefore, in order to offer an on-demand, highly elastic channel in future PONs, from the physical layer perspective, reconfigurable optical transceivers (ROTs) are considered key PON components, embedded in the ONUs and the OLT, which have variable transmission parameters including data rate, signal spectral location, signal bandwidth and modulation format, etc., allowing dynamic allocation of available network resources and reconfiguration of the PON according to transient traffic demand, thus flexibly

sharing the PON capacity and achieving highly efficient use of the network. It is also critical that ROTs, together with other essential networking devices, enable SDN-controlled multiplexing of multiple, dynamically configurable, independent channels on a single optical wavelength. The associated PON, incorporating multiple independent channels, thus allows key features such as i) converged fixed and mobile transport in a single PON, ii) on-demand, customer specific, virtual private networks (VPNs) and iii) network slicing which is a highly important feature needed to support the highly heterogeneous requirements of 5G services[15]. By exploiting DSP, ROTs can be implemented to support dynamically configured advanced modulation formats and elastic channels, thus supporting SDN-based programmability to provide the aforementioned variable transmission parameters [16, 17].

An example of a flexible transceiver device for future networks is the high-capacity sliceable bandwidth variable transceiver (S-BVT) based on DD, making it suitable for inter-data centre communications and elastic metro/regional networks[18]. The S-BVT is managed by a centralised SDN controller to allow it to achieve efficient resource usage, enabling unique bandwidth granularity and flexibility. The S-BVT also has extended features to make it more adaptable and reconfigurable by supporting the on-demand configuration of programmable network functions, such as bit rate, bandwidth, path adaptation, switching and sliceability. The S-BVT transmitter consists of adaptive DSP-based multicarrier modulation which is either OFDM or discrete multitoned modulation (DMT) (OFDM located at baseband), to achieve the required high transmission speed, followed by the DAC to convert to an analogue domain signal, an array of tunable laser sources (TLS) and Mach-Zehnder modulators are also employed to convert the generated signal to the optical domain which are then aggregated by a spectrum selective switch (SSS) as an optical filtering process. The aggregated flow can be sliced to serve multiple destination nodes at variable rate and bandwidth. While the receiver side adopts the reverse process of the transmitter side.

In addition to the ROT, the ROADM is considered as another key component to greatly enhance the utilisation of future PONs by enabling their integration into CANs. Existing ROADMs with various advanced architectures are reported in detailed in section 3.3.1, however, these ROADMs can only work at the wavelength level and they are also expensive and too bulky for application in the converged metro/access networks due to the utilisation of hard-wired switching elements, which significantly limits the ROADM's flexibility, upgradability, as well as its adaptability and cost-effectiveness[19]. To meet the challenging

requirements of CANs which integrate future PONs, it is easy to comprehend that it is critical that new ROADMs are developed that are equipped with new features for highly flexible operation at both wavelength and multiple sub-wavelength levels, whilst also meeting the associated cost, power and size restrictions of the metro/access networks. To provide suitable ROADMs, soft-ROADMs are proposed for application CANs which are presented in detail in section 3.3.2 and experimentally demonstrated in chapter 7.

3.2.2 Digital Filter Multiple Access PONs

To provide the highly desirable dynamic software-reconfigurable networking in a cloud access network scenario down to the physical layer, a new multiple access technique termed DFMA has been proposed, which is applicable to both PONs and their associated CANs. The DFMA technique uses the power of optical transceiver-embedded DSP to realise SDN controlled channel multiplexing/demultiplexing to allow multiple users and/or services to dynamically share a common fibre transmission medium [16]. The DFMA technique enables PONs to support reconfigurable and elastic connections which can be dynamically configured by a centralised SDN controller according to the transient network requirements. Furthermore, when combined with optical filter- and E-O-E conversion-free ROADMs that perform DFMA channel add/drop operations at the wavelength, sub-wavelength and orthogonal sub-band levels, the DFMA technique can also enable highly flexible CAN network architectures that exploit rapid traffic-dependent reconfiguration to efficiently utilise CAN network resources[20].

3.2.2.1 Digital Orthogonal Filtering-based Channel Multiplexing

The DFMA PON concepts are built upon the principle of DSP-based channel multiplexing using digital orthogonal filters. This technique employs channel multiplexing/demultiplexing operations that are fully implemented by DSP functions in the digital domain using digital orthogonal filters. This allows great flexibility in network connectivity due to the intrinsic versatility of DSP. Employing purely IC-based DSP implies that the technique can be highly cost effective due to the inherent low cost of mass produced digital ICs and the fact that no additional analogue electrical or optical components are required. Fig. 3.1, illustrates the basic principle of channel multiplexing/demultiplexing in a PTP IMDD optical link, where reconfigurable digital orthogonal filters embedded in digital ICs within the optical transceivers are used to multiplex/demultiplex N bandwidth-variable

channels. For each channel, an independently modulated signal is first up-sampled via the insertion of M-1 zeros between two consecutive samples, thus the up-sampling factor is M, denoted as (M↑).
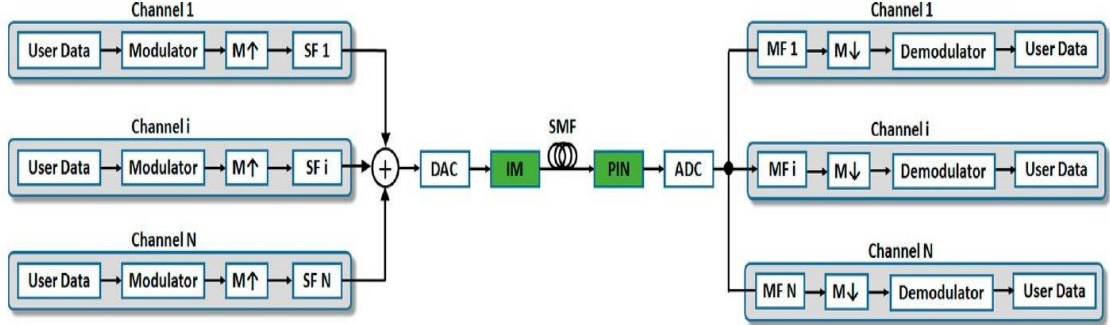

Fig. 3.1. Digital orthognal filtering-based channel multiplexing SF, shaping filter; DAC, digital to analogue converter; IM, intensity modulator; ADC, analogue to digital converter; MF, matching filter; M↑, up-sampling by factor M; M↓, down-sampling by factor M.

The up-sampling generates M/2 double-sideband spectral images within the Nyquist frequency band, the up-sampling factor, therefore, allows control of the generated channel bandwidth (bandwidth = sampling frequency/M). Subsequently, a digital shaping filter (SF) is employed to select the appropriate spectral image to locate the signal at the desired spectral location, that is, in the desired sub-wavelength channel.

By using Hilbert-pair filters, two signals can be co-located in the same sub-wavelength channel. The Hilbert-pair filters generate orthogonal channels as the In-phase (I) filter applies a 0° phase shift to all frequency components, whereas the Quadrature-phase (Q) filter applies a −90° phase shift to all frequency components, thus two orthogonal sub-band channels occupy the same sub-wavelength channel. The two orthogonal channels are thus denoted as I (In-phase) and Q (Quadrature-phase) channels. The generated channels are all summed together in the digital domain and fed to a single DAC. The resulting analogue electrical signal then drives a suitably biased optical IM and the optical signal is launched into an IMDD network employing standard single mode fibre (SSMF). After transmission through the network, in the receiver a photo detector (PD) converts the optical signal to an electrical for digitisation by an ADC, the digital signal is then fed to one or more DSP-based receivers, each dedicated to recovering a specific channel. In the DSP receivers the digital signal is first filtered by the appropriate digital matching filter (MF) to demultiplex the desired channel from the aggregated signal, subsequent down-sampling by a factor of M,

denoted as (M↓), is performed by selecting every M-th sample, which returns the signal to baseband at the original sample rate. Sample timing alignment is necessary for the receiver (not shown in Fig. 3.1) to ensure correct filter operation. Finally, the received signal from each channel is demodulated according to the adopted signal modulation to recover the encoded binary data. Fig. 3.2(a,b) show example spectra of different combinations of digital orthogonal filter multiplexed channels for the cases of equal and varying channel bandwidths respectively. Here it is worth highlighting a vitally important characteristic of the aforementioned channel multiplexing technique, which is that channels can be routed and switched completely in the optical domain without the need for optical-electrical-optical (OEO) conversion or optical bandpass filters (OBPFs), thus allowing the realisation of low-cost, low-latency network switching devices which are crucial for the cost-sensitive CAN scenarios, these network devices are soft-ROADMs which are described in detail in section 3.3.2.
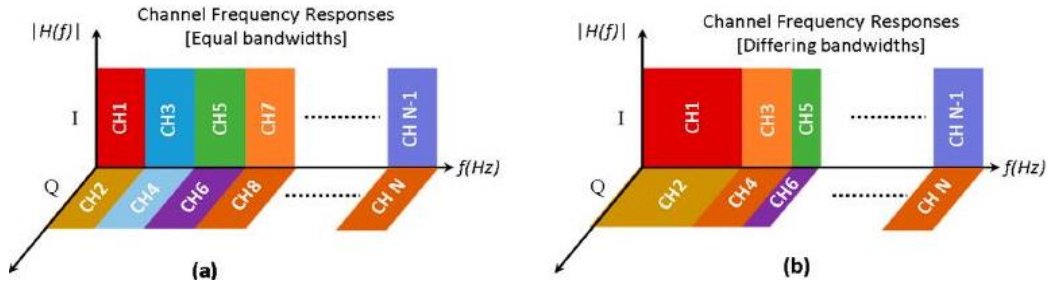

Fig. 3.2. Example electrical spectra of combinations of digital orthogonal filter multiplexed channels a) Equal bandwidth channels b)Varying bandwidth channel

The Hilbert-pair approach is employed to implement the necessary digital orthogonal filters. The *ith* Hilbert-pair filters, $h_i(t)$ have impulse responses of

$$s_i^I(t) = p(t)\cos(2\pi f_{ci}t)$$

$$s_i^Q(t) = p(t)\sin(2\pi f_{ci}t) \tag{3.1}$$

where the spectrally overlapped in-phase and quadrature phase Hilbert-pair filter components are designated by the superscripts "I" and "Q," respectively, f_{ci} is the *ith* Hilbert pair filter central frequency, and *p(t)* is the baseband pulse with a square-root raised-cosine expressed as:

$$p(t) = \frac{\sin[\pi(1-\alpha)t'] + 4\alpha t' + \cos[\pi(1+\alpha)t']}{\pi t'[1-(4\alpha t')^2]}, \quad t' = \frac{t}{T_s} \tag{3.2}$$

where T_s is the sampling period preceding the up-sampling, and the 'α' parameter governs the excess of bandwidth of $p(t)$ in the frequency domain. The corresponding impulse responses for the receiver-side Hilbert-pair matching filters for the *ith* sub-band, are $m_i^I(t)$ and $m_i^Q(t)$ where:

$$m_i^I(t) = s_i^I(-t)$$

$$m_i^Q(t) = s_i^Q(-t)$$

$$\tag{3.3}$$

For simplicity, a point-to-point DFMA PON system conveying two channels, orthogonally occupying the same spectral region, is considered, thus for this case i=1. The Hilbert pair-based digital filters achieve orthogonality between these two sub-band channels such that:

$$s_i^A(t) \otimes m_i^A(t) = \begin{cases} p(t)\cos(2\pi f_{ci}t), & A = B \\ 0, & A \neq B \end{cases} \tag{3.4}$$

where the superscripts A and B each denote I or Q and $p(t)$ is the baseband pulse of associated filters.. In addition, assuming that the DAC and the ADC have identical sampling speeds of F_s, the central frequencies, f_{ci}, of the *ith* Hilbert-pair is given by:

$$f_{ci} = (2i-1)\frac{F_s}{2N}, \quad i=1,2,3,\ldots\ldots \tag{3.5}$$

Thus if the inputs to the in-phase channel and quadrature-phase channel are $d_I(t)$ and $d_Q(t)$ respectively and there is an ideal, zero loss and zero delay channel from the shaping filter outputs to the matched filter inputs, the output signal $d_I'(t)$ from the in-phase matched filter is:

$$d_I'(t) = [d_I(t) \otimes s_1^I(t) \otimes m_1^I(t)] + [d_Q(t) \otimes s_1^Q(t) \otimes m_1^I(t)] \tag{3.6}$$

Using the orthogonality property of the Hilbert-pair filters defined in Eq. (3.4), the first convolution term in Eq. (3.6) becomes a delayed version of $d_I(t)$ and the second term becomes zero, thus:

$$d'_I(t) = [d_I(t) \otimes \delta(t - T_{CH})]$$

$$(3.7)$$

Here T_{CH} is included to represent the total system propagation delay between the transmitter's shaping filter input and the receiver's matching filter output. Similarly, the output signal from the quadrature-phase matched filter in the receiver is a delayed version of the input signal at the quadrature-phase shaping filter in the transmitter, thus:

$$d'_Q(t) = \left[d_Q(t) \otimes \delta(t - T_{CH})\right]$$

$$(3.8)$$

Thus for the ideal channel case and with ideal filter responses, perfect orthogonality between the spectrally-overlapped orthogonal channels is maintained and the digital filter multiplexing and demultiplexing operations do not introduce any interference between these two channels. The practical FIR digital filters employed provide an approximation to the ideal, infinitely long, Hilbert-pair filter impulse responses, however the filter lengths can be suitably truncated to practical lengths as demonstrated in [7][19].
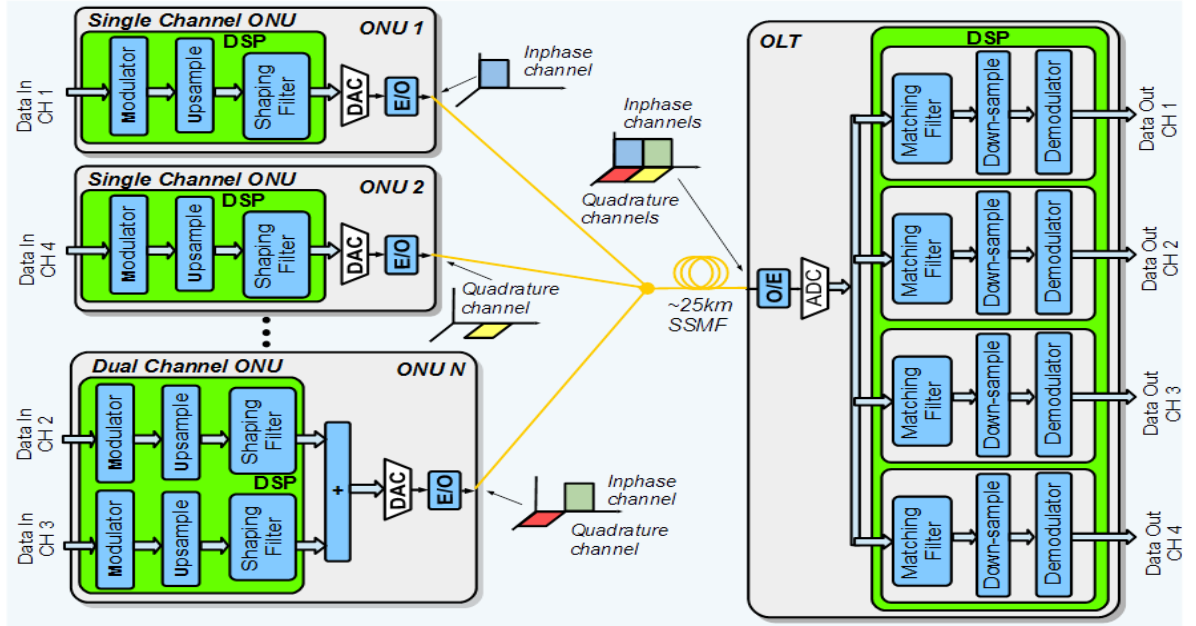
3.2.2.2 DFMA PON Operating Principle

Fig. 3.3. DFMA-PON top level architecture

The DFMA PON employs the digital orthogonal filtering-based channel multiplexing technique, as described in the section 3.2.2.1. In the downstream direction of the PTMP DFMA PON, all channels are multiplexed in the digital domain in the OLT transmitter, with each ONU receiver configuring its FIR-based matching filters according to its allocated channel(s). Fig. 3.3 depicts a simplified top level architecture of a DFMA PON, where only the upstream direction is shown. In the upstream direction of the DFMA PON, each ONU generates one or more channels and the multiple channels from different ONUs are now multiplexed in the optical domain using the passive OC at the remote node, the optical signal emerging from the OC, then propagates through the shared fiber transmission link to the OLT. The channel demultiplexing is then performed in the digital domain in the OLT receiver. As multiplexing in the downstream direction is performed in the digital domain within the DSP of the common OLT transmitter, the common clock signals thus inherently synchronise all downstream channels. However, in the upstream direction, in addition to the sample timing synchronisation needed at all receivers, as described in section 3.2.2.1, suitable upstream timing synchronisation is necessary between ONUs occupying the same sub-band in order to maintain channel orthogonality. However, if the OLT uses a single ADC to receive all channels from all ONUs, then synchronisation between all ONUs on the PON is required. A control loop is therefore required between the OLT and ONUs to monitor and

adjust the transmitted signal timings and delays to achieve the correct inter-ONU STO, thus ensuring the correct timing relationship between orthogonal channels is maintained. It should also be emphasised that an individual ONU can also support multiple channels simply by implementing multiple FIR filter instances in parallel, as shown in Fig. 3.3, thus allowing an ONU to support multiple independent and isolated network connections. Furthermore, multiple ONUs can also share the same orthogonal sub-band channel by employing multiple access modulation formats. For example, OFDM supports multiple subcarriers which can be independently allocated to different ONUs sharing the same channel.

As the overall configuration of the DFMA PON is dependent on reconfigurable DSP functions, a centralized SDN-controller communicates, via a protocol such as extended OpenFlow, with transceiver-embedded DSP controllers to dynamically configure the DFMA PON in terms of the characteristics of the involved digital filters, to configure the channels in terms of optimum spectral locations and required bandwidths and to avoid any channel contention between ONUs. Thus highly reconfigurable, dynamic and elastic bandwidth provision is achievable in the DFMA PON. A crucial characteristic of the DFMA PON, is that the independent and essentially isolated channels allow key features such as i) converged fixed and mobile transport in a single PON, ii) on-demand, customer specific, virtual private networks (VPNs) and iii) network slicing which is a highly important feature needed to support the highly heterogeneous requirements of 5G services[15]. Other salient advantages of DFMA PONs can be summarized as follows:

- Extension of SDN control functionalities to the physical layer. Thus, drastically improving dynamic network reconfigurability, ease of network virtualisation and channel bandwidth elasticity.
- Inherent backwards compatibility with all existing PONs.
- Transparency to underlying signal parameters such as modulation format.
- Enhanced data security in the physical layer due to the arbitrary nature of the digital filter configurations, i.e. full knowledge of the filter parameters is required to correctly demultiplex a channel from the aggregate signal.
- Inherent network scalability for "pay-as-you-gow" operation due to the ability to incrementally add capacity by exploiting a modular DSP solution in the OLT.
- The low cost associated with large scale, mass-produced digital integrated circuits can keep PON CAPEX levels commercially viable.

3.3 ROADMs for Application in CANs

3.3.1 Evolution of ROADM Technologies

3.3.1.1 OEO based Add Drop Multiplexers

During the 1980s and 1990s, the Synchronous Optical Network/Synchronous Digital Hierarchy (SONET/SDH) standards were developed to transfer multiple digital bit streams over optical fiber using lasers at varying transmission data rates, where all of the data processing and switching is done in the electrical domain. The SONET/SDH standards were further developed to accommodate the increasing capacity demands, but the maximum capacity achieved on a single fiber was of the order of a several 10s Gb/s and costly electronic regenerators where required between add drop locations [21]. By the mid-1990s, WDM technology was maturing, which enabled multiple wavelengths, each carrying a high capacity signal, to be multiplexed in one single fiber. The WDM technology thus had the effect of dramatically increasing the network's optical transmission capacity and the emergence of multi-wavelength optical amplifiers for signal regeneration in the optical domain, enabled large scaling up of SONET/SDH connectivity in a highly cost effective way [22]. The network nodes are the sites in the network where traffic is sourced, terminated, and switched, a switching node, or ADM is shown in Fig. 3.4[22].
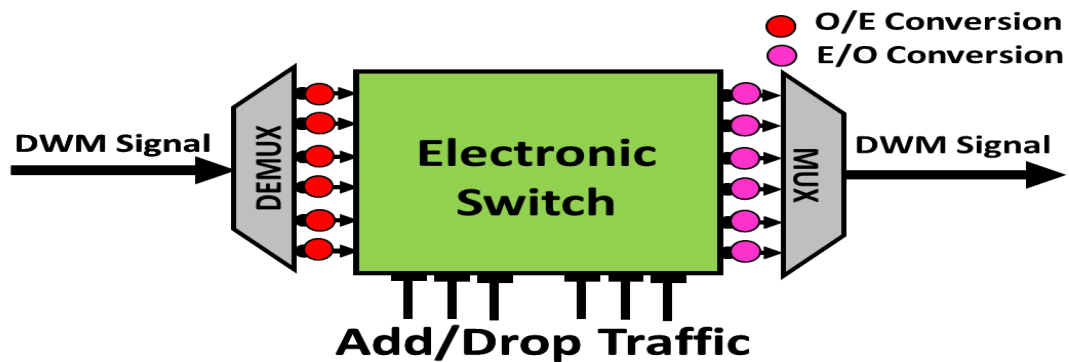

Fig. 3.4 Network Node with O-E-O architecture

In the incoming direction, the optical demultiplexer (demux) splits the incoming aggregate WDM signal into separate individual wavelengths. Each single wavelength will then pass into an optical-to-electrical (OE) converter to transform the signal from optical to electrical

domain after entering the node. Subsequently, the electrical signals undergo switching and the add/drop functions are applied electronically, the outgoing signals are transformed back to the optical domain by electrical-to-optical (EO) conversion, thus forming an optical-electrical-optical (OEO) architecture[21]. In the outgoing direction, the individual optical signals are combined by an optical multiplexer (mux) to form an outgoing WDM signal. Note that Fig 3.4. shows only one optical signal direction (from West to East), however this architecture is applicable in both directions (East to West and West to East). The nodal traffic is classified into bypass, add and drop traffic. The bypass traffic is traffic that is transiting the node on its way to its final destination, while the drop traffics carries the data that is extracted at the node and the add traffic carries the data that is sourced at the node. For all types of traffic in the O-E-O architecture, a dedicated O/E (E/O) is required for every incoming (outgoing) wavelength. The main disadvantage of this architecture is the need for a large number of O/E and E/O converters which increases the cost, power requirement and physical space of the node. Furthermore the electronic switching fabric does not scale easily when increasing the network capacity and so forms an "electronic bottleneck", thus an all optical network, where a network connection is maintained and switched in the optical domain from source to destination is highly desirable.

3.3.1.2 **Optical Add Drop Multiplexer (OADM) Functionality**

Fig. 3.5 illustrates the architecture of the basic Optical Add Drop Multiplexer (OADM) which was introduced commercially in the mid-1990s. In this innovation, the OADM keeps the E/O and O/E converters for the electrical add/drop traffic and eliminates them for the bypass traffic as all the transiting traffic passes through the node in the optical domain without needing O-E-O conversions[23]. Therefore the aforementioned disadvantage of the O-E-O architecture are drastically reduced as O-E-O conversions are not needed for the bypass traffic.
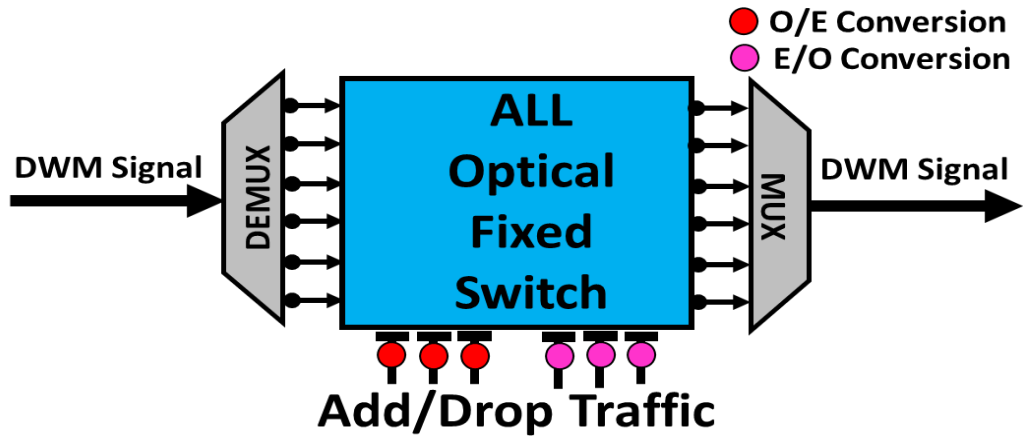
Fig. 3.5 OADM using E/O and O/E conversion only in Add/Drop ports

A traditional OADM, is depicted in Fig.3.5. It consists of three main parts, an optical demux, an optical multiplexer and an optical routing device located between the optical demux and multiplexer to direct the light paths, together with a set of ports for adding and dropping signals. The routing of the light paths is fixed and can only be changed by manual reconfiguration of the OADM, i.e. changing the filters. For an OADM, "drop" refers to extracting a wavelength, from multiple wavelengths in a fiber. While "add" refers to inserting a new wavelength into the aggregated output signal along with the pass through wavelengths [24]. An example of wavelength add/drop operations is shown in Fig. 3.6 where 2 channels $\lambda 1$, $\lambda 6$ are dropped at the drop outputs respectively from the input port, simultaneously, 2 different channels with the same wavelengths $\lambda 1$, $\lambda 6$ are added through the add ports into the signal stream at the output port. Thus, OADMs control the network architecture and provide add/drop functionality at the wavelength level. To achieve control of network interconnections and add/drop functionality at a lower sub-wavelength level, such as frames, timeslots or packets, an electronic switch fabric is however still required.
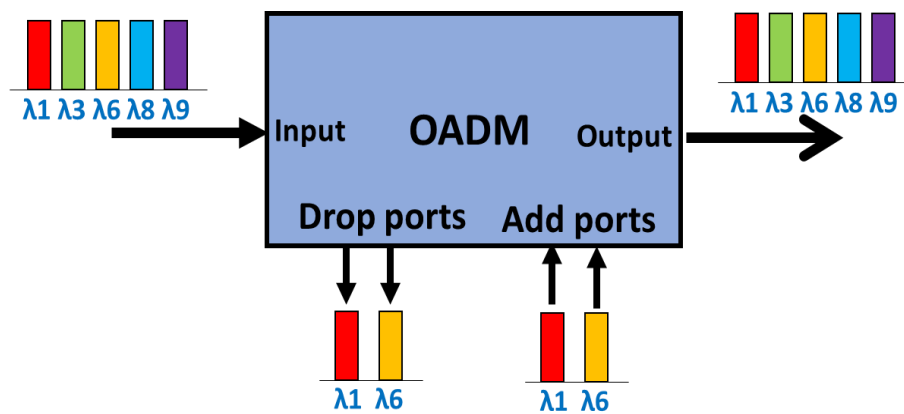

Fig. 3.6 Functionality of a typical OADM

Electric thin film filters (TFF) and fibre Bragg gratings (FPG) are the main technologies that are commonly used to realize OADMs [25]. In each case, an appropriate filter is selected according to the wavelength to be dropped/added. In the TFF architecture, as shown in Fig. 3.7, the first narrow bandpass filter [25] is used in the drop side to pass the wavelengths to be dropped from the wavelength multiplexed signal and reflect the bypass wavelengths through the node. The second narrow bandpass filter is used in the add side to pass the add wavelengths into the output port and reflect the bypass wavelengths to the output port.
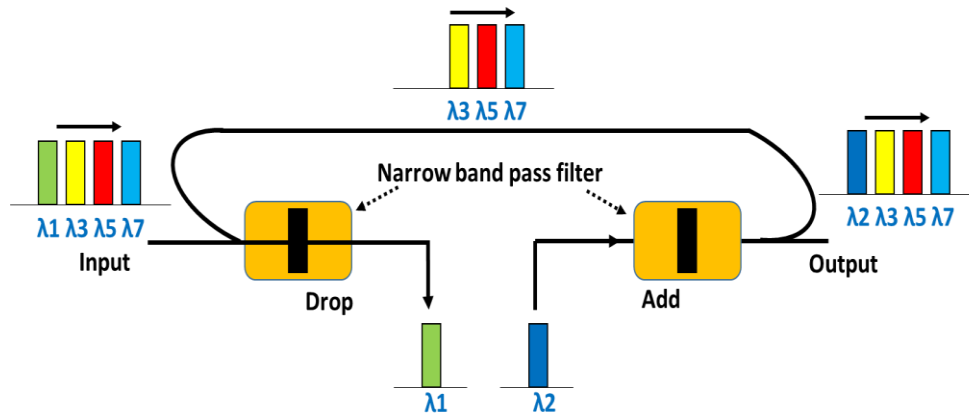

Fig. 3.7 A typical OADM configuration using TFF

Fig. 3.8 illustrates the OADM using the FBG configuration. The FBG is selected according to the wavelengths to be added/dropped. The FBG which is located in the middle of the node between the two circulators connecting to the add and drop ports, is used to reflect the desired drop wavelength signals from the wavelength multiplexed signal, where the reflected signals would be dropped to the drop port via the circulator and the remaining wavelength signals pass through the first circulator, the FBG and the second circulator, thus passing through the whole node.
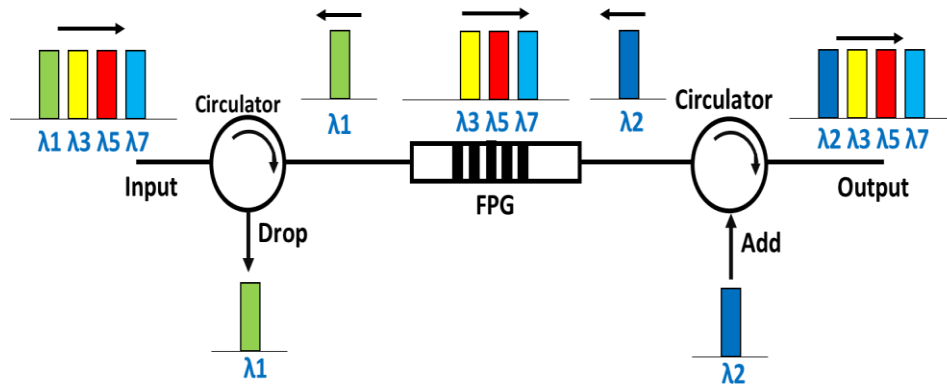

Fig. 3.8 A typical OADM configuration using FBG

At the same time, new wavelength signals incident on the circulator in the add side, are reflected by the FBG and added into the bypass WDM signal that is transmitted via the circulator to the node output. The TFF configuration can offer lower cost and a more simple design than the FBG[25]. Both OADM designs have the key advantage of avoiding the use of WDM DEMUXs and MUXs which would reduce optical signal power levels due to their high insertion losses. To conclude, the added/dropped channels at each OADM in the network are only manually reconfigurable therefore it does not allow easy control of the network architecture and also limits OADM controlled network connectivity to the optical wavelength level only.

The traditional OADM is also called a fixed OADM due to the add/drop of fixed wavelengths to specific fixed ports[26]. So, if the add/drop configuration must be changed, a technician must visit the OADM site to manually update the OADM configuration. There are some other disadvantages related to OADMs such as: firstly, a separate filter(s) is required according to the add/drop configuration. As the site must be visited by an engineer the fixed filter based OADM requires a long time to reconfigure the node. Secondly, it requires a large inventory of filters to add/drop a preselected wavelength from the arbitrary wavelengths. Finally, the OADM reconfiguration will interrupt the prevailing traffic. The OADM therefore has significant limitations when considering the rapid reconfigurability of the network.

3.3.1.3 Reconfigurable Optical Add Drop Multiplexer (ROADM) Functionality

Reconfigurable optical add drop multiplexers (ROADMs) are a key technology that allows the network to be reconfigured remotely to dynamically add/drop selected wavelengths and control the routing of different wavelengths in the network, this obviously has a clear advantage over the OADM that requires manual intervention to reconfigure the connectivity [27]. ROADMs were developed as an upgraded version of OADMs to provide high speed rerouting of light paths to accommodate dynamic changes in traffic patterns, greater network configuration flexibility, bypassing of faulty connections and easing the upgrade to newer WDM technologies. As the network can be remotely reconfigured as required and regular changes in traffic patterns can be predicted, the utilisation of ROADMs can lead to huge flexibility in both network design and management for more effective use of network

resources. Multi-degree ROADMs can be implemented, where the degree refers to the number of switching directions carrying aggregated WDM signals.

There are two common architectures for multi-degree ROADMs, known as broadcast and select (B&S) [28] and route and select (R&S)[29]. In the B&S architecture as shown in Fig. 3.9, 1xN power splitters (PS) and Nx1 wavelength selective switches (WSS) are employed where N is equal to the degree of the ROADM. Thus, an N degree ROADM requires N PSs and N WSSs. The principle of B&S is based on broadcasting the whole multi-wavelength input signal from each degrees' input via a PS, to an AWG feeding the drop ports and WSSs feeding each degrees' output. The WWSs are also fed from an AWG which connects to the add ports[28]. In this architecture, the optical PSs will limit the number of degrees of the ROADM as insertion loss is proportional to N. The maximum number of degrees is therefore limited to a small number, typically not exceeding more than 8.
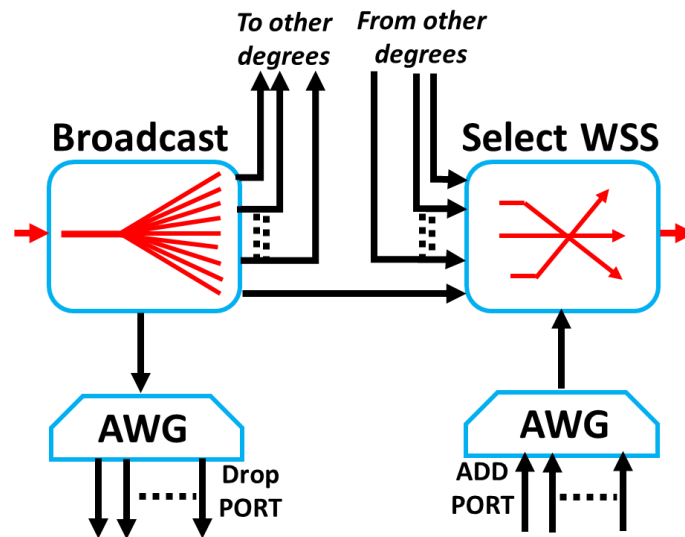
Fig. 3.9 A broadcast and select multi-degree ROADM architecture

In order to eliminate the limitation on the number of degrees in B&S-based ROADMs and thus increase the scalability in the ROADM architecture, the PS can be replaced with a WSS in every degree in the B&S architecture to form the route and select (R&S) ROADM architecture, illustrated in Fig. 3.10. Two WSSs are now required in every nodal degree, hence for an N degree ROADM, 2N WSSs are required, which has the drawback of increased cost and power consumption. However, as the insertion loss of the WSS is independent of N the degree of the ROADM is not limited and so degrees up to around 16, can be achieved

with the R&S ROADM architecture. The use of only WSSs can also provide superior isolation and so reduce leakage between wavelengths.
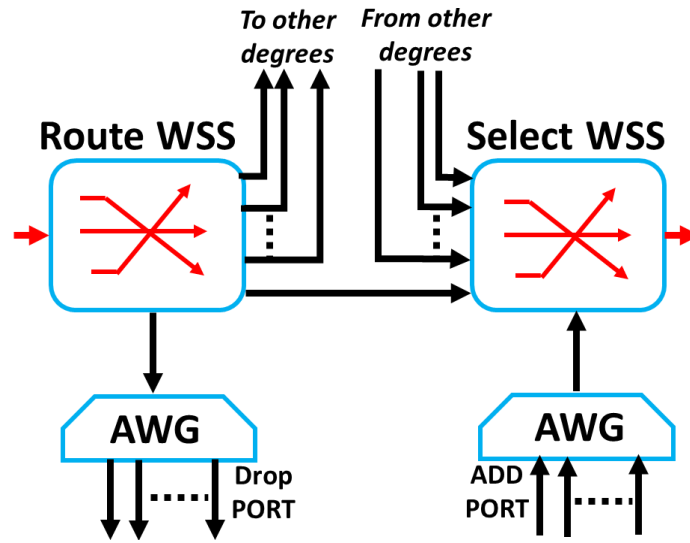

Fig. 3.10 A route and select multi-degree ROADM archeticture

In addition to offering high flexibility and good scalability, ROADMs have continued to evolve to meet the challenges in future optical networks. Colourless, directionless and contentionless (CDC) [10-12] are the three key ROADM features to also be considered when fully evaluating ROADM performance. Colourless means that no dedicated wavelength is specific to a certain add/drop port, therefore, any wavelength could be added/dropped at any port in the ROADM. While directionless refers to the redirection of new added channels from any nodal port to any other outbound nodal degree, and vice versa. In other words, add/drop ports at a node are not nodal degree selective. The contentionless feature prevents light path blocking, this can occur when two wavelengths of the same colour converge at the same WSS at the same time, thus causing network contention.
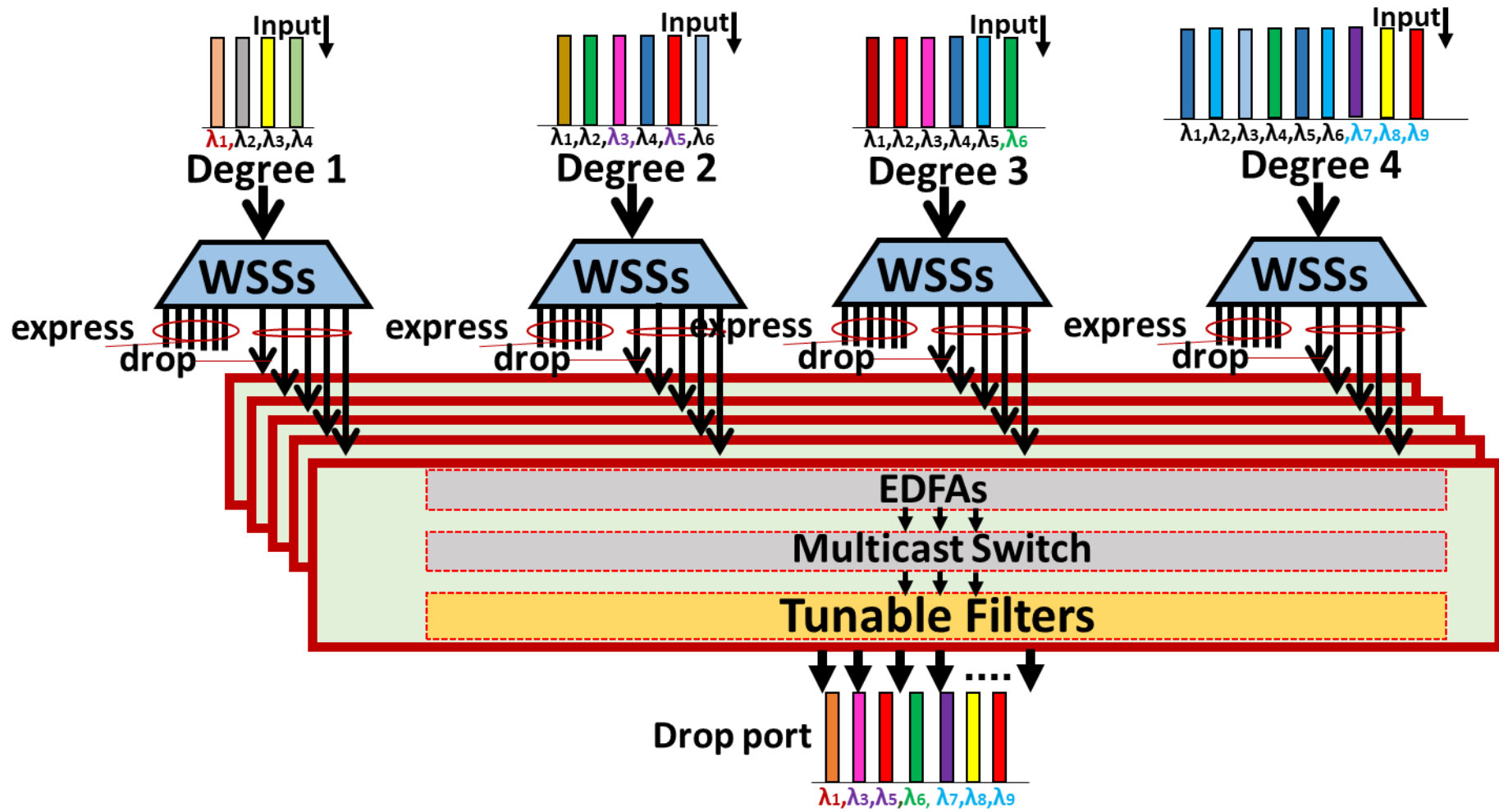
Fig. 3.11 Drop Functionality in a MCS-based CDC ROADM with Multi-Degree Archeticture

There are different ways to implement ROADM designs giving varying levels of performance and cost. The micro electromechanical systems (MEMS) [30]or Liquid Crystal on Silicon (LCOS) [31]based WSSs are the key optical devices to build colourless and directionless (CD) ROADM architectures. While multiple cascaded WSSs [32] and planar lightwave circuit (PLC)-based multicast switches (MCSs) [16-18] are the key optical devices used to construct a full CDC ROADM architecture[33]. Fig. 3.11, illustrates an example of the drop function in a 4 degree (North, South, East and West) CDC ROADM employing WSSs and MCSs. The architecture is designed to allow multiple MCS cards to be added as needed, allowing the total number of add/drop ports to be increased incrementally for greater cost effectiveness.

For the drop functionality in Fig. 3.11, a WSSs is employed in each degree to demultiplex the incoming traffic into multiple groups of wavelengths and each wavelength group is assigned as an input to a N×M MCS, where N refer to the number of degrees and M refers to the number of drop ports, thus each input of a MCS is fed with a group of wavelengths from an individual degree. In a MCS, as depicted in Fig. 3.12, N 1×M splitters are used to distribute the wavelength groups from each direction to M N×1 switches which operate as a gate to select one of the N wavelength groups form the required degree. Tuneable filters, as shown in Fig. 3.12, are required in the case of direct-detection optical systems, to allow the optical receiver at each drop port to detect only the required wavelength's traffic. Tuneable filters are not needed for the case of coherent optical systems as the coherent receiver's tuneable laser-based local oscillator would select the desired wavelength. It should be noted that the EDFAs, shown in Fig. 3.12, are required to compensate the high losses associated with the optical PSs. A similar architecture is employed for the add direction, as shown in Fig. 3.12, except the tuneable filters are not required at the add port inputs as only single wavelengths are applied to each port. An MCS achieves "colourless" operation as the ROADM can add/drop any arbitrary wavelength signal to/from any port via a tuneable filter. In other words, no input/output ports are specific to certain wavelengths. The MSC achieves "directionless" operation as any wavelength from any direction can be added/dropped to any output port by the associated N×1 switch. The MCS achieves "contentionless'' operation because each N×1 switch only selects wavelengths from a single direction at any time, so it is not possible for the same colour wavelengths coming from different nodal degrees to collide with each other. Therefore, with the help of the MCS, the CDC ROADM enables

add/drop of any wavelength to/from any port to/from any direction with no contention thus achieving the CDC operation.
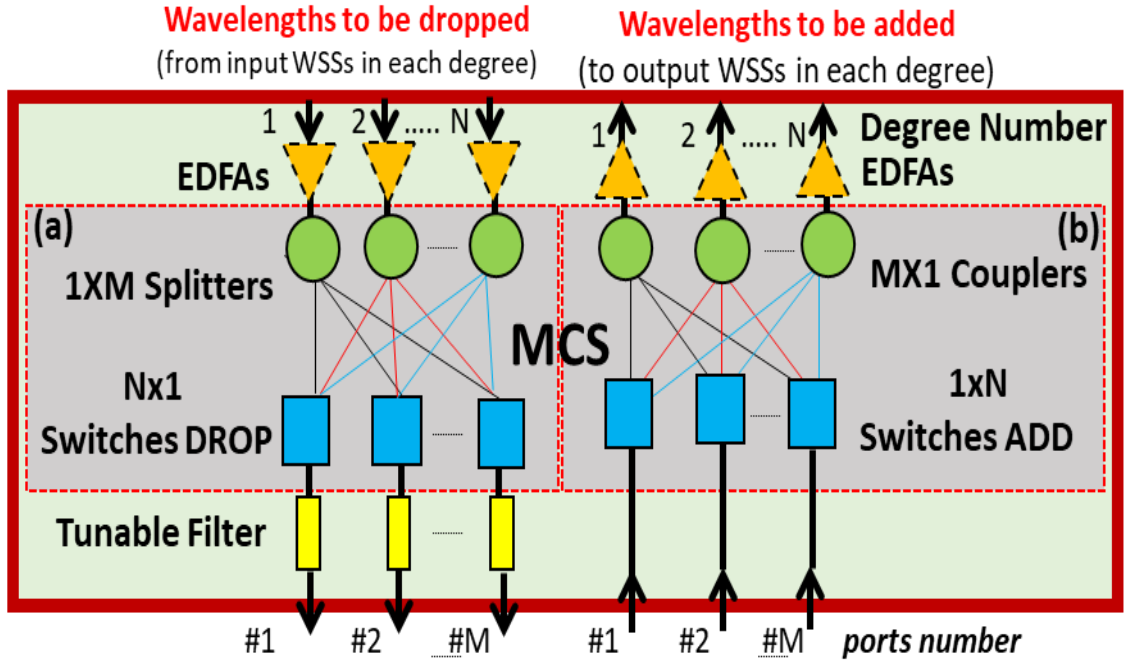

Fig. 3.12 A Multicast Switch Archeticture in CDC ROADM (a) Drop port (b) Add Port

Existing ROADMs and the emerging advances in ROADM technology mainly target long haul optical backbone networks and only provide advanced wavelength level switching functionalities in term of the aforementioned colourlessness, directionlessness, contentionlessness and also WDM gridlessness. As a direct result of such course wavelength-level switching functions and their associated high equipment costs, these ROADMs are therefore incompatible with cost sensitive CANs. As such, cost-effective ROADMs that can provide flexible channel switching at the wavelength level and sub-wavelength levels and that are fully compatible with SDN-based network control are an essential required for implementing highly reconfigurable, elastic and transparent CANs.

3.3.2   Soft-ROADMs for CANs

As mentioned in the above section the existing ROADMs are not suitable for CAN applications as they only provide advanced wavelength level switching functionalities and do not have sufficiently low cost. Therefore, new ROADMs, termed here as soft-ROADMs [19-21], have been proposed with low cost DSP-enabled optical-domain add/drop operations

that can provide flexible channel switching at the wavelength, sub-wavelength and orthogonal sub-band levels and that are fully compatible with SDN-based network control. The soft-ROADMs are considered an essential requirement for implementing highly reconfigurable, elastic and transparent CANs. The soft-ROADM operations are independent of the underlying signal and channel characteristics, so they are highly versatile in their applications. They also have very simple architectures, comprising of passive OC -based add elements and IM-based drop elements without incorporating either costly narrowband optical tuneable bandpass-filters (OTBPFs) or O-E-O signal conversions [19-21]. Enabled by DSP, the soft-ROADM provides the aforementioned SDN-controllable, dynamic and flexible optical switching at wavelength, sub-wavelength and spectrally-overlapped orthogonal sub-band levels, in IMDD-based DFMA CANs and/or PONs.

3.3.2.1 Soft-ROADM application in CANs

The CAN optical layer consists of three distinct channel levels. The top level is the wavelength level as in a typical WDM-based optical network, with each wavelength consisting of two different sub-levels of sub-channels[22, 23], the upper sub-level consists of multiple sub-wavelength (Sub-λ) bands located at different RF center frequencies (CFs), and the lower sub-level is formed by each Sub-λ band consisting of two spectrally overlapped orthogonal sub-bands (Sub-B) with their associated RF carriers located at the same CF but with a relative phase difference of 90°, these sub-bands are therefore orthogonal and are denoted as I and Q (In/Quadrature-phase). A full explanation of the generation of the digital orthogonal filtering-multiplexed Sub-λ and Sub-B channels is presented in section 3.2.1.1. Fig. 3.13 illustrates an example of a CAN employing soft-ROADM-based channel switching at all of the aforementioned three channel levels. The soft-ROADM providing on-line reconfigurable connectivity between an OLT in the central office and various ONUs to transparently support both fixed and/or mobile traffic as shown in Fig. 3.13. The CAN is also able to dynamically provision fronthaul links between BBUs and RRHs physically located at different sites in the CAN.
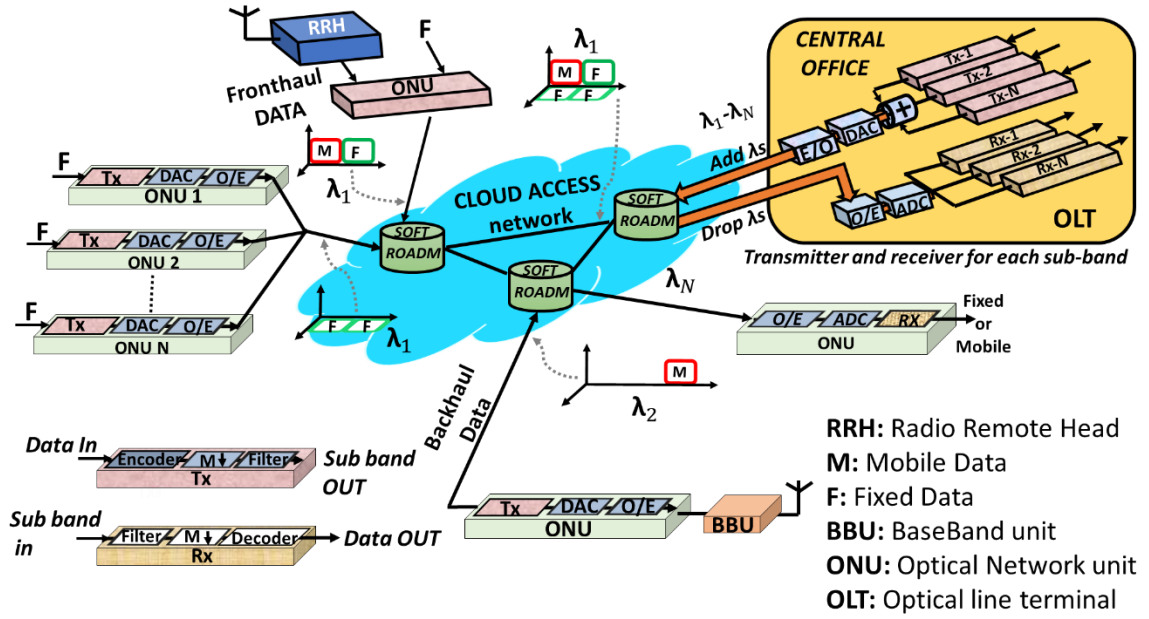
Fig. 3.13 DSP enabled soft-ROADMs in a cloud access network.

Although 5G is just one of many network scenarios supported by the CAN, it is important to highlight some key features of the digital orthogonal filter-based channel multiplexing technique and the soft-ROADM-enabled channel switching technique to illustrate the potential performance characteristics of a CAN and thus the alignment with the targeted requirements of 5G mobile networks:

- *Higher system capacity:* The technique can support a large number of aggregated elastic channels, which is highly scalable. The soft-ROADM can also transparently accommodate different channel bandwidths achieved using various signal modulation formats including advanced modulation formats with high spectral efficiency. The wide channel bandwidth dynamic range with fine granularity allows more efficient use of the available network resources as statistical multiplexing can be fully exploited. The bandwidth of available ADC/DACs is perhaps the key bottleneck in terms of maximum per wavelength capacity, however the latest generation of converter technologies offers sampling rates in excess of 100GS/s.

- *Massive device connectivity*: The highly elastic channels with fine granularity, combined with inherent transparency to multiple access techniques and modulation formats, allows for a high count of low bandwidth connections.

- *Reduced latency*: As the soft-ROADM operates purely in the optical domain, the soft-ROADM operation-induced latency can be considered as negligible.

- *Low-cost*: The soft-ROADMs completely avoid expensive and bulky optical filters and O-E-O conversions, which significantly reduces overall cost.

- *Energy saving*: The data carrying signals do not require conversion and processing in the electrical domain in order to add and drop sub-wavelength/sub-band channels, consequently this results in a huge saving in power consumption, as high speed electronic switching circuits are completely eliminated.

It is also interesting to highlight the backwards compatibility of the soft-ROADM with existing ITU-T and IEEE standards-based networks and transmission technologies, which permits a gradual migration to a CAN from the existing networks. There are three key aspects of backwards compatibility to highlight, i) full compliance with the ITU-T WDM grid which allows interoperability with conventional fixed-grid ROADMs, ii) whole wavelengths can be added and dropped allowing wavelengths carrying conventional optical signals to be switched by the soft-ROADM, and iii) the channels are transparent to modulation format so signals adopting standardized modulation formats can be transported. More specifically, the soft-ROADM in combination with a CDC architecture is also expected to be compliant to the ITU-T G.672 multi-degree ROADM characteristics at wavelength level.

3.3.2.2 Soft-ROADM top-level architecture

In the soft-ROADM, as illustrated in Fig. 3.14, the incoming WDM optical signal at the aggregated input port is first demultiplexed into separate wavelengths via an AWG. Each wavelength is split into two parts via an optical splitter, the first part of each wavelength then passes through a drop element, where a targeted Sub-B (TSB) channel can be dropped to a drop port. Multiple drop elements are thus required for each wavelength, however the drop elements are colourless so all drop elements are identical. The second part of the wavelength then passes through an add element, where one or more channels, fed into an add port, can be added to the pass-through channels, before multiplexing the wavelength into the WDM output signal via an AWG. Similar to conventional ROADMs, additional WDM demux/mux can also be implemented at the add/drop ports. The architecture in Fig. 3.14 depicts the West-East traffic direction, however the East–West direction would be implemented in a similar manner forming a 2-degree ROADM. As the soft-ROADMs would typically be configured in a ring architecture, as shown in Fig. 3.13, 2-degrees of switching is sufficient to allow low cost, flexible and dynamic allocation of the aggregated ring capacity throughout the CAN.

It is perfectly feasible, however, to construct multi-degree soft-ROADMs by employing a B&S architecture [35] in the express paths based on 1xN (N = degree) PSs and WSSs. Furthermore, the B&S architecture inherently supports directionless operation. Generally speaking, the soft-ROADMs in combination with the CDC architecture can support similar wavelength-level network performances as conventional ROADMs. However, it should be emphasised that soft-ROADMs are designed to provide optical add/drop operations at sub-wavelength and/or sub-band levels, which provide fine granularity, elastic sub-channels below the wavelength level, essential for the targeted CAN applications.
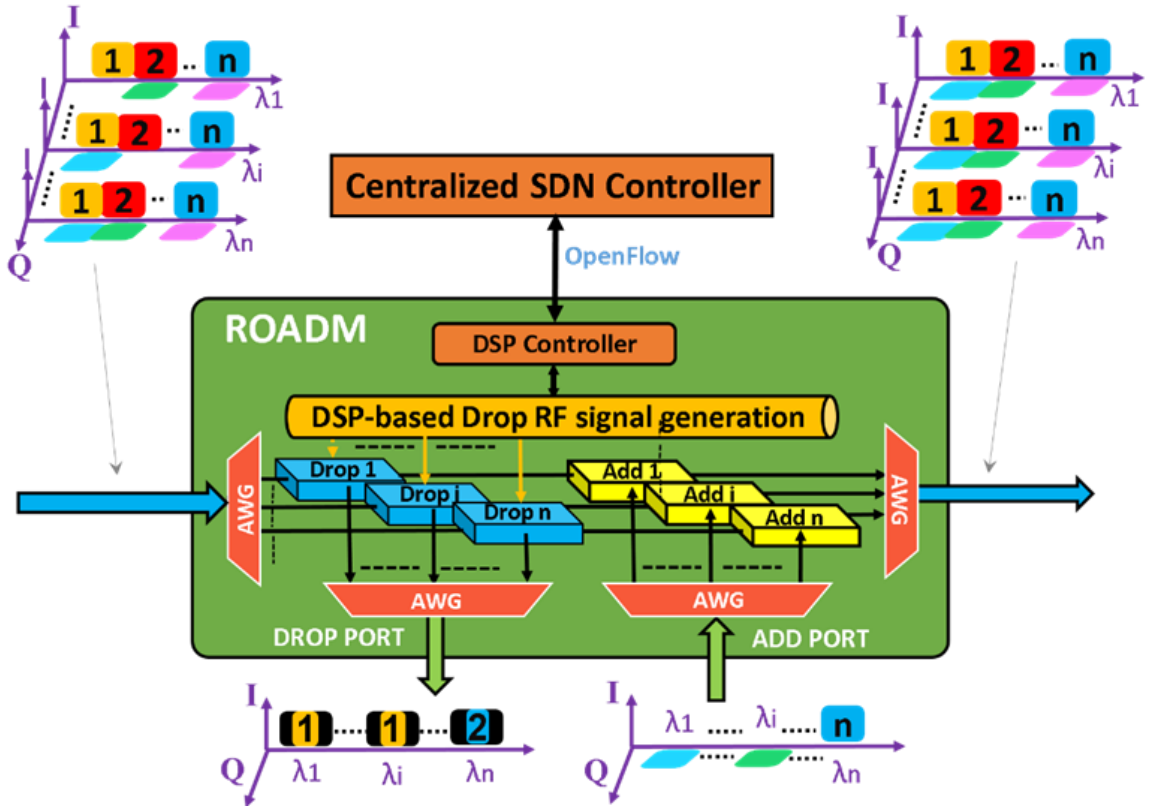
Fig. 3.14 Block diagram of basic soft-ROADM architecture..

The use of AWGs, as shown in Fig. 3.14, makes the soft-ROADM colourless at sub-wavelength levels only, however, utilizing WSSs would achieve colourlessness at the wavelength level also. Furthermore, as the contentionless feature is controlled by the SDN control plane, it is thus feasible to implement soft-ROADMs with CDC functionality. To dynamically configure the required network interconnectivity, a centralized SDN controller communicates, via a protocol such as extended OpenFlow, with embedded DSP controllers in the soft-ROADMs and the terminal equipment transceivers (TETs). The required signalling channel could be implemented as an optical supervisory channel (OSC) carried

by a dedicated wavelength outside the WDM wavelength band, as is the case in conventional ROADM technologies. Alternatively, a low bandwidth sub-band channel embedded in a multi-channel wavelength could potentially be employed as the signalling channel.

Network latency is a critical factor in CANs supporting 5G traffic. Minimisation of network latency can be achieved by employing soft-ROADMs with a CDC architecture in combination with a low latency enabled control plane such as a hierarchical SDN control architecture[24, 25]. It is also important to highlight the fact that the drop and add elements each impose a 3dB loss in optical power on the pass-through wavelengths, the combined 6dB loss is however comparable to a conventional ROADM. This implies that the scalability of the soft-ROADM is similar to the conventional ROADM. However, the performance of concatenated soft-ROADMs is still an important area to be studied to assess for example i) the trade-off between the number of concatenated soft-ROADMs and the overall CAN performance, and ii) the need and application of optical amplifiers in various CAN scenarios.

Other practical factors influencing the scalability of the soft-ROADM architecture are also important to consider. For a specific application scenario, the maximum wavelength count is only restricted by the employed AWG or WSS devices. The aggregated signal bandwidth is ultimately limited by the bandwidth of the DAC/ADCs embedded in the TETs, as discussed in section 3.2.2.2. Maximum Sub-λ channel count on a single wavelength is limited by DSP implementation complexity in the TETs, however, the DSP complexity due to the channel filtering does not scale linearly with channel count [36], in fact DSP complexity can reduce with channel count as each transceiver processes a narrower bandwidth channel. For the case of a soft-ROADM dropping multiple channels to a PON with multiple ONUs, the ONU-count dependent performance of the PON has been investigated in [17] which showed that aggregated PON capacity is virtually independent of ONU-count and minimum received optical power increases by 1.7 dB when the number of ONUs is doubled, which is very similar to that observed in orthogonal frequency-division multiple access (OFDMA) PONs.

3.3.2.3 Add Operation Principle

A simple passive OC performs the add operation by simply adding the involved channels passively in the optical domain. Fig. 3.15 illustrates two representative examples of different add operation cases. An SDN controller configures the associated TETs' DSP to locate their

channel(s) at a free location(s) in a specific wavelength's digital filtering space to avoid possible channel contention in the add element. A two-port optical coupler would be utilized to add the soft-ROADM's pass-through optical signal to a single tributary input signal as shown in Fig. 3.15(a). It is also feasible to use a multi-port coupler to add multiple signals simultaneously to the pass-through signal, thus providing a soft-ROADM with multiple add ports, as shown in Fig. 3.15(b). Furthermore, the tributary input signal(s) to be added can consist of multiple channels, as the centralised SDN-controller ensures the corresponding wavelength has free channel spaces in the aggregated soft-ROADM input signal.
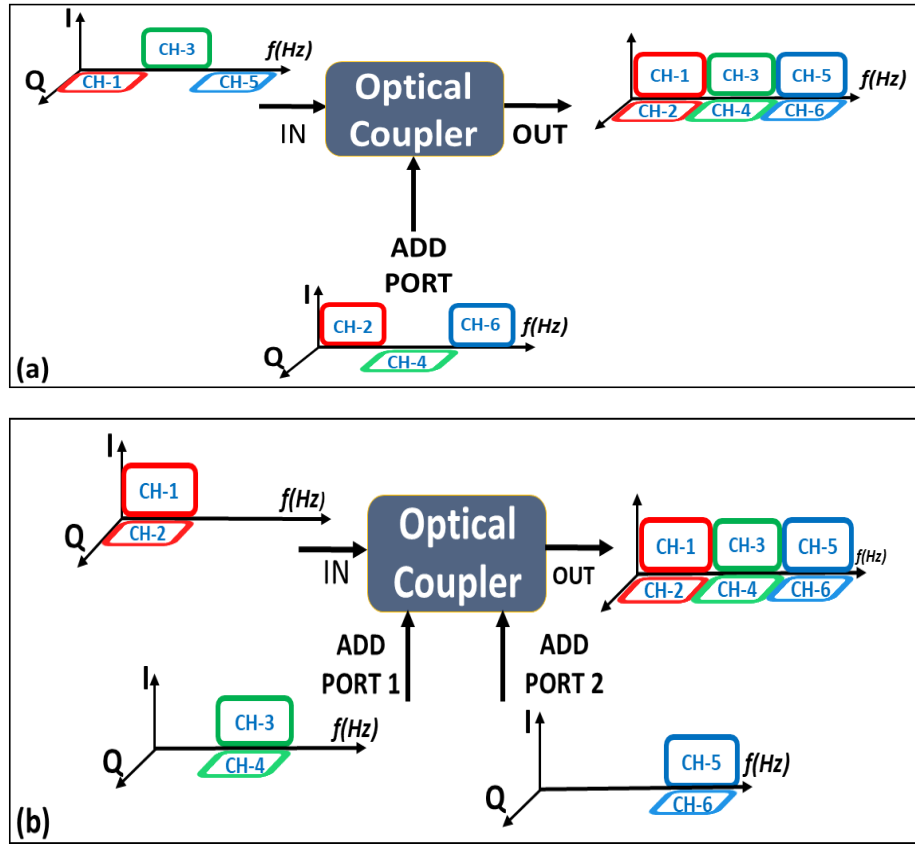
Fig. 3.15 Add operations with example signal spectra. (a) Sub-B add operation with single add port, (b) Sub-λ add operation with multiple add ports

Optical couplers characteristically support a wide range of operating wavelengths, thus a single OC component type can be utilised for the soft-ROADM add element of all WDM wavelengths. This facilitates a cost saving advantage due to the associated reduction in component inventory. It should also be noted that the soft-ROADM add operation-induced time delay is negligible which is also highly advantageous when considering the low latency requirements of 5G mobile connections.

3.3.2.4 **Drop Operation Principle**

In the soft-ROADM drop operation element, as shown in Fig. 3.16, a 'drop and continue' configuration is adopted as an optical splitter divides the incoming optical signal of a single wavelength into two parts, as mentioned above, one signal passes via an add operation element to form the outgoing signal and the other signal is fed to an optical IM in order to drop the TSB. By driving the IM with a local oscillator (LO)-generated sinusoidal drop RF signal which has both its frequency and phase matched to the TSB, the TSB is down-converted to the baseband spectral region at the IM's output with a spectral reversal occurring. As all Sub-Bs are frequency shifted by $\pm f_{LO}$, where f_{LO} is the LO frequency, the non-targeted Sub-Bs become ruined and thus are unrecoverable Sub-Bs (RUSBs) [20, 21] at the output of the drop operation element, these RUSBs are easily eliminated by simple analogue or digital filtering after O-E conversion with similar performances achieved by both filter types[34]. The drop element also has the capability to provide full wavelength level drop functionality simply by driving its IM with a suitable bias voltage and switching off the drop RF signal, the IM then acts as an optical passway.
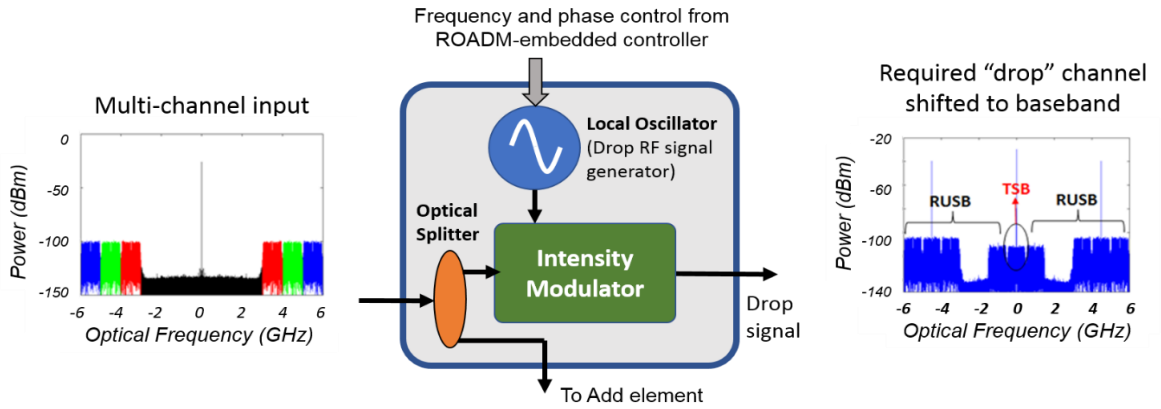
Fig. 3.16 Soft-ROADM drop element structure with example input and output signal spectra relative to carrier. (TSB: Targeted sub-band. RUSB: Ruined and unrecoverable sub-bands)

The remote SDN controller manages the soft-ROADM-embedded controller to set the drop RF signal's frequency and phase [19]according to the channel to be dropped. Fine tracking adjustments of the drop RF signal can be made using pilot signals for detecting optimum performance. The dropped channel's receiver DSP then compensates for the spectral reversal. As the two orthogonal channels have an effective relative phase of 90°, the drop RF signal phase is simply altered by 90° to select the I or Q channel. Some example signal

spectra before and after the drop operation are shown in Fig. 3.16 for an optical wavelength supporting 6 channels. To optimize drop channel performance, the optical signal-to-noise ratio (OSNR) of the dropped signal has to be maximized, this can be conducted by optimising the drop RF signal power[19]. The drop elements 'drop and continue' configuration importantly minimises cost by avoiding optical filtering, but it also allows a multicast function whereby a channel employing different signal modulation formats and multiple access techniques can be dropped at multiple soft-ROADMs and shared by users at different locations in the CAN. Also, due to the low filter complexity enabled, large digital filter space and the fact that the number of cascaded soft-ROADMs in a CAN would not be so high, the non-reuse of channels is not a significant issue for representative application scenarios, as the capacity allocation in the CAN is highly flexible and elastic allowing efficient use of the available filtering space.

Apart from the advantages easily seen from the above description, another advantageous feature of the drop operation is a significant relaxation of required receiver component bandwidths and digital filter complexity, this results in cost and power savings as the receiver detecting the dropped Sub-B only needs to support the channel bandwidth and not the aggregated signal bandwidth. The reduced operating bandwidth can be highly significant, particularly in terms of reducing DAC sample rate requirements and DSP processing power requirements. In a typical CAN the soft-ROADM's drop signals can feed an entire network, thus all ONUs on the network can benefit from the drop operation-induced reduction in operating bandwidth. Furthermore, another key advantage is that the CAN capacity can be incrementally increased by adopting additional channels when required, thus increasing the aggregated bandwidth without the need to upgrade the ONU receivers as the channel bandwidth is unchanged. It should also be noted that, similar to the add operation, the soft-ROADM drop operation-induced latency is also negligible, which is highly advantageous for supporting 5G mobile connections.

References

[1]   J. M. Senior, P. Kourtessis, M. Milosavljevic, and W. Lim, "OFDMA-PON for future generation metro-access networks," 2012 Photonics Glob. Conf. PGC 2012, no. 248654, pp. 1–5, 2012.

[2]   J. I. Kani, S. Kuwano, and J. Terada, "Options for future mobile backhaul and fronthaul," Opt. Fiber Technol., vol. 26, pp. 42–49, 2015.

[3]   E. Al-Rawachy, R. P. Giddings, and J. M. Tang, "Real-time experimental demonstration of DSP-enabled soft-ROADMs with multi-level flexible add/drop functions for cloud access networks," Opt. Express, vol. 27, no. 1, p. 16, 2019.

[4]   R. Giddings, "Real-time digital signal processing for optical OFDM-based future optical access networks," J. Light. Technol., vol. 32, no. 4, pp. 553–570, 2014.

[5]   M. Morant, T. M. F. Alves, R. Llorente, and A. V. T. Cartaxo, "Broadband impairment compensation in hybrid fiber-wireless OFDM long-reach PONs," J. Light. Technol., vol. 32, no. 7, pp. 1387–1393, 2014.

[6]   Peter J. Winzer, "Advanced modulation formats for high-bit-rate optical networks," J. Light. Technol., vol. 24, no. 12, 2006.

[7]   I. Morita, "Advanced modulation format for 100-Gbit/s transmission," LEOS Summer Top. Meet., vol. 3, pp. 252–253, 2007.

[8]   J. Wei, Q. Cheng, R. V. Penty, I. H. White, and D. G. Cunningham, "400 Gigabit Ethernet using advanced modulation formats: Performance, complexity, and power dissipation," IEEE Commun. Mag., vol. 53, no. 2, pp. 182–189, 2015.

[9]   J. Tang et al., "Real-Time Optical OFDM Transceivers for PON Applications," 2011 Opt. Fiber Commun. Conf. Expo. Natl. Fiber Opt. Eng. Conf., p. OTuK3, 2013.

[10]   J. D. Ingham, R. Penty, I. White, and D. Cunningham, "40 Gb/s Carrierless Amplitude and Phase Modulation for Low-Cost Optical Datacommunication Links," 2011 Opt. Fiber Commun. Conf. Expo. Natl. Fiber Opt. Eng. Conf., p. OThZ3, 2013.

[11]   X. Li, "Simulink-based Simulation of Quadrature Amplitude Modulation (QAM) System," Proc. IAJC-IJME Int. Conf. …, vol. 11, 2008.

[12]   K. Szczerba et al., "4-PAM for High-Speed Short-Range Optical Communications," J. Opt. Commun. Netw., vol. 4, no. 11, p. 885, 2012.

[13]   R. Giddings, X. Duan, E. Al-Rawachy, and M. Mao, "A Review of DSP-based enabling technologies for Cloud Access Networks," Futur. Internet, vol. 10, no. 11, 2018.

[14]   Z. Lin, X. Du, H. H. Chen, B. Ai, Z. Chen, and D. Wu, "Millimeter-wave propagation modeling and measurements for 5g mobile networks," IEEE Wirel. Commun., vol. 26, no. 1, pp. 72–77, 2019.

[15]   P. Popovski, K. F. Trillingsgaard, O. Simeone, and G. Durisi, "5G wireless network slicing for eMBB, URLLC, and mMTC: A communication-theoretic view," IEEE Access, vol. 6, pp. 55765–55779, 2018.

[16]   M. Bolea, R. P. Giddings, and J. M. Tang, "Digital orthogonal filter-enabled optical OFDM channel multiplexing for software-reconfigurable elastic PONs," J. Light. Technol., vol. 32, no. 6, pp. 1200–1206, 2014.

[17]   M. Bolea, R. P. Giddings, M. Bouich, C. Aupetit-Berthelemot, and J. M. Tang, "Digital Filter Multiple Access PONs With DSP-Enabled Software Reconfigurability," J. Opt. Commun. Netw., vol. 7, no. 4, p. 215, 2015.

[18]   M. Svaluto Moreolo et al., "SDN-Enabled Sliceable BVT Based on Multicarrier Technology for Multiflow Rate/Distance and Grid Adaptation," J. Light. Technol., vol. 34, no. 6, pp. 1516–1522, 2016.

[19]   W. Jin et al., "DSP-Enabled Flexible ROADMs Without Optical Filters and O-E-O Conversions," J. Light. Technol., vol. 33, no. 19, pp. 4124–4131, 2015.

[20]   E. AL-Rawachy, R. P. Giddings, and J. M. Tang, "Experimental Demonstration of Cross-Channel Interference Cancellation for Digital Filter Multiple Access PONs," vol. 25, no. 4, p. Th3C.5, 2016.

[21]   J. Berthold, S. Member, A. A. M. Saleh, L. Blair, J. M. Simmons, and S. Member, "Optical Networking : Past , Present , and Future," J. Light. Technol., vol. 26, no. 9, pp. 1104–1118, 2008.

[22]   A. A. Saleh and J. M. Simmons, "All-Optical Networking-Evolution , Benefits , Challenges , and Future Vision," Proc. IEEE, 2012.

[23]   J. M. Simmons, "Optical Network Design and Planning," Springer, 2014.

[24]   M. M. A. Eid, "Optical Add Drop Multiplexers with UW-DWDM Technique in Metro Optical Access Communication Networks," Int. J. Comput. Sci. Telecommun., vol. 2, no. 2, pp. 5–13, 2011.

[25]   M. Kagawa, H. Tsukada, and M. Yoneda, "Optical add-drop multiplexers for metro/access networks," Furukawa Rev., no. 23, pp. 59–64, 2003.

[26]   A. Tzanakaki, I. Zacharopoulos, and I. Tomkos, "Optical add/drop multiplexers and optical cross-connects for wavelength routed networks," Int. Conf. Transparent Opt. Networks, vol. 1, pp. 41–46, 2003.

[27]   P. Pavon-Marino and M. V. Bueno-Delgado, "Dimensioning the Add/drop contention factor of directionless ROADMs," J. Light. Technol., vol. 29, no. 21, pp. 3265–3274, 2011.

[28]   N. A. A Boskovic, M Sharma, "Broadcast and select OADM nodes application and performance trade-offs," in Optical Fiber Communication Conference. Optical Society of America, 2002, pp. 65–66.

[29]   M. Filer and S. Tibuleac, "N-degree ROADM architecture comparison: Broadcast-and-select versus route-and-select in 120 Gb/s DP-QPSK transmission systems," Conf. Opt. Fiber Commun. Tech. Dig. Ser., no. c, pp. 14–16, 2014.

 [30]   H. Yang, B. Robertson, P. Wilkinson, and D. Chu, "Low-Cost CDC ROADM Architecture Based on Stacked Wavelength Selective Switches," J. Opt. Commun. Netw., vol. 9, no. 5, p. 375, 2017.

[31]   K. Suzuki, K. Seno, and Y. Ikuma, "Application of Waveguide/Free-Space Optics Hybrid to ROADM Device," J. Light. Technol., vol. 35, no. 4, pp. 596–606, 2017.

[32]   S. Gringeri, B. Basch, V. Shukla, R. Egorov, and T. Xia, "Flexible architectures for optical transport nodes and networks," IEEE Commun. Mag., vol. 48, no. 7, pp. 40–50, 2010.

[33]   W. I. Way, "Next Generation ROADM Architectures," Asia Commun. Photonics Conf., p. AS1G.3, 2012.

 [34]   Jin, W. Zhang, C., Duan, X., Kadhum, M. R., Dong, Y. X., Giddings, R. P., ... & Tang, J. M. "Improved Performance Robustness of DSP-Enabled Flexible ROADMs Free from Optical Filters and O-E-O Conversions," J. Opt. Commun. Netw., vol. 8, no. 8, p. 521, 2016.

[35]   W. I. Way, "Optimum Architecture for M×N Multicast Switch-Based Colorless, Directionless, Contentionless, and Flexible-Grid ROADM," in National Fiber Optic Engineers Conference. Optical Society of America, 2012, p. NW3F.5.

 [36]   R. M. Dorward, M. J. Anderson, and R. P. Giddings, "Technical and market feasibility of high-speed software-reconfigurable OOFDM/DFMA-based Optical transceivers for Next Generation Access Network PONs," Int. Conf. Transparent Opt. Networks, vol. 2016-Augus, pp. 1–4, 2016.

4. Channel Interference in DFMA PON-based CANs

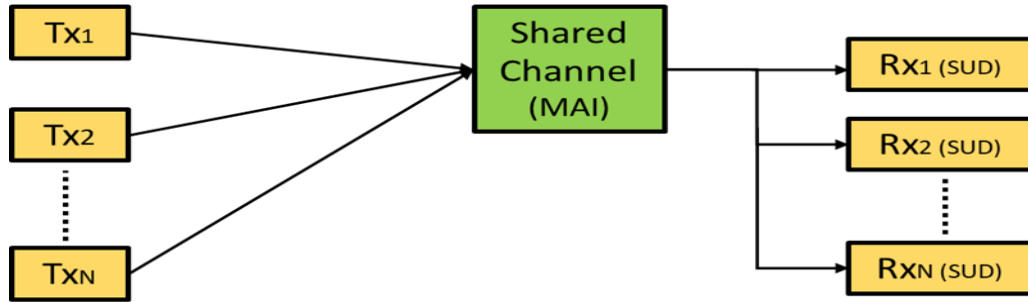## *Contents*

4.1 **Multiple Access Interference**

Fig. 4.1 General system using shared transmission medium resulting in MAI

Multiple access interference (MAI), as illustrated in Fig. 4.1, refers to the interference between users accessing and sharing the same channel to reach the targeted user. In other words, the MAI problem occurs due to power leakage to/from different users caused by other users' transmissions when multiuser environments are considered. MAI manifests mainly in communication systems employing orthogonal signals, such as Code Division Multiple Access (CDMA) and OFDM. For example, OFDM systems are highly susceptible to carrier frequency offset (CFO) and symbol timing offset (STO). The CFO occurs due to the frequency mismatch between RF oscillators which causes synchronization errors between different transmitters and receivers, and wireless channel induced Doppler shifts for mobile users. STO is caused by the finite accuracy of the employed symbol alignment alogorithms, resulting in non-perfect symbol alignment. The effect of CFO and STO is orthogonality degredation between subcarriers which leads to inter carrier interference (ICI). Channel fading, CFO and STO constitute the most important effects that are responsible for interference generation and, more specifically, for the ICI effect in OFDM systems [1, 2]. MAI can also occur in multiple access systems using non-orthogonal signals such as WDM systems. Kerr effect-induced nonlinearities occur when multiple optical wavelengths propagate through the same fibre, for example cross-phase modulation (XPM), causes one optical wavelength to affect the phase of another optical wavelength, thus leading to interference [2].

When considering the downlink case in a multi-access system as the signals are multiplexed for all users and sent by the same transmitter (e.g. a base station) it is possible to maintain the orthogonality between the subcarriers. Downlink MAI can, therefore, be avoided by

preserving a tight frequency and time synchronization at the transmitter. For the more challenging uplink scenario, the MAI effect is present due to the different CFOs and STOs between users. In this case, there are two different approaches for minimising MAI, feedback and compensation [1]. In the feedback case the frequency synchronization (symbol alignment) is accomplished using CFO (STO) feedback from the uplink receiver to the multiple users in order to allow regular adjustments to the users' transmitter frequency offsets (symbol timing). The compensation method requires advance signal processing techniques to compensate the ICI between multiple users and it can be necessary to use interference cancellation techniques to sufficiently reduce MAI-induced ICI between users.

For a more in-depth look at MAI, a generic orthogonal channel-based system will be taken as an example. In orthogonal systems, MAI is the result of the random time and frequency offsets between signals [3, 4] which makes it impossible to design the data carrying waveforms to be completely orthogonal. MAI consequently limits the capacity and overall system performance. The conventional single user detector (SUD) deals only with its own signal and treats other users as noise. Therefore, MAI cannot be suppressed by the conventional SUD [1] and the input received signal *r(t)* to the SUD is given by:

$$r(t) = \sum_{k=1}^{K} A_k(t) S_k(t) b_k(t) + n(t) \qquad (4.1)$$

where $A_k(t)$, $S_k(t)$, $b_k(t)$ and *n(t)* are the amplitude, orthogonal waveform, modulated data of the kth user and channel noise respectively. A diagram of a conventional orthogonal system detector, based on multiple correlators, is depicted in Fig. 4.2. The conventional orthogonal system detector applies the following processes: firstly, the orthogonal reference waveform of each user, as used in the transmitter, is regenerated at the receiver. Secondly, the regenerated orthogonal reference waveforms are correlated with the input received signal by using a bank of correlators, which consist of multiply and integration functions, with a separate correlator required for each user. Finally, after sampling the correlated signal at the appropriate bit/symbol times, the decision will be taken independently for each user resulting in either a single bit value or one of multiple symbols being determined.
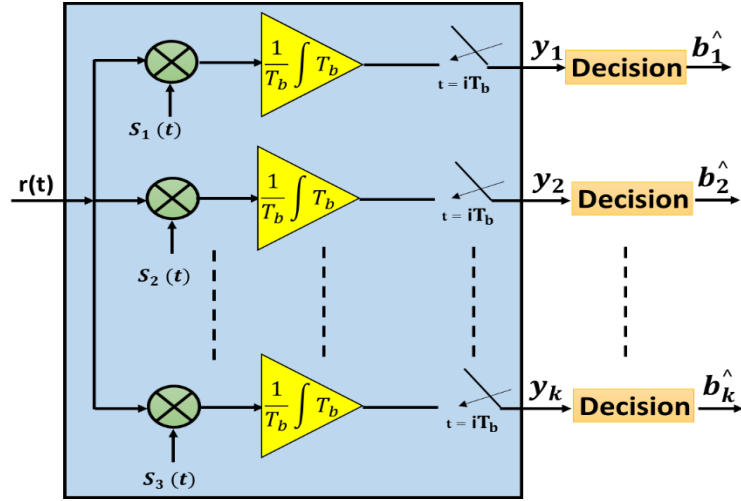
Fig. 4.2 The conventional correlation-based detector

In the detector, as a user's signal auto-correlates with it's orthogonal waveform it recovers the user data. However, MAI is generated when a user's data is cross-correlated with the other users' orthogonal waveforms, as they are not perfectly orthogonal. MAI will thus also increase with the number of users. The generation of the required data signal and the MAI is shown in Eq.(4.2) [3]. Whereas Y_k is the output of the kth correlator.

$$Y_k = \frac{1}{T_b} \int_0^{T_b} r(t) S_k(t) dt$$

$$Y_k = \frac{1}{T_b} \int_0^{T_b} \left[\sum_{j=1}^{K} A_j b_j S_j(t) + n(t) \right] S_k(t) dt$$

$$Y_k = A_k b_k + \sum_{\substack{j=1 \\ j \neq k}}^{K} P_{jk} A_j b_j + \frac{1}{T_b} \int_0^{T_b} S_k(t) n(t) dt \qquad (4.2)$$

Where
$$P_{kj} = \frac{1}{T_b} \int_0^{T_b} S_k(t) S_j(t) dt \qquad (4.3)$$

The first, second and third terms on the right of Eq.(4.2) represent the recovered user signal, the MAI signal and the correlation with the channel noise, respectively, for the kth user. The MAI term results from the cross-correlations of the orthogonal reference waveform of the kth user and the other users. The orthogonal reference waveforms are designed to minimise the cross-correlation elements, however in practice the cross-correlation will have a finite value. To recover the user's data the decision function simply selects the bit/symbol nearest to the detector's output. When the received power from different users can vary, clearly the

low signal power users suffer more MAI interference effect than the higher power signal users [3]. To solve the MAI problem present in SUDs, multi-user detectors (MUD) emerged to improve the system's capacity and performance by supressing the MAI interference. The MUD operates by detecting all users' data, which is then exploited to mitigate the MAI effect. As a result, the MUD implementation has a higher complexity than the SUD [5].

4.2 The Cross-Channel Interference Effect in DFMA-based Systems:

As decribed in section 3.2.2, the DFMA technique employs a channel-multiplexing operation which can be implemented in the digital or optical domain typically corresponding to point-to-point or multipoint-to-point architectures respectively. A full mathematical description and examples of the system are covered in detail in section 3.2.2.1 in terms of the ideal channel case. When the channel is ideal, during transmission perfect orthogonality between the spectrally overlapped orthogonal channels is preserved. The aforementioned ideal channel is characterised by a flat frequency response, and there is no channel frequency response roll-off effect.

(a)   *(b)*

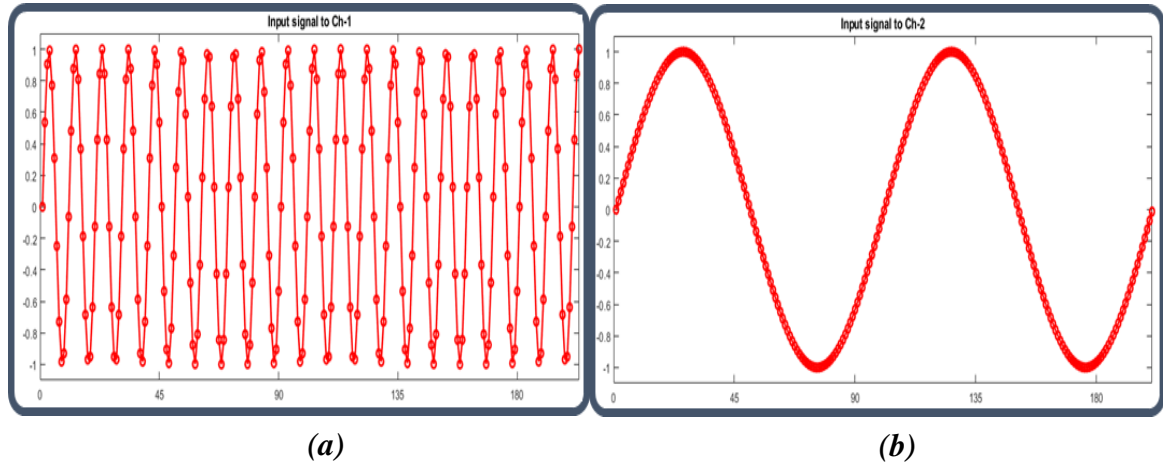*Fig. 4.3 Sinusoidal input signals of a) A high frequency b) A low frequency*

The following examples show the impact of the physical channel frequency response-induced loss of channel orthogonality and the subsequently generated CCI, for the cases of systems with ideal and non-ideal channel frequency responses. A 2-channel system is employed with input signals, shown in Fig. 4.3 (a,b), applied in both cases. Firstly, the case

of a system with an ideal physical channel is considered, as illustrated in Fig. 4.5. The sinusoidal input signals, shown Fig. 4.3 (a,b), are first up-sampled a factor of 2 by inserting a zero-valued sample between two successive samples. The up-sampled signals are each applied to orthogonal shaping filters. The discrete impulse responses of the shaping filters forming a Hilbert-pair in the transmitter are shown in the Fig. 4.4 (a,c). As a result two channels with 90° phase shift difference between them, referred to as cosine and sine channels are generated, as shown in Fig. 4.5 (a,b) respectively. The two digitally filtered channels are then directly added as shown in Fig. 4.5 (e). Here it is important to highlight that the Hilbert-pair shaping filters main function is to create the orthogonality between the multiplexed channels. Therefore, non-zero samples output from any channel's filter coincide with the zero-valued samples output from the orthogonal channel's filter, as depicted in Fig. 4.5 (c) and also the magnified figure in Fig. 4.5 (d). The multiplexed channels are then transmitted through a channel with a flat frequency response and no phase distortion, thus there is no channel frequency response roll-off.
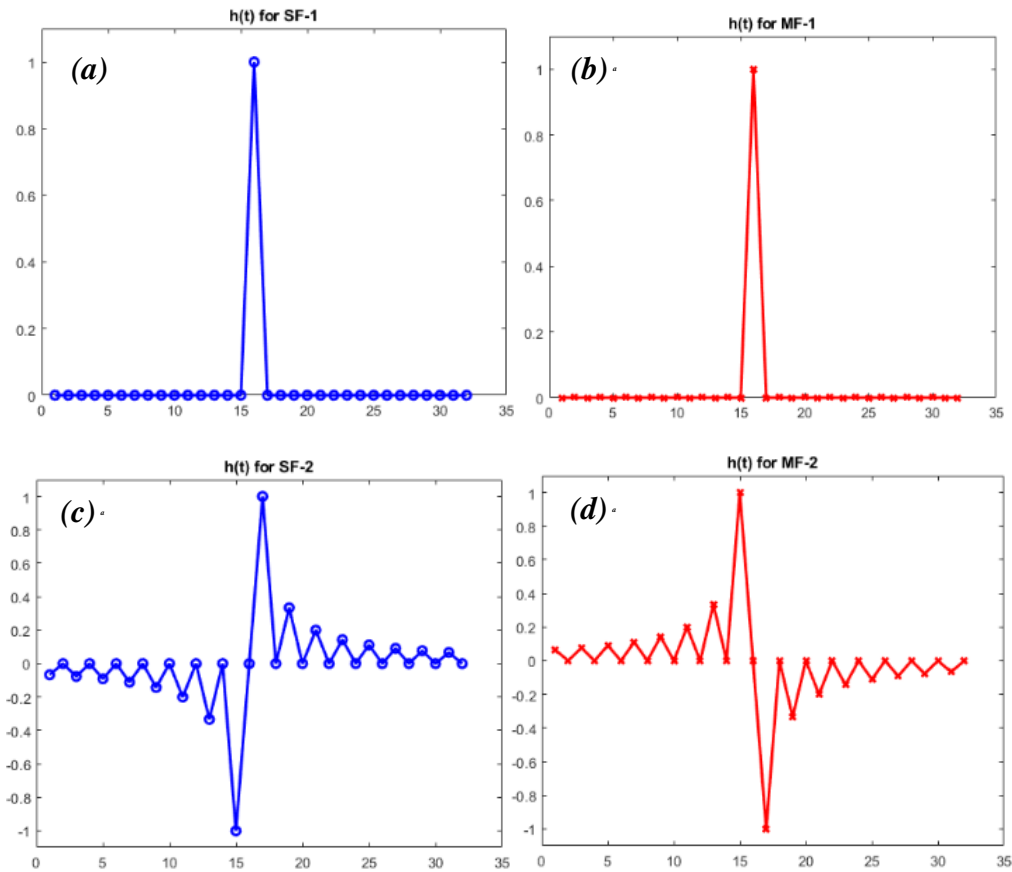
Fig. 4.4 The impulse responces of the filters a) Shaping Cosine Filter, b) Matching Cosine Filter, c) Shaping Sine Filter, d) Matching Sine Filter.
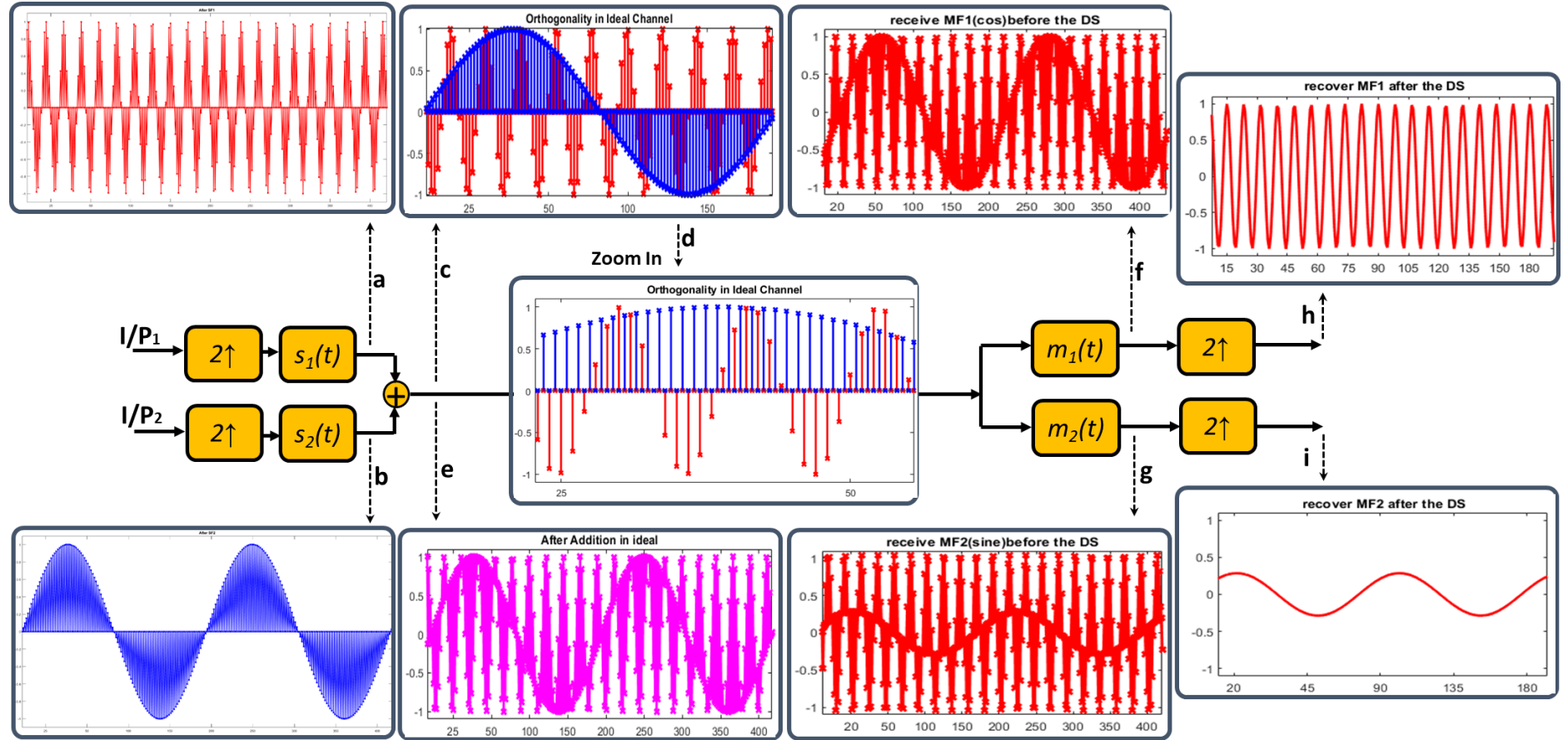
Fig. 4.5 Various signals in a 2-channel system with an ideal channel a) the upsampled high frequency signal after the Cosine shaping filter, b) the upsampled low frequency signal after the Sine shaping filter, c) the overlaid summed signal, d) zoomed version of the overlaid summed signal, e) the summed signal, f). signal after Cosine matching filter, g) signal after Sine matching filter, h) the high frequency recoverd signal, i) the low frequency recoverd signal

In the receiver side, the matching filters detect the corresponding target signal as in Fig 4.5 (f,g) followed by the 2x down sampling process to recover the targeted signals as show in Fig 4.5 (h,i). The matching filter $m_1(t)$ is used to detect the high frequency signal while the matching filter $m_2(t)$ is used to detect the low frequency signal. The matching filters' impulse responses are depected in Fig 4.4 (b,d). The recovered signals show no CCI as depicted in Fig. 4.5 (h,i), which are the same as the input signals in Fig. 4.3(a,b) respectively.

The DFMA system performance is highly reliant on the preservation of spectrally overlapped channel orthogonality which can be dependent on effects such as component and physical channel frequency responses as well as the nonlinearities mainly associated with optical signal transmission. CCI occurs when channel orthogonality is not perfect, and the CCI level increases as the level of channel orthogonality decreases. The CCI effect leads to reduced system performance due to the unwanted signal leakage between orthogonal channels. In a real transmission system, the overall physical channel frequency response between the digital transmitter-side and digital receiver-side must be considered, which includes all RF and optical componets, and typically exhibits a significant frequency response roll-off characteristic, i.e. physical channel attenuation increases with frequency. The frequency response roll-off effect is a major contributor to loss of channel orthogonality and is mainly attributed to: i) the sin(x)/x response associated with zero-order-hold DACs, ii) the low-pass response of the DAC/ADC analogue front-ends, iii) the frequency response characteristics of RF and optical transceiver components, and iv) the frequency selective channel fading effect associated with the IMDD transmission system.

Next, the non-ideal physical channel case is considered to illustrate the impact of the frequency response roll-off effect. The same processes as in the ideal case are repeated except the physical channel's impulse response $h(t)$ is applied to the system. The orthogonality of the added channels is perfectly preserved before the physical channel as shown in Fig 4.6(c), where the zero-valued samples from the cosine (sine) channel coinside with the non-zero-valued samples from the sine (cosine) channel. The added signals are then transmitted through a physical channel with 5dB roll-off. As a result of the low pass filtering effect of the physical channel, which attenuates the higher frequency signal components, the signal from each channel can no longer maintain its zero-valued samples, as shown in the overlaid signals in Fig. 4.6(e), and also the magnified signals in Fig. 4.6(f). As the originally zero-valued samples now have a finite value and combine with the corresponding orthogonal

channel's non-zero-valued samples, they will generate CCI, as shown in the combined signal after the physical channel in Fig. 4.6(g). The outputs of the the cosine and sine matching filters are shown in Figs. 4.6(h) and 4.6(i), respectively. The corresponding signals after down-sampling are shown in Figs. 4.6(j) and 4.6(k), respectively. The interference between the orthogonal channels is now clear, as Fig. 4.6(j) shows the high frequency sinusoid applied to the cosine channel with leakage from the low frequency sinusoid applied to the sine channel, thus an attenuated version of the low frequency signal is directly superimposed on the wanted high frequency signal. The leakage from the cosine channel to the sine channel is also clearly seen in Fig. 4.6(k).

It is important to consider the case where the two spectrally overlapped orthogonal channel signals are OFDM modulated signals, each containing multiple subcarriers at harmonically related, discreet frequencies. The above example used different frequency sinusoids to help illustrate the CCI effect clearly. However, in an OFDM system there is theoretically no interference between subcarriers at different frequencies. The upsampling in the DFMA system, however, generates a double sideband (DSB) signal spectra and the subcarrier images in the upper and lower sidebands from each orthogonal channel will overlap. CCI between these overlaid subcarrier images thus results in interference leakage between the orthogonal channels. Hence, the inherent orthogonality between OFDM subcarriers, means CCI is only problematic between subcarriers at the same frequency and not between subcarriers of different frequencies.
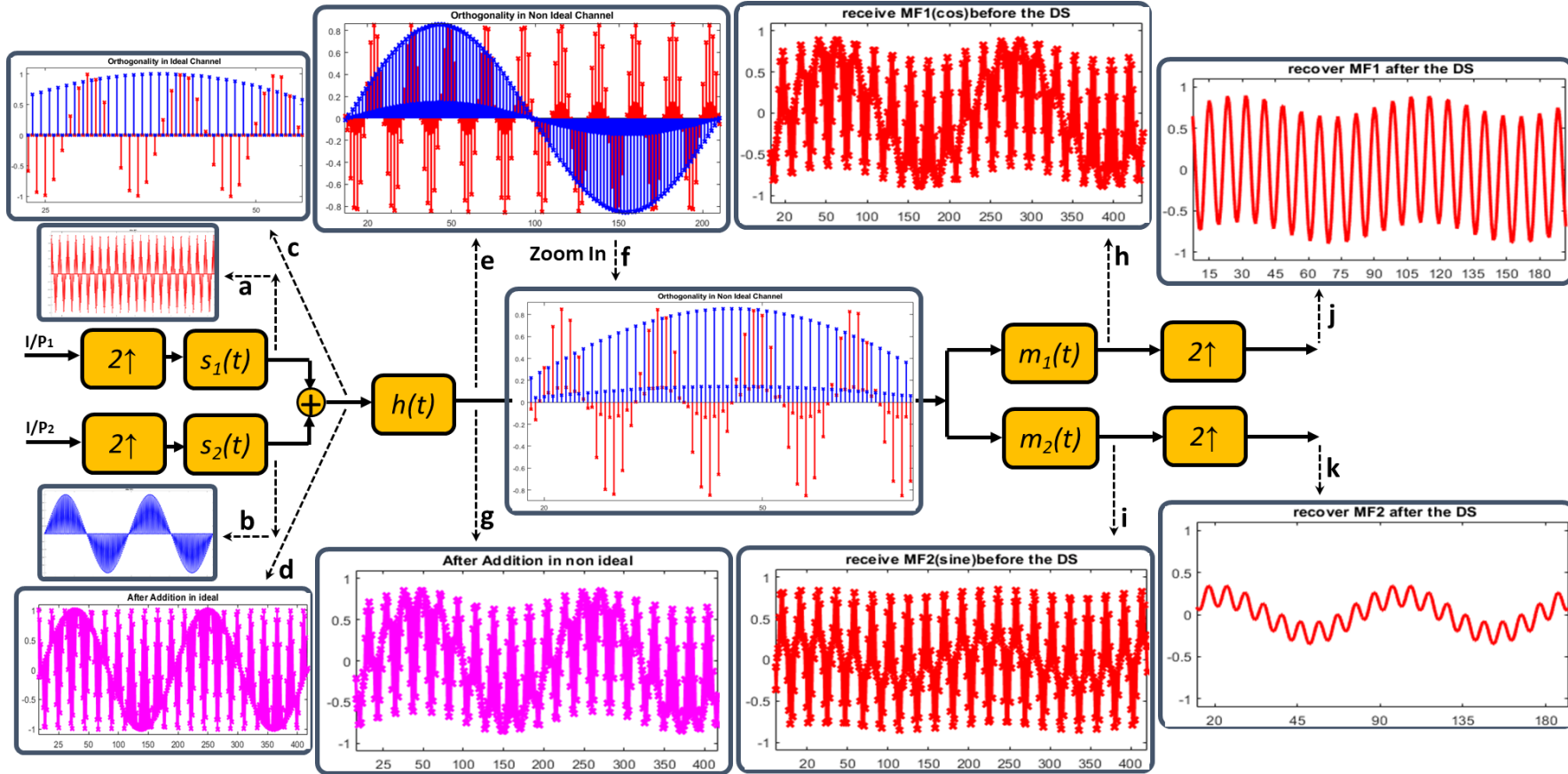
Fig. 4.6 Various signals in a 2-channel system with a non-ideal channel a) the upsampled high frequency signal after the Cosine shaping filter, b) the upsampled low frequency signal after the Sine shaping filter, c) the overlaid summed signal before the channel, d) the summed signal before the channel, e) the overlaid summed signal after the channel, f) zoomed version of the overlaid summed signal after the channel, g)summed signal after channel, h) signal after Cosine matching filter, i) signal after Sine matching filter, j) the recovered high frequency signal with CCI from low frequency signal, k) the recovered low frequency signal with CCI from high frequency sign

4.3 **General Interference Cancellation Techniques**

4.3.1 **Background**

Interference cancellation (IC) techniques can be exploited to reduce the MAI effect and thus enhance overall transmission system performance. Pre-interference cancelation (pre-IC) and post-interference cancelation (post-IC) are the two main categories of the IC techniques [6]. The IC technique classification thus depends on the location of the interference cancelling operation. Pre-IC (Post-IC) refers to the implementation of the IC technique at the transmitter (receiver) side. The pre-IC focuses on the suppression of interference on a *priori* basis by establishing an appropriate precoding technique that allows the transmitted signal to be suitably modified to suppress interference with other users' signals, precoding techniques applied to OFDM systems are, for example, the Selected Mapping (SLM) [7], the Partial Transmit Sequences (PTS) [8] and the Dirty Paper Coding (DPC) [9]. The appropriate precoding technique employed in the transmitter is combined with a knowledge of channel state information (CSI), for each user, to efficiently pre-estimate the level of the ongoing interference at the receiver side and optimise the precoding for minimum interference. Exchange of reliable CSI via signalling overhead is required to efficiently pre-estimate the amount of the ongoing interference, and a detailed update of the interference information for all users must be kept at the transmitter side. However, the effectiveness of the pre-IC implementation becomes more challenging as the number of users in the multi user system is increased, due to key factors including i) the practical realisation of accurate CSI is considerably harder to achieve, ii) accuracy of the interference profiling for all the transmitting users reduces as CSI accuracy reduces, iii) the signalling overhead for CSI information exchange increases resulting in reduced system efficiency and large latency [6].

Post-IC techniques are based on decoding the desired user information and then using this information along with channel estimates to supress the received interference from the overall received signal [4] . Post-IC thus only uses signal processing after the detector to cancel the interference on a *posteriori* basis. In contrast to the pre-IC, the signalling overhead between the transmitter and the receiver side is not necessary although CSI can still be critical. Therefore, post-IC represents quite an adaptable IC methodology and can be preferable to use in comparison with pre-IC [6]. Post-IC can generally be divided into two

main categories, parallel interference cancellation (PIC) and successive interference cancellation (SIC). Due to the way the user data is decoded, the parallel technique operates by detecting all the users' data simultaneously, whereas the successive technique operates by detecting users' data consecutively.

4.3.2 **Post-Interference Cancelation**

The post-IC technique is considerably preferable to use in suppressing the effect of the MAI, as it is simpler to implement compared with pre-IC due to the aforementioned challenges associated with large users counts. The Post-IC methods can also be called subtractive interference cancellation detectors, as the basic principle is to create an estimate of the interference contributed by the other users accessing the channel and then subtract the interference from the total received signal.

4.3.2.1 **Successive Interference Cancellation**

The SIC technique consists of multiple processing stages in a serial approach, where each successive process detects a single user's data and cancels the MAI interference it has generated from its input signal for passing to the next processing stage, hence the detector operates as a MUD system. To explain the SIC process, its application in a generic orthogonal channel-based system is used, where it is assumed that the component orthogonal signals have significantly varying power levels, hence low power signals can suffer high MAI from high power signals. The conventional corellation-based detector, the orthogonal reference waveform regenerator and the subtractor represent the main elements of each stage in the SIC MUD system, as shown in Fig. 4.7. The initial stage of the SIC detector (not shown in Fig. 4.2) ranks the component received input signals from the highest to the lowest power user signal, where power levels are estimated from the outputs of conventional correlator-based detectors. The highest power signal has the largest signal to interference ratio (SIR) and the lowest power signal has the smallest SIR, thus processing the signals in the order of highest to lowest power maximises the SIC due to the improved interference estimation accuracy of the higher power signals..

For the SIC detector in Fig 4.7 , $r(t)$ denotes the total received input signal to the detector, $s_1(t - T_b)$ refer to the reference orthogonal waveform of the highest power user signal, $\hat{b}_1(t)$ refers to the estimated data of the highest power user signal and $r_1(t)$ denotes the output

signal after subtracting the interference of the higher power user from $r(t)$. The interference signal is regenerated by the waveform regenerator, based on the detected user data and the corresponding user's orthogonal reference waveform. The subtraction of the MAI of the highest power user from the total received signal results in a higher quality signal in comparison to the total received signal. The second highest power user takes advantage of receiving the higher quality signal with lower interference as the interference impact of the first higher power user has been removed from the total received signal [5]. The process of detecting a user's signal and removing the interference continues at each stage until the user with the smallest power signal is reached and the input signal now has the lowest interference contribution.
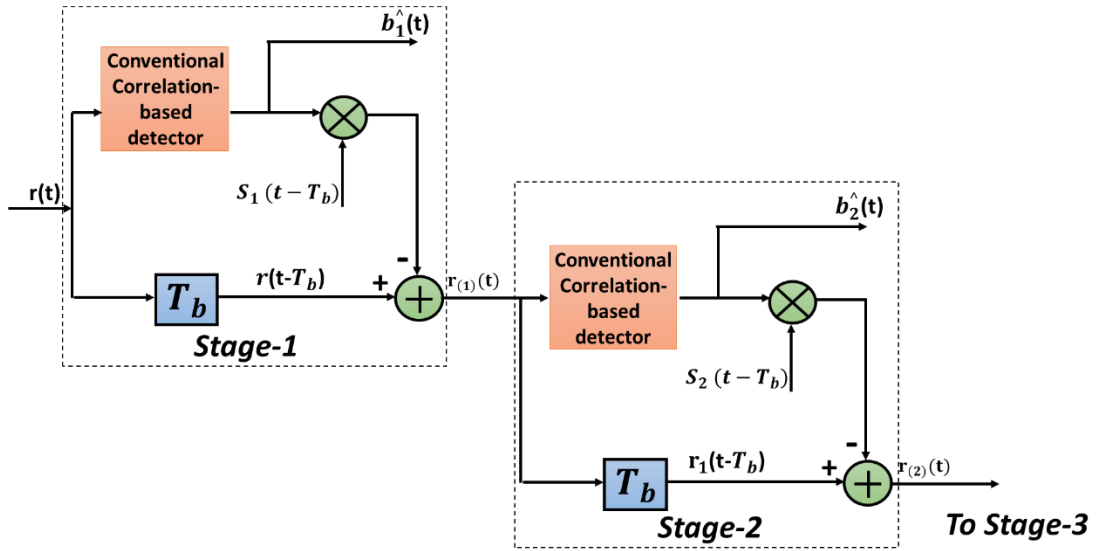

Fig. 4.7 The successive interference cancelation technique

4.3.2.2   **Parallel Interference Cancellation**

The PIC technique is also based on the idea of estimating and subtracting the MAI from the received signal before processing it. However, there is no need to sort the users one by one depending on to their signal power levels as in SIC. The MAI in MUD-PIC are estimated and subtracted for all users in parallel. The idea of the PIC technique is based on removing the interference simultaneously from each user produced by all the remaining users accessing the channel. Therefore, in contrast to the SIC, the PIC can remove the interference for all users simultaneously as it is not necessary to process the users sequentially depending on their signal power levels [12], so can achieve lower processing latency.

The PIC technique, as shown in Fig. 4.8, consist of a set of processes as follows: A bank of conventional corellation-based detectors is used to give an initial estimate of the received symbols for each user accessing the channel. Afterwards, a parallel process is applied to regenerate the transmitted signal waveform by applying the appropriate orthogonal reference waveform, to give an estimate of the MAI generated by each user. The MAI reduction for one user is achieved by subtracting the regenerated transmitted signal estimate for all other users from the total received signal, resulting in a cleaner signal. This MAI reduced signal is used as an input to a second bank of conventional correlation-based detectors to produce a new sequence of detected bits/symbols.

A multistage PIC (MPIC) process can be introduced to improve performance by reducing the interference error further in each PIC stage, as the new set of bit/symbol estimates from the previous stage are used as input bits/symbols to the next stage. In a MPIC-based MUD, the process begins by detecting all users and simultaneously eliminating the aggregated interference from all other users in the primary stage, thus generating user signals with improved SIR. The process is then repeated over multiple stages to further cancel the interference as each stage further improves the SIR of each users signal.
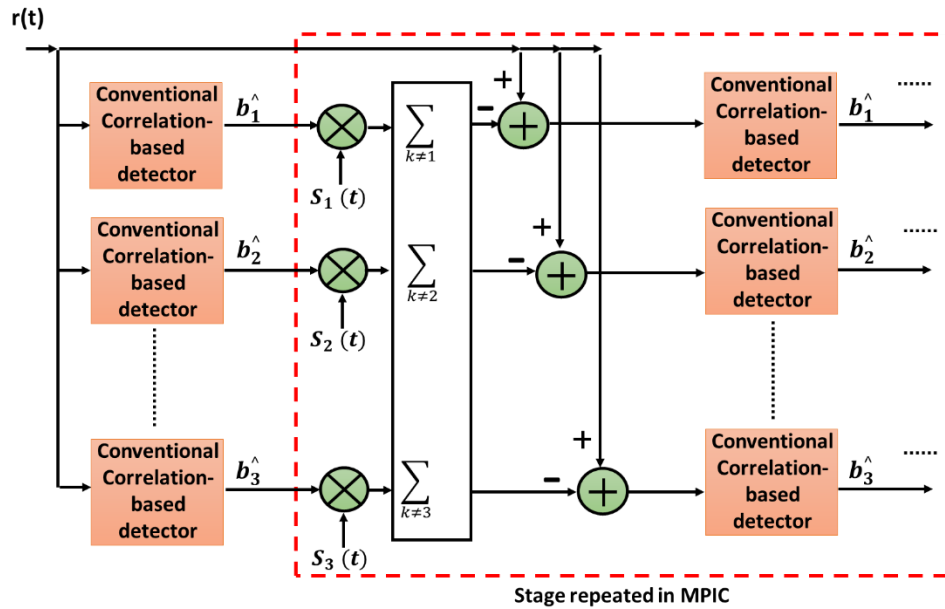

Fig. 4.8 The parallel interference cancelation technique

Both of the PIC and SIC techniques enhance the overall system performance by introducing different ways of removing the effect of the MAI. SIC outperforms the PIC in term of the

system complexity because the PIC requires all the users to be detected simultaneously in parallel. The PIC can surpasses the SIC in terms of latency, as the latter introduces larger delay, because removing the interference in every subsequent user in SIC will cause one bit/symbol delay, therefore, a large number of users could cause an unacceptable delay. Finally, the expected level of the received users' power will determine which of the MUD techniques would perform better. PIC would provide better performance if all the users are received with approximately equal power, but the SIC would perform better if all the users are received with significantly varying power [10].

4.3.2.3   **Least Mean Square Equalisation**

In digital transmission systems, a common problem is the ISI phenomenon which results in an overlap between neighbouring transmitted pulses corresponding to different symbols [13]. The wired and wireless transmission channels' transmission medium can play an important role in magnifying the ISI problem. In other words, the band-limited channel of wired transmission and the multipath propagation problem of wireless communications are the main reasons for the ISI problem. Thus, the non-flat frequency response of a transmission system can causes severe interference between a transmitted symbol and it's neighbouring symbols, and so leads to a degradation of the system performance. Where neighbouring symbols originate from different users sharing the same channel, the ISI can thus lead to MAI, as the ISI results in interference between symbols from different users [6]. Therefore, it is crucial to eliminate the effect of the interference and an equalizer can be employed to overcome this issue. The principle of the equalizer is to provide an inverse response compared to the channel response resulting in an overall flat channel frequency response, thus overcoming the channel impairments and enhancing the system performance.

However, the channel response can vary with time, for example non-stationary channels as in wireless communications. Consequently, an adaptive equalizer is employed and is therefore preferable to utilize in an unknown, dynamic environment over the static equalizer [14]. An adaptive equalizer, as shown in Fig. 4.9, consists of a digital filter with adjustable tap coefficients to automatically adapt its characteristics over time, according to an adaptive algorithm, and so follows the time dependent characteristics of the communication channel.
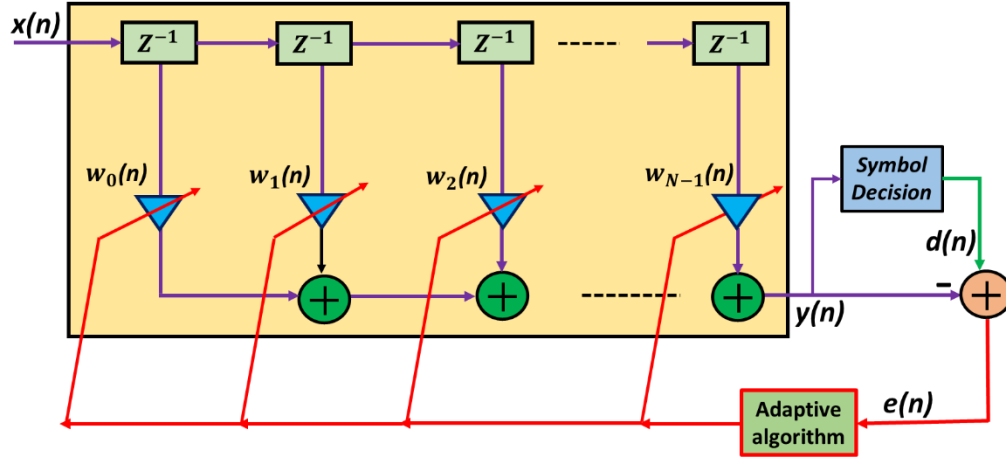
Fig. 4.9 Structure of the function of the adaptive filter

The least mean square (LMS) algorithm is a class of adaptive filter, based on the gradient descent method, which continuously updates the filter's variable coefficient values, to minimise the mean square error between the desired signal and the actual signal. Thus, the LMS filter converges to an approximation of the inverse channel response of the transmission system. Fig. 4.10 shows the signal flow graph representation of the LMS algorithm. The input signal *x(n)* is given as a transposed vector containing the present sample followed by *N-1* previous samples. The output value of the finite impulse response (FIR) filter is a product between the transposed input and a vector of *N* filter coefficients *w(n)* as shown in Eq. (4.4, 4.5):

$$w(n) = \begin{bmatrix} w1(n) \\ w2(n) \\ ... \\ wN(n) \end{bmatrix}, \quad x(n) = \begin{bmatrix} x(n) \\ x(n-1) \\ ... \\ x(n-N+1) \end{bmatrix} \tag{4.4}$$

The output of the filter *y(n)*, at time n=1,2, 3, ... is computed as:

$$y(n) = w(n)x^T(n) \tag{4.5}$$

and the error signal *e(n)* is computed as:

$$e(n) = d(n) - y(n) \tag{4.6}$$

Whereas the *d(n)* represent the desired signal and the updated coefficients of the LMS filter are calculated as follows:

$$w(n+1) = w(n) + 2\mu * e(n) * x(n) \tag{4.7}$$

Assuming the output of the process is known, the error signal *e(n)* can be described as the difference between the desired signal *d(n)* and the output signal from the digital filter *y(n)* as shown in Eq. (4.6). As the output is essentially unknown, the recovered signal after the symbol decision is used as an approximation to *d(n)*. The coefficients of the filter are interatively updated to minimize the output mean squared error $E[((d(n) - y(n))^2]$. Coefficient vector *w(n + 1)* for the next iteration is obtained from the sum of the current coefficient vector *w(n)* with the weighted input vector *x(n)* as shown in Eq. (4.7). The input vector is scaled with the error value *e(n)* and the step size μ [15]. The selection of the value μ will therefore control the convergence rate of the filter. A small μ value results in a slower convergence speed, but it can improve the accuracy of convergence and reduce the steady state noise. On the other hand, if the μ value is large, then the convergence speed will be faster and but accuracy can be lower and steady state noise will be higher. If the μ value is too large, oscillation can occur during the convergence. Therefore, the μ value should be chosen to achieve the optimum combination of accuracy and convergence speed.
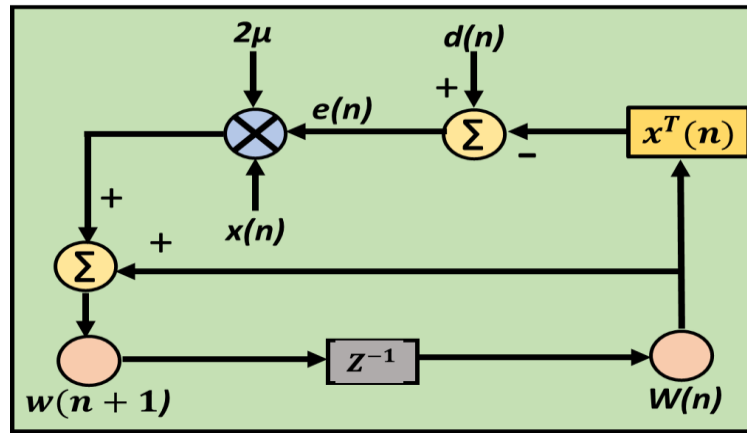

Fig. 4.10 Signal flow graph representation of the adaptive LMS algorithm

In summarise the LMS process is as follows: For each iteration the data input vector is multiplied with the weighted filter coefficient vector to produce the actual recovered signal. Then, the recovered signal is subtracted from the desired signal (after symbol decision), the resulting signal is the error signal and this is used to update the weighted filter coefficient vector. This process continues iteratively, until the filter coefficients converege to match as close as possible to the inverse channel response of the transmission system [15, 16]. If the channel response changes, the filter will then adapt accordingly.

4.4 Cross Channel Interference Cancellation Technique for Application in CANs

To mitigate the CCI induced by linear and nonlinear effects, two of the previously described DSP-based techniques can potentially be applied, these are the SIC [19], as described in section 4.3.2.1 and LMS-based equalization [18], as described in section 4.2.3 [19]. The LMS-based equalization has the disadvantages of: i) a large number of iterations can be required to achieve the performance convergence, which contributes to an increase in the total switching delay during network reconfiguration ii) high convergence sensitivity to initial conditions, which means convergence cannot always be guaranteed, and iii) the optimum tap count and step size can also be system-dependent [10]. On the other hand, to receive a strong signal in the presence of a weaker signal, the SIC technique typically involves complicated DSP procedures including: i) the full bit-level decoding of the stronger signal, ii) the reconstruction of the modulated signal and its subtraction from the combined received signal, and finally iii) the decoding of the weaker signal's data from the residual signal. It may be possible to adapt and apply the SIC technique to address the CCI problem, however the need to fully decode the signal to the bit-level and reconstruct the modulated signal results in the following three disadvantages: i) implementation dependence on signal modulation format, ii) very high DSP complexity, which would be especially high for the case of OFDM modulation, and iii) unacceptably high latency.

As the physical channel frequency response effect is a principal factor contributing to loss of channel orthogonality, to effectively mitigate the resulting CCI a simple but highly effective, DSP-based CCI cancellation (CCIC) technique, suitable for any DFMA-based transmission system, has been proposed. The CCIC technique is designed to compensate for linear effects and cannot eliminate interference due to nonlinear effects as this would require the reproduction of the actual channel nonlinearities which is highly complex, however as the linear effects are dominant in the IMDD PON the CCIC technique can be highly effective [17]. The CCIC technique operates by estimating and subsequently cancelling the CCI signals associated with IMDD DFMA-PON systems and DFMA-based CANs. The proposed CCIC technique is modulation format-independent, has low DSP complexity, requires only a single CCIC iteration and it is completely free from dependence on any initial conditions.
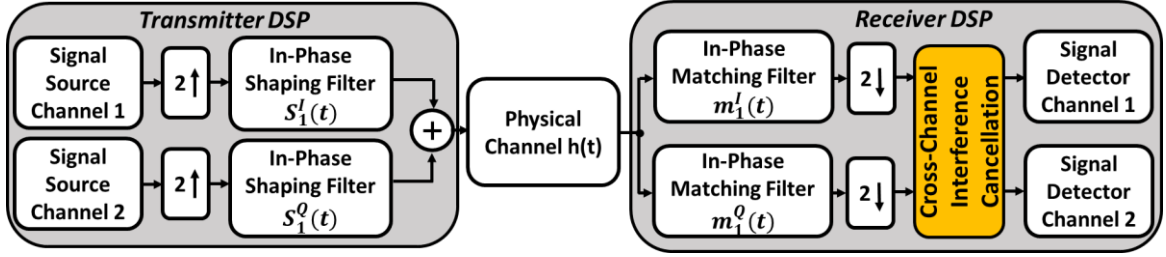
Fig. 4.11 A 2-channel point-to-point DFMA system incorporating a DSP-based CCIC function

For simplicity, but without losing generality, the proposed CCIC technique is described for a 2-channel, point-to-point, DFMA system, as shown in Fig. 4.11, where the the location of the CCIC DSP block is clearly shown in the receiver side DSP. If $h(t)$ represents the overall channel impulse response of the complete physical channel between the shaping filter output(s) in the transmitter and the matching filter inputs in the receiver, and $s_1^I(t), s_1^Q(t), m_1^Q(t)$ and $m_1^Q(t)$ represent the impulse responses of the in-phase and quadrature shaping filters and matching filters respectively, as definitioned in Eq.(3.4 -3.8) for the case of $i=1$. The signal output from the in-phase matching filter, $d'_I(t)$ is now:

$$d'_I(t) = [d_I(t) \otimes s_1^I(t) \otimes h(t) \otimes m_1^I(t)] + [d_Q(t) \otimes s_1^Q(t) \otimes h(t) \otimes m_1^I(t)] + w_I(t) \qquad (4.8)$$

The first term on the right of Eq. (4.8) reflects the wanted signal $d_I(t)$ which is however subject to the effect of $h(t)$. The second term on the right is now non-zero and so the output of the in-phase matched filter also contains a component dependent on $d_Q(t)$, thus the received signal on the in-phase channel consists of a wanted component originating from the in-phase channel and an unwanted CCI component originating from the quadrature-phase channel. $w_I(t)$ represents the received noise component on the in-phase channel due to all noise sources in the transmission system. It can be shown in a similar manner that there exists CCI from the in-phase channel to the quadrature-phase channel, thus, the signal output from the quadrature-phase matching filter, $d'_Q(t)$ is:

$$d'_Q(t) = [d_Q(t) \otimes s_1^Q(t) \otimes h(t) \otimes m_1^Q(t)] + [d_I(t) \otimes s_1^I(t) \otimes h(t) \otimes m_1^Q(t)] + w_Q(t) \quad (4.9)$$

where $d_Q(t)$ *is the* wanted signal and $w_Q(t)$ represents the received noise component on the quadrature-phase channel due to all noise sources in the transmission system, such as

DAC/ADC quantisation noise, RF amplifier noise and photodetector associated noise. The unwanted CCI components generated between orthogonal channels can result in a severe degradation of the transmission performance of both channels, therefore it is highly advantageous if a simple and highly effective transceiver-embedded DSP algorithm can be exploited to mitigate the effect of the CCI.

The interference signal, $c_{QI}(t)$ from the quadrature-phase channel to the in-phase channel as determined in Eq. (4.8) is:

$$c_{QI}(t) = d_Q(t) \otimes s_1^Q(t) \otimes h(t) \otimes m_1^I(t) \tag{4.10}$$

It is shown in Eq. (4.10) that, in order to ideally reconstruct the interference signal at the receiver, the transmitted signal $d_Q(t)$ must be known at the receiver. However as $d_Q(t)$ is obviously unavailable, the actual received signal on the quadrature-phase channel, $d'_Q(t)$, can be used as an estimate as it closely approximates to a scaled version of $d_Q(t)$. Thus as the shaping and matching filter responses are known and as the channel impulse response can be easily determined by a training sequence-based, channel estimation DSP function in the receiver, an estimate of the interference signal, $e_{QI}(t)$, can be generated as follows:

$$e_{QI}(t) = [d'_Q(t) / S_Q] \otimes s_1^Q(t) \otimes h(t) \otimes m_1^I(t) \tag{4.11}$$

where S_Q represents the scaling factor of $d'_Q(t)$, relative to $d_Q(t)$. Thus to generate $e_{QI}(t)$ it is clear from Eq. (4.11) that a 3-stage DSP filter process is required, which corresponds to convolution by $s_1^Q(t)$, $h(t)$ and $m_1^I(t)$, with scaling by S_Q^{-1}. It is also necessary to apply 2× up-sampling (2× down-sampling) before (after) the filtering and scaling functions to replicate the exact signal path that generates the CCI effect. A similar approach can be used to estimate the interference signal, $e_{IQ}(t)$, from the in-phase channel to the quadrature-phase channel. The generated CCI signal estimates are then subtracted from suitably delayed versions of the received signals on each channel to cancel out the CCI, thus;

$$\begin{aligned}
d_I''(t) &= d_I'(t - T_E) - e_{QI}(t), \\
d_Q''(t) &= d_Q'(t - T_E) - e_{IQ}(t)
\end{aligned} \tag{4.12}$$

where $d''_I(t)$ [$d''_Q(t)$], is the new received signal estimate for the in-phase channel [quadrature channel] and T_E is the delay of the interference estimation function. T_E is therefore the delay which is applied to the received signals to align the actual and estimated interference signals. The resultant received signals are then passed to the appropriate demodulation functions for data recovery. The value of T_E can be determined from the knowledge of the estimate of $h(t)$ and the corresponding shaping and matching filters in the interference estimation function. If the CCIC function does not completely remove the CCI component in the received signal and as the resultant signals are improved estimates of the transmitted signals, the new received signal estimates could then be applied to a second CCIC iteration stage, which in theory could further reduce any remaining CCI signal components. It is feasible that multiple CCIC iterations may be beneficial, however the need for multiple iterations will naturally be dependent on the accuracy of the CCI signal estimates.

The detailed internal functions of the CCIC block are detailed in Fig. 4.12(a), which shows the implementation of two CCIC stages. Within each CCIC stage, there are two interference estimation functions, one function estimates the interference from channel 1 to channel 2 and the second function estimates the interference from channel 2 to channel 1. Within each CCIC stage, the incoming signals are suitably delayed before the estimated interference signals are subtracted. The output signals from CCIC stage 1 then pass to the CCIC stage 2 where the same process is repeated. Fig. 4.12(b,c) shows the internal operations of the interference estimation functions, which consist of the aforementioned up-sampling/down-sampling, filtering and scaling operations.
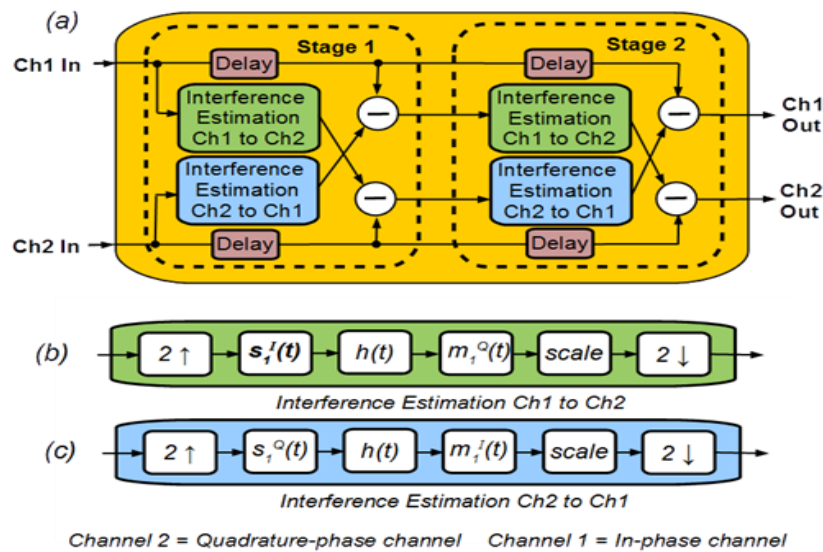

Fig. 4.12 (a) 2 stage Cross-Channel Interference Cancellation function. Interference estimation functions: (b) Channel 1 to Channel 2 and (c) Channel 2 to Channel 1.

References

[1]   S. Sharma and K. Thakur, "Carrier frequency offset in OFDM systems," Proc. 2nd Int. Conf. Inven. Syst. Control. ICISC 2018, no. Icisc, pp. 369–373, 2018.

[2]   R. Jose, "Estimation of channel and Carrier Frequency Offset in OFDM systems using joint statistical framework," Phys. Commun., vol. 25, pp. 139–147, 2017.

[3]   S. Moshavi, "Multi-user detection for DS-CDMA communications," IEEE Commun. Mag., vol. 34, no. 10, pp. 124–135, 1996.

[4]   G. Kebede, "Performance Evaluation of Interference Cancellation using SIC and PIC for WCDMA Systems," 2007.

[5]   T. Huovinen, "Independent Component Analysis in DS-CDMA Multiuser Detection and Interference Cancellation," PhD Thesis, Tampere Univ. Technol. Finl., p. 88, 2008.

[6]   N. I. Miridakis and D. D. Vergados, "A survey on the successive interference cancellation performance for single-antenna and multiple-antenna OFDM systems," IEEE Commun. Surv. Tutorials, vol. 15, no. 1, pp. 312–335, 2013.

[7]   J. B. H. Bauml, Robert W., Robert FH Fischer, "Reducing the peak-to-average power ratio of multicarrier modulation by selected mapping," Electron. Lett., vol. 32, no. 22, pp. 6–7, 1996.

[8]   J. C. Chen, "Partial transmit sequences for peak-to-average power ratio reduction of OFDM signals with the Cross-Entropy method," IEEE Signal Process. Lett., vol. 16, no. 6, pp. 545–548, 2009.

[9]   H. Li, "LDPC-LDGM based dirty paper coding techniques for multicell cooperative communication system," Proc. 2009 Pacific-Asia Conf. Circuits, Commun. Syst. PACCS 2009, pp. 7–10, 2009.

[10]   J. G. Andrews, "Interference cancellation for cellular systems: A contemporary overview," IEEE Wirel. Commun., vol. 12, no. 2, pp. 19–29, 2005.

[11]   J. G. Andrews, W. Choi, and R. W. Heath, "Overcoming interference in spatial multiplexing mimo cellular networks," IEEE Wirel. Commun., vol. 14, no. 6, pp. 95–104, 2007.

[12]   D. Divsalar, M. K. Simon, and D. Raphaeli, "Improved Parallel Interference Cancellation for CDMA," vol. 46, no. 2, pp. 258–268, 1998.

[13]   P. Sharma, P. Gupta, and P. Singh, "Performance Comparison of ZF, LMS and RLS Algorithms for Linear Adaptive Equalizer," Ripublication.Com, vol. 4, no. 6, pp. 587–592, 2014.

[14]   L. Mahmood et al., "Adaptive filtering algorithms for channel equalization in wireless communication," Indian J. Sci. Technol., vol. 8, no. 17, 2015.

[15]   I. Kempi, "Adaptive Chanel equalization.," 2015.

[16]   R. Chandrakant Sanghvi and H. B. Soni, "Experiments with LMS Algorithm," Indian J. Sci. Technol., vol. 9, no. 48, pp. 1–5, 2016.

[17]   A. Amari, "Nonlinear effects compensation for long-haul superchannel transmission system," Télécom ParisTech, 2016.

[18]   L. Tao, Y. Wang, Y. Gao, A. P. T. Lau, N. Chi, and C. Lu, "40 Gb/s CAP32 system with DD-LMS equalizer for short reach optical transmissions," IEEE Photonics Technol. Lett., vol. 25, no. 23, pp. 2346–2349, 2013.

[19]   A. L. C. Hui and K. Ben Letaief, "Successive interference cancellation for multiuser asynchronous DS/CDMA detectors in multipath fading links," IEEE Trans. Commun., vol. 46, no. 3, pp. 384–391, 1998.

5. Experimental demonstration of a DSP-based cross-channel interference cancellation technique for application in digital filter multiple access PONs

Contents

5.1   **Introduction**

The importance of preserving the orthogonality between spectrally overlapped channels in a DFMA-based network is explained in detail in section 3.2. As described in detail in section 4.2, CCI is the result of reduced orthogonality due to the physical channel roll-off effect and nonlinearities mainly associated with optical signal transmission. To alleviate the effect of CCI, section 4.4 presents an extensive description, including a mathematical analysis and illustrative diagrams of the proposed, highly effective, CCIC technique suitable for any DFMA-based transmission system. In this chapter, in-depth experimental investigations are performed to examine the CCIC-induced system performance improvements in a digital orthogonal filter multiplexed IMDD and SMF-based, point-to-point system employing two spectrally overlapped channels, carrying OFDM modulated signals. Performance improvements are assessed in terms of individual OFDM subcarrier BERs, total signal transmission capacity and optical power budget. The results presented in this chapter demonstrate that the CCIC technique can lead to substantial performance improvements when applied to IMDD DFMA PONs.

5.2   **Experimental system setup**

Figure 5.1 shows the considered point-to-point DFMA-PON experimental system setup with key system parameters listed in Table 1. A field programmable gate array (FPGA)-based real-time transmitter with an 8-bit DAC operating at 2GS/s, as detailed in appendix A, is employed to generate and multiplex via digital filtering two orthogonal DFMA channels. An RF gain stage sets the optimum RF signal voltage at 2.2Vpp for combination, via a bias-T, with an optimum DC bias of −0.7V. The resultant RF signal intensity modulates a 10GHz electro-absorption modulator (EAM) within an EML. The 1550nm DFB laser in the EML is driven with a 125mA bias current. The EML's optical output is launched at an optical power of 2dBm into varying lengths of an SMF IMDD system. At the receiver, the received optical signal passes through a variable optical attenuator (VOA) to control the ROP level, optical-electrical conversion is then performed by a 12.4GHz photodetector with integrated transimpedance amplifier, this is followed by a RF gain stage and a low pass filter to optimize the electrical signal level fed into a DSO.

The DSO samples the signal at 25GS/s and then performs off-line DSP using MATLAB^{TM}. The off-line DSP function first resamples the signal to 26GS/s before down-sampling to 2GS/s to match the transmitter sample rate. As the absolute STO of the sampling instances in the receiver is critical for maintaining channel orthogonality, the off-line DSP determines the optimum STO when down-sampling from 26GS/s to 2GS/s. By varying the sample offset when down-sampling the STO can be changed in increments of 38.46ps, due to the two times up-sampling it is necessary to sweep the STO across two sample periods at 2GS/s (1ns). The total BER for the in-phase channel is computed for the 26 possible STO values to identify the optimum STO for use with the remaining receiver DSP functions. The subsequent off-line DSP functions performed are as follows: in-phase and quadrature-phase match filtering, two times down-sampling, CCIC signal processing according to the principle described in section 4.4 and OFDM signal demodulation for each of the two received signals.
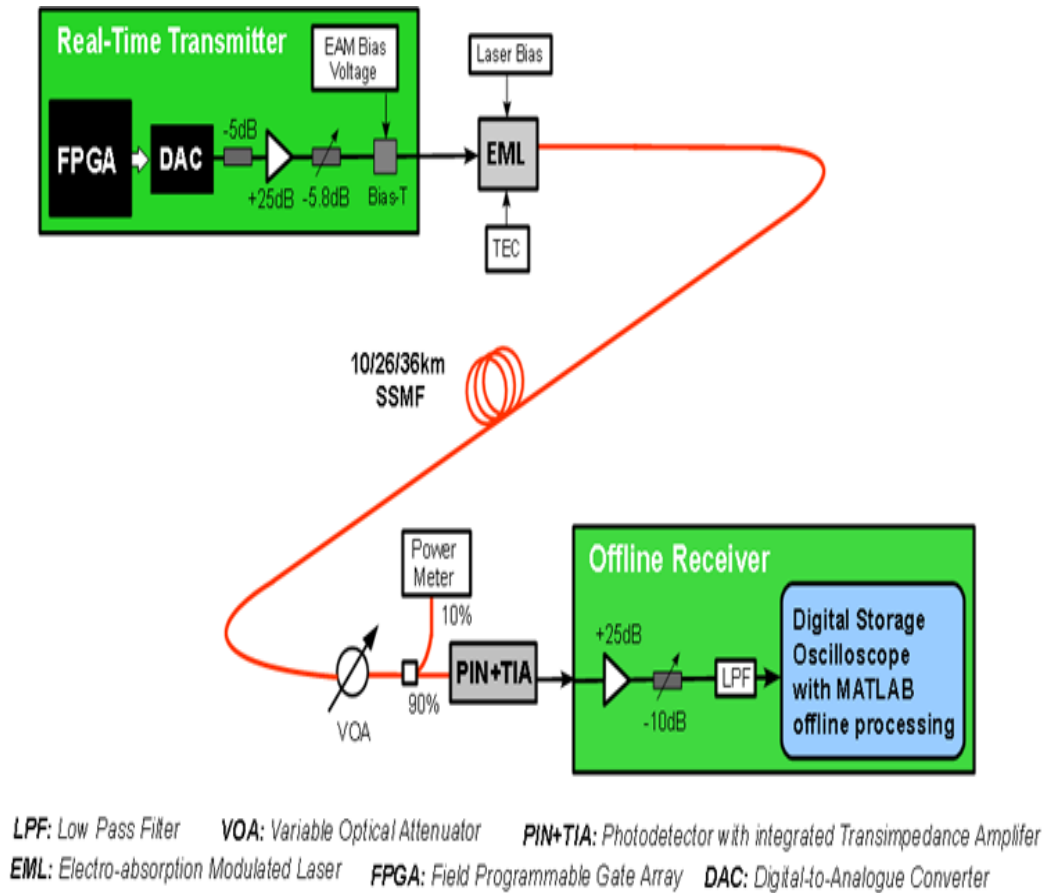

Fig. 5.1 Point-to-point two-channel DFMA-PON experimental system setup

Table 1. Transceiver and system parameters

Parameter	Value
Total number of IFFT/FFT points per channel	32
Maximum data-carrying subcarriers per channel	15
n-th subcarrier frequency	n×31.25MHz
Modulation formats on all subcarriers	16-QAM
DAC sample rate	2GS/s
DAC resolution	8 bits
Oscilloscope sample rate [re-sampled rate]	25GS/s [2GS/s]
OFDM symbol rate	25MHz [#]
Samples per symbol (IFFT)	32 samples (32ns) [#]
Cyclic prefix	8 samples (8ns) [#]
Total samples per symbol	40 samples (40ns) [#]
EML laser wavelength	1550nm
3-dB EML modulation bandwidth	10GHz
Laser bias current	125mA
EAM bias voltage	-0.7V
EML driving voltage	2.2Vpp
PIN detector bandwidth	12.4GHz
PIN detector sensitivity	-19dBm[*]
System frequency response roll-off (signal spectral region)	10.5dB

\# Before up-sampling and after down-sampling
* Corresponding to 10 Gb/s non-return-to-zero data at a BER of 1.0×10^{-9}

5.3   Experimental results

5.3.1   Channel Frequency Response and Impulse Response

Figure 5.2 shows the normalised amplitude and phase profiles of the channel frequency response H(f) of the complete physical point-to-point IMDD DFMA-PON system between the digital domains in the transmitter and the receiver. The complete system consists of the transmitter side elements comprising a DAC, a RF gain stage and an EML intensity modulator, the 26km SMF optical link, as well as the receiver side elements comprising a variable optical attenuator, a PIN photodetector, a RF gain stage and a DSO-embedded ADC. The system frequency response is measured with a conventional optical OFDM system at the 15 discrete OFDM subcarrier frequencies spaced at 62.5MHz (with no digital filtering or up/down-sampling, the conventional OFDM subcarrier frequencies are twice that of the DFMA system). As expected, Fig. 5.2(a) and Fig. 5.2(b) show that the overall frequency response roll-off across the 0-1GHz spectral region is 10.5dB, and that the phase profile has an almost linear developing trend across the same signal spectral region.

For the results in this section obtained using the CCIC technique, the required discrete system impulse response h(t) is determined by performing a 32 point inverse fast Fourier transform (IFFT) on the doubled sided spectrum of H(f). The fact that H(f) is normalised to the gain at the first subcarrier frequency is simply compensated for by an adjustment to the

linear scaling factor used in the interference estimation function. As the frequency selective channel fading effect associated with the IMDD dispersive system is just one of several factors contributing to the total system frequency response roll-off effect, H(f) does not vary significantly for the different lengths of SMF employed in the measurements, therefore the discrete system impulse response h(t) determined at 26km SMF is also used for all fiber lengths.
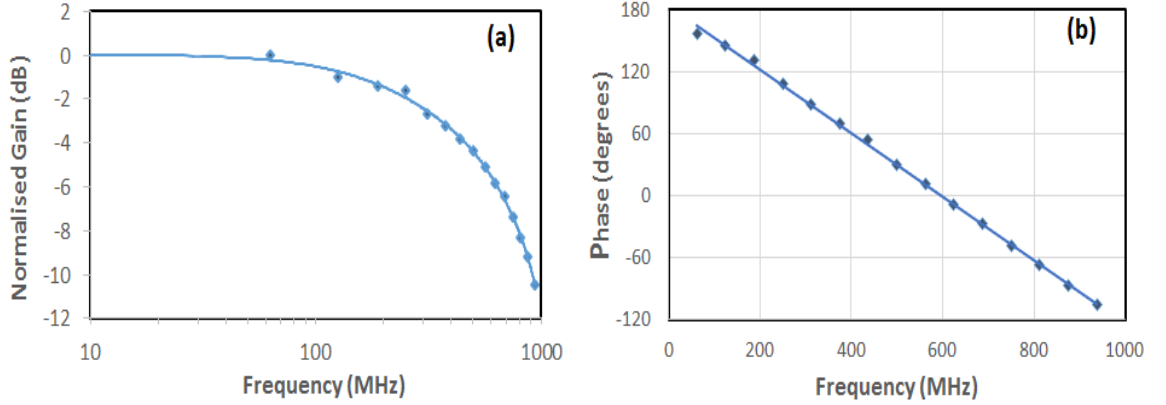

Fig. 5.2 (a) Normalized amplitude response |H(f)| and (b) Phase response ∠H(f) of the physical point-to-point DFMA-PON system from DAC input to (DSO) ADC output with 26km SSMF included. The response is normalized to the gain at the first subcarrier.

5.3.2 OFDM Subcarrier BER Improvements

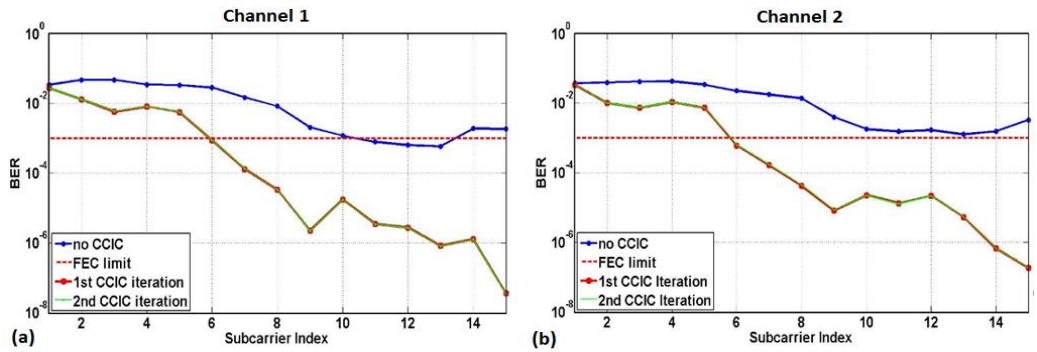*Fig. 5.3 BER vs. subcarrier index with and without the CCIC technique at a received optical power of -14dBm (a) Channel 1, (b) Channel 2*

The improvements in individual OFDM subcarrier BERs due to the CCIC technique are first explored in this subsection. For transmission over 26 km of SMF at a ROP of -14dBm, Fig. 5.3 shows the BERs for each individual data-carrying OFDM subcarrier for the cases of: i)

no CCIC applied, ii) one CCIC iteration applied and iii) two CCIC iterations applied. Fig. 5.3(a) is plotted for channel 1 (in-phase) and Fig. 5.3(b) is plotted for channel 2 (quadrature-phase). It is clear in Fig.5.3 that at the ROP of -14dBm, when the CCIC technique is not applied, very few subcarriers can comply with the adopted FEC limit of 1.0×10^{-3}, in fact only 3 subcarriers on channel 1 are only marginally below the FEC requirement. However, when one iteration of the CCIC technique is applied, Fig. 5.3 shows that the subcarrier BERs are substantially improved and a total of 20 subcarriers (6-15 on each channel) now achieve BER levels below the adopted FEC limit. The total BER for subcarriers 6-15 on channel 1 (channel 2) is now as low as 1×10^{-4} (6×10^{-5}). Also, a single iteration of the CCIC technique achieves a highly notable improvement in BER of more than 1000 times on some individual subcarriers. An important result also shown in Fig. 5.3 is that the second CCIC iteration does not improve the subcarrier BER performance any further, thus as convergence has been reached further higher order iterations cannot achieve any additional improvements in BER performance. The results therefore indicate that the CCIC technique is powerful enough to only require a single iteration.

It can also be seen in Fig.5.3 that higher frequency subcarriers of both channels experience greater improvements in BER compared to lower frequency subcarriers. This can be attributed to the fact that the signal spectrum after up-sampling and digital filtering by the shaping filter, consists of two mirrored spectral images having an upper sideband and a lower sideband with subcarrier images mapped to both sidebands. In comparison with the higher frequency subcarriers, the images from the lower frequency subcarriers see greater frequency separations and thus greater amplitude variations at the receiver due to the system frequency response roll-off effect. The removal of the unwanted signal in the receiver relies on the frequency components from each image sideband cancelling out after the down-sampling function as the aliasing effectmaps both images to the same baseband spectral region but with phase differences of 180°, the larger the difference in amplitude of the two frequency components, the weaker the signal cancellation effect is. Any non-ideal phase response can also lead to greater relative phase shifts between the lower frequency subcarrier images which also reduces the effectiveness of the sideband cancellation. Lower frequency subcarriers thus suffer from greater CCI and the CCIC technique is less effective at lower frequencies. As such the aforementioned difference occurs.

A very common characteristic of long IMDD links with wide signal spectra is the presence of frequency response nulls in the signal spectral regions. The work presented in [64], has shown that the CCIC-induced performance gains are not significantly impacted by the nulls because the associated reduction in optical signal-to-noise ratio (OSNR) also plays a significant role in determining the maximum achievable transmission performances.

5.3.3 **Capacity versus Reach Improvements**

To explore the maximum improvements in capacity versus reach performance due to the CCIC technique, the following experimental procedures are adopted: without CCIC enabled in a fixed SMF fiber length of 36km, the ROP is reduced until the lowest possible aggregated signal transmission capacity is reached at a BER below 1×10^{-3}. At a ROP of -16.6dBm only a single subcarrier on channel 1 can be supported, whilst on channel 2 there does not exist a single subcarrier capable of carrying information. Under these conditions, as 16-QAM modulation is employed, the total net bit rate of is only 0.1Gb/s. With the identified ROP of -16.6dBm and CCIC still disabled, maximum signal transmission capacities are also determined for each channel at different fiber lengths of 26km and 10km. The maximum signal transmission capacities on each channel are then determined for these three fiber lengths with CCIC enabled. In exploring the maximum signal transmission capacities for different fibre lengths with and without the CCIC technique, the receiver RF signal levels are always adjusted for each fibre length to maximize the corresponding signal transmission capacity at a BER below 1×10^{-3} on each subcarrier.

Figure 5.4(a) shows the net signal transmission capacity versus reach for each channel with and without CCIC enabled. It is shown that without CCIC channel 2 cannot support any data transmission even at a fiber length of 10km, whereas channel 1 can only support two subcarriers when fiber length is reduced to 10km. However, when CCIC is enabled channel 1 (channel 2) can now support 10 (9) subcarriers, thus giving a net signal transmission capacity of 1 (0.9) Gb/s. The reason why channel 2's performance with and without CCIC is always worse than channel 1 at the adopted ROP is due to the fact that channel 2 is the quadrature-phase channel, whose filter impulse response deviates further from the ideal filter response compared to the channel 1's in-phase filter [31].
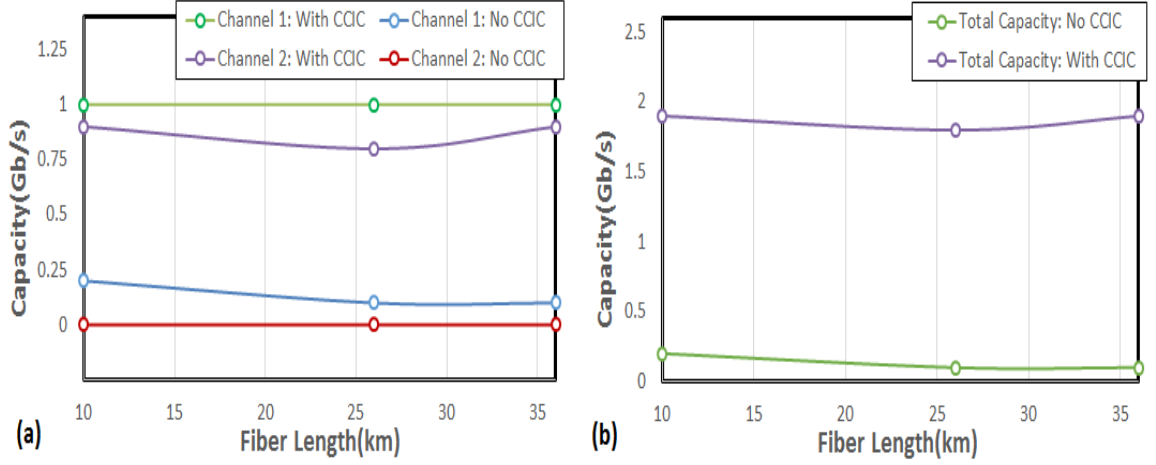
Fig. 5.4. Capacity vs. reach with and without the CCIC technique at a ROP = -16.6dBm.
(a) Two individual channels (b) Combined channels

Figure 5.4(b) shows the total aggregated net signal transmission capacity versus reach for both channels combined. Here the total signal transmission capacity can increase from 0.1Gb/s to 1.9Gb/s due to the CCIC technique, thus CCIC achieves an increase in signal transmission capacity as large as 19 times. It is also important to note that Fig. 5.4 reveals that signal transmission capacities are not dependent on the adopted fiber lengths, this indicates that the DFMA technique preserves the OFDM signal tolerance to the chromatic dispersion effect.

5.3.4 Power Budget Improvements

Finally, the improvements in power budget due to the CCIC technique are investigated in Fig.5.5. To provide a suitable CCIC-free reference operating point, for a 36km SMF transmission system, an appropriate adjustment is made to ROP to ensure that the 6 highest frequency subcarriers on each channel are capable of operating at BERs below the adopted FEC limit of 1.0×10^{-3} for the cases of with and without the CCIC technique applied. The aggregated total net signal transmission capacity is 1.2Gb/s (0.6Gb/s per channel). Under these conditions, Fig. 5.5 shows the BER versus ROP curves for each channel with and without CCIC enabled. It can be seen that both channels exhibit very similar BER developing trends in each case. The power budget improvement can be as large as ~3.5dB for each channel, when the aggregated signal transmission capacity is fixed.
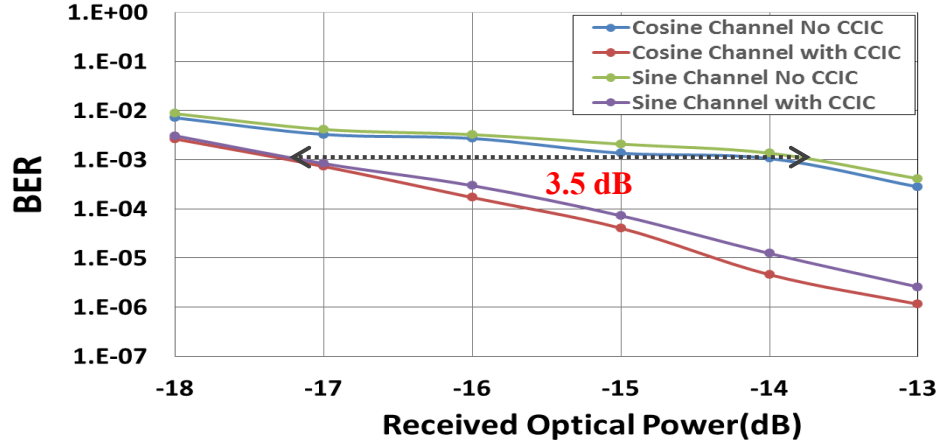
Fig. 5.5. BER vs. received optical power with and without the CCIC technique for transmission over 36km SMF.

5.4 **Conclusions**

The CCI effect between two orthogonal channels sharing the same spectral region can severely degrade the transmission performance in an IMDD-based DFMA PON system. A DSP-based CCIC technique has been experimentally demonstrated which is shown to have relatively low complexity and be highly effective at mitigating the CCI effect for significantly improving the DFMA PON performance. The CCIC technique has the following four unique characteristics; i) the performance rapidly converges after only a single CCIC iteration, ii) the DSP operation is not dependent on the employed modulation formats, iii) the DSP complexity is lower compared to other techniques such as SIC and iv) the performance is not dependent on initial system conditions.

The CCIC technique has been experimentally demonstrated in a two channel point-to-point IMDD DFMA PON system, detailed investigations of the CCIC impact on transmission performance have been undertaken with the following substantial improvements observed: i) reduction in individual subcarrier BERs of over 1000 times, ii) increase in aggregated signal transmission capacity by a factor of 19 times and iii) increase in optical power budget of ~3.5dB. This work demonstrates that the CCIC technique is potentially capable of radically improving the transmission performance in DFMA-PONs. Subsequent research work has investigated the application of a modified CCIC technique in an upstream DFMA-PON with multiple ONUs [64], the modified CCIC technique is also shown to be highly effective for multi-channel DFMA systems.

References

[1]   Y. Dong, E. Al-Rawachy, R. P. Giddings, W. Jin, D. Nesset, and J. M. Tang, "Multiple Channel Interference Cancellation of Digital Filter Multiple Access PONs," J. Light. Technol., vol. 35, no. 1, pp. 34–44, 2017.

[2]   M. Bolea, R. P. Giddings, M. Bouich, C. Aupetit-Berthelemot, and J. M. Tang, "Digital Filter Multiple Access PONs With DSP-Enabled Software Reconfigurability," J. Opt. Commun. Netw., vol. 7, no. 4, p. 215, 2015.

6. Experimental Demonstration of a Real-Time Digital Filter Multiple Access PON with Low Complexity DSP-Based Interference Cancellation

Contents

6.1 **Introduction**

As it is vital to verify the practical implementation of DFMA PONs, in this chapter, we report for the first time the experimental demonstration of a completely real-time DSP-based upstream, 26km SMF, DFMA PON based on IMDD. By employing two real-time reconfigurable ONUs and a real-time reconfigurable OLT, we successfully demonstrate multiple upstream transmissions with various channel configurations, verifying that the real-time DSP-based orthogonal filters can be implemented with sufficient accuracy and operating speed, with software-controlled reconfiguration to dynamically select the ONUs' operating channel(s). In the real-time IMDD DFMA PON, incorporating four independent OFDM-modulated channels, subject to CCI, we demonstrate the integration of the aforementioned CCIC technique, implemented in real-time DSP in the OLT, to verify its practical implementation and explore its performance under different DFMA PON channel configurations. The CCIC function is also fully optimised for low DSP complexity as it requires only 44 scalar multiplier elements, corresponding to only 11 multipliers per signal sample. The CCIC function is demonstrated to significantly improve the performance and robustness of the IMDD DFMA PON in terms of, i) significant improvements in BER versus received optical power, with the BER of individual OFDM subcarriers being reduced by factors as large as $100 - 300$ times, ii) significant increase in total channel capacity, of the order of ≥ 12 times, iii) reduction of sensitivity to ONU synchronisation as the inter-ONU STO range can be increased by a factor of up to 15 times, and iv) excellent transparency to the interfering channel's modulation format, as negligible change in subcarrier BERs was observed when applying two different modulation formats on the interfering signal. Furthermore, we analyse the minimum DSP complexity requirements of the digital orthogonal filters and CCIC filters and show that their complexity does not scale with the implemented channel count. In addition, a crucial result for the CCIC filters is that each generated sample in the estimated interference signal only requires the processing of ~10 samples from the interference-inducing signal, such that only as few as ~10 scalar multipliers are required per parallel CCIC FIR filter. The results presented in this chapter therefore verify that an ultra-low complexity CCIC function is technically feasible and it leads to substantial improvements in the performance and robustness of IMDD DFMA PONs.The operating principle of the DFMA PON is described in section 3.2.2.2, and the operating

principle of the CCIC technique is described in section 4.4. Fig 6.1 depicts the Dsp architecture of the CCIC enabled DFMA PON transceiver.
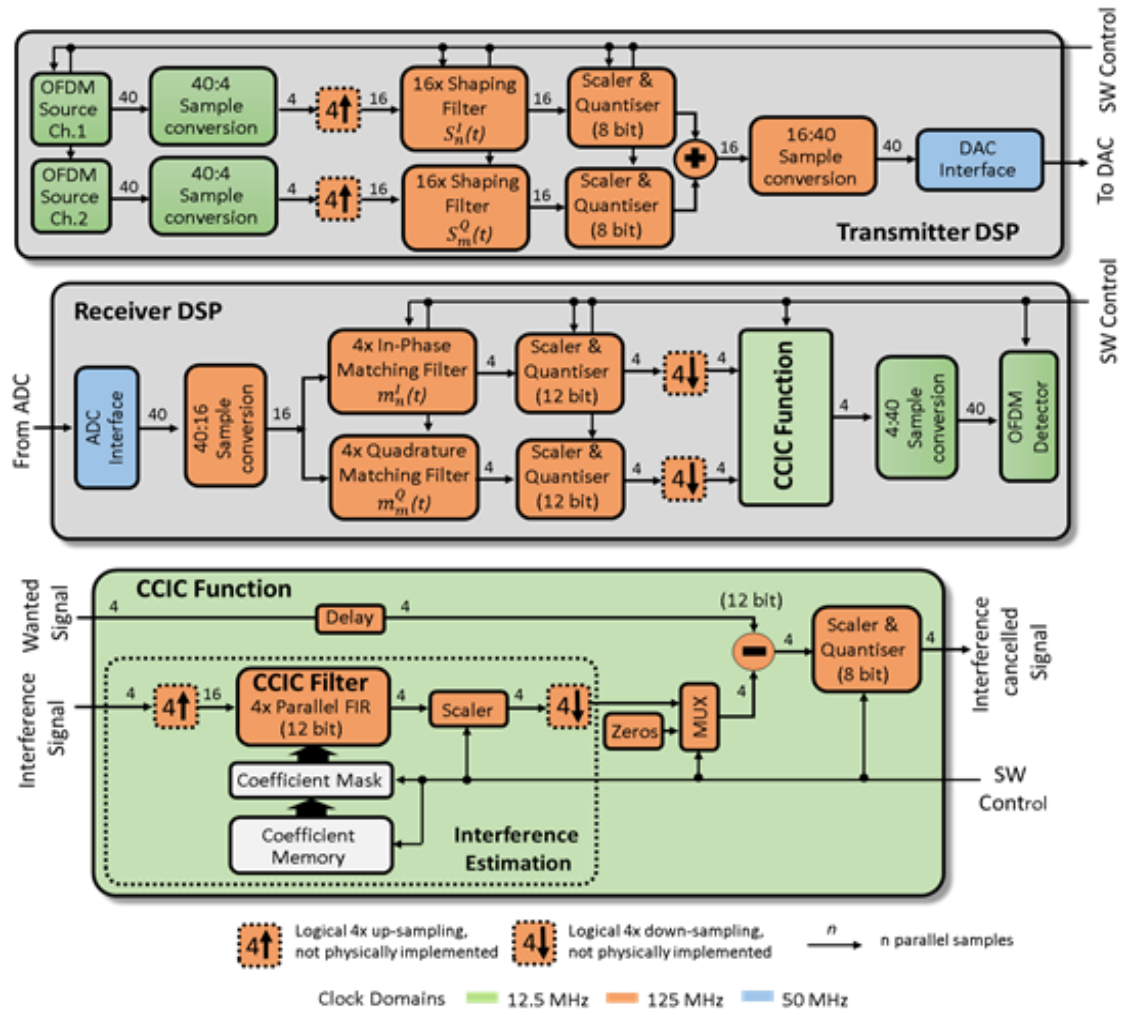

Fig. 6.1. Top level DSP architecture of the 4-channel CCIC-enabled DFMA PON transceiver

.

6.2   Real-time DFMA PONs Incorporating Low Complexity CCIC

6.2.1   DSP architecture of CCIC-enabled real-time transceivers

Fig. 6.1 shows the top-level DSP architecture for the optical transceiver's transmitter and receiver elements, which are implemented in FPGAs. The presented architecture shows the implemented DSP, which is based on the reconfigurable transceiver described in[1], which supports a two-channel system with Hilbert pair-based digital orthogonal filters for channel multiplexing. The transceivers employed here are designed to support a 4-channel system so an up-sampling factor of 4 is employed. An adaptive OFDM signal source[2], with PRBS test data and key parameters as specified in Table. I, provides a data signal for each channel. As the employed DAC operates at 2GS/s, the SF consists of 16 parallel FIR filters, with software-controlled tap coefficients, operating at 125MHz to achieve the required sample throughput. An on-line adjustable scaling function with 8-bit quantisation follows the SF to allow signal power adjustment. Two channel instances are implemented in a single transmitter, with their outputs digitally summed, before application to the DAC interface. As the 8-bit, filter tap coefficients are software-controlled each SF can be dynamically configured to support any one of the four possible channels. Full details of the SF DSP design for low complexity are discussed in section 6.4.2. As the DAC/ADC sample rate is 2GS/s, the four transmitter generated channels are an I (Q) channel in the baseband region from 0–0.5GHz designated as BB-I (BB-Q) and an I (Q) channel in the passband region from 0.5–1GHz designated as PB-I (PB-Q).

The inset in Fig. 6.2 shows example electrical spectra at the ONUs of the two sub-wavelength bands. The architecture of the receiver's DSP is also based on that presented in[1], however here the design supports 4 channels and two FIR-based, reconfigurable, MFs are implemented. Full details of the low complexity, MF DSP design are discussed in section 6.4.2. The first MF recovers the wanted signal and the second MF recovers the interference-generating signal in the corresponding orthogonal channel. For demonstration purposes only one OFDM decoder function is implemented to decode and analyse the BER of the wanted, CCIC-compensated, channel, however in a practical implementation both orthogonal channels could be recovered.

Table I. Transceiver and system parameters

Parameter	Value
OFDM IFFT/FFT size	32 points
Maximum data carrying OFDM subcarriers per channel	15
Subcarrier frequency spacing	15.625 MHz
Subcarrier modulation format	16-QAM
DAC and ADC sample rate / bit resolution	2GHz / 8 bits
OFDM encoder/decoder clock rate	12.5MHz
Data sequence length for error counting	88,500 Symbols
Samples per symbol* IFFT/Cyclic prefix/Total	32 / 8 / 40 Samples
Line rate per channel (13 subcarriers enabled)	812.5Mb/s
Adopted FEC limit	1.0×10^{-3}
EML wavelength/modulation bandwidth	~1550nm[&] / 10GHz
EML laser bias current/EAM bias voltage/MZM DC bias	125 mA / -0.75V / 1.43V
EML/MZM driving voltage	2 / 1.2 Vpp
TLS wavelength/MZM modulation bandwidth	~1550nm[&] / 20GHz
EML/MZM optical launch power before EDFA	2.6 / -2.3 dBm
EML and MZM optical launch power after EDFA	4.5 dBm
Electrical signal amplitude at ADC	340 mVpp
PIN bandwidth/noise	12.5 GHz / 2.8mVrms
PIN responsivity at 1550nm	0.55 A/W
SSMF length	26 km

* Before up-sampling and after down-sampling
& Wavelength spacing =0.3nm
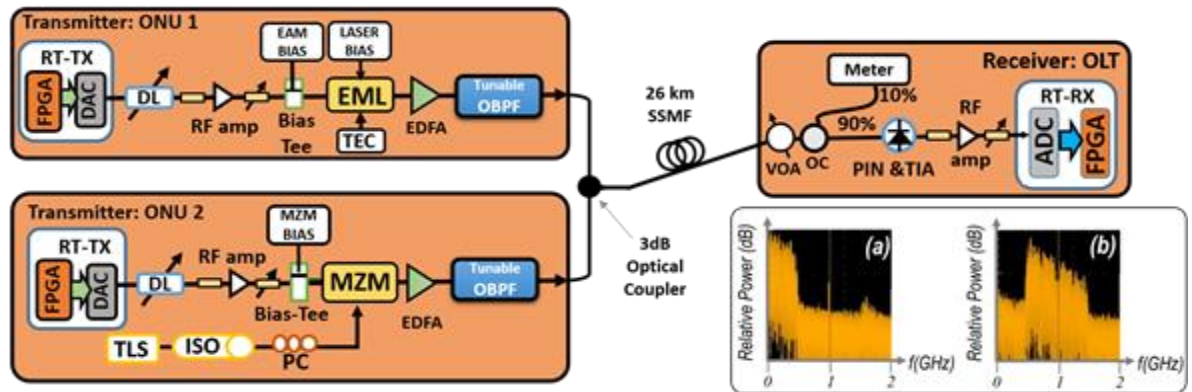
Fig. 6.2. Real-time DFMA PON upstream experimental system setup. Inset: Example electrical spectra at the ONUs with all subcarriers enabled (a) BB-I+BB-Q, (b) PB-I+PB-Q. Note: Image spectra shown from 1-2GHz. DL: Delay line; EML: electro-absorption modulated laser; TEC: thermo-electric controller; MZM: Mach-Zehnder modulator; VOA: variable optical attenuator; OBPF: optical bandpass filter; TLS: tunable laser source; PC: polarization controller; PIN+TIA: photodetector with integrated transimpedance amplifier; EDFA: erbium doped fiber amplifier; ISO: Isolator; RT-TX: real-time transmitter; RT-RX: real-time receiver

The recovered interference-generating signal is applied to the CCIC function, as illustrated in Fig. 6.1, where, after suitable up-sampling, it is applied to the CCIC filter, suitably scaled and down-sampled to generate an estimate of the interference signal. The 12-bit, estimated interference signal is then subtracted from the 12-bit, suitably delayed wanted signal, before signal decoding, channel/subcarrier BER analysis and subcarrier constellation observation in the OFDM decoder function. The CCIC function operates with 12-bit samples as this resolution limits complexity and minimises the quantisation noise effect to achieve good CCIC performance at the lower interference levels present at the higher signal frequencies. The CCIC function also incorporates additional functionality for the purpose of performance analysis only. Firstly, the interference cancellation can be disabled via a multiplexer, shown in Fig. 6.1, which allows the interference estimation signal to be set to zero-valued samples thus allowing the system performance to be observed without CCIC enabled. Secondly, as it is important to optimise the complexity of the CCIC filter to minimise implementation cost and power consumption, whilst maintaining sufficient performance, the CCIC filter design incorporates a coefficient mask located between the 64-tap coefficient memory and the CCIC filter coefficient inputs. This software-controlled mask can dynamically limit the effective filter tap count by setting the unwanted tap coefficients to zero. This allows full investigation of the trade-off between complexity (tap-count) and performance. The coefficient mask is designed to limit CCIC filter tap count to 64, 54, 42, 32, 16 or 8.

6.2.2 **Experimental System Setup**

The upstream DFMA PON experimental system setup and the associated transceiver/system parameters are given in Fig. 6.2 and Table. I, respectively. The employed real-time DSP platform is described in appendix A The more challenging upstream transmission is experimentally demonstrated as it involves the optical summation of different channels with timing synchronisation necessary between ONUs to maintain channel orthogonality. The setup consists of two ONUs (with dual-channel transmitters) and one OLT (with a single-channel receiver). Both ONUs, incorporating the aforementioned DSP and DACs, include an RF delay line for fine adjustment of signal timing, an RF gain stage based on a fixed gain RF amplifier and variable gain electrical attenuator, an IM for E/O conversion, and an EDFA for optical power boost and control with a tuneable 0.8nm OBPF to minimise out-of-band, amplified spontaneous emission noise (ASE). The IM in ONU1 is an electro-absorption modulated laser (EML) which integrates a DFB laser, as its light source, with an electro-

absorption modulator (EAM), both of which are subject to optimised operating conditions including DC biasing, temperature control and driving voltage as specified in Table. I. The IM in ONU2 consists of a tuneable laser source (TLS) and a Mach-Zehnder modulator (MZM). The TLS output passes via an isolator and an optimally adjusted polarization controller prior to feeding the MZM input. By adopting different IMs in each ONU, the performance of the DFMA PON and the CCIC technique when operating with different types of IM can be easily observed. The MZM is biased at its quadrature point. During MZM operation, the bias voltage and driving voltage amplitude are fine-tuned for best performance. The output powers of both EDFAs are adjusted to 4.5 dBm. The optical signals from the ONUs are combined in a 3dB passive optical coupler, representing the remote node of the PON, before the optically combined signal is launched into a 26km SSMF. Both ONUs operate at a nominal wavelength of 1550nm, however a wavelength spacing of 0.3nm is employed to avoid the DD-induced OBI effect [3]. During the photo-detection process, the optical beating between multiple adjacent optical wavelengths generates unwanted interference components within the wanted signal frequency range, by ensuring sufficient spacing between wavelengths, the interference components will fall outside the wanted signal frequency range and can be removed by filtering after photo-detection. In practice wavelength control can be achieved by laser thermal detuning [4] or alternative OBI mitigation methods [5, 6] may be employed after suitable modifications. For experiments involving a PTP configuration, ONU1 and the 3dB optical coupler are omitted so that ONU2 connects directly to the 26km SSMF link. The OLT-based receiver consists of a variable optical attenuator (VOA) to adjust the ROP level, a 90:10 optical splitter for ROP measurement, a 12.5GHz linear PIN photodetector with integrated transimpedance amplifier (TIA) for direct detection of the optical signal, an RF gain stage, similar to that employed in the ONUs, to optimise the analogue signal level, a 2GS/s, 8-bit ADC and finally an FPGA for the receiver DSP operations. It should be noted that the ADC incorporates a suitable antialiasing filter to remove out-of-band receiver noise before signal sampling.

The frequency responses of the two paths, i.e. from ONU1 to the OLT employing the EML and from ONU2 to the OLT employing the MZM, are measured using a pilot tone-based channel estimation method. This provides the discrete channel frequency response coefficients from 62.5MHz to 937.5 MHz in 62.5MHz intervals. The discrete channel impulse responses are then computed for use in the CCIC filters. Both paths show a reasonably similar frequency response with a total roll-off of 10.5 - 12dB over the 1GHz

spectral region, therefore, the same channel impulse response is utilized when determining the four different CCIC filter responses corresponding to the four channels. In addition, as the level of frequency response roll-off is relatively high, it has a high probability of representing worst-case practical scenarios, thus providing an excellent environment for evaluating the CCIC technique's performance.

6.2.3   Performance of Low Complexity CCIC in Point-to-Point SMF Links

To verify the performance of the real-time CCIC function and investigate the impact on performance of CCIC filter tap count, a 26km SSMF PTP optical link is adopted as described in section 6.2.2, and shown in Fig. 6.2, with the parameters specified in Table. I. Thus the PTP link uses ONU2 with a TLS and MZM for optical intensity modulation. The PTP link is adopted as it allows reliable evaluation of the CCIC function's performance by eliminating any possible inter-ONU STO-induced channel leakage [7] caused by non-optimised inter-ONU synchronisation. To assess the performance of the real-time CCIC function, BER versus ROP measurements are performed. The adopted measurement procedure is as follows; the OFDM subcarriers are set for 16-QAM modulation with a flat subcarrier power loading profile, then with only one sub-band channel enabled all parameters are optimised (as in Table. I) for minimum channel BER. To optimise the receiver's sample timing, whole sample interval adjustments are made in the ONU's OFDM encoder and sub-sample interval adjustments are made with the manual RF delay line in the ONU. All transceiver and system parameters are thus optimised for a minimum channel BER. For the BB (PB) sub-wavelength band only the highest frequency 11 (14) subcarriers are enabled as the 3 (1) lower frequency subcarriers have BERs in excess of the FEC limit. When the first sub-band channel is operational, the corresponding orthogonal sub-band channel is then enabled and parameters such as RF gain and digital scaling values are adjusted to minimise the total BERs of both channels simultaneously. Fig. 6.3shows measured BER versus ROP curves for each of the four channels with a different number of CCIC taps enabled and with the CCIC function disabled.

The BER measurements in Fig. 6.3 clearly show that when no CCIC is applied, there are significant levels of CCI, which prevents all channels from achieving a BER below the FEC limit, regardless of the ROP level, as indicated by the flat characteristic of the BER curves. However, the real-time CCIC function substantially improves BER performance to

acceptable levels on all channels when enabled with a sufficient number of filter taps. Fig. 6.3 clearly shows that in all cases, a minimum of 32 taps are required to achieve a BER below a FEC limit of 1×10^{-3} (corresponding to 7% overhead [14]). To allow some margin however, 42 taps can be considered to provide a good trade-off between the CCIC filter complexity and the channel performances. It is also interesting to note that the general BER developing trends observed in Fig. 6.3, of very shallow curves with CCIC off and steeper curves with CCIC on, is also observed in both the offline [8] and theoretical [7] CCIC results.
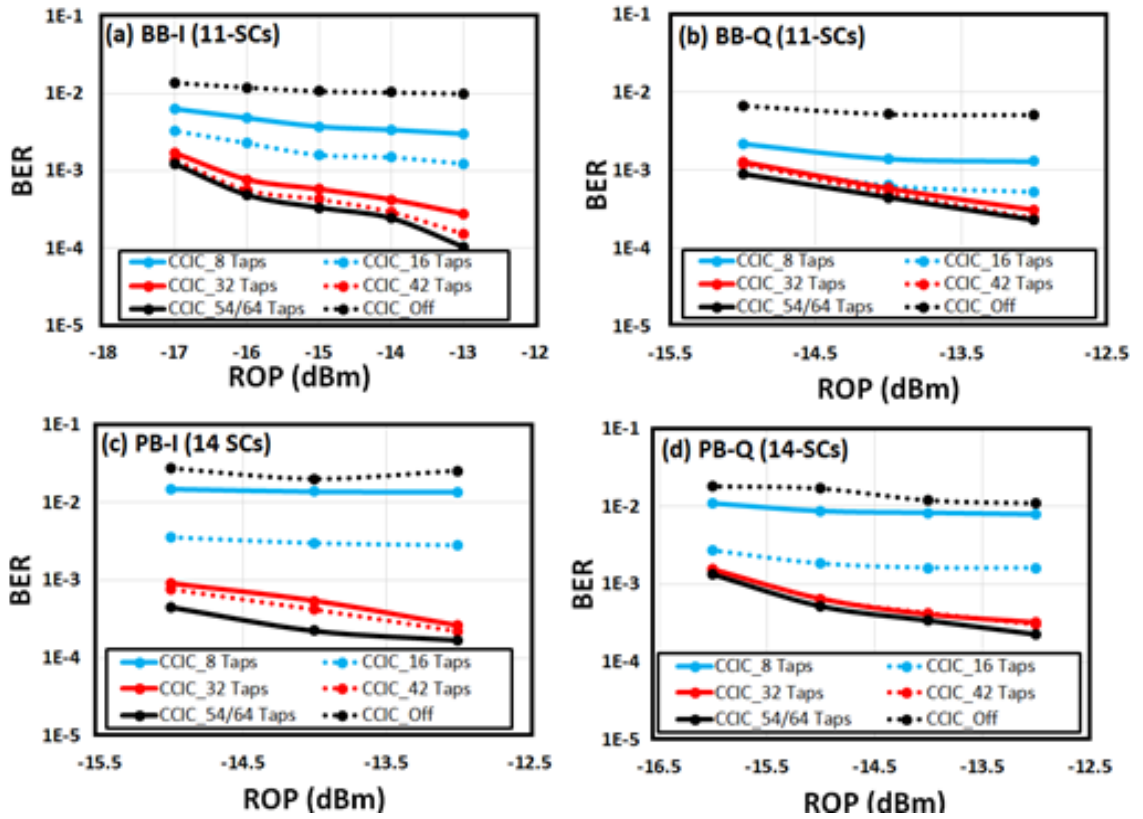

Fig. 6.3. Fig. 3. BER vs. ROP for (a) BB-I, (b) BB-Q, (c) PB-I, (d) PB-Q for varying CCIC filter complexity for point-to-point 26km SSMF transmission

6.2.4 **Performance of Low Complexity CCIC in DFMA PONs**

Having validated the CCIC function in a PTP optical link, it is essential to verify its operation in a practical IMDD DFMA PON scenario. For this experiment, the setup in Fig. 6.2 is adopted with all associated parameters set as specified in Table. I, and the CCIC filter tap count is set to the optimum value of 42 taps as determined in section 6.2.3. The ONUs are configured such that ONU2 (ONU1) generates channels BB-Q and PB-I (BB-I and PB-Q), this provides a worst case channel configuration scenario as inter-ONU STO timing must be

correctly adjusted to maintain orthogonality between channels in the same sub-wavelength band. All OFDM subcarriers are enabled in order to observe the CCIC function's effectiveness across the entire signal spectral range. The total ROP is set to -10dBm, which corresponds to a ROP for each ONU of -13dBm.

The method adopted to configure the system for optimum upstream performance is as follows: firstly, only ONU1 is enabled and configured to generate channels BB-I and PB-Q, this logical PTP set up is optimised, as described in section 6.2.3, following the same procedure for receiver sample timing adjustment. Secondly, ONU2 is enabled and configured to generate the BB-Q and PB-I channels. The integer valued, sample timing offset is adjusted in the OFDM encoder in ONU2 to ensure the correct samples are recovered in the receiver and the inter-ONU STO is adjusted via the manual RF delay line in ONU2. Finally, to simultaneously minimise the BERs of all channels the RF gains and SF/MF digital scaling values are adjusted as necessary.

To receive a specific channel the MFs and CCIC filter in the receiver are configured with the appropriate impulse responses. The real-time BER of each individual subcarrier within a channel is then observed in order to plot the BER versus subcarrier index for each channel, as shown in Fig. 6.4. To observe the effectiveness of the CCIC function on each channel, the CCIC is disabled, whilst keeping all other parameters unchanged, and the BER versus subcarrier index for this case is measured as shown in Fig. 6.4. Furthermore, to observe the impact on BER performance of the neighbouring sub-wavelength band, for each channel the BER versus subcarrier index is plotted with the 2 channels in the neighbouring sub-wavelength band disabled, for the cases of CCIC enabled and disabled, as shown in Fig. 6.4.

Table II. Working subcarrier count with and without CCIC enabled

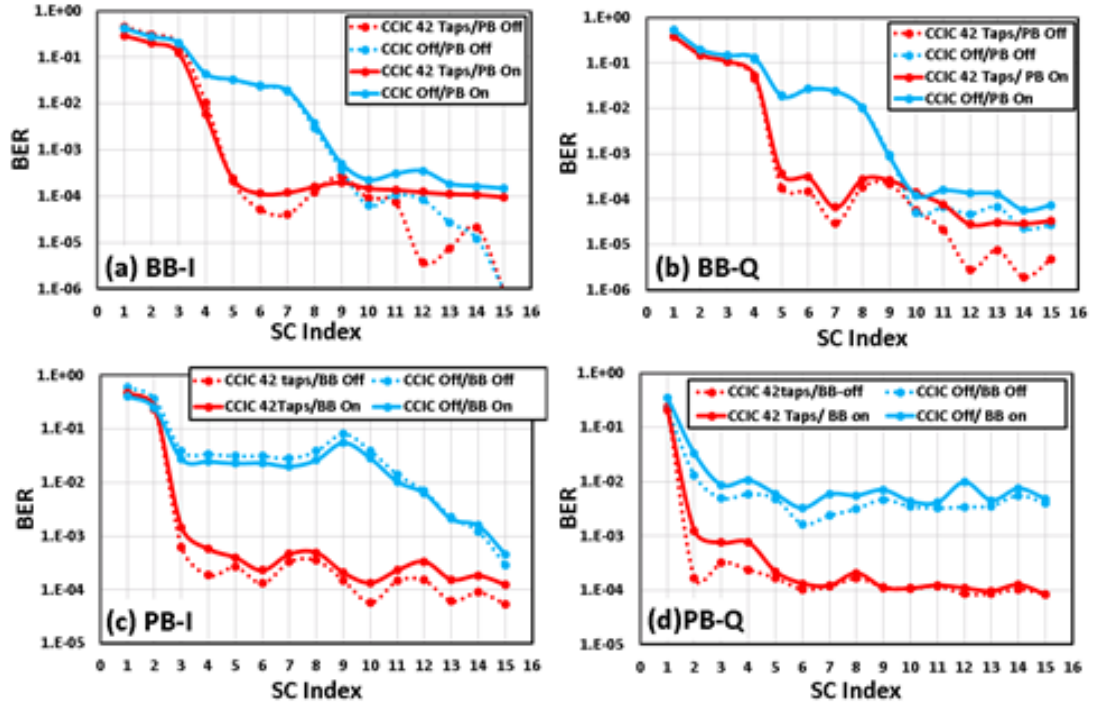| Channel	SCs when CCIC off	SCs when CCIC on	Capacity Increase Factor
BB-I	7	11	1.6
BB-Q	7	11	1.6
PB-I	1	12	12
PB-Q	0	13	∞

Fig. 6.4. BER vs. subcarrier index for 26km SSMF DFMA PON transmission at a total ROP of -10dBm with 42 tap CCIC filters a) BB-I, b) BB-Q, c) PB-I and d) PB-Q.

The observed results verify that the CCIC function, implemented with only a 42 tap filter, is highly effective in removing CCI between orthogonal channels in the 26km SSMF DFMA PON. When considering the channel capacity in terms of the number of subcarriers with BERs below 1×10^{-3}, the observed CCIC-induced increases in channel capacity for the cases of CCIC off and CCIC on are illustrated in Table. II. It would also be possible in practice for an ONU, to further maximise the capacity of its dynamically allocated and hence variable channel, by exploiting the adaptive bit and power loading feature of OFDM.

It can also be inferred from Fig. 6.4 that the dominant CCI occurs between spectrally overlapped orthogonal channels as there is minimal reduction in subcarrier BERs when the neighbouring sub-wavelength band is turned off, hence, there is a finite, yet very low level of interference from a channel's adjacent sub-wavelength band, which is due to the large, but finite, out-of-band attenuation of the digital filters. This important result is in full agreement with the results from the numerically investigated DCIC technique presented in[7].

When considering the BER vs. subcarrier index curves in Fig. 6.4(a-d), for the case of CCIC disabled, there is a general trend of lower frequency subcarriers suffering higher BERs,

which is consistent with the fundamental CCI mechanism, as the lower frequency subcarriers are located at the outer edges of the sidebands and so suffer more from the sideband power imbalance effect. Also, the frequency response profile for the PB channels has a higher roll-off (~7dB) compared to the BB channels (~4dB) which explains why the PB channels, in comparison to the BB channels, have virtually no subcarriers with a BER below the FEC limit for the CCIC-disabled cases. The general variation between the curves can be due to the fact that the CCI levels are dependent on the specific channel frequency response profiles. When considering the CCIC enabled case, the curves show a trend of a reasonably flat BER but rising sharply at the lower frequency subcarriers, the flatness indicating that the CCIC is equally effective for different levels of CCI. The aforementioned sharp rise in BER can be attributed to the finite tap count-induced enhancement of digital filter frequency response ripples, which leads to higher attenuation at the filter edges, where the low frequency subcarriers are located. Furthermore, unwanted subcarrier-subcarrier-intermixing (SSI) products [9] are generated upon square-law photon detection, where characteristically the noise power is higher at lower signal frequencies, thus the impact of SSI is more severe in the BB region, which can explain why the BB curves show high BERs at more of the lower frequency subcarriers. The shape of the curves with CCIC enabled is also dependent on the accuracy of the channel estimation used in the CCIC function. However, an important result shown in Fig. 6.4, is that the CCIC function significantly improves the BER of a substantial number of subcarriers by factors of up to ~360, interestingly this is of a similar order to that observed in the off-line CCIC experiment in [8].

In the off-line CCIC experiment in [8], which uses a very similar optical link between the ONU and OLT, hence has a similar physical channel response, the BER versus subcarrier index curves show a general trend of CCIC performance increasing with subcarrier frequency, however a similar trend is not apparent in the plots in Fig. 6.4. This can be due to differences in the sub-wavelength band frequency response profiles [10], as here (in[8]) each sub-wavelength band occupies half (all) of the 1GHz aggregate signal bandwidth. Also, the real-time DSP hardware employs fixed-point calculations (max 12 bit) in comparison to the high precision, floating-point calculations of the off-line processing approach. This can reduce the CCIC effectiveness at low CCI power levels, nevertheless, the finite precision of the real-time DSP implementation is demonstrated to be sufficient to achieve highly effective CCIC.

6.3 Real-Time DFMA PON Performance

To further explore the effectiveness of the CCIC function and its impact on system robustness, in this section further analyses is undertaken of the performance of a real-time DFMA PON incorporating low complexity CCIC, in terms of BER performance, impact on tolerance to inter-ONU STO and transparency of the CCIC function to the interfering signals modulation format.

6.3.1 Low complexity CCIC-Induced Improvement in DFMA PON Performance

The IMDD DFMA PON system employing a 26km SSMF link, as described in section 6.2.4, is employed with ONU1 (ONU2) generating the PB (BB) sub-wavelength bands. The BER performance of both the PB-I and PB-Q channels, with BB-I and BB-Q channels being present, is measured with 13 subcarriers enabled (3rd to 15th) allow a fair comparison and ensure all subcarriers operate with BERs below the adopted FEC limit of 1×10^{-3}. Small adjustments to the subcarrier power loading profiles are made to reduce the BER of low frequency subcarriers with BERs close to the FEC limit. BER measurements are performed with and without the 42-tap count CCIC function enabled, and to further verify that 42 taps are adequate, comparative BER measurements are also performed with 54 and 64 taps enabled. Fig. 6.5(a) shows the BER versus ROP for the PB-I channel, in the region of the adopted FEC limit, for the aforementioned cases and Fig. 6.5(b) shows the corresponding measurements for the PB-Q channel. The BB-I and BB-Q channel performances are not shown in Fig. 6.5 as their performances are similar to the PB-I and PB-Q channels.
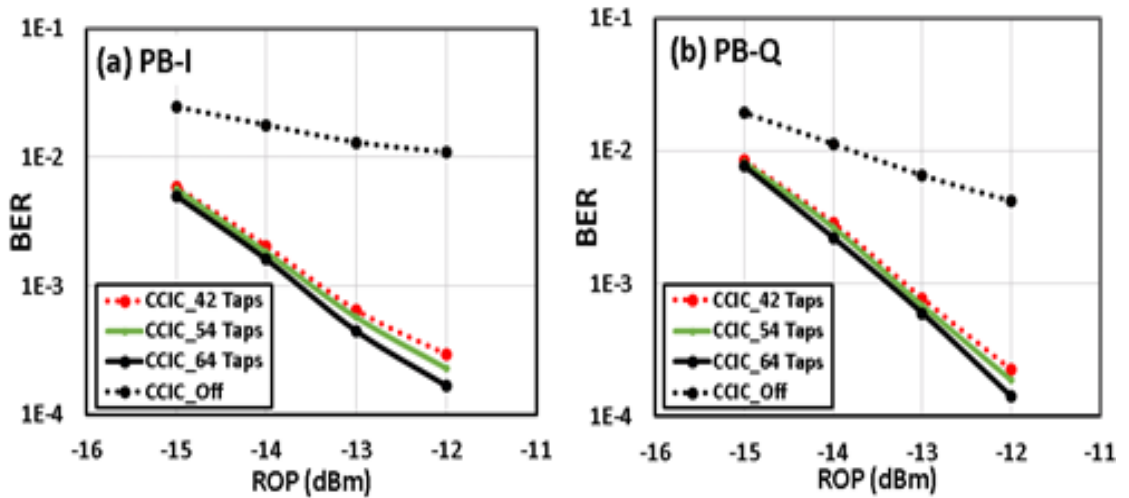
Fig. 6.5 BER vs. ROP for passband channels using varying CCIC filter complexity for

26km SSMF MPTP transmission using 13 subcarriers (a) PB-I (b) PB-Q

It is clear that without CCIC the total channel BERs greatly exceed the FEC limit, whereas when CCIC is enabled with 42 taps, both channels can operate below the FEC limit when the total ROP level is ≥-13.4dBm (≥-13.2dBm) for the PB-I (PB-Q) channel. Considering ROP per ONU, to allow comparison with the PTP case, the corresponding ROPs for PB-I (PB-Q) at the FEC limit are -16.4dBm (-16.2dBm), which are ~1dB lower than the corresponding PTP case, this can be due to the fact that, in the DFMA PON case a second, high BER, subcarrier has been dropped. This fact can also be the reason for the increased slope of the BER curves. It is also evident that there is now only an extremely small variation in performance between the 64, 54 and 42 tap count cases, which is smaller than that observed in the corresponding PTP case plotted in Fig. 6.3.

This can also be due to the aforementioned dropping of the low performance 2nd subcarrier. Fig. 6.5, thus further validates 42 taps as the optimum CCIC filter tap count. As 16-QAM is adopted on each subcarrier the total line rate of each channel is 812.5 Mb/s, or 1.625Gb/s aggregate line rate for the PB subwavelength band, corresponding to a spectral efficiency of 3.25b/s/Hz. Hence, an aggregate signal bandwidth of 15GHz could support ~50Gb/s.
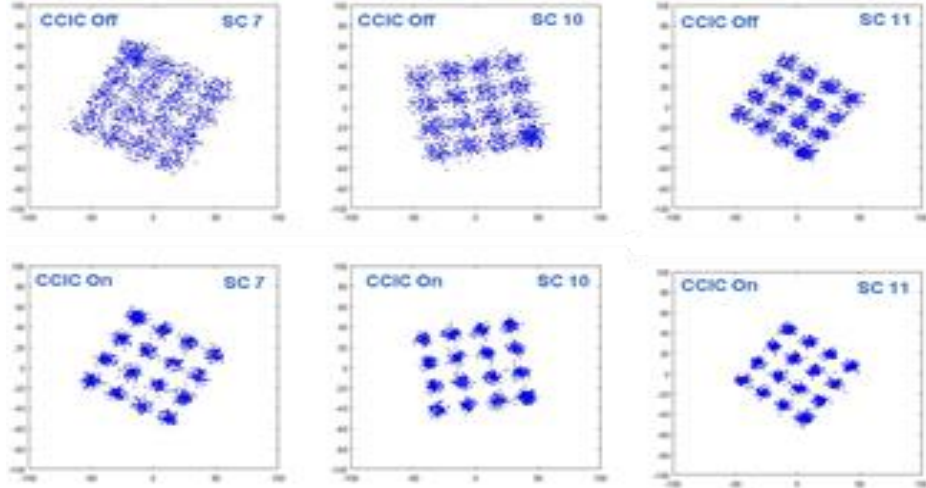

Fig. 6.6 Example unequalised PB-I subcarrier constellations for the cases of CCIC disabled and enabled in a 25km SSMF DFMA PON at -10dBm total ROP and 42 tap CCIC filters. (SC: subcarrier)

For the PB-I channel, Fig. 6.6 shows example unequalised subcarrier constellations for the cases of CCIC enabled and disabled, for the conditions corresponding to the measurement case in Fig. 6.5(a) and a total ROP of -10dBm. As would be expected, the constellations with CCIC enabled show a clear reduction in CCI compared to the case when CCIC is disabled, which is fully consistent with the observed reductions in the subcarrier BERs. It is also observed that each of the 16-QAM constellation points has a more square (round) shape for the case of CCIC disabled (enabled). This is due to the fact that, the CCI at a specific subcarrier frequency originates from the corresponding spectrally overlapped subcarrier in the orthogonal sub-band, which has a characteristic square shape due to the square-shaped 16-QAM constellation. Whereas when CCIC is enabled, the predominant noise is additive white Gaussian noise (AWG) from sources such as the PIN photodetector and the RF amplifiers and so it generates the characteristically rounded constellation points.

6.3.2   Impact of Real-Time CCIC on Inter-ONU STO Tolerance

Achieving suitable timing synchronization between ONUs occupying the same signal spectral region is essential for the DFMA PON operation. Therefore, the effect of the CCIC function on the tolerance of the DFMA PON to inter-ONU STO is explored in this section. The PON system employing a 26km SSMF link, as described in section 6.2.4 , is employed with ONU1 (ONU2) generating the BB-I and PB-Q (BB-Q and PB-I) channels, such that orthogonal sub-bands originate from different ONUs. To allow inter-ONU STO range comparisons for the cases of CCIC enabled and disabled, and as the range is dependent on the number of enabled subcarriers and the ROP, only the 6 highest frequency subcarriers are employed in each channel with ROP set to -9dBm, to ensure channel BERs below the FEC limit of 1×10^{-3} can still be achieved when the CCIC function is disabled. All subcarriers adopt 16-QAM modulation and all other parameters are as specified in Table. I. The CCIC function also employs the previously identified optimum tap count of 42. Here, the inter-ONU STO range is defined as the maximum signal time delay variation range of the ONU with varied sample time, which maintains the BER of the ONU with fixed sample time, below the adopted FEC limit, thus, loss of channel orthogonality is purely generated by inter-ONU STO as receiver STO is maintained at the optimum value. To measure the inter-ONU STO range, the inter-ONU STO between the transmitters in the ONUs and the receiver STO at the OLT are optimised for minimum BER on all channels. Then, using the RF delay lines

the signal timing of ONU1 (ONU2) is advanced and delayed in relation to its optimum value
in steps of 12.5ps, whilst the BER of PB-I (BB-I) is monitored.

Fig. 6.7(a) shows the BER variation of the BB-I channel from ONU1, as the timing of the
BB-Q channel from ONU2 is varied for the cases of CCIC enabled and disabled. In the
figure, 0ns corresponds to the optimum ONU synchronisation case. A significant increase in
inter-STO timing range is achieved from 0.04ns with CCIC off to 0.2ns with CCIC on,
corresponding to a five-fold increase. Fig. 6.7(b) shows the corresponding case for the PB-I
channel from ONU2 when the timing of the PB-Q channel from ONU1 is varied, here an
approximate fifteen-fold increase in inter-STO range is achieved from ~0.01ns for CCIC off
to 0.15ns for CCIC on. The PB-I channel is observed to be more sensitive to the inter-ONU
STO compared to the BB-I channels, which is expected as the PB channels operate at higher
frequencies where a given time offset results in a greater signal amplitude deviation. The
CCIC-induced improvements in inter-ONU STO ranges now significantly relaxes the ONU
synchronisation requirements as the ranges now correspond to 40% (30%) of the 500ps
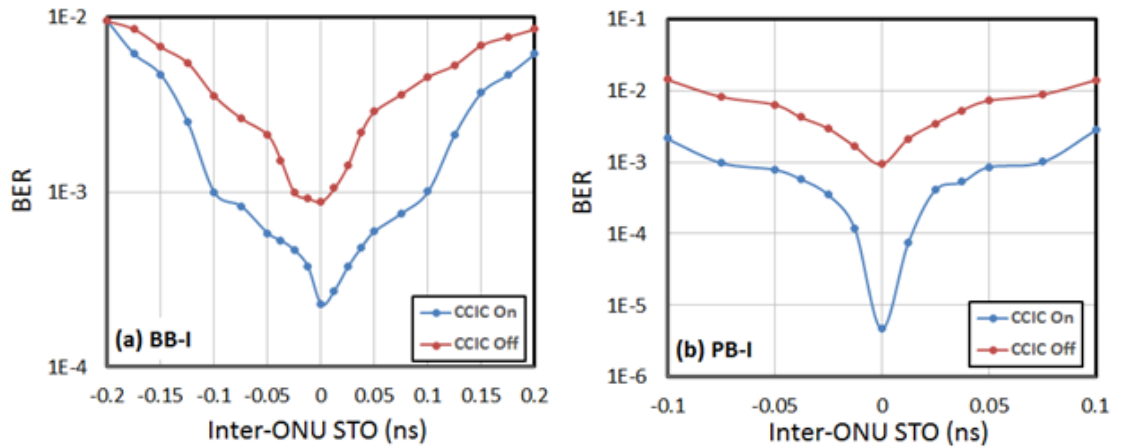sample interval for BB-I (PB-I).

*Fig. 6.7 Variation of BER with Inter-ONU STO for (a) BB and (b) PB in-phase channels
with and without CCIC enabled*

The precision of practical clock sources such as temperature compensated crystal oscillators
(TCXOs), can be as low as 1 part per million (PPM) or less, therefore the above determined
STO range will mean that required rate of the clock timing adjustment is realistic. In a
practical system it is necessary to implement sufficiently accurate and automatic control of
the relative inter-ONU STO. Ideally DSP algorithms embedded inside the ONUs and OLT,

can estimate the STO and compensate accordingly, this is because DSP-based solutions which avoid the need for external discrete components such as RF delay lines, are unquestionably more preferable from a cost-effectiveness perspective. A potential approach is for the OLT to monitor the STO dependent recovered signal power and instruct the ONU to adjust signal timing via an embedded variable fractional delay filter [13], which provides a sub-sample interval timing adjustment.

6.3.3   **Transparency of CCIC to Signal Modulation Format**

In this section, the transparency of the CCIC function to the interfering channel's modulation format is investigated. The DFMA PON, with all parameters as specified in Table I, is employed, with a total ROP of -10dBm. The ONUs are configured such that ONU1 (ONU2) generates the BB-I and PB-Q (BB-Q and PB-I) channels, thus the CCI-inducing orthogonal channels originate from different ONUs. The CCIC function is set for the previously determined optimum tap-count of 42. To evaluate the transparency to modulation format across the whole spectral region of a sub-band channel, all subcarriers are enabled and the BER versus subcarrier index is measured for PB-I and PB-Q for two different cases. For case 1, all channels adopt 16-QAM on all subcarriers and the system is optimised for minimum channel BERs using the procedure described in Section 6.2.4. For case 2, the ONU generating the interfering orthogonal channel is configured to generate 32-QAM on all subcarriers on both of its channels, whilst all other transmitter and receiver settings remain unchanged. The BER versus subcarrier index for both cases is plotted for ONU2 (16-QAM on PB-I) and ONU1 (16-QAM on PB-Q) in Fig. 6.8(a) and Fig. 6.8(b) respectively. The results clearly show that the CCIC function is highly effective with either 16-QAM or 32-QAM modulation on the interfering orthogonal channel, showing that the CCIC function is highly flexible and transparent, as its operation is independent of modulation format, and the required CCIC function's configuration is also completely independent of the modulation format.
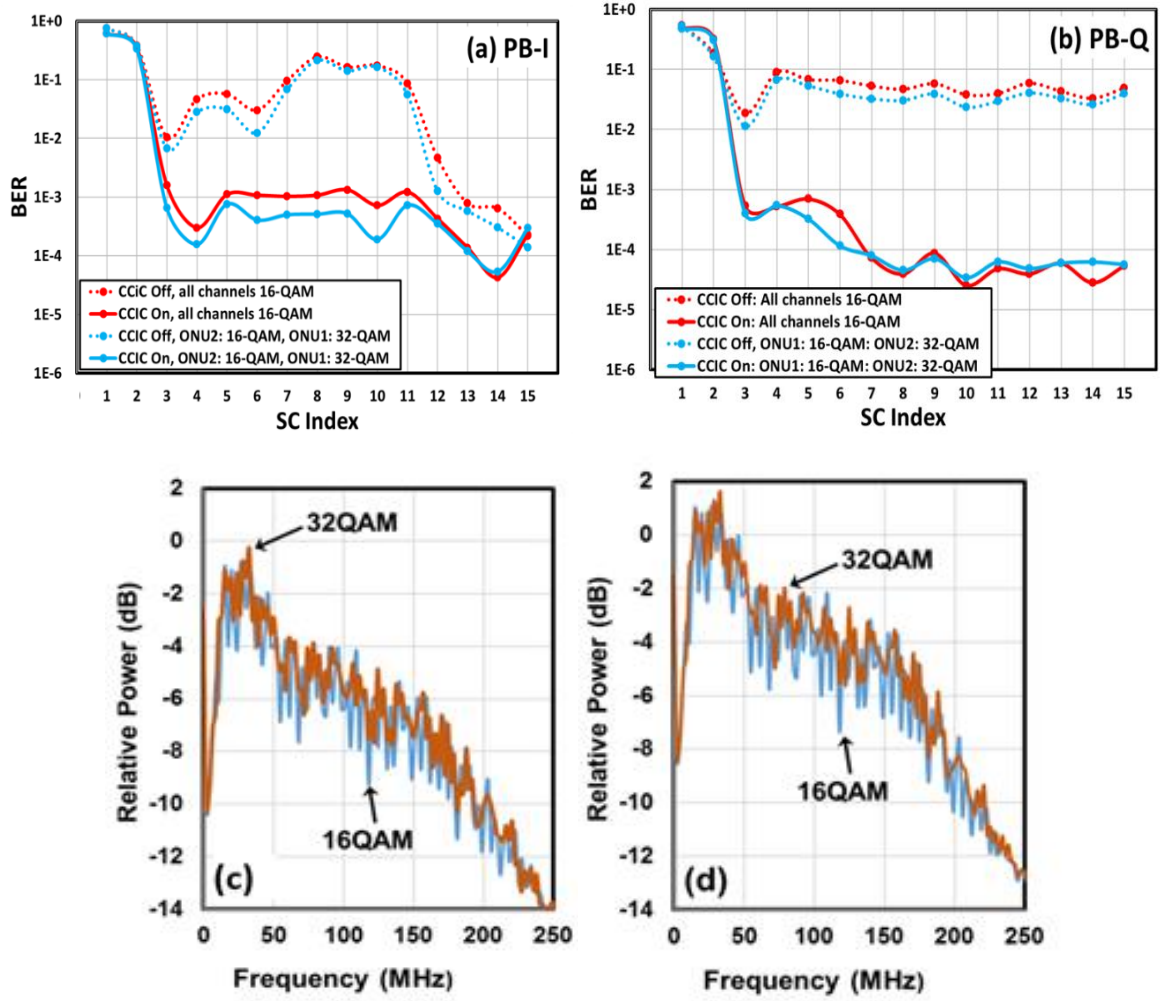
Fig. 6.8 BER vs. subcarrier index for 26km SSMF multipoint-to-point transmission at an ROP of -10dBm for (a) PB-I from ONU2, (b) PB-Q from ONU1 and corresponding interfering signal spectra (c) PB-I, (d) PB-Q

Also, it can be seen in Fig. 6.8 that the shape of the BER versus subcarrier index curves are very similar for the two aforementioned cases, indicating the 16-QAM and 32-QAM interfering signals generate a similar spectral distribution of interference signal power, this supposition is validated by the fact that the frequency spectra of the 16-QAM and 32-QAM interference signals are also very similar, as shown on Fig. 6.8(c) and Fig. 6.8(d) for the cases of recovering the PB-I and PB-Q channels respectively. As the real-time receiver DSP is not designed to allow observation of the actual interference signal within the FPGA, the aforementioned spectra are generated using a Simulink-based simulation model of the experimental DFMA PON system, employing a digital FIR filter to represent the physical channel's response (DAC, E/O, fibre, O/E, ADC).

6.4   DSP Complexity Analysis

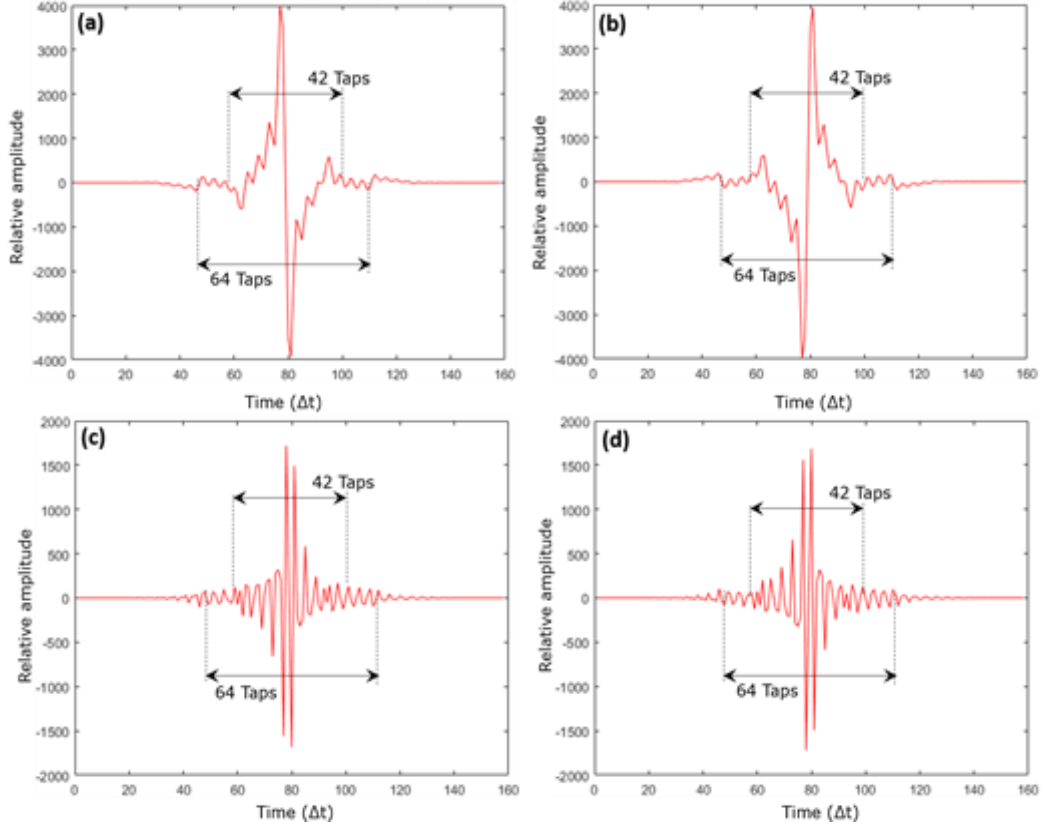### 6.4.1   Complexity Optimisation of DSP-Based CCIC Filter

Fig. 6.9. Full length (158 tap) impulse responses of CCIC filters (a) BB-I, (b) BB-Q, (c) PB-I, (d) PB-Q

In this sub-section, we examine the responses and the associated complexity of the CCIC filters for the 4 channel DFMA PON. Assuming the SFs and MFs are 64 taps in length and the determined channel response is 32 taps in length, the full length CCIC filters resulting from the convolution of the three concatenated filters would be 158 taps in length. Fig. 6.9 (a-d) shows the CCIC filter impulse responses for the cases of receiving the BB-I, BB-Q, PB-I and PB-Q channels respectively. By inspection, it is easy to see that truncating the impulse responses to 64 taps would lead to minimal deviation from the full-length filter response, thus a tap count of 64 is selected as the starting point for the CCIC filter tap count optimisation study.

In section 6.2.3, it was concluded that 42 taps is a good trade-off between CCIC filter complexity and performance. To further validate this conclusion, Fig. 6.10 plots the BER values for each channel against tap count, extracted from the BER curves in Fig. 6.3, at a total ROP of -14dBm. Fig. 6.10 shows that as tap count decreases below 42 the BER sharply increases as the CCIC filter's impulse response rapidly deviates from its desired response, thus reducing the accuracy of the estimated interference signal. However, as tap count increases above 42 the relatively small weighting of the additional taps gives little improvement in the accuracy of the CCIC filter's impulse response, and consequently little improvement in the accuracy of the estimated interference signal. Hence, 42 taps provide an optimum CCIC filter size. The CCIC filter complexity in terms of tap count (scalar multiplier count) is therefore reduced by 73% in comparison to the full-length CCIC filter.
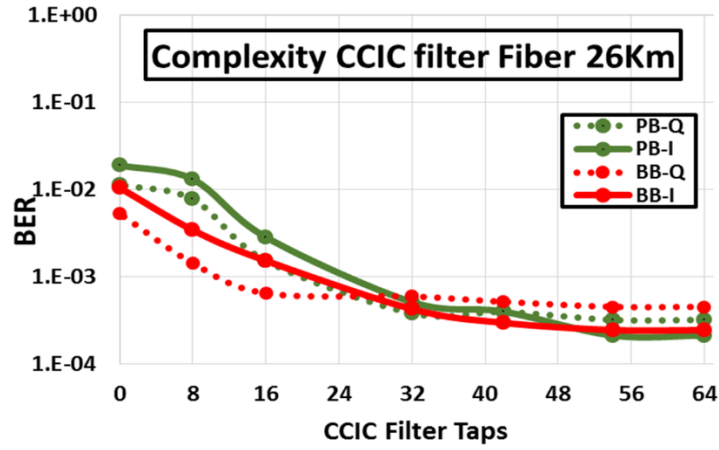

Fig. 6.10. BER vs. CCIC filter tap count for 26km SSMF point-to-point transmission at ROP of -14dBm

6.4.2 Complexity of Shaping, Matching and CCIC Filters in Multi-Channel DFMA PONs

In this section the complexity of the SF, MF and CCIC filters, in terms of scalar multiplier count (tap count), is explored to determine the interdependency on the following parameters: channel count N, DAC/ADC sampling rate S (proportional to total aggregate signal bandwidth) and maximum filter digital logic clock frequency, K. It should be noted that the required multiplier elements for all the digital filters are scalar, fixed-point multipliers and not the more logic resource hungry, complex, floating-point multipliers. Also, for the

demonstrated DFMA PON incorporating CCIC, in the SF and MF (CCIC) filters, multipliers with only 8x8-bit (8x12-bit) resolution are employed.
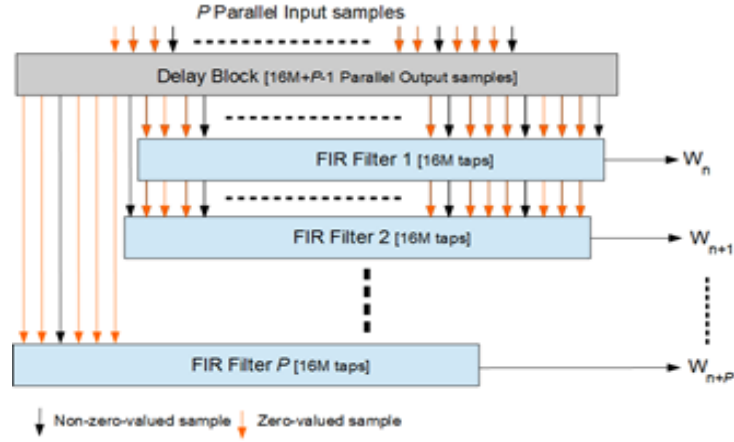

Fig. 6.11. Shaping Filter DSP Architecture

The DSP architecture of the digital SF is shown in Fig. 6.11. Parallel FIR filters are employed, as typically the digital logic clock frequency is significantly lower than the ADC/DAC sample rate. As the sampling rate of the ADC/DAC is S samples/s and the clock frequency of the digital logic is K Hz, P can be considered as a parellisation factor and is defined as the ratio of S to K, i.e. P=S/K, and so the required effective number of parallel filters is P. For P parallel filters, P parallel input samples are input to the filter bank and a delay function generates the necessary delayed samples to feed all FIR filters. To minimise the SF complexity in terms of the number of scalar multiplier elements required for the FIR filters, P is selected to be an integer multiple of the up-sampling factor M. This ensures that the zero-valued samples, generated by the up-sampling function, are always located at the

same inputs on each FIR filter, this arrangement is therefore exploited to minimise the SF complexity. Fig. 6.11, illustrates the architecture for the case of $M = 4$ as an example, however the structure is valid for the general case for all M values, where every M^{th} input sample is non-zero. In Fig. 6.11, the zero-valued (non-zero valued) samples are indicated by the orange (black) coloured arrows. In [11] an optimum length of the SF FIR filters was shown to be 16×M, therefore each FIR filter always has 16 non-zero valued input samples irrespective of the up-sampling factor M. As the required number of parallel FIR filters, P, is S/K, the total number of scalar multipliers, X_{SF}, required for the SF is:

$$X_{SF} = 16(S/K) = 16P \tag{6.1}$$

Note that as P must be a multiple of M, the value of K would be adjusted accordingly. As the maximum number of channels N, is equal to the up-sampling factor M [11], this leads to the important result that the complexity of the SF is totally independent of N, thus scaling of the channel count does not lead to excessive SF complexity.As the adopted sample rate is 2GS/s and the SF clock rate is 125MHz, P=16, therefore using Eq.(6.1), the number of scalar multipliers employed in the implemented SF described in section 6.2.1 is $16 \times 16 = 256$. Also, as an example, a system operating at 50GS/s and with a digital logic speed of 390.625MHz (i.e. P=128), would require $16 \times 128 = 2048$ scalar multipliers, which is entirely practical with modern high density application specific integrated circuit (ASIC) or FPGA technology[12].The DSP architecture of the digital MF is shown in Fig. 6.12, where P parallel FIR filters are again required to restrict the digital clock frequency to a practical value. The length of the FIR filters in terms of taps is again $16 \times M$ [11], however now there are no continuously zero-valued samples at the filter inputs so all FIR filters must employ $16 \times M$ scalar multipliers. If the filter bank operates on P parallel input samples, a similar delay block as in the SF, is employed to generate all the appropriately delayed samples for the filter inputs. As there are P parallel inputs to the MF there should be P parallel outputs, however the subsequent down-sampling function discards M-1 samples in every M samples, this fact can be exploited to completely eliminate the corresponding redundant FIR filters in the parallel filter bank, thus the total number of physically
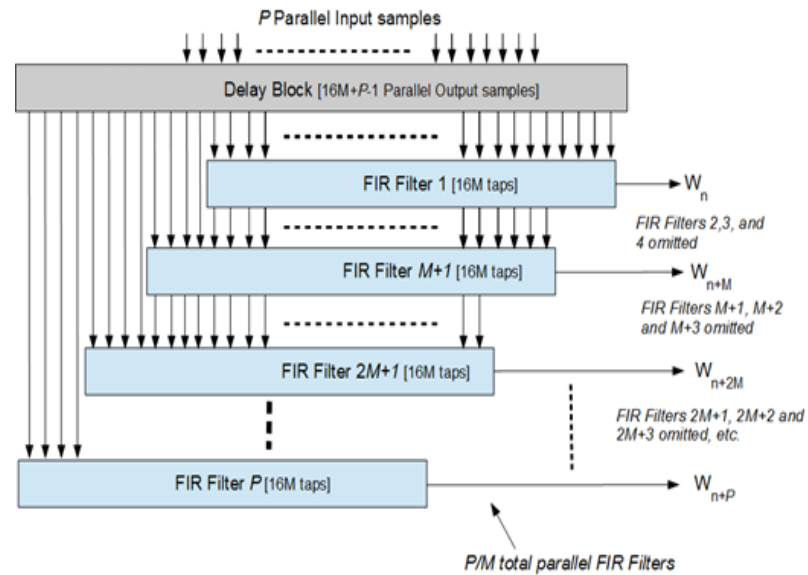

Fig. 6.12. Matching Filter DSP Architecture

implemented parallel filters is *P/M*, a reduction by a factor of (*M*-1)/*M*. It should be noted that *P* must again be a multiple of *M* to ensure the down-sampling discarded samples always originate from the same FIRs, and *P*≥*M* must be valid as there must be at least one FIR filter, corresponding to the case when *P*=*M*. As there are *P/M* parallel FIR filters each with 16×*M* scalar multipliers, and assuming *P*≥*M*, there are a total of X_{MF} scalar multipliers in the MF, given by:

$$X_{MF} = 16M(P/M) = 16P \tag{6.2}$$

This is identical to the SF case and more importantly shows X_MF is independent of the maximum channel count N, so MF complexity also does not scale with channel count. The implemented MF described in section 6.2.1, thus also employs 256 scalar multipliers.

The DSP architecture of the CCIC filter is shown in Fig. 6.13, which is based on a combination of the SF and MF filter structures. As the CCIC filter is preceded by up-sampling and followed by down-sampling, it can exploit the multiplier redundancies present in both the SF and MF filter architectures, specifically, no multipliers are required for zero-valued input samples and no FIR filters are needed where the output sample is discarded in down-sampling. For the demonstrated 4 channel case, each filter supports a tap count of 42, thus with M=4 the number of scalar multipliers per FIR is 11. As P=16 and M=4 the number of parallel FIR filters is 4, so there are only 11×4=44
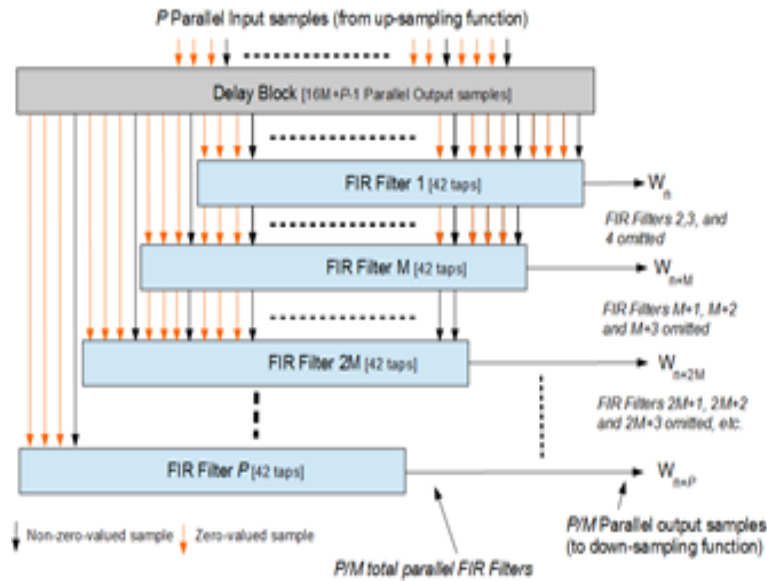

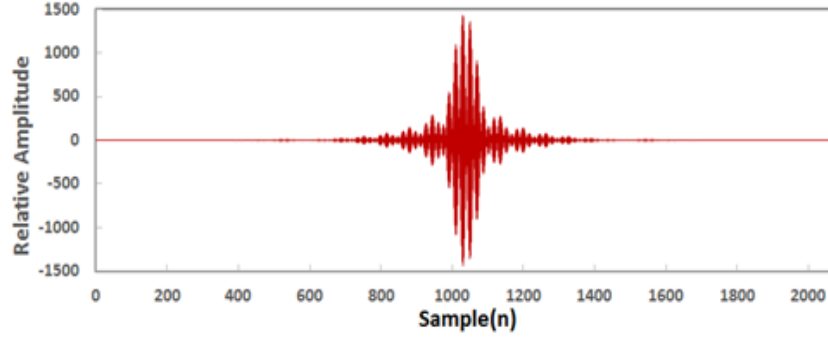*Fig. 6.13. CCIC Filter DSP Architecture*

Fig. 6.14. CCIC filter impulse response for the highest frequency sub-wavelength band in a system with 64 channels, for the case of interference from I channel to Q channel.

scalar multipliers in the implemented CCIC function, thus an ultra-low complexity DSP design is achieved.

It is also important to consider how the complexity of the CCIC filter scales with parameters such as, channel count N and the aforementioned P value. To explore the possibility of truncating the CCIC filter impulse responses for DFMA PONs employing higher channel counts, Fig. 6.14 shows the CCIC filter impulse response for the case of 64 channels, CCI from I to Q on the sub-wavelength band with the highest central frequency and using the channel impulse response of the experimental system. It is clear that the resultant 2078-tap filter can be truncated to approximately 30% of the full length giving a ~ 600-tap filter. CCIC filter responses for other tap counts and sub-wavelength bands are found to have a similar property.

The CCIC filter complexity in terms of total scalar multiplier count X_{CCIC}, can be determined for the general case, assuming tap count truncation to 30% of original count and adopting the DSP architecture of Fig. 6.13. Here we assume the channel count N is maximum such that N=M [11]. The nominal length of the CCIC filter in taps will be $T_{SF} + T_{MF} + T_{CH}$ -2, where T_{SF}, T_{MF}, T_{CH} are the tap counts of the SF, MF and the estimated channel impulse response respectively. The non-truncated CCIC filter tap count is therefore 16M+16M+32-2= 32M+30, assuming T_{CH}=32. The truncated CCIC filter tap count is therefore:

$$X_{TR} = \lceil 0.3(32M + 30) \rceil = \lceil 9.6M + 9 \rceil \tag{6.3}$$

where [a] denotes the minimum integer not smaller than real value a. The number of scalar multipliers per FIR filter is reduced by a factor of 1/M, due to zero-valued sample insertion by the M× up-sampling function, thus multiplier count per FIR is:

$$X_{FIR} = \lceil\lceil 9.6M + 9\rceil/M\rceil = \lceil 9.6 + (9/M)\rceil \tag{6.4}$$

The number of parallel FIR filters taking into account the redundancy due to M× down-sampling, is $\lceil P/M\rceil$ and therefore the total number of scalar multipliers is given by:

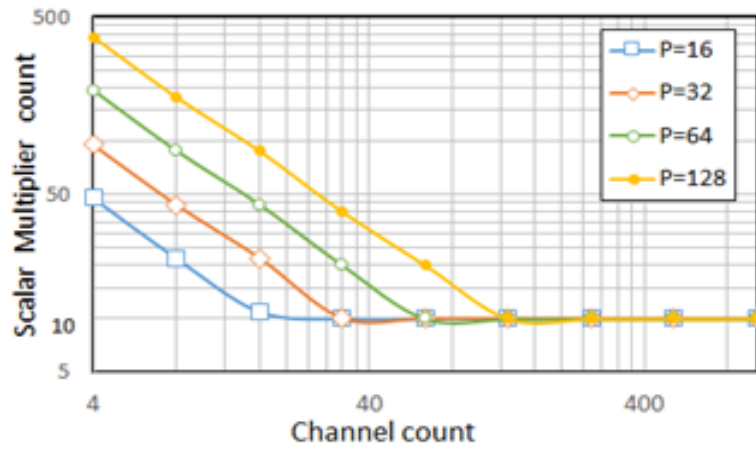$$X_{CCIC} = \lceil 9.6 + (9/M)\rceil\lceil P/M\rceil \tag{6.5}$$

Fig. 6.15. CCIC filter scalar multiplier count XCCIC, variation with channel count N (where N=M) for varying P values

A highly significant result here is that as M, and therefore channel count N, increases X_CCIC in fact decreases and approaches a fixed value of only 10. Therefore, ultra-low CCIC filter complexity is achievable for high channel count DFMA PONs. This key result shows that for M≥4 the CCIC filter complexity in terms of scalar multipliers is ~10×[number of parallel FIRs]. The implemented CCIC filters comply with this fact as the optimum tap count of 42 results in 11 scalar multipliers per parallel FIR filter. Therefore, as each parallel FIR generates a separate output sample, only ~10 sequential.

A non-zero valued samples from the CCI-inducing signal are required to produce each interference-estimate signal sample. This indicates that only 10 samples from the CCI-inducing signal generate significant interference in a single sample in the CCI-impacted signal. Fig. 6.15 illustrates the scalar multiplier count, X_{CCIC}, as defined by Eq. (6.5), for various channel counts up to 1024 channels, for four different *P* values. It is clear that

complexity decreases with channel count and as M approaches P the complexity X_{CCIC} approaches a fixed value of only 10 multipliers. It can therefore be concluded that the complexity of the DSP required for the ONUs and OLT in a DFMA PON does not scale with channel number, and as a channel is used by one or more ONUs, it does not scale with ONU count. The OLT requires DSP hardware per connected ONU, however using a modular hardware design would allow the aforementioned "pay-as-you-grow" PON deployment.

6.5   **Conclusion**

DFMA PONs can achieve SDN-controlled, physical layer network reconfigurability to offer highly efficient use of network resources, elastic bandwidth provisioning and fixed and mobile network convergence. To technically validate the DFMA PON technique a fully real-time upstream DFMA PON incorporating four independent OFDM modulated channels, has been experimentally demonstrated in a 26km SSMF, IMDD-based PON consisting of two ONUs and an OLT, all of which are dynamically reconfigurable and operate completely in real-time. As physical channel frequency response-induced CCI severely degrades the performance of two spectrally overlaid orthogonal channels, the OLT receiver incorporates a low complexity real-time DSP-based CCIC function, which is shown to considerably improve the performance and robustness of the four ONU channels, this is evidenced by: i) individual OFDM subcarriers exhibit a reduction in BER by factors as large as 100 – 300 times, ii) for the adopted FEC limit, the achieved channel capacities are significantly increased in terms of operational subcarrier count, for one channel 13(0) of 15 subcarriers can be employed when the CCIC is enabled (disabled), iii) sensitivity to ONU synchronisation is reduced as the inter-ONU STO range can be increased by a factor of up to 15 times, and iv) excellent transparency to the interfering channel's signal modulation format. The CCIC function is fully optimised for low DSP complexity and it has been shown that the associated CCIC filter requires as few as only ~10 scalar multipliers per parallel signal sample, which is independent of the implemented channel count. Furthermore, the DSP complexity analysis of the SFs and MFs, has also shown that their complexity in terms of scalar multiplier count is independent of channel count. This work therefore demonstrates the technical feasibility of achieving high performance IMDD DFMA PONs incorporating DSP-based transceivers with low complexity digital orthogonal filters, and furthermore, that ultra-low complexity CCIC functions are highly effective in mitigating the CCI due to the non-flat physical channel responses.

References

[1]   X. Duan et al., "Real-time experimental demonstrations of software reconfigurable optical OFDM transceivers utilizing DSP-based digital orthogonal filters for SDN PONs," Opt. Express, vol. 22, no. 16, p. 19674, 2014.

[2]   R. P. Giddings, E. Hugues-Salas, and J. M. Tang, "Experimental demonstration of a record high 11.25 Gb/s real-time optical OFDM transceiver supporting 25km SMF end-to-end transmission in simple IMDD systems," Opt. Express, vol. 20, no. 18, p. 20666, 2012.

[3]   X. Q. Jin and J. M. Tang, "Experimental investigations of wavelength spacing and colorlessness of RSOA-based ONUs in real-time optical OFDMA PONs," J. Light. Technol., vol. 30, no. 16, pp. 2603–2609, 2012.

[4]   A. Tsokanos et al., "Reductions of peak-to-average power ratio and optical beat interference in cost-effective OFDMA-PONs," Photonic Netw. Commun., vol. 26, no. 2–3, pp. 44–52, 2013.

[5]   S.-M. Jung, S.-M. Yang, K.-H. Mun, and S.-K. Han, "Optical beat interference noise reduction by using out-of-band RF clipping tone signal in remotely fed OFDMA-PON link," Opt. Express, vol. 22, no. 15, p. 18246, 2014.

[6]   Z. Li, M. S. Erkilinç, R. Bouziane, B. C. Thomsen, P. Bayvel, and R. I. Killey, "Simplified DSP-Based Signal-Signal Beat Interference Mitigation Technique for Direct Detection OFDM," J. Light. Technol., vol. 34, no. 3, pp. 866–872, 2016.

[7]   Y. Dong, E. Al-Rawachy, R. P. Giddings, W. Jin, D. Nesset, and J. M. Tang, "Multiple Channel Interference Cancellation of Digital Filter Multiple Access PONs," J. Light. Technol., vol. 35, no. 1, pp. 34–44, 2017.

[8]   E. AL-Rawachy, R. P. Giddings, and J. M. Tang, "Experimental Demonstration of Cross-Channel Interference Cancellation for Digital Filter Multiple Access PONs," vol. 25, no. 4, p. Th3C.5, 2016.

[9]   A. J. Lowery, "Improving sensitivity and spectral efficiency in direct-detection optical OFDM systems," OFC/NFOEC 2008 - 2008 Conf. Opt. Fiber Commun. Fiber Opt. Eng. Conf., no. February 2008, 2008.

[10]   Duan X et al, "Performance Tolerance of IMDD DFMA PONs to Channel Frequency Response Roll-Off," IEEE Photonics Technol. Lett., vol. 29, no. 19, pp. 1655–1658, 2017.

[11]   M. Bolea, R. P. Giddings, M. Bouich, C. Aupetit-Berthelemot, and J. M. Tang, "Digital filter multiple access PONs with DSP-enabled software reconfigurability," J. Opt. Commun. Netw., vol. 7, no. 4, 2015.

[12]   Intel, ""Stratix 10 GX/SX Device Overview, Table. 4," 2018. [Online]. Available: https://www.intel.com/content/dam/www/programmable/us/en/pdfs/literature/hb/stratix-10/s10-overview.pdf, 2018.[13]   Deng, T.B., 2009. Hybrid structures for low-complexity variable fractional-delay FIR filters. IEEE Transactions on Circuits and Systems I: Regular Papers, 57(4), pp.897-910.

[14   J. Cho, C. Xie, and P. J. Winzer, "Analysis of soft-decision FEC on non-AWGN channels," Opt. Express, vol. 20, no. 7, p. 7915, Mar. 2012.

7. Real-Time Experimental Demonstration of DSP-enabled Soft-ROADMs with Multi-level Flexible Add/Drop Functions for Cloud Access Networks

Contents

7.1 Introduction

The work presented in this chapter validates the technical feasibility of the proposed soft-ROADM in a fully real-time system consisting of four independent and guard-band free, digital orthogonal filtering multiplexed channels in terms of dynamically switching signals in real-time at sub-wavelength and spectrally-overlapped orthogonal sub-band levels. In addition, the work presented in this chapter also rigorously evaluates the soft-ROADM's physical layer dynamic performance and its robustness in terms of: i) add operation tolerance to differential optical power for various add operation combinations and ii) drop operation tolerance to variations in the characteristics of the drop RF signal (used to select the drop channel). As such, this chapter provides some deep insights into the technical aspects associated with the application of the soft-ROADMs in CAN scenarios. For an adopted FEC limit of 1.0×10^{-3}, it is shown that the soft-ROADM induces maximum power penalties of just 1.4dB and 2dB for the add and drop operations, respectively. Furthermore, to maintain all channel BERs below the adopted FEC limit, the add operation can tolerate a maximum differential optical power dynamic range of 6.5dB (1.5dB) for the sub-wavelength (sub-band) add operation, and the drop operation can tolerate variations in the drop RF signal's amplitude of 5dB and its phase of 16°. The results indicate that the proposed soft-ROADM exhibits good tolerance to variations in practical network operating conditions.

7.2 Real-Time Transceivers and Soft-ROADM Experimental System Setup

7.2.1 DSP-Based Real-Time Transmitters And Receivers

For signal generation and detection, the experiment employs a dual channel, sub-wavelength transmitter and a single channel receiver, each employing a FPGA to implement real-time DSP processing. The DSP architecture is based on the reconfigurable transceiver described in[1], which supports a two channel system and employs Hilbert pair-based digital orthogonal filters for channel multiplexing. In this work, appropriate modifications are implemented to support a 4 channel system (2 Sub-λ channels each with two Sub-B channels). In the transmitter an up-sampling factor of 4 [2] is adopted and 16 parallel, 64-tap finite impulse response (FIR) filters are used to implement each channel's shaping filter. Also, as filter coefficients are scaled to use the full range of the 8 bit coefficients and as the

155

specific filter impulse response can impact filtered signal amplitude[1], the outputs of the shaping filters pass through on-line adjustable scaling functions to allow the signal amplitudes in each channel to be closely matched.

For the matching filter in the receiver, 16 parallel, 64-tap FIR filters are theoretically required, however as a down-sampling factor of 4 is employed, the number of parallel filters physically implemented is reduced to 4. All FIR filters are dynamically software-reconfigurable by on-line reprogramming of the tap coefficients, thus the transmitter filters can be configured as one of four shaping filters, and the receiver filters can also be configured as one of four matching filters or as a LPF for use in the drop operation case.

On each individual channel any signal modulation format would be suitable for the soft-ROADM. Here, for simplicity but without losing any generality, OFDM is adopted, with pseudo random bit sequences (PRBS) employed as test data. Details of the OFDM parameters are given in Table 1. It should be noted that, in addition to demodulation, the OFDM receiver DSP performs essential functions including symbol alignment and channel equalisation as well as BER analysis for each subcarrier. A slight modification to the OFDM receiver block is also needed for the drop operation demonstration, as it must implement subcarrier conjugation and order reversal to mitigate the drop operation-induced spectral reversal effect.

The employed DACs and ADC are each 8 bit, 2GS/s devices which result in one Sub-λ channel occupying the 0-0.5GHz region, referred to as baseband (BB), and one Sub-λ channel occupying the 0.5-1.0GHz region, referred to as passband (PB). The associated I and Q Sub-Bs are denoted as BB-I, BB-Q, PB-I and PB-Q, respectively. The double-sided amplitude responses of the corresponding 64-tap shaping/matching filters are illustrated in Fig. 7.1.
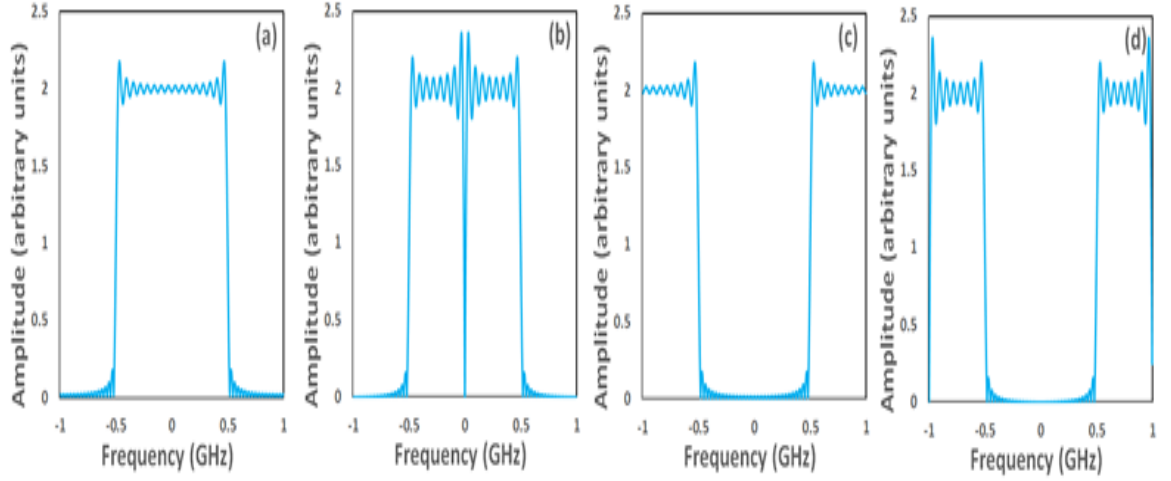
Fig. 7.1. Shaping and matching filter double-sided amplitude responses (a) BB-I, (b) BB-Q, (c) PB-I, and (d) PB-Q.

7.2.2 Experimental System Setup
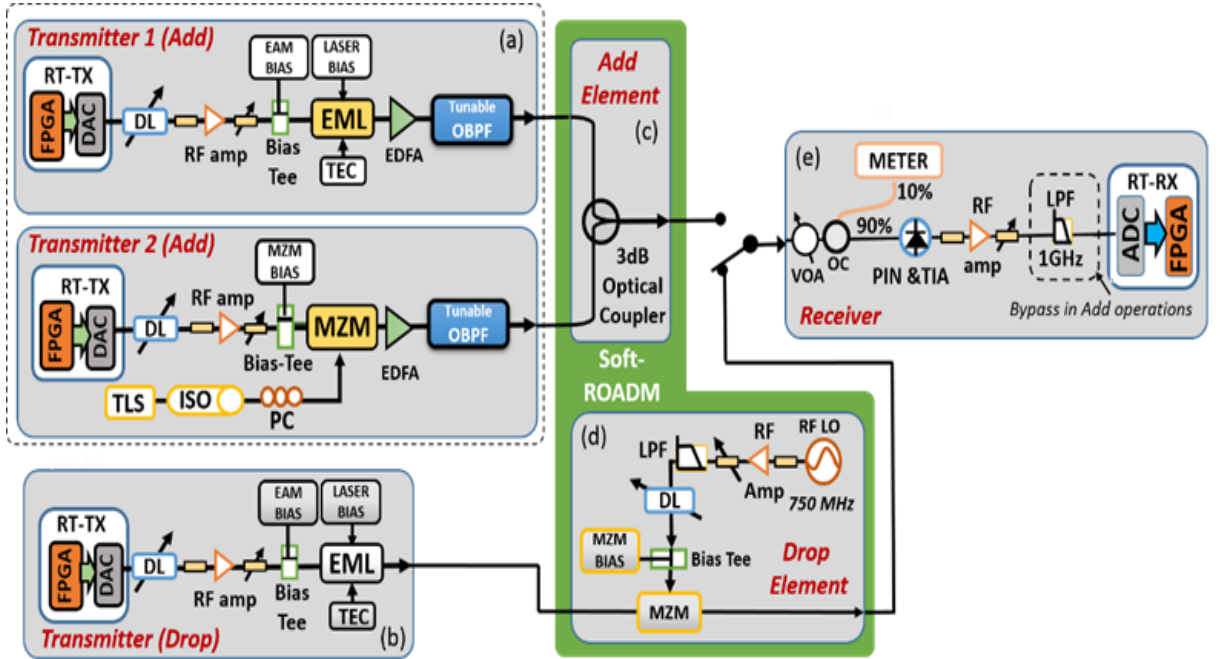
Fig. 7.2 Soft-ROADM add and drop operations experimental system setup. (a) transmitter system for add operations, (b) transmitter system for drop operation, (c) add element, (d) drop element, and (e) receiver system. DL: Delay line; LPF: low-pass filter; LO: local oscillator; EML: electro-absorption modulated laser; TEC: thermo-electric controller; MZM: Mach-Zehnder modulator; VOA: variable optical attenuator; OBPF: optical bandpass filter; TLS: tunable laser source; PC: polarization controller; PIN+TIA: photodetector with integrated transimpedance amplifier; EDFA: erbium doped fiber amplifier.

Fig. 7.2 shows the soft-ROADM add/drop operation experimental system setup with the adopted experimental system parameters listed in Table 1. The employed real-time DSP platform is described in appendix A. Fig. 7.3 shows examples of Sub-B/Sub-λ and dropped signal electrical spectra measured before and after the soft-ROADM add/drop operations. The adopted transmitter details are shown in Fig. 7.2 (a) for the add operation experiment and Fig. 7.2 (b) for the drop operation experiment. In both Fig.7.2 (a) and Fig.7.2 (b), the RF delay lines (DL) after the DACs are required as the entire end-to-end system operation is dependent on correct signal synchronisation. Transmitted signal delays must therefore be adjusted to ensure: i) correct sample timing at the receiver for correct filter operation, and ii) correct relative signal timing between the transmitters to maintain orthogonality when orthogonal channels are added. When channels in different Sub-λ bands are added, their relative transmitter timing is not critical, however the receiver's absolute timing must still be adjusted for each channel independently. The DLs are manually adjusted to achieve optimum sample timing, which gives rise to minimum BERs for the considered channel. The DL adjustment procedure adopted for all add cases, is to firstly enable a single transmitter and set its DL for minimum BERs on its associated channels, thus attaining correct receiver timing, then the second transmitter is enabled and its DL adjusted for minimum BERs on all channels, thus attaining optimum relative transmitter timing. Moreover, the drop RF signal levels are also adjusted to the optimum voltage with an RF amplifier and a fixed and variable electrical attenuator in order to drive the optical IM. In addition, the drop RF signals are combined in a bias-Tee with an optimum DC bias voltage for the IMs. In the first transmitter, the IM is an EML which has an integrated DFB laser as its light source. The DFB laser is optimally biased and its temperature optimised by an external temperature controller. An erbium doped fibre amplifier (EDFA) with a 0.8nm OBPF, amplifies the EML output to control the optical signal power and allow balancing of the powers from both transmitters.

Table 1. Transceiver and system parameters

Parameter	Value
OFDM IFFT/FFT size	32 points
Maximum data carrying OFDM subcarriers per channel	15
add/drop data-carrying subcarriers per sub-band	6/7
Subcarrier modulation format	16-QAM
DAC and ADC sample rate / bit resolution	2GHz /8 bits
FIR filter clock rate	125MHz
OFDM encoder/decoder clock rate	12.5MHz
Data sequence length for error counting	88,500 Symbols
Raw bit rates per add/drop channel	0.3/0.35 Gb/s
Samples per symbol* IFFT/Cyclic prefix/Total	32/8/40 Samples
EML wavelength/modulation bandwidth	~1550nm$^\&$/10GHz
EML laser bias current/EAM bias voltage	124 mA/-0.75V
EML/MZM driving voltage for Sub-λ add operation	2.3/1.0 Vpp
EML/MZM driving voltage for Sub-B add operation	2.3/0.6 Vpp
MZM DC bias for Sub-λ/Sub-B add operation	1.3/1.47 V
TLS wavelength/MZM modulation bandwidth	~1550nm$^\&$/20GHz
PIN sensitivity[#]/Bandwidth	-19 dBm /12.4 GHz
Add/drop optical launch power	4.5/3.1 dBm
EML Sub-λ frequency response roll-offs (BB/PB)	8.5/4 dB
MZM Sub-λ frequency response roll-offs (BB/PB)	8/5 dB
Electrical signal amplitude at ADC	300 mVpp
EML/MZM driving voltage for drop operation	2.3/3 Vpp
MZM DC bias for drop operation	1 Vpp

* Before up-sampling and after down-sampling
& wavelength spacing =0.3nm
\# Corresponding to 10 Gb/s non-return-to-zero data at a BER of 1.0×10^{-9}

The second transmitter is similar to the first except that the IM is implemented with a tuneable laser source (TLS) and a MZM. After an isolator, a polarization controller prior to the MZM input is adjusted for optimum performance. The MZM is biased at its quadrature point and is fine-tuned during operation to attain the optimum setting. The MZM output power is set via an EDFA with an OBPF. In the add operation experiment, the DD-induced OBI effect can occur when operating at similar nominal wavelengths, a wavelength spacing of 0.3nm is therefore employed between the two light sources, as this is sufficient to eliminate the OBI effect[3].
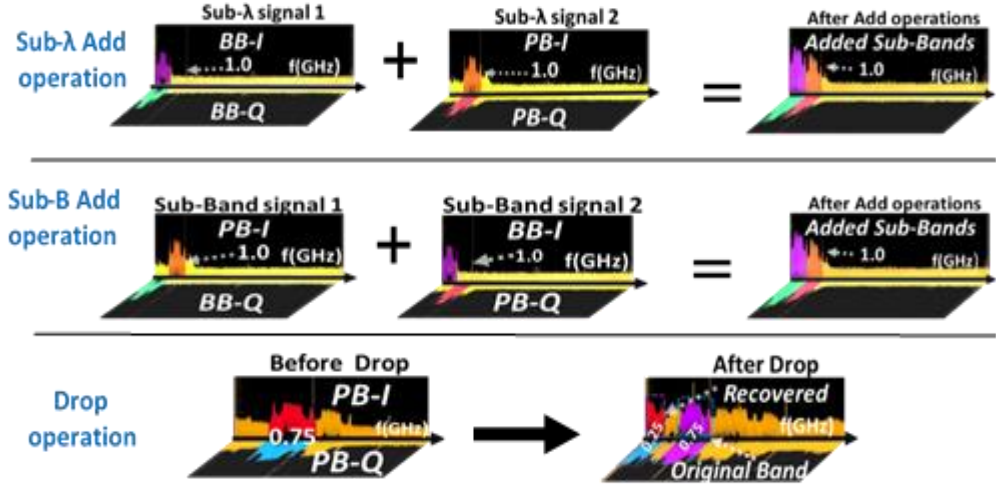
Fig. 7.3 Representative Sub-λ and Sub-B signal spectra measured before and after the soft-ROADM add/drop operations

It is also worth noting that the end-to-end optical connections established in the add operation experiments exhibit frequency response roll-off, as detailed in Table 1, which can lead to non-perfect channel orthogonality-induced CCI and subsequent overall system performance degradations[4, 5]. This effect is however strictly.

To configure the soft-ROADM add operation, the add element consisting of a two input 3dB passive optical coupler, as shown in Fig. 7.2 (c), is connected to the outputs of both transmitters in Fig. 7.2 (a), with both transmitters set for an optical output power of 4.5dBm. The output of the add element then feeds the receiver as shown in Fig. 7.2 (e). In the receiver, a VOA allows the adjustment of received optical power to the required value before direct detection of the optical signal with a PIN+TIA. A coupler is used before the PIN to tap off 10% of the optical power for system monitoring purposes. The electrical signal after the PIN is amplified and variably attenuated to optimise the signal level, before being digitized by the ADC. The samples from the ADC are then processed by DSP implemented in an FPGA as described in Section 7.2.1. The bit error counts for each OFDM subcarrier are monitored in real-time using the FPGA's embedded logic analyser function. To assess the penalties due to the add operations, before-add (BAD) BER measurements are also made, in conducting this, the optical cables of both transmitters are kept connected to the OC, with both lasers on, then only the considered Sub-λ/Sub-B to be measured is enabled in the DSP. This avoids optical connector-induced power variations and negligible differences are observed in BAD measurements with the unmodulated laser on or disconnected. On the other hand, the after-

add (AAD) BER measurements are performed when the Sub-λ/Sub-B channels are simultaneously activated in both transmitters' DSP. To fully examine the soft-ROADM add performance for different add combinations, we define Sub-λ Add as: BB-I+BB-Q optically added to PB-I+PB-Q, and Sub-B Add as: BB-Q+PB-I optically added to BB-I+PB-Q. Furthermore, to examine the add operation robustness to differential optical input power, the gain of the EDFAs in each transmitter in the AAD setup is adjusted to induce a difference in optical signal power at the add element inputs. The impact of differential power on system performance is presented in Section 7.3.2.

For the drop operation experiment, a single dual-channel transmitter is employed as shown in Fig. 7.2 (b), which generates a PB Sub-λ containing spectrally overlapped and orthogonal PB-I and PB-Q channels. The transmitter is the same as the EML-base transmitter used in the add operation experiment except the EDFA and OBPF are omitted as power balancing is not an issue as there is now only a single transmitter in the experimental setup for the drop operation. For the before-drop (BDR) case, the transmitter in Fig.7.2 (b) connects directly to the receiver in Fig.7.2 (e), thus bypassing the drop element, here data is recovered as in the BAD/ADD case, i.e. using appropriate matching filters. To configure the setup for the soft-ROADM after-drop (ADR) operation, the drop element in Fig.7.2 (d) is now inserted between the aforementioned transmitter and receiver. The soft-ROADM drop element employs a MZM-based IM with a manually controlled LO for the drop RF signal generation. To drop either Sub-B from the PB Sub-λ, the RF drop signal's frequency is set to the PB Sub-λ CF (0.75GHz). The drop RF signal's amplitude is optimised by an RF amplifier and a variable RF attenuator, and the phase is manually controlled by a variable RF DL to select either the PB-I or PB-Q channel and is finely tuned to give a minimum BER for the dropped channel. To recover the OFDM signal from the baseband-shifted Sub-B, a 1GHz analogue LFP is introduced before the ADC to remove unwanted remaining sub-bands above the Nyquist frequency and the receiver's digital FIR filter is configured as a LPF with a 250MHz bandwidth which corresponds to the bandwidth of the wanted channel located at baseband. The modified OFDM demodulator for signal spectral reversal is also adopted. To analyse the robustness of the drop operation to drop RF signal variations, manual adjustments are made to its amplitude and phase using a variable electrical attenuator and RF DL respectively, whilst the corresponding variations in drop channel BERs are observed. The impacts of drop RF signal variations on system performance is presented in Section 7.3.3.

7.3 Experimental Results

The overall BER performance of an established optical connection can be affected by transceiver/system-related effects, including, for example, i) limited filter tap count-induced enhancement of digital filter frequency response ripples; ii) unwanted subcarrier-subcarrier-intermixing (SSI) products generated upon square-law photon detection, and iii) frequency response roll-off-induced CCI between the orthogonal channel pairs. As all of these effects are more predominant for lower frequency subcarriers, to effectively highlight the soft-ROADM operation impairments only, a number of low frequency subcarriers are thus deactivated in each 16-QAM-encoded OFDM signal to ensure that acceptable BER levels for each subcarrier in each Sub-B are always obtainable before and after the soft-ROADM operations. Specifically, the 6 (7) highest frequency subcarriers are employed in each Sub-B for the ROADM add (drop) operations.

7.3.1 Performance of add and drop operations

Based on the experimental setups and parameters presented in Section 7.2.2, the BER curves versus ROP of each added signal, measured before and after the add operation for Sub-λ and Sub-B add operations, are shown in Fig. 7.4 (a, b) and Fig. 7.4 (d, e) respectively. For the Sub-λ add case the BB (PB) channels are generated by the EML-based (MZM-based) transmitter, whereas for the Sub-B add case the BB-Q + PB-I (BB-I + PB-Q) channels are generated by the EML-based (MZM-based) transmitter. At the FEC limit of 1×10^{-3} the measured Sub-λ and Sub-B add penalties for all channels are summarised in Table 2. The key physical effects impacting the experimentally observed add operation penalties are: i) finite filter length-induced non-perfect digital filter orthogonality with finite out-of-band attenuation, ii) increase in DD-induced SSI products (particularly due to Sub-λ add-induced increases in both signal bandwidth and power) which characteristically have higher power at lower frequencies, iii) residual frequency response roll-off induced CCI between orthogonal channels, and iv) inter-channel STO, which causes the higher PB frequencies to suffer higher STO sensitivity. It should also be highlighted that all these aforementioned physical effects are purely dependent on transceiver implementation rather than the soft-ROADM. The SSI products have more impact at lower frequencies which can explain i) the higher penalties observed for BB channels compared to PB channels in the Sub-λ add case, and ii) why BB channels see a higher penalty in Sub-λ add than Sub-B add due to the

increased number of intermixing products generated by the doubling of signal bandwidth due to the Sub-λ add operation. The roll off-induced CCI only contributes to the add penalty in the Sub-B add cases as this effect is already present in the Sub-λ add case before the add operation. The exact frequency response profile in each Sub-λ also influences the level of generated CCI. Also, in the Sub-B add case as the orthogonal channels within a Sub-λ originate from different transmitters, their inter-channel STO can be non-zero, thus the resulting CCI contributes to the add penalty. As the PB is more sensitive to STO, this gives rise to the higher penalty observed in the PB for the Sub-B add case.
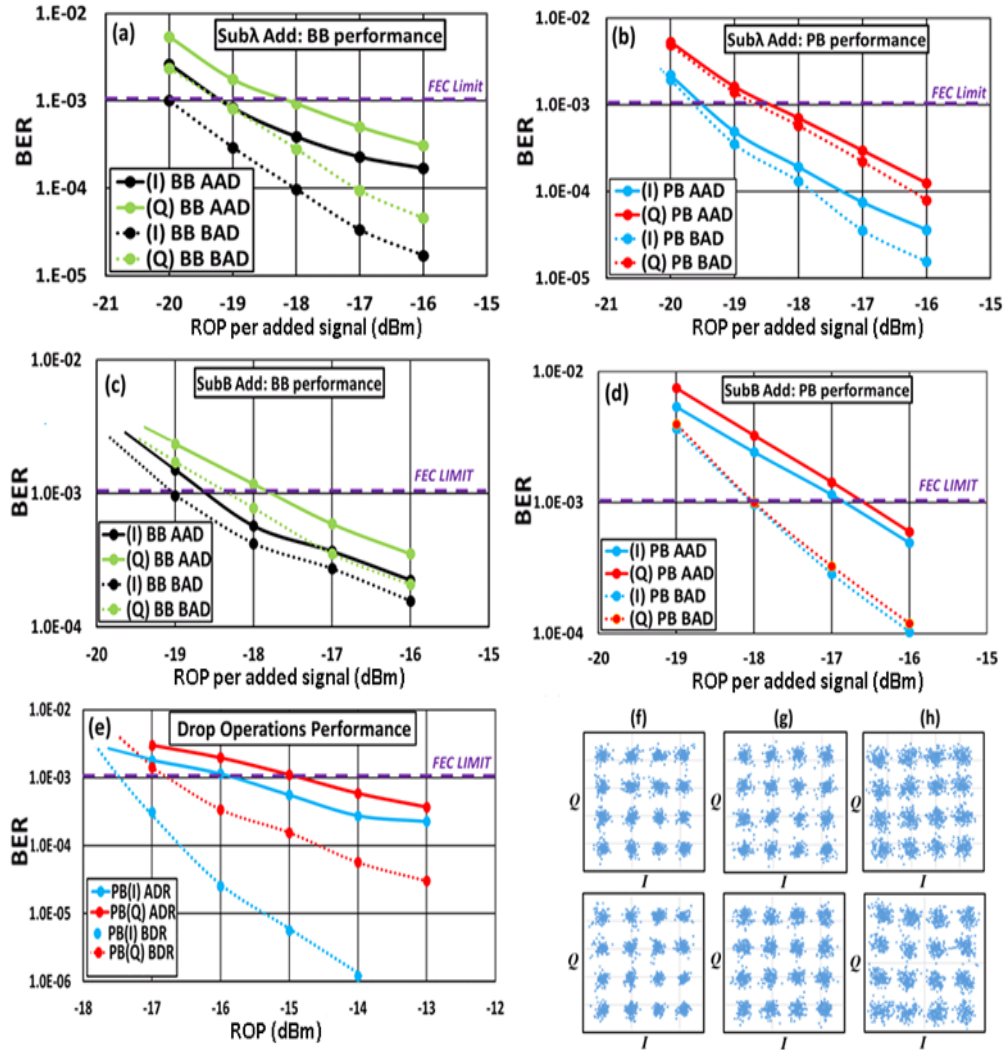

Fig. 7.4. BER curves for (a),(b) each Sub-B before/after Sub-λ add, (c),(d) each Sub-B before/after Sub-B add, (d) before/after the drop operation; Example subcarrier constellations at -18dBm for the BB-I (upper) and PB-I (lower) after (f) Sub-λ add, (g) after Sub-B add; Example subcarrier constellations at -14dBm after the drop operation for (h) PB-I (upper) and PB-Q (lower).

Table 2. Add operation penalties (dB)

	Sub-λ Add		Sub-B Add	
	I	Q	I	Q
BB	0.8	1.0	0.3	0.5
PB	0.1	0.2	1.2	1.4

Fig. 7.4 (c) shows the measured BER curves for the cases of before and after drop operation on PB-I and PB-Q Sub-Bs. As expected from theoretical [30] and experimental [39] results, it can be seen in Fig. 7.4 (c) that the drop operations give rise to similar BER developing trends on both channels. There is also a similar drop penalty of ~2dB for both channels at the adopted FEC limit, which arises mainly due to imperfect MZM-IM transfer function-induced signal distortions [7].

For all of the measured add/drop performances presented in Fig.7.4, the Q channel has slightly inferior performance in all cases due to the finite filter length-induced filter frequency response ripples being more prominent for the quadrature filters, as shown in Fig. 5. Similar behaviours have also been experimentally observed in [39]. Equalized and overlaid example constellations of the received subcarriers for add (BB-I/PBI) and drop (PB-I/PB-Q) cases, at ROPs of -18dBm and -14dBm respectively, are shown in Fig. 7.4 (f-h).

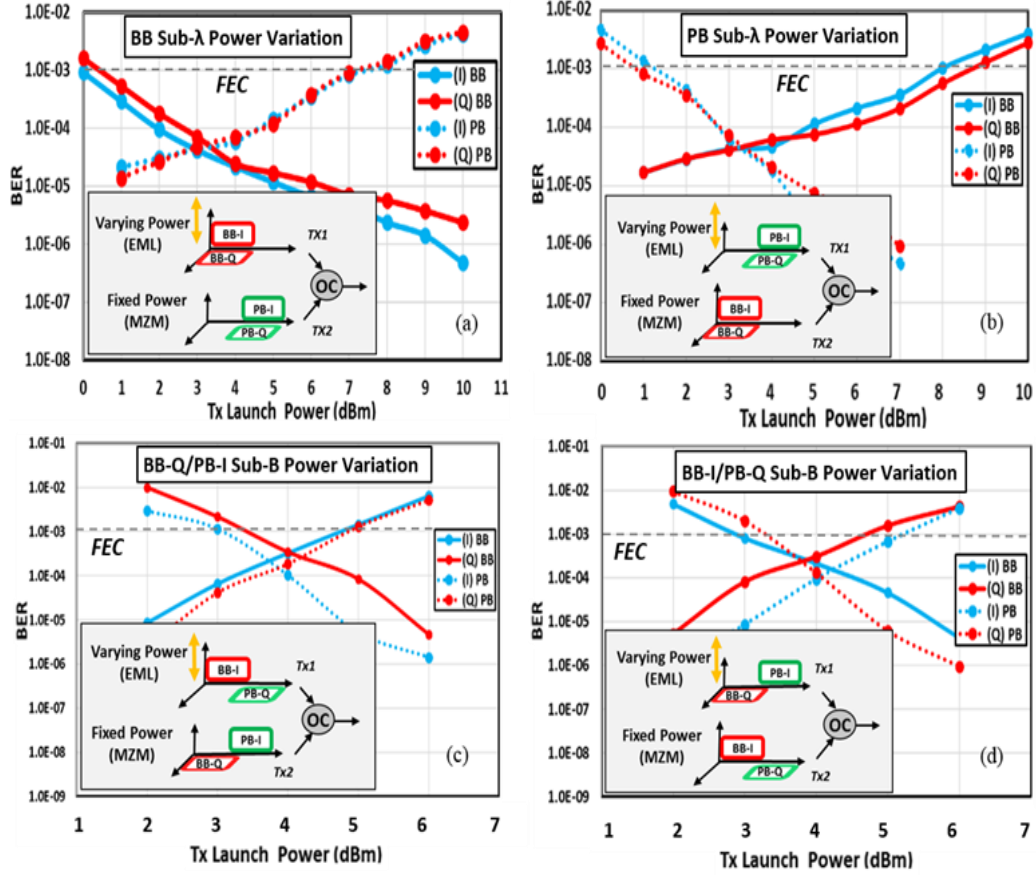## 7.3.2 Add operation robustness to differential optical input power

Fig. 7.5 Differential optical input dynamic range at -10dBm ROP for power variation of: (a) BB Sub-λ (b) PB Sub-λ (c) BB-Q/PB-I Sub-B (d) BB-I/PB-Q Sub-B.

As optical signal power levels can vary within a network, there can be variation between the signal powers present at the soft-ROADM add element ports, it is therefore essential to explore the performance of the soft-ROADM add operation when subject to such power variations in order to evaluate the add operation robustness to differential optical input power. Soft-ROADM Sub-λ/Sub-B add operations can ideally tolerate a large differential optical input dynamic range, which is the maximum variation in the input optical power at one of the add element ports which maintains all channel BERs below a predefined FEC limit.

For all Sub-λ/Sub-B add measurement cases presented in this section, the power of the EML-based transmitter is varied, thus it has a variable optical power (VOP) whereas the MZM-based transmitter has a fixed optical power (FOP) of 4dBm. Furthermore, for all

measurements the received optical power is fixed at -10dBm. Fig. 7.5 (a-d) shows the add configurations and the corresponding allowable differential input optical power for Sub-λ/Sub-B add operations. As seen in Fig. 7.5, two different channel configurations are implemented for each Sub-λ/Sub-B add case so that the effect of power variations on all channels can be explored. The results in Fig. 7.5 show that in all cases, as the optical output power of the VOP transmitter increases (decreases) the BER of its associated channels decrease (increases), whereas for the transmitter with FOP the BER of the associated channels increase (decreases). For a FEC limit of 1×10^{-3}, the observed differential input optical power dynamic range for both Sub-B add cases is ~1.5dB, whereas for the Sub-λ add cases the differential optical input dynamic range is ~6.5dB. As the received optical power is fixed, the dependency of receiver OSNR on transmitted signal powers clearly explains the observed trends of the curves in Fig. 7.5. The physical mechanism underpinning the lower differential optical input dynamic range for the Sub-B add case is due to the transceiver and transmission link frequency response roll off-induced residual CCI between the orthogonal Sub-Bs [32], thus as the optical power variation induces a corresponding power variation between orthogonal channels in the same Sub-B, this results in increased (decreased) CCI for the lower (higher) power channel, therefore causing a more rapid change in the effective channel OSNRs which leads to the lower differential optical input dynamic range [32]. For the Sub-λ add cases the aforementioned CCI effect is not an issue, so a considerably larger differential optical input dynamic range occurs, this indicates that the observed optical input power dynamic range in the Sub-B add case is not a limitation of the soft-ROADM but a consequence of transceiver/link induced CCI.

It is also worth mentioning the following two aspects: i) The upper limit of the observed differential optical input dynamic range is determined by the minimum OSNR allowed by the fixed-power optical signal, whilst the lower limit of the differential optical input dynamic range is determined by the minimum OSNR allowed by the variable-power signal; ii) As a direct result of the above statement, the ROP at the destination TET has an important impact on the achievable differential optical input dynamic ranges for the add operations. Under practical conditions, our experiments have shown that the differential optical input dynamic range in dB is almost proportional to total ROP in dBm for Sub-λ add operation.

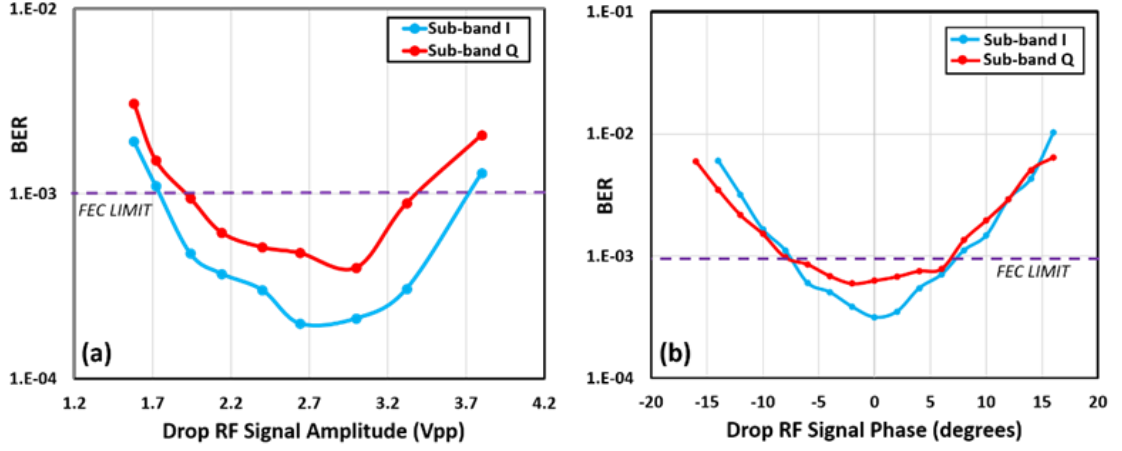### 7.3.3 Drop operation robustness to drop RF signal characteristics

Fig. 7.6 Variation in soft-ROADM dropped signal BERs (a) as a function of drop RF signal amplitude (b) as a function of drop RF signal phase offset.

To explore the robustness of the soft-ROADM drop operation to variations in the drop RF signal characteristics, the BER performance of the dropped PB-I and PB-Q channels are measured as the amplitude and phase of the drop RF signal are varied about their optimum values. Using the experimental system setup and parameters for the drop operation as described in Section 7.2.2and with a received optical power of -11dBm, Fig. 7.6 (a) shows, with optimum phase setting, how the BER of each dropped channel varies as the drop RF signal amplitude is varied about the optimum value of ~3Vpp. The fundamental principles underpinning the observed results are that as the drop RF signal amplitude is reduced below ~2.5V, the power of the dropped optical signal reduces [8], thus reducing the dropped signal's OSNR at the receiver. Whereas, when increasing drop RF signal amplitudes above ~3.3V, the amplitude dependent non-linearity effect of the IM induces increasing dropped signal distortions. Whilst maintaining both channel BERs below the FEC limit of 1×10^{-3}, the tolerated amplitude variation is 1.4Vpp (1.9Vpp – 3.4Vpp) corresponding to a power variation of ~5dB, thus the soft-ROADM drop operation is exceedingly robust to the drop RF signal amplitude variations. As such it does not require an amplitude control loop or highly precise setting of the drop RF signal amplitude.

With both PB-I and PB-Q channels enabled, Fig. 7.6 (b) shows, with optimum amplitude setting, the BER variation of each dropped channel as the drop RF signal phase is varied about the optimum value for the given channel (shown as 0°). Any deviation from the

optimum phase results in phase-offset-induced CCI, as the power from the unwanted orthogonal channel is also down-converted to the baseband spectral region. For the given conditions, the allowed phase offset variation range to maintain BERs below the FEC limit of 1×10^{-3} is ~16°. It should be noted that, similar to the differential optical input dynamic range case presented in Section 7.3.2, the allowed phase variation range is also dependent on the dropped signal's ROP level, since the BER subject to a zero phase-offset is ROP dependent. However, for a given phase offset there is a fixed ratio of unwanted channel leakage power to wanted channel power, this ratio is ROP-independent, and more predominant at higher ROPs. The relatively shallow slope of the curves in Fig. 7.6 (b) about the optimum phase indicates that the BER has reasonably low sensitivity to phase offset.

Additionally, the level of orthogonality between the two channels in the targeted drop Sub-λ band can also impact the maximum allowed phase variation range, perfect orthogonality being necessary for negligible drop operation-induced CCI, therefore increased filter length-induced improvement in shaping filter characteristics improves channel orthogonality, thus enhancing the allowed phase variation range. As a drop RF signal phase control loop is required to lock to and track the TSB's phase, the observed results show that if a suitable margin is adopted between the zero phase-offset BER and the FEC limit, combined with the very low sensitivity to drop RF signal power, it should be practically feasible to implement the required phase control loop. The SDN control would initialise and optimise the RF drop signal parameters by monitoring the dropped chanel's BER in the ROT by the use of known training sequences. The subsequent drift in the drop RF signal parameters of the soft-ROADM would also be tracked by BER performance monitoring in the ROTs, the SDN controller would then provide a feedback loop between ROTs and the soft-ROADMs to maintain the required RF drop signal parameters for minimum drop channel BER.

7.4 Conclusions

Making use of DSP-based orthogonal digital filtering, intensity modulation and passive optical coupling, simple, flexible and cost effective soft-ROADMs free from both optical filters and O-E-O conversions have been experimentally demonstrated in a fully real-time 4-channel system. The soft-ROADMs successfully perform DSP-enabled dynamic add and drop operations at sub-wavelength and spectrally overlapped orthogonal sub-band levels. Detailed experimental investigations of the physical-layer add and drop operation

performances have been undertaken, the robustness of the add operation to variations in differential optical power and the robustness of the drop operation to variations in the drop RF signal characteristics have also been investigated.

It has been shown that the soft-ROADM introduces maximum optical power penalties as low as 1.4dB for the add operation and 2dB for the drop operation. Furthermore, the results show the add operation can tolerate a differential optical input dynamic range of 1.5dB (6.5dB) for the Sub-B (Sub-λ) add case. The soft-ROADM drop operation has also been shown to be robust to variations in the drop RF signal characteristics, allowing ~5dBm amplitude variation and 16° of phase variation for the adopted conditions. The very low BER sensitivity to amplitude variations and the observed BER sensitivity to phase offset indicates that it should be practically feasible to implement the required drop RF signal phase control loop.

The fully real-time, proof-of-concept demonstration of the soft-ROADM is a significant step in demonstrating the technical feasibility of the proposed soft-ROADM technology, which can enable cloud access networks to converge fixed and mobile networks supporting key features such as dynamically sliceable networks with ultra-low latency for effective support of 5G mobile networks.

References

[1]   X. Duan et al., "Real-time experimental demonstrations of software reconfigurable optical OFDM transceivers utilizing DSP-based digital orthogonal filters for SDN PONs," Opt. Express, vol. 22, no. 16, p. 19674, 2014.

[2]   M. Bolea, R. P. Giddings, and J. M. Tang, "Digital orthogonal filter-enabled optical OFDM channel multiplexing for software-reconfigurable elastic PONs," J. Light. Technol., vol. 32, no. 6, pp. 1200–1206, 2014.

[3]   X. Q. Jin and J. M. Tang, "Experimental investigations of wavelength spacing and colorlessness of RSOA-based ONUs in real-time optical OFDMA PONs," J. Light. Technol., vol. 30, no. 16, pp. 2603–2609, 2012.

[4]   Duan X et al, "Performance Tolerance of IMDD DFMA PONs to Channel Frequency Response Roll-Off," IEEE Photonics Technol. Lett., vol. 29, no. 19, pp. 1655–1658, 2017.

[5]   E. AL-Rawachy, R. P. Giddings, and J. M. Tang, "Experimental Demonstration of Cross-Channel Interference Cancellation for Digital Filter Multiple Access PONs," vol. 25, no. 4, p. Th3C.5, 2016.

[6]   X. Duan, M. L. Deng, W. Jin, R. P. Giddings, S. Mansoor, and J. M. Tang, "Experimental Demonstration of DSP-enabled Drop Operations of Flexible ROADMs Excluding Optical Filters and O-E-O Conversions," 2016 Opt. Fiber Commun. Conf. Exhib., no. Im, p. M3E.4, 2016.

[7]   W. Jin et al., "Improved Performance Robustness of DSP-Enabled Flexible ROADMs Free from Optical Filters and O-E-O Conversions," J. Opt. Commun. Netw., vol. 8, no. 8, p. 521, 2016.

[8]   W. Jin et al., "New ROADMs with DSP-enabled dynamic and flexible operations for elastic optical networks," in Optical Fiber Communications Conference and Exhibition (OFC), 2015, 2015, pp. 1–3.

8. Conclusions and Future Work

Contents

8.1 **Conclusions:**

It is crucial that future optical networks evolve to accommodate emerging trends such as; i) the rapid increase in the required data traffic capacity, ii) the explosive growth in the range and dynamicity of data traffic characteristics, due to aspects such as the increasing variation in the types of devices connected the network, together with the evolution of new disruptive technologies such as the IoT, iii) new emerging 5G services and ecosystems with heterogeneous requirements such as eMBB, uRLLC and mMTC and iv) the need to provide a network slicing function where dedicated network resources provide effectively isolated interconnections for different services with differing QoS requirements. To meet the abovementioned trends, the future networks should be highly agile, have a significantly more dynamic and reconfigurable architecture, be very cost effective and allow the network operators to also decouple the data capacity provision from their revenue thus enabling a more on-demand, customer or service specific, network service provision.

To address the above requirements CANs, as discussed in chapter 3, have been proposed as a cost-effective "future-proof" network solution. CANs aims to provide a flexible integration of traditional optical access networks, metropolitan area optical networks and 4G/5G MFH and MBH networks. CANs are equipped with the vital networking function of SDN-based, dynamic online network reconfigurability and bandwidth provisioning with fine granularity, which is performed at wavelength, sub-wavelength and/or sub-band levels. Furthermore, CANs are also envisaged to transparently accommodate a diverse range of important network design features such as signal modulation formats, signal detection schemes, flexible WDM grids, diversified network topologies and multiple access techniques, to achieve ultra-high flexibility and elasticity in network provisioning.

The work in this thesis includes an extensive exploration of off-line processing-based experiments and real-time DSP-based experimental demonstrations to investigate the technical feasibility of the practical implementation of novel proposed techniques vital for future CANs. The work ranges from the DSP function level to device level to network architecture level. The research specifically explores; i) a CCIC technique based on a real-time transmitter and a DSO running MatLab, as an offline receiver, employing a two-channel DOF-multiplexed, PTP IMDD SMF-link of various lengths, ii) an OLT embedded CCIC technique demonstrated in a completely real-time system, employing a four-channel IMDD-

based, 26km SMF, DFMA PON, and iii) a fully real-time soft-ROADM using real-time DSP-based transceivers for signal generation and detection, with commercially-available low-cost electrical/optical components for application in CANs

The CCIC technique applied in a two channel DOF-multiplexed PTP SMF-link successfully cancelled the interference between the orthogonal channels in the same spectral region to significantly improve the network transmission performance. In chapter 4, the CCIC operating principle is explained in detail, while in chapter 5, in depth experimental explorations are performed to explore the technical feasibility of the proposed technique. The CCIC technique has some unique features in comparison with various interference cancellation techniques presented in chapter 4, such as i) lower DSP complexity, ii) the CCIC operation is not dependent on the modulation format, iii) a single iteration is sufficient to achieve the performance convergence and iv) operation is not dependent on any initial conditions. To validate the proposed CCIC technique, for the first time, the experimental demonstration, based on the aforementioned DOF-multiplexed PTP transmission system, employs a real-time transmitter and offline receiver to effectively mitigate the CCI effect between two orthogonal channels. The transmission performance is experimentally investigated in terms of individual OFDM subcarrier BER, total signal transmission capacity and optical power budget using 25km SSMF-IMDD systems. The results showed that the CCIC technique achieves a significant improvement in the system performance and so making it highly suitable for application in CANs.

In chapter 6, a two ONU, DFMA-PON supporting four independent channels with OOFDM-modulated signals, is experimentally demonstrated for the first time. The DFMA PON providing a key element for the realisation a CAN. The employed ONUs and OLT are all based on real-time DSP with dynamic reconfigurability. Extensive explorations, with dynamic performance optimization, are undertaken on the low complexity CCIC function embedded in the OLT's receiver to investigate its impact on system performance. The results showed that the fully real-time CCIC implementation achieved significant performance improvements for all four channels and the observed performance also corresponds to the abovementioned offline CCIC performance. It is shown that the real-time CCIC has a big impact on the DFMA PON transmission system by considerably enhancing the performance and the robustness in term of significant reductions in individual subcarrier BERs and total channel BERs. Moreover, the experimental result also shown that the ONU synchronisation

sensitivity decreased when the CCIC is enabled, as the inter-ONU STO range is considerably increased. The optimization of the CCIC function's filter to obtain the optimum trade-off between the DFMA PONs performances and tap count is also investigated.

To realise highly reconfigurable, elastic and transparent CANs, channel switching functionality at wavelength, sub-wavelength and orthogonal sub-band levels is essential, which is provided by new network elements known as soft-ROADMs. The soft-ROADMs, explained in chapter 3, are designed to be highly flexible, very cost effective and fully compatible with SDN-based network control. In chapter 7, a soft-ROADMs is experimentally demonstrated using a passive optical coupler-based add element and an intensity modulator-based drop element which is free from both optical filters and O-E-O conversions. Furthermore, the utilisation of commercially available components enables the provision of highly cost effective soft-ROADMs. The physical-layer add/drop operations are evaluated together with the performance robustness to real-time operating condition variations, both are fully investigated to validate the feasibility of the soft-ROADMs in real-time. The obtained result shown that the soft-ROADMs induced low power penalties for both add and drop operations. The result also show that the soft-ROADM can tolerate large differential optical input power for various add operation combinations. Furthermore, as the drop RF signal deviates from the optimum value the BER sensitivity to the associated phase and amplitude variations is shown to have a sufficient level of robustness, indicating that the required drop RF signal control function should be practically feasible. The fully real-time, proof-of-concept demonstration of the soft-ROADM is a significant step in demonstrating the technical feasibility of the proposed soft-ROADM technology for enabling cloud access networks.

8.2 Future Work

Comprehensive experimental research work has been implemented in this thesis to validate key functionality of the proposed reconfigurable CANs, which includes real-time demonstration of the proposed technologies, however, there are some technical aspects that still need to be researched in more details in order to fully validate and verify the technical and commercial feasibility of the associated CAN technologies. Some of the suggested areas of future research work for further investigation are as follows:

1) Transceiver clock frequencies and sample timings in DFMA based CANs.

As illustrated in the experiment demonstrations presented in this thesis, the STOs between the ONUs operating in the same spectral frequency region need to be adjusted to achieve a high level of channel orthogonality for the best transmission system performance. In the experiments manually adjusted RF delay lines were used to obtain the optimum sample timing, however, in a practical system it is thus necessary to implement sufficiently accurate and automatic control of the relative inter-ONU STO. Therefore, it is necessary to explore and develop DSP algorithms for embedding inside the ONUs and OLT, which estimate the STO and compensate accordingly. Fully DSP-based solutions which avoid the need for external discrete components such as RF delay lines, are unquestionably more preferable from a cost-effectiveness perspective. Furthermore, it is also a requirement to adjust the absolute STO in the receivers in the DFMA PON. Therefore, in the same way as the inter-ONU STO control, a receiver embedded DSP algorithm is required to automatically adjust the absolute receiver STO. DSP algorithms are also required to compensate the sampling frequency offset (SFO) between transceivers, which will result in STO drift. Therefore, due to this inter-relationship it is necessary to explore algorithms to address both SFO and STO in combination. It is important to emphases that a centralised SDN controller manages all the network elements, thus it can be used to implement control information exchange between the connected transceivers in a CAN, which can help to simplify the DSP transceiver embedded SFO/STO algorithms.

2) Automatic control of drop RF signal amplitude, frequency and phase in flexible ROADMs.

As illustrated in the experimental work in the chapter 7, the drop operation in the soft-ROADM is based on the manual setting of both of the frequency and the phase of the drop RF signal to select the channel to be dropped. Automatic control needs to be designed and implemented in DSP to adjust the instantaneous phase and frequency of the drop RF signal to optimize drop operation performance for each sub-band. The SDN control would initialise the RF drop signal parameters while for optimum performance the set values have to be consistently monitored to track and adjust any drift in the drop signal parameters. The drift in the drop RF signal parameters of the soft-ROADM can be tracked by BER performance monitoring in the ROTs and the SDN controller can be employed once again to provide a feedback between ROTs and the soft-ROADMs. Alternatively it may be possible to employ

power level monitoring of the dropped signal within the soft-ROADM as dropped signal power is dependent on the drop RF signal parameters.

3) The impact on transmission performance of concatenated flexible ROADMs in a CAN.

As explained in the chapter 3, from a practical deployment point of view, multiple soft-ROADMs can be connected in ring-type network in a CAN. Consequently, it is necessary to research, both numerically and experimentally, the trade-off between the number of concatenated soft-ROADMs and the CAN performance for different scenarios, and thus determine the corresponding maximum number soft-ROADMs where acceptable network performance is maintained.

4) Experimental evaluation of DFMA PONs and CANs with large channels counts and high aggregated capacities.

In [1] numerical explorations where performed of a DFMA PON with 32 ONUs, with one channel allocated per ONU, and an aggregated capacity of >30Gb/s. This is currently the highest channel count and aggregated capacity employed in a numerical simulation which investigates the performance characteristics of DFMA PONs. To fully validate the DFMA PON and CAN operation, real-time experimental investigations with high channel counts and high aggregate capacity are required over a wide range of network scenarios. To implement DFMA-based networks with suitably high aggregated capacity, higher DAC/ADC sampling rates are crucial to support the higher total required bandwidth. The sampling rate of the employed DACs/ADCs in this dissertation research was 2GS/s for all real-time demonstrations, whereas to achieve the higher and capacities as adopted in [31], a sample rate of 12.5 GS/s is required to give a total transmission capacity of >30Gb/s. Consequently, to support aggregate capacities of the order of 100 Gb/s sample rates of >40GS/s are required. The latest high speed DACs/ADCs, however, can now achieve sample rates in the region of 100GS/s or more. Furthermore, when operating at high signal bandwidths the associated RF and optical components must have suitably high bandwidths. As the characteristics of the high bandwidth devices will impact on the DFMA PON and CAN performance, it is this critical to assess their performance experimentally in the aforementioned high capacity, high channel count networks.

References

[1]   M. Bolea, R. P. Giddings, M. Bouich, C. Aupetit-Berthelemot, and J. M. Tang, "Digital Filter Multiple Access PONs With DSP-Enabled Software Reconfigurability," J. Opt. Commun. Netw., vol. 7, no. 4, p. 215, 2015.

References
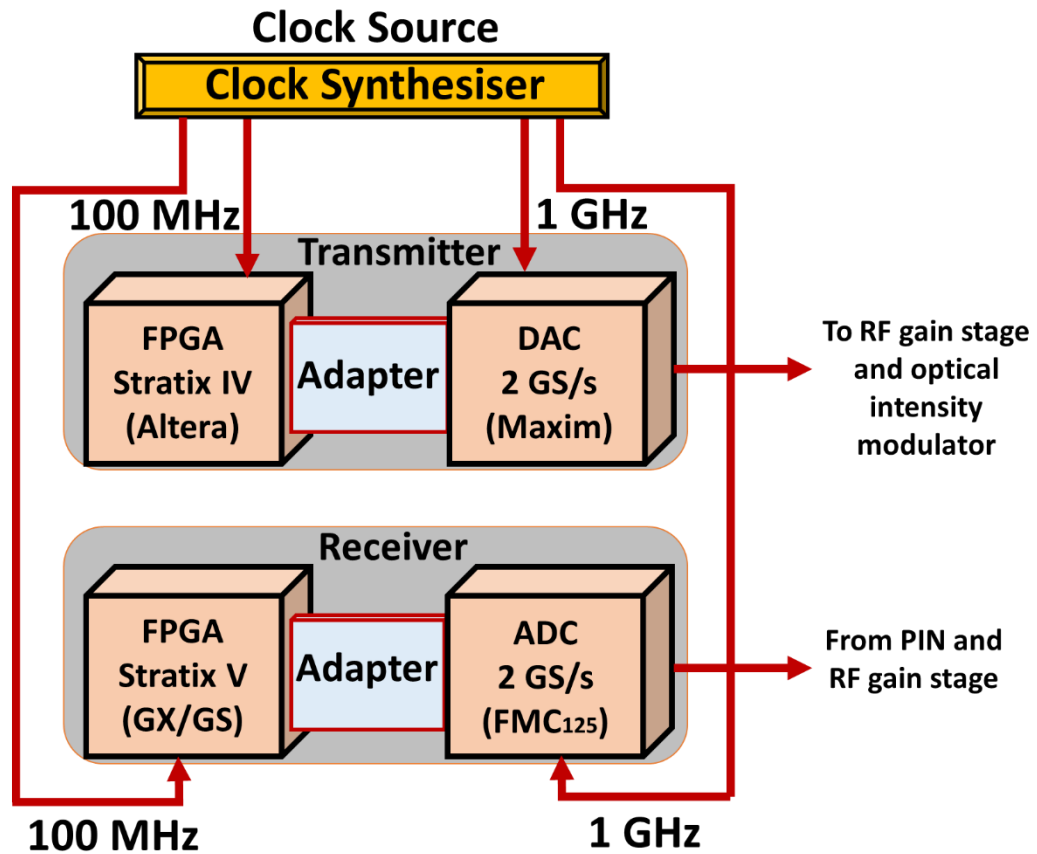
Appendix: A

A.1 **Real-time DSP Platform**

Fig. A1.1 Real-time transceiver DSP platform basic architecture.

The real-time transceiver DSP platform is shown in Fig. A1.1, which consist of FPGAs, digital interface adaptors, DAC/ADC and clock sources (RF gain stages and optical front ends are not shown). Figs. A1.2 to A1.3 show photographs of the real-time transceiver platform. The key component specifications are listed in Table A1.

Fig. A1.2 Real-time transceiver DSP platform (Transmitter top, Receiver bottom)
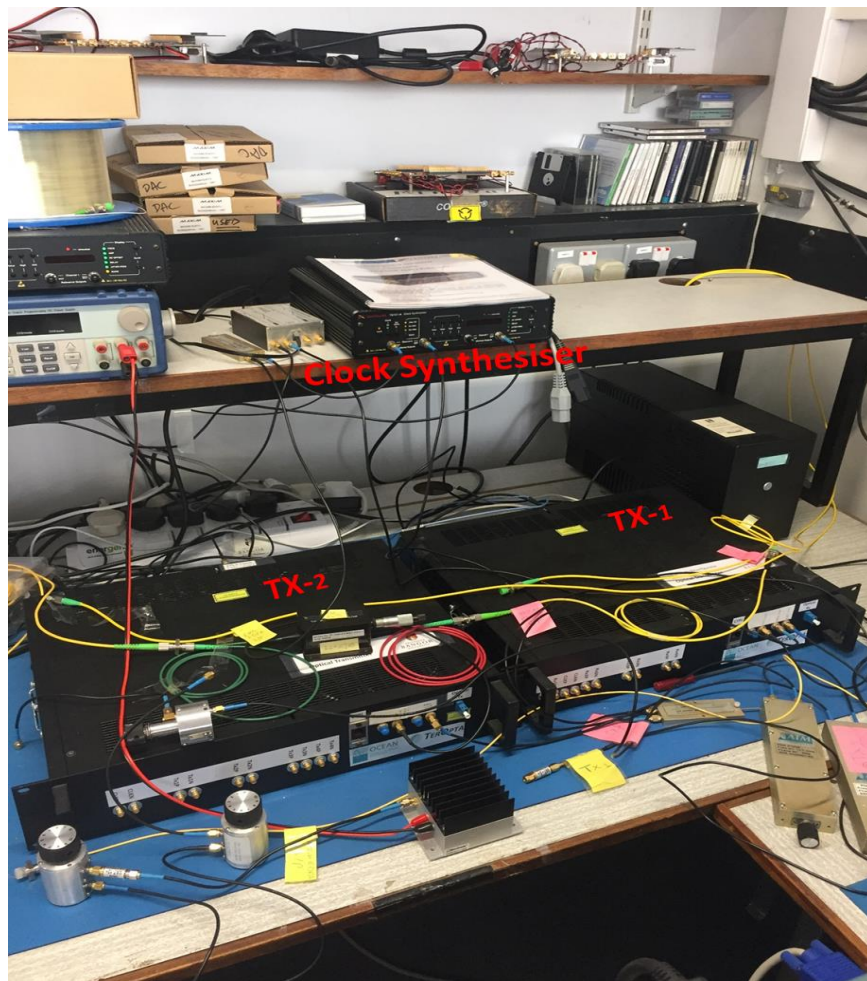
Fig. A1.3 Real-time transceiver DSP platform (Two transmitters)

Table A1. Key Component Parameters

Component	Type	Key Parameter
FPGA (TX)	Altera: Stratix IV GX EP4SGX230KF40C2	■ 228k logic elements (LEs) ■ 1288 18×18 multipliers ■ 0.6 Gbps-6.5 Gb/s high-speed transceivers ■ Up to 17,133 Kb of total memory
DAC	Maxim: MAX5881	■ Resolution: 12-bit ■ Sample rate: 4.3GS/s ■ Output voltage: 660mVpp ■ 4×8-bit LVDS ports
FPGA (RX)	Altera Stratix® V GX/GS 5SGXEA7K3F40C3	■ 952k logic elements (LEs) ■ 3,926 18×18 multipliers ■ 32 full-duplex, multi-gigabit transceivers up to 14.1 GHz ■ 1.4 Gb/s LVDS performance ■ Up to 62 Mb of embedded memory ■ Embedded Hard Copy Blocks
ADC	E2V Quad ADC: EV10AQ190	■ Quad - Dual - Single 10-Bit Channel Operation 4-Channel 1.25 GS/s A/D conversion Mode ■ Resolution: 10-bit ■ ENOB: 7.1 bits@5GS/s ■ Sample rate: 5GS/s ■ 4×8-bit LVDS ports ■ Selectable analogue input range (500mVpp / 625mVpp)
Clock Source	Centallax: TG1C1A Clock Synthesiser	■ Frequency Range: 0.5 – 13.5 GHz ■ Accuracy: ±3.0 ppm ■ differential output channels ■ Sub-rate trigger output: (Clock/N)

A.2 **DSP Design Environment**

A complete DSP system modelling, simulation and design environment with graphical user interface (GUI) is provided by MATLAB[TM], Simulink[TM] and Intel's DSP Builder[TM], which supports hierarchical system models. Component libraries in MATLAB[TM] and Simulink[TM] provide comprehensive sets of fundamental building blocks to create the required system

models. Such models provide processing in discreet-time via Simulink^{TM} for conformity with digital logic circuits. Simulink^{TM} also supports multi-rate systems such as in the case of a multiple clock logic system. The design environment allows the designer to implement the model design and verification in various stages and allows rapid evaluation of diverse designs. If the verified design in Simulink^{TM} is built purely from DSP Builder^{TM} library components it can be directly compiled into a hardware description language (HDL) such as Verilog or VHDL.

Appropriate test circuitry, not restricted to DSP Builder components, is added to provide input signals and to view/analyse output signals. For example Vector Scopes can be used to view constellation diagrams. Simulink^{TM} allows the designer to rapidly modify the model to easily evaluate alternative logic designs and assess the effect of parameters such as sample bit resolution. Variable system control parameters can be used in the DSP design which can be implemented as writable memory locations in the FPGA to allow real-time control of various DSP parameters, allowing real-time control of functions such as signal scaling factors and quantisation levels, etc, for performance optimisation. When the Simulink^{TM} simulation process successfully verifies the design's functional operation, it can be transferred to the FPGA design for evaluation in the real-time system.

A.3 DSP Design

The whole system design of both ONUs, channel filter (used to modelling the roll-off of the physical channel) and OLT are depicted in Fig. A3.1. Fig. A3.2 shows the internal ONU DSP design which contains the main processing elements for implementing the digital orthogonal filtering in the transmitter side as follows: signal up-sampling, FIR-based shaping filters and a re-quantisation processes. The input to the aforementioned DSP is the output of an existing OFDM generator function, where a suitable delay is used to generated two uncorrelated OFDM signals. It should be noted however, that in the final FPGA design, two separate OFDM generators are used to allow independent control of subcarrier bit and power loading. Fig A3.3 depicts the internal OLT DSP design including the main processing elements for implementing the digital orthogonal filtering in the receiver side and for the CCIC process, thus the main functions are; the corresponding FIR-based matching filters (one for the wanted channel and one for the interfering channel), the CCIC filtering process and the subtraction process (subtracts interference estimate from wanted signal). The output

of the aforementioned DSP is the input to an existing OFDM detector function. It should also be noted that all filters have real-time controllable parameters including tap coefficients, output signal scaling factor, variable delays and quantisation control. Fig A3.4 shows the sub-functions of the matching filter function, including programmable FIR filter, quantiser and the controllable down-sampler function (to dynamically select the required samples). It should be noted that in an optimised design no down-sampling function would be physically implemented in the receiver as the discarded samples are simply not generated. The same FIR filter design is used in the shaping, matching and CCIC filters except that in the CCIC filter a higher sample resolution was used (12 bit vs. 8 bit) and a tap mask was included to control the effective tap count. The FIR filter internal design is shown in Fig A3.5, which consists of an up-sampler, a delay block to generate parallel samples and 16 parallel FIR filters, each containing multiple multipliers and adders (not visible).
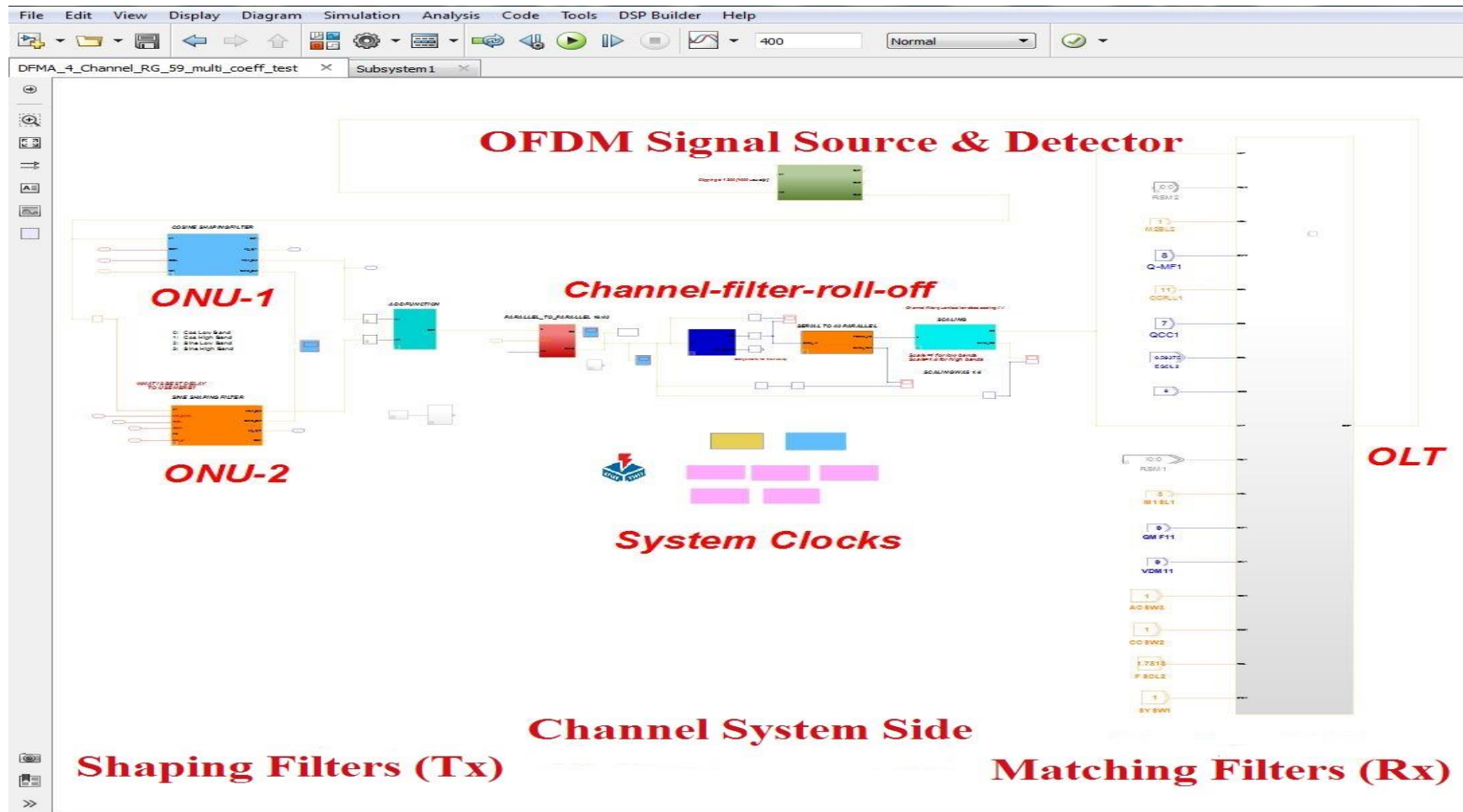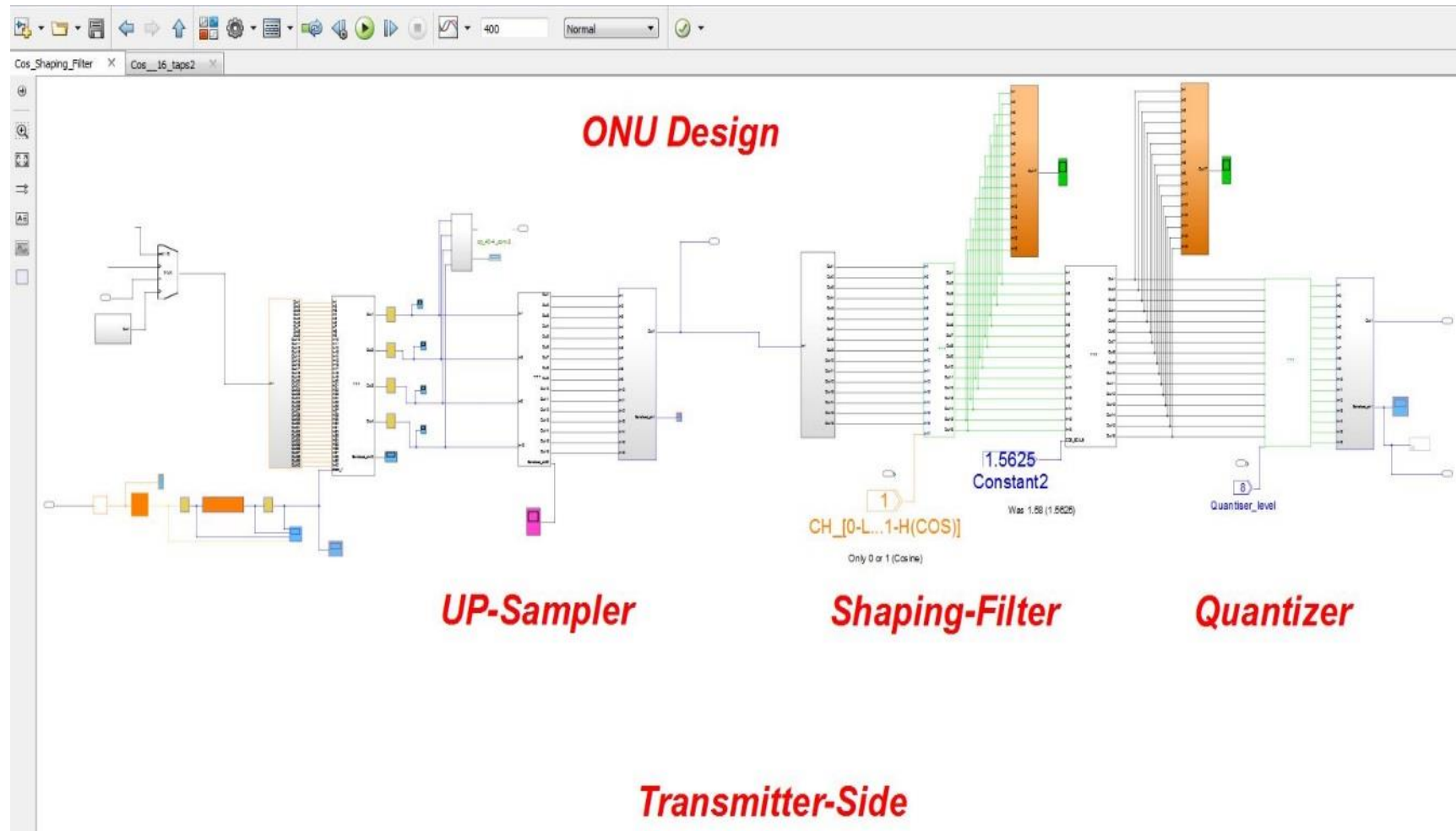
Fig. A3.1 Simulink model of whole system design
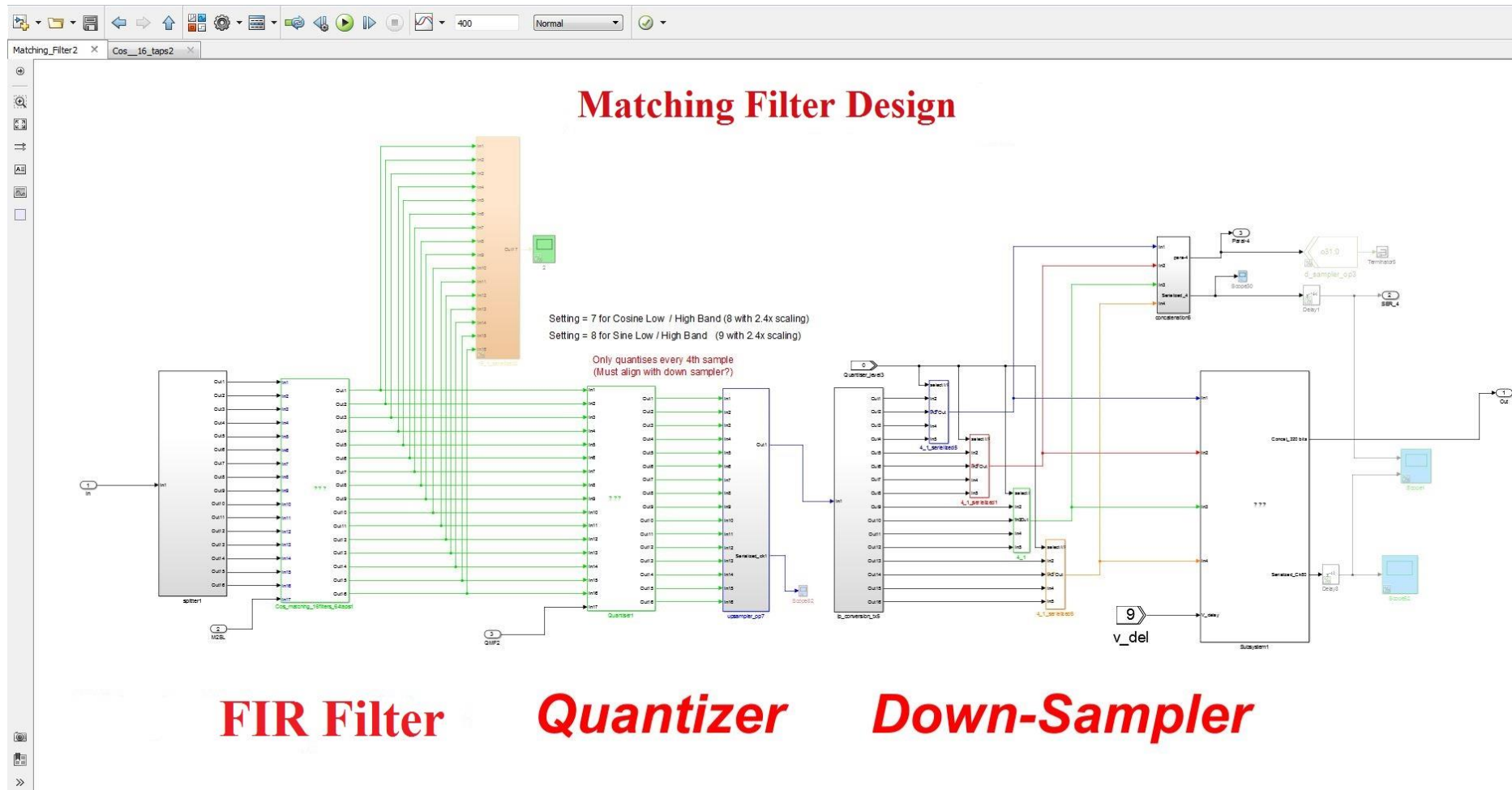
Fig. A3.2 Simulink model of internal ONU design

Fig. A3.3 Simulink model of OLT including embedded CCIC function

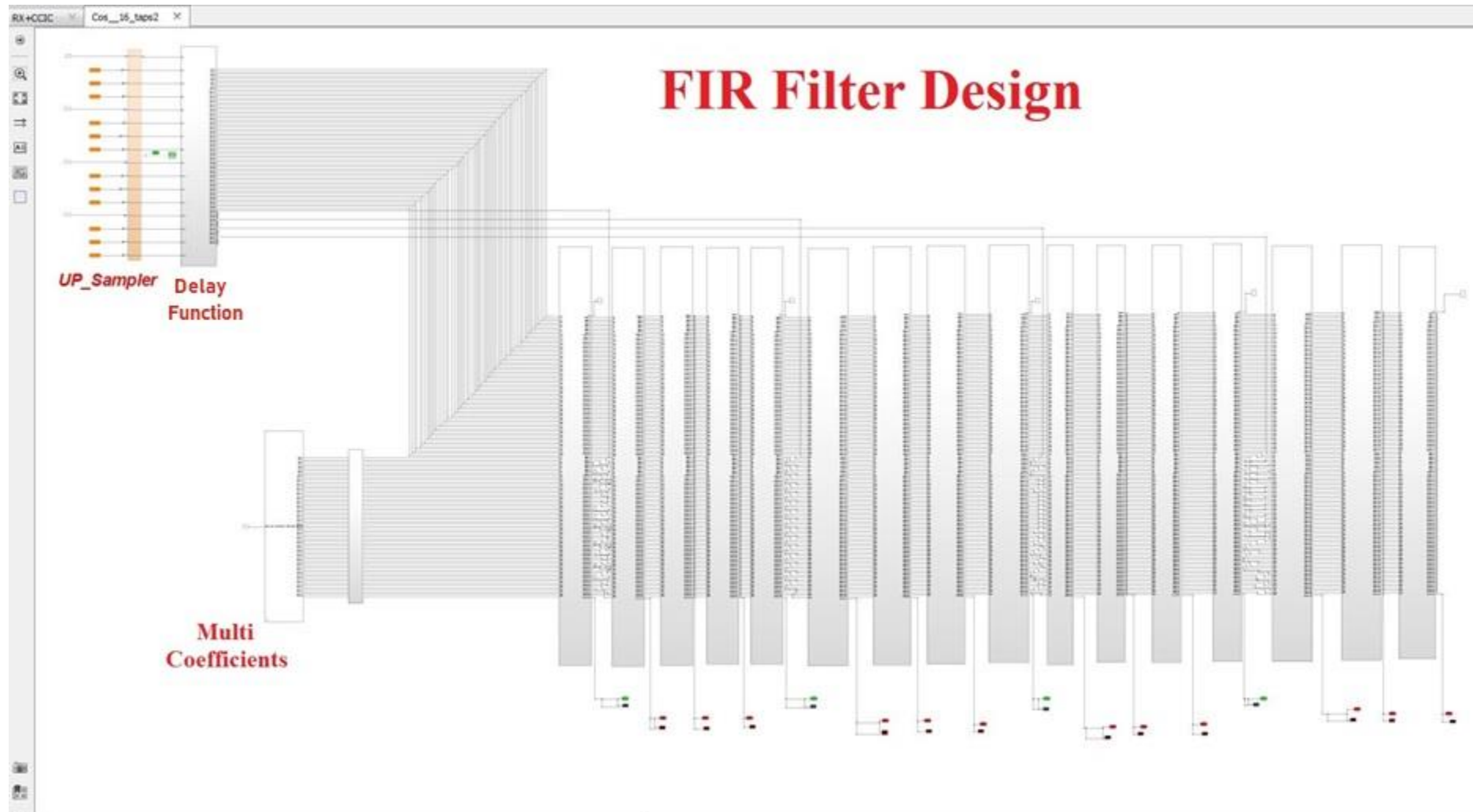*Fig. A3.4 Simulink model for matching filter design*

Fig. A3.5 Simulink model of FIR filter design

The Simulink™ *Signal Compiler* process is used to automatically generate a VHDL representation of the Simulink™ design, which is first partitioned into different functional components to be compiled separately. These compiled functional components are then represented as different blocks in the FPGA schematic design, which is built in the Quartus Prime FPGA design environment. Quartus Prime automatically generates the required schematic symbols, which can also be edited if required, from the VHDL files. It is important to mention that VHDL generation from DSP Builder™ models cannot generate highly optimised logic, in terms of logic resources or power consumption, compared to direct coding in VHDL. However, for the proof-of-concept purpose extensive, highly detailed logic optimisation is not so critical. However, the DSP itself can of course be designed to control the high level design complexity, such as minimising the use of logic consuming elements such as multipliers, for example.

Multiple VHDL-based functional blocks therefore integrated together in a single FPGA logic design. The top level FPGA designs for the transmitter, the receiver and the receiver with embedded CCIC are depicted in Fig. A3.6, Fig. A3.7 and Fig. A3.8 respectively. The logic synthesis process for the whole design is performed to generate a netlist based on primitive logic gates. The netlist is then fitted to the FPGA's logic array and its fixed logic functions, such as multipliers, to produce the FPGA programming file. SignalTap II™ is an embedded logic analyser tool that can monitor the state of internal FPGA signals and provides a user interface as part of the Quartus Prime™ software. SignalTap II™ thus allows the state of predefined nodes to be probed during FPGA operation, this can be employed for design debugging purposes and to extract key system performance parameters during operation such as bit error counts and channel response. Fig. A3.9 shows an example of the SignalTap II™ output. Quartus Prime™ also contains a memory content editor tool to allow the aforementioned system control parameters located in embedded FPGA memory to be changed in real-time. It can thus provide instantaneous update of parameters to adapt to real-time system variations and users demands. This feature is fully exploited to enable the rapid online optimisation of various system parameters which directly impact system performance. In addition, it is also used to change the filter coefficients in real-time to select the transmitted and received channel(s), thus this feature is used to make the transceiver real-time reconfigurable.
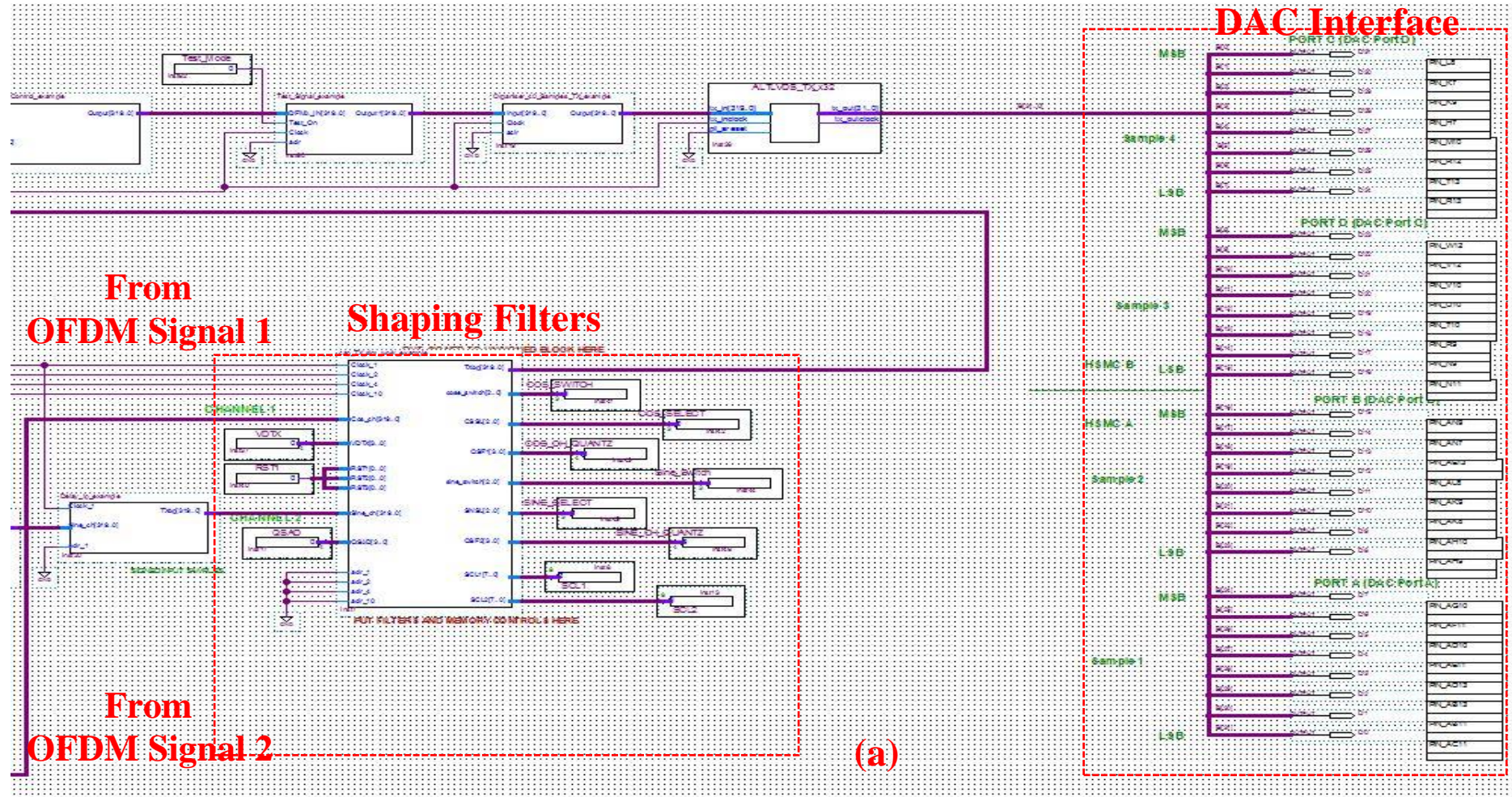
Fig. A3.6 (a) Quartus Prime top-level design for the transmitter side showing the shaping filters and DAC interface.
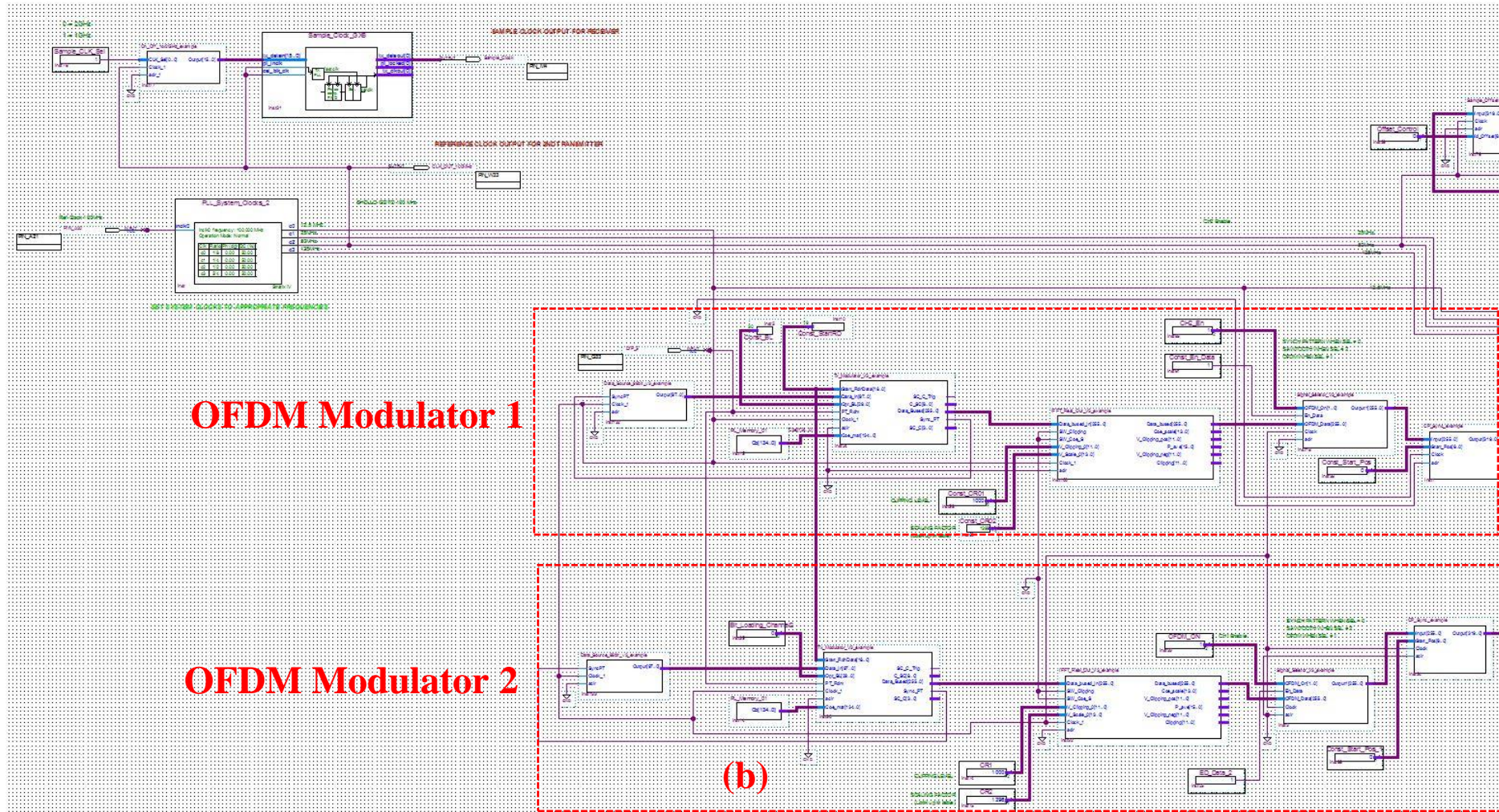
Fig. A3.6 (b) Quartus Prime top-level design for the transmitter side showing the two OFDM modulators.
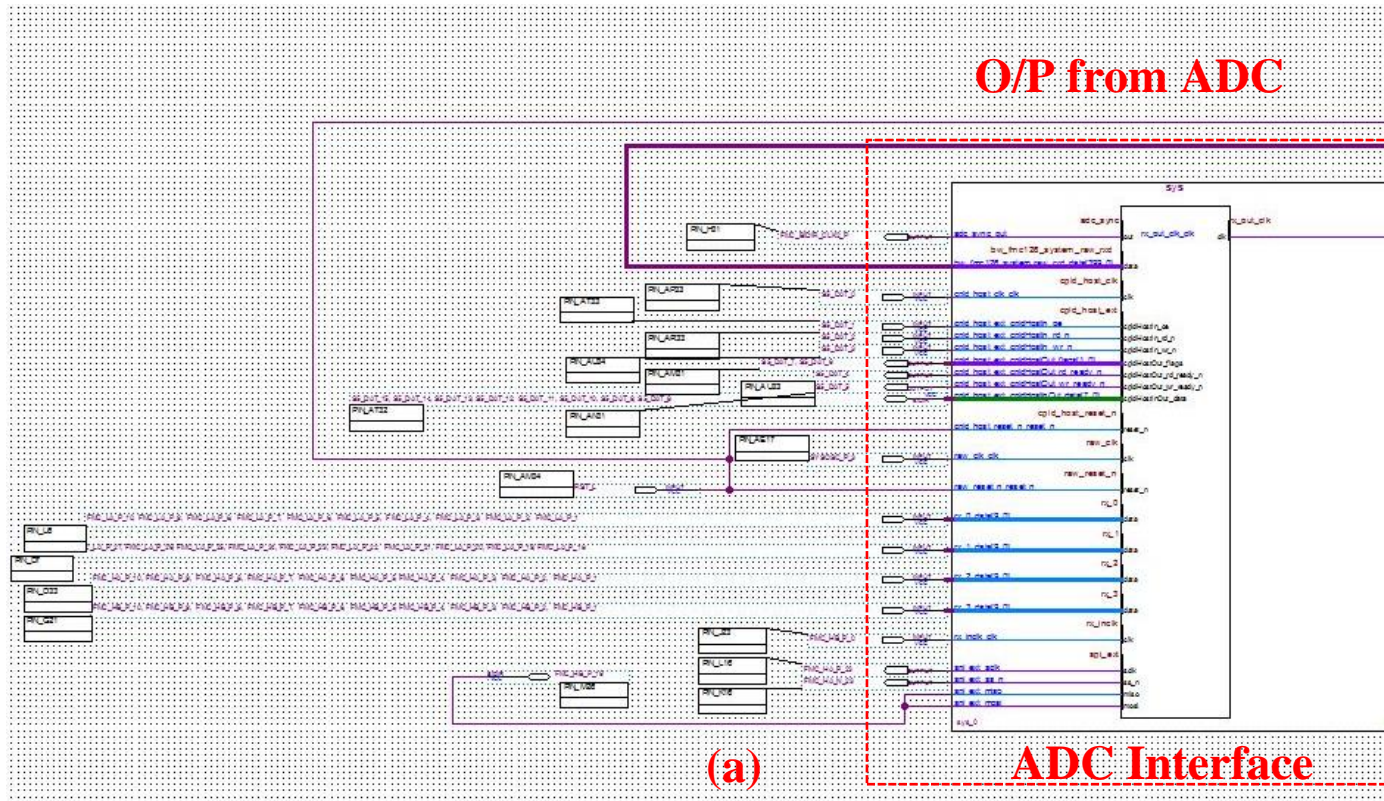
Fig. A3.7 (a) Quartus Prime top-level design for the receiver side showing the ADC interface.
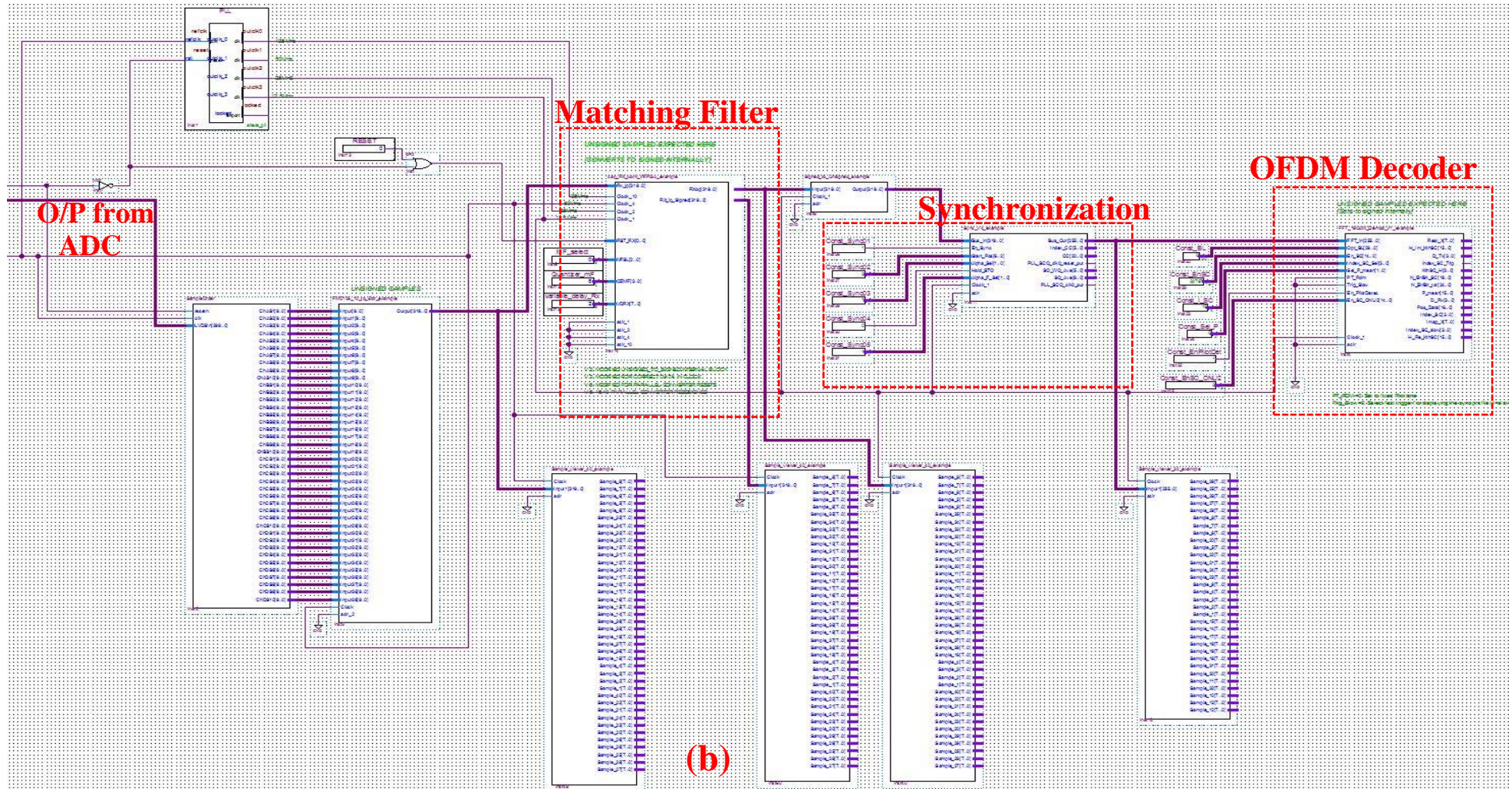
Fig. A3.7 (b) Quartus Prime top-level design for the receiver side showing matching filter, synchronisation and OFDM decoder blocks.
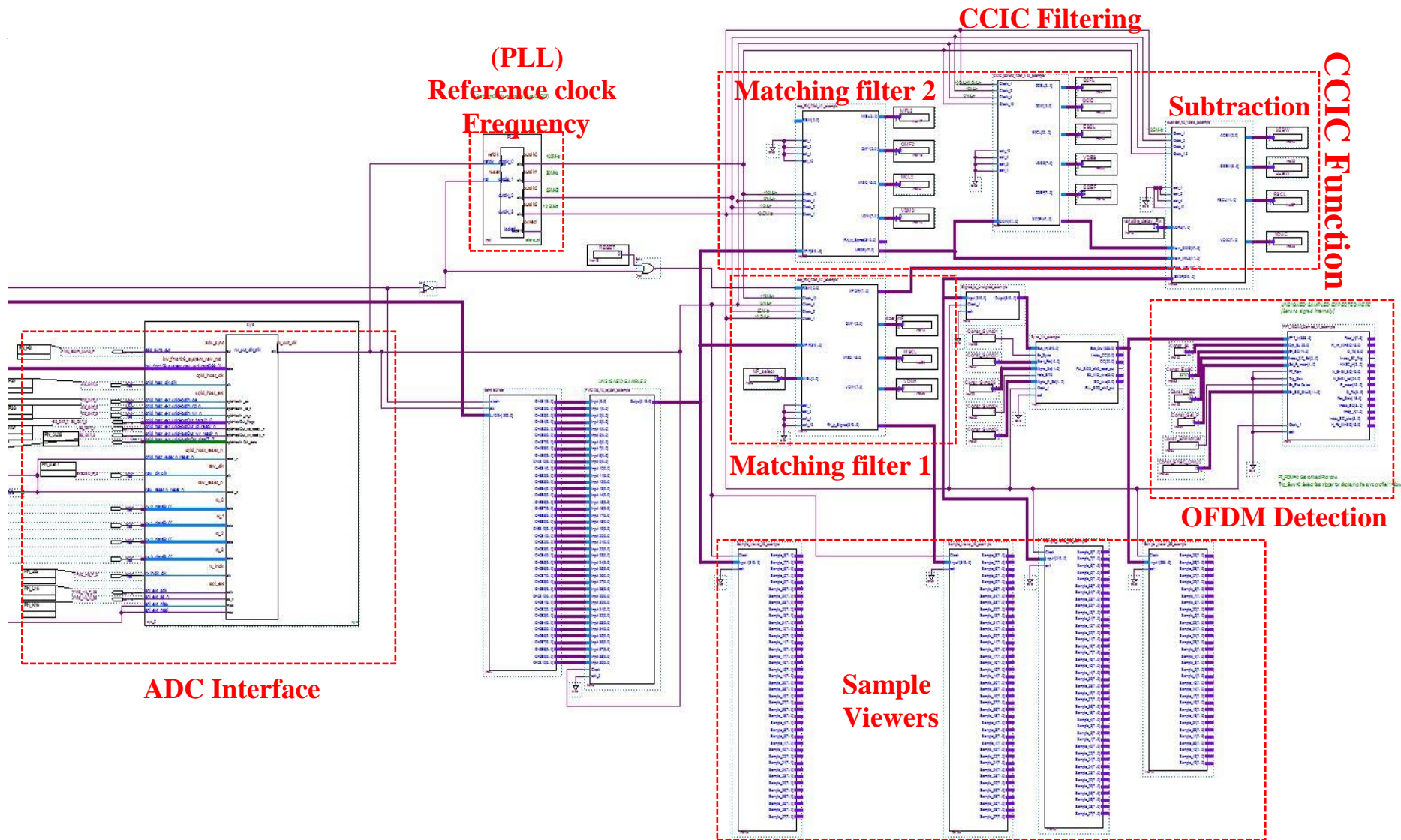
Fig. A3.8 Quartus Prime top-level design for the receiver side with the embedded CCIC function

Fig. A3.9 Performance monitoring with Signal Tap II Embedded Logic Analyser

A.4 **Journal Publications**

[1] **Ehab Al-Rawachy**, Roger Philip Giddings, and Jianming Tang. "Experimental demonstration of a DSP-based cross-channel interference cancellation technique for application in digital filter multiple access PONs." Optics express 25.4 (2017): 3850-3862.

[2] Dong, Yixian, **Ehab Al-Rawachy**, Roger Philip Giddings, Wei Jin, Derek Nesset, and J. M. Tang. "Multiple channel interference cancellation of digital filter multiple access PONs." Journal of Lightwave Technology 35, no. 1 (2016): 34-44.

[3] **Ehab Al-Rawachy**, Roger Philip Giddings, and Jianming Tang. "Real-time experimental demonstration of DSP-enabled soft-ROADMs with multi-level flexible add/drop functions for cloud access networks." Optics express 27.1 (2019): 16-33.

[4] Giddings, Roger, Xiao Duan, **Ehab Al-Rawachy**, and Mingzhi Mao. "A Review of DSP-Based Enabling Technologies for Cloud Access Networks." Future Internet 10, no. 11 (2018): 109.

[5] **Ehab Al-Rawachy**, Roger Philip Giddings, and Jianming Tang. "Experimental Demonstration of a Real-Time Digital Filter Multiple Access PON With Low Complexity DSP-Based Interference Cancellation." Journal of Lightwave Technology 37.17 (2019): 4315-4329.

A.5 **Conference Publications**

[1] **Ehab Al-Rawachy**, Roger Philip Giddings, and Jianming Tang. "Experimental demonstration of real-time add/drop operations in DSP-enabled flexible ROADMs for converging fixed and mobile networks." In Optical Fiber Communication Conference, pp. W2A-33. Optical Society of America, 2018.